PB85-190890

U.S./U.S.S.R. Symposium on Particulate Control (3rd) Held at Suzdal, U.S.S.R. on September 10-12, 1979

(U.S.) Environmental Protection Agency
Research Triangle Park, NC

Apr 85

U.S. Department of Commerce
National Technical Information Service
NTIS

PB85-190890

EPA/600/9-85/011
April 1985

THIRD U.S./U.S.S.R. SYMPOSIUM ON PARTICULATE CONTROL

EPA Project Officer: Jaroslaw Pekar

Air and Energy Engineering Research Laboratory
Research Triangle Park, North Carolina 27711

AIR AND ENERGY ENGINEERING RESEARCH LABORATORY
OFFICE OF RESEARCH AND DEVELOPMENT
U.S. ENVIRONMENTAL PROTECTION AGENCY
RESEARCH TRIANGLE PARK, NC 27711

REPRODUCED BY
NATIONAL TECHNICAL
INFORMATION SERVICE
U.S. DEPARTMENT OF COMMERCE
SPRINGFIELD, VA. 22161

TECHNICAL REPORT DATA

(Please read Instructions on the reverse before completing)

1. REPORT NO. EPA-600/9-85-011	2.	3. RECIPIENT'S ACCESSION NO. PB85 190890 /AS
4. TITLE AND SUBTITLE Third U.S./U.S.S.R. Symposium on Particulate Control*		5. REPORT DATE April 1985
		6. PERFORMING ORGANIZATION CODE -
7. AUTHOR(S) Miscellaneous		8. PERFORMING ORGANIZATION REPORT NO.
9. PERFORMING ORGANIZATION NAME AND ADDRESS NA		10. PROGRAM ELEMENT NO.
		11. CONTRACT/GRANT NO. NA (Inhouse)
12. SPONSORING AGENCY NAME AND ADDRESS EPA, Office of Research and Development Air and Energy Engineering Research Laboratory Research Triangle Park, NC 27711		13. TYPE OF REPORT AND PERIOD COVERED Proceedings; September 1979
		14. SPONSORING AGENCY CODE EPA/600/13

15. SUPPLEMENTARY NOTES AEERL project officer is Jaroslaw Pekar, Mail Drop 60, 919/541-3995. (*) Symposium held in Suzdal, U.S.S.R., September 10-12, 1979.

16. ABSTRACT The proceedings document the Third U.S./U.S.S.R. Symposium on Particulate Control, September 10-12, 1979, in Suzdal, U.S.S.R. Papers covered such topics as: predicting back-corona formation and fly ash resistivity, improved electrostatic precipitator (ESP) mathematical modeling, calculating effects of back corona in wire-duct ESPs, chemical conditioning of flue gas before an ESP on a 500-MW power unit, sodium conditioning tests with EPA's mobile ESP, fly ash dielectric properties and critical current density, general industrial application of precipitating electrodes for ESPs, performance analysis of a hot-side ESP, dynamics and strength of corona electrodes in industrial ESPs, ESPs for use at high temperatures and high pressures, cleaning hot aspirated air from sinter machines and clinker coolers, ESP modeling with the TI-59 calculator, removing fly ash at electric power stations, particle collection by granular bed filters and dry scrubbers, filter materials for cleaning gases and possible areas of their application, high temperature ceramic filters, measuring the size of finely dispersed particles less than 0.3 micrometer for process gases, particle measurement in the U.S., aerosol dispersion analysis, automatic monitoring of particle-size distributions, measuring the dew point of process emissions, and designing an improved impactor.

17. KEY WORDS AND DOCUMENT ANALYSIS

a. DESCRIPTORS		b. IDENTIFIERS/OPEN ENDED TERMS	c. COSATI Field/Group	
Pollution	Mathematical Models	Pollution Control	13B	12A
Particles	Electrostatic Precipitators	Stationary Sources	14G	
Dust		Particulate Matter	11G	13I
Aerosols	Flue Gases	Russia	07D	
Coronas	Measurement	Back Corona	20C	14B
Fly Ash	Ceramics		21B	11B

18. DISTRIBUTION STATEMENT Release to Public	19. SECURITY CLASS *(This Report)* Unclassified	21. NO. OF PAGES 345
	20. SECURITY CLASS *(This page)* Unclassified	22. PRICE

EPA Form 2220-1 (9-73)

NOTICE

This document has been reviewed in accordance with U.S. Environmental Protection Agency policy and approved for publication. Mention of trade names or commercial products does not constitute endorsement or recommendation for use.

ABSTRACT

The Third U.S./U.S.S.R. Symposium on Particulate Control was sponsored by the Particulate Control Technology Project Group of the U.S./U.S.S.R. Stationary Source Air Pollution Control Technology Working Group under the U.S./U.S.S.R. Environmental Agreement. Papers were presented by Soviet specialists from scientific research and design institutes and by representatives of the United States Environmental Protection Agency and representatives of the private sector. The topics included: prediction of back corona formation, fly ash resistivity prediction, improved ESP mathematical model, calculation of effects of back corona in wire-duct electrostatic precipitators, study of chemical conditioning of flue gas before an ESP on a 500 MW power unit, sodium conditioning test with EPA mobile ESP, fly ash dielectric properties and critical current density, improved design for general industrial application of precipitating electrodes for ESP's, performance analysis of a hot-side ESP, dynamics and strength of corona electrodes in industrial ESP's, progress on electrostatic precipitators for use at high temperatures and high pressures, cleaning of hot aspirated air from sinter machines and clinker coolers, ESP model for the TI-59 calculator, problems of fly ash removal at electric power stations, particle collection by granular bed filters and dry scrubbers, filter materials for cleaning gases and possible areas of their application, high temperature ceramic filters, methods and instruments for measuring size of finely dispersed particles less than 0.3 micron for process gases, particle measurement in the U.S.A., current trends in aerosol dispersion analysis, instruments for automatic monitoring of particle-size distributions, methods and instruments for measuring the dew point of process emissions, and design of an improved impactor.

Table of Contents

Page

Abstract iii

Foreword viii

Forcasting the Occurrence of Back Corona in Electrostatic Precipitators, (USSR) 1

I.K. Reshidov
V.M. Tkachenko
A.Ya. Rachek
A.T. Lyapin
V.A. Rodionov

A Technique for Predicting Fly Ash Resistivity, (USA) 13
Roy E. Bickelhaupt
Leslie E. Sparks

An Advanced Mathematical Model for Electrostatic Precipitator Calculating 23
(USSR)
I.V. Ermilov
T.I. Dmitrieva
Yu.M. Morozov

Calculations of Effects of Back Corona in Wire-Duct Electrostatic Precipitators, (USA) 41
Phil A. Lawless
Leslie E. Sparks

Study of Chemical Conditioning of Stack Gases before Electrostatic Precipitation at 500 MW Power Station (USSR) 69
I.A. Kizim
B.V. Zolotaryov
A.A. Troitsky
M.A. Golosov

Sodium Conditioning Test with EPA Mobile ESP, (USA) 80
Steven P. Schliesser

Improving Electrical Feeding System for Electrostatic Precipitators, (USSR) 114
V.I. Sikorskiy
V.V. Kutlyashov

Fly Ash Dielectric Properties and Critical Current Density, (USA) . . . 126
John P. Gooch
Jack R. McDonald
Leslie E. Sparks

Preceding page blank

Table of Contents (cont'd)

Page

Research, Development and Introduction of Advanced Precipitating Electrode Designs of Industrial Purpose Electrostatic Precipitators (USSR) 140
A.I. Zavyalov
V.B. Mescheryakov

Performance of a Hot-Side Electrostatic Precipitator, (USA) 145
G.H. Marchant
John P. Gooch
Leslie E. Sparks

Study of the Dynamics and Strength of Coronal Electrodes in Electrostatic Precipitators, (USSR) 155
E.N. Kurbatskiy
V.B. Meshcheryakov
E.N. Rudometov

Progress on Electrostatic Precipitators for Use at High Temperature and High Pressure, (USA) 161
George Rinard
Donald Rugg
Robert Gyepes
James Armstrong
Dennis Drehmel

Purification of Hot Aspirated Air from Sintering Machines and Clinker Coolers, (USSR) 172
V.M. Tkachenko
V.A. Rodionov
A.D. Malgin

A Model of Electrostatic Precipitation for TI-59 Calculator, (USA) 178
Leslie E. Sparks

Urgent Problems of Ash Trapping at Thermal Power Stations, (USSR) 186
L.I. Kropp
G.S. Chekanov

Particle Collection by Granular Bed Filters and Dry Scrubbers, (USA) 199
Dennis Drehmel
R. Parker
S. Calvert

Table of Contents (cont'd)

Page

Filtering Material for Gas Cleaning and Possible Areas for Its Use, (USSR) 212
I.K. Goryachev
Yu.V. Abrosimov

High Temperature Ceramic Filters, (USA) 218
Dennis Drehmel
R. Parker
S. Calvert

Methods and Equipment for Measuring of Finely Dispersed Particle-Size Less Than 0.3 Micron for Industrial Gases, (USSR) 228
N.G. Bulgakova
D.L. Zelikson

Particle Measurement in the USA, (USA) 239
W.B. Smith
K.M. Cushing
D.B. Harris

Present-Day Tendencies of Aerosol Disperson Analysis, (USSR) . . . 268
D.L. Zelikson
N.G. Bulgakova

Instruments for Automatically Monitoring Particle-Size Distribution, (USA) 275
W.M. Farthing
W.B. Smith
W.B. Kuykendal

Methods and Devices for Measuring Industrial Gases' Dew Point (USSR) 303
A.I. Manyurov
N.G. Bulgakova
E.I. Akopov

Design of an Improved Impactor, (USA) 317
W.B. Smith
K.M. Cushing
D.B. Harris

FOREWORD

The primary objective of the Third U.S.-U.S.S.R. Symposium on Particulate Control, held September 10-12, 1979, in Suzdal, U.S.S.R., was to discuss work done by American and Soviet specialists on particulate control and measurement technology.

The two symposium co-chairmen were: (U.S. side) A. B. Craig, Deputy Director of the Industrial Environmental Research Laboratory,* U.S. Environmental Protection Agency, North Carolina; and (Soviet side) I. K. Reshidov, Director of the Scientific Research Institute of Industrial and Sanitary Gas Cleaning (NIIOGAZ), Moscow, U.S.S.R.

The following organizations participated:

U.S.A. - Industrial Environmental Research Laboratory,* U.S. Environmental Protection Agency, Research Triangle Park, N.C. 27711

U.S.S.R. - Scientific Research Institute of Industrial and Sanitary Gas Cleaning (NIIOGAZ), Moscow

- Semibratovo Branch of NIIOGAZ
- Zapozozhye Branch of NIIOGAZ
- Special Dasign Office for Gas Cleaning and Dust Eliminating Equipment (SKBGPO), Semibratovo
- State Institute for Gas Cleaning Equipment Desing (GIPROGAZOOCHISTKA), Moscow
- All-Union Heat Engineering Institute imeni Dzerzhinskiy (VTI), Moscow
- State Research and Design Institute for Environmental Protection in the Building Materials Industry (NIPIOSTROM), Novorossiysk
- Moscow Energy Institute (MEI), Moscow
- Moscow Transport Engineering Institute (MIIT), Moscow
- All-Union Electrotechnical Institute imeni Krzhyzhanovskiy (VEI), Moscow

---

(*) Now, Air and Energy Engineering Research Laboratory.

I.K. Reshidov, V.M. Tkachenko, A.Y. Rachek, A.G. Lyapin,
E.N. Andrusenko, G.I. Vyalkova, V.A. Rodionov

FORECASTING THE OCCURENCE OF BACK CORONA IN ELECTROSTATIC PRECIPITATORS

For efficient removal of high-resistance dusts from gases in electrostatic precipitators, it is important to know under what gas-cleaning parameters that back corona may arise in the equipment.

Predicting back corona by the magnitude of resistivity in the dust layer is not always justifiable, since the resistivity magnitude depends not only on properties of the dust and gas, but also on dust layer forming methods and dust resistence measurements. Furthermore, back corona is caused not only by dust resistivity, but also by current density in the precipitator. Therefore, it is most advisable to directly record back corona and establish the parameters under which it may occur.

A method for detecting back corona and for determining the critical parameters of its occurence has been developed by NIIOGAZ, This method is based on various effects of the dust layer in the precipitating electrodes upon the voltampere characteristics of the corona in relation to the dust's resistance.

It is known that, in the case of non-high-resistance dust and absence of back corona, the voltampere characteristics of dust-laden electrodes have less slope than clean precipitating electrodes. This is caused by a a drop in voltage in the dust layer and by blocking of coronal discharge by volumetric charging of dust.

In the case of high-resistance dust, various effects of the dust layer in the precipitating electrodes on the corona voltampere characteristics may occur. Fig.1 shows the voltampere coronal characteristics in a "conductor-plane" electrode system in the presence of a high-resistance fly-ash layer from ekibastuz coal on the plane's surface as well as during its absence. Discharge distances are the same in all cases and comprised 125mm. For needle coronal electrodes (fig.1a), the current magnitude of the corona characteristic at the beginning section in the presence of a layer is somewhat less than corresponding current values in the absence of a dust layer. This is caused by blocking action of the layer's potential. With further voltage increase, the slope of the characteristic increases and intersects the characteristic in clean electrodes. This is related to the manifestation of back corona. As seen from fig.1b, it is obvious that by using bar wire electrode, back corona manifests itself practically simultaneously with the base corona, despite the fact that under these circumstances the average value of the specific current of the corona per unit of length is less than that for a needle-type electrode. This occurence is caused by considerable change in the bar wire corona current with respect to time and the maximal current density value for the bar wire electrode is significantly higher, than for a needle electrode (1).

The dependence of corona current differences for clean and dusty-laden electrodes on voltage (fig.2) is plotted on the basis of the considered voltampere characteristics. In the case of needle electrodes, it has variable character both according to its magnitude, and to its sign. Corona current difference for bar wire electrodes increases with the rise of voltage. but has a negative sign. These represent typical relationships for high-resistance dust.

The correct approach for determining voltage in the dust layer on precipitating electrodes before the onset of back corona according to corona voltampere characteristics for clean and dust-laden electrodes (2) has been established by probe measurement. It is shown that back corona formation corresponds to the maximum of the dependence of voltage difference for dust-laden and clean electrodes on corona current. This is confirmed by the occurence of glow on the precipitating electrode and also because the probe measurement begins to trap opposite-sign ions.

Consequently, the maximum of corona current difference dependence for clean and dust-laden electrodes on voltage corresponds to the start of back corona occurence. It is obvious from fig.2 that the largest value of corona current difference for needle electrodes is reached at the critical voltage $U_{critical}$ = 30 kilovolts. At this voltage, corona current in the discharge intervals with dust-laden electrodes (fig.1a) is equal to the critical value $J_{critical}$ = 0.06 milliamperes/m.

A knowledge of critical values for corona current density $\dot{j}_{critical}$ in the precipitating electrode and voltage in a dust layer $U_{c.-critical}$ of determined thickness δ allows the resistivity critical value of the dust layer to be found:

$$\rho_{critical} = \frac{E_{critical}}{\dot{j}_{critical}} = \frac{U_{c\ -critical}}{\delta \cdot \dot{j}_{critical}}$$

Use of the stated method gives the opportunity to determine not only critical electrical parameters for back corona occurence, but also critical values such as, for example, temperature and gas humidity. In order to do this, it is necessary to change the parameter of interest until that time when the back corona occurs or disappears. In this manner it is possible to establish an area of implementation of back corona during the ~~trapping~~ collection of high-resistance dusts in the precipitator.

The developed method may be realized in principle in a multi-field precipitator, if the last field is going to have clean electrodes.

A special complex of equipment was created at NIIOGAZ, which allows the determination of critical parameters of back corona occurence in laboratory as well as in industrial conditions by means of direct dust and ga sampling from the gas-duct in a model precipitator. Electric heaters for gas and a steam generator installed at the inlet of the model, which has both clean and dust-laden electrodes make it possible to vary the temperature and moisture content of the studied gas.

Aspirated dust, sampled from the hopper of a DVPNI-4x20 precipitator in a center plant at a metalurgical works, was studied in the laboratory uder various air temperature with the aid of this equipment complex. Aspirated air, entering the unit at a temperature of about 110°C from various sections of the sintering machine, is cleaned in this precipitator.

It has beeen established as a result of research that the probability of a back corona occurence during trapping of the indicated dust will appear at air temperatures of more than 70°C, moisture content of 9-10g/m^3 (of moist gas), and during an exceeding of average current density of 1.3-2.5 milliamperes/m^2. At lower current densities, the back corona does not occur during an increase of air temperature to 150°C.

At NIIOGAZ's Zaporozhe branch, another method has been developed which also makes it possible to determine several quantitative characteristics of back corona. The impulse characteristics of discharge from the surface of the high-resistance dust layer serve as the basis of this method. A differential sensor, which gives basic corona signals and constant interference source signals and separates only the back corona ionization process impulses, is proposed for the measurement of back corona impulses (3,4). The initial back corona voltage can be determined by the manifestation of the first pulses while back corona intensity can be determined by the repetition frequency of these pulses.

By placing the differential sensor together with the discharge ~~coronizing~~ electrode directly in the gas-duct or in a separate chamber, it is possible to predict the conditions of back corona occurence prior to construction of industrial precipitators.

A general view of the unit with coronizing intervals is shown in fig.3. The unit's discharge interval consists of a coronizing electrode (1) and a back corona sensor (2). Part of the gas from the duct (9) enters the chamber (3) through the connecting (5). In the corona discharge field, a dust layer is formed on the working surface of the sensor (2). The amount of gas and its temperature is controlled in the unit. According to sensor signals, the beginning back corona occurence conditions are determined (current density, averaged electrical field intensity) and its intensity.

A back corona measuring device was used for study of back corona occurence conditions in a gas-dust stream from the casting-bed of a high-capacity blast furnace in a metallurgical works, from electric-arc ovens for synthetic corundum smelting in an abrasive mill and from electric-arc ovens for silicon smelting in aluminum plants. In all cases, the gas-dust stream passed through the coronizing interval. The test results have shown that the sensor works satisfactorily.

The measurement results taken are introduced in fig.4-6. At a humidity more than $10g/nm^3$, the back corona is not present until breakdown voltages in the gage on dust from blast-furnace cast-houses (fig. 4) In this case, there are no back corona impulses. On high-resistance synthetic corundum dust, the back corona occurs at a voltage of 9.3 kv in the coronizing electrode and with a 9.7 microampere current through the discharge interval (fig.5). Under the increase of voltage back corona impulse frequency grows and reaches 10kHz.

The measuring device allows monitoring of corona parameters during introduction into the dust-gas stream of moisture,necessary for its removal. The temperature of gases from from silicon smelting furnaces decreases in relation to the amount of directly introduced moisture, and the intensity of back corona drops simultaneously. At 200°C, the

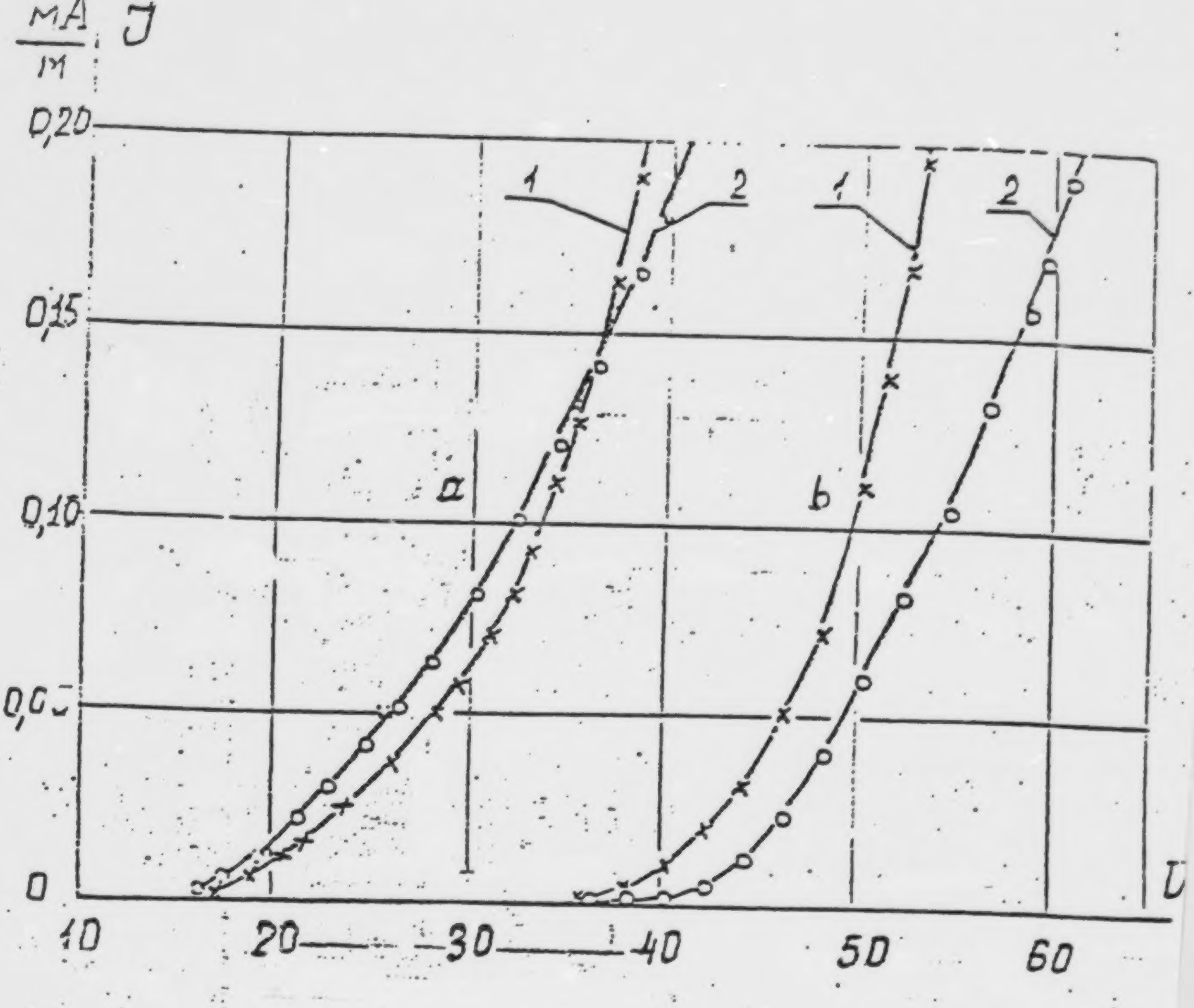

fig.1. Voltampere characteristics of the corona for a "wire-plane" electrode system:

1. during the presence of a dust layer on the plane surface.
2. for clean electrodes

a. neddle electrode

b. bar wire

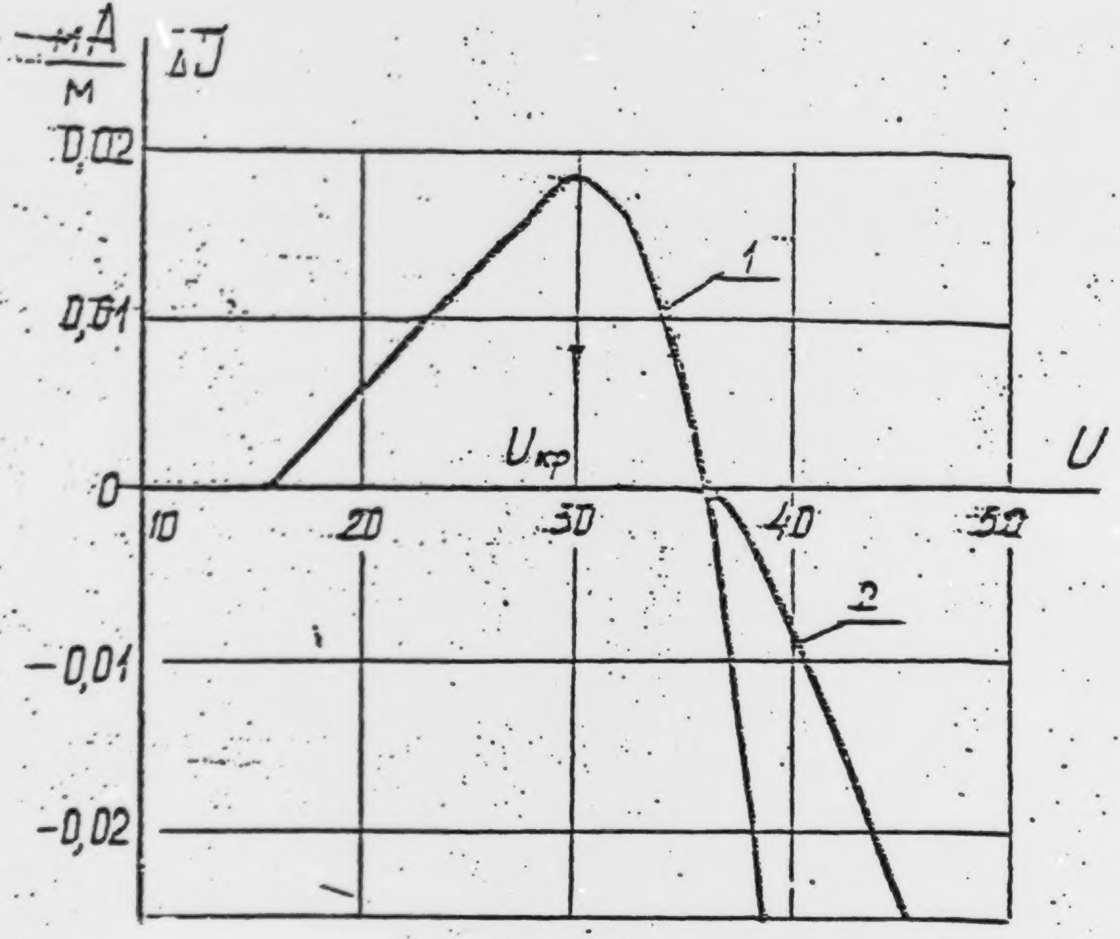

fig.2. Relationship of corona current variability for clean and dust-laden electrodes:

1. needle electrode
2. bar wire.

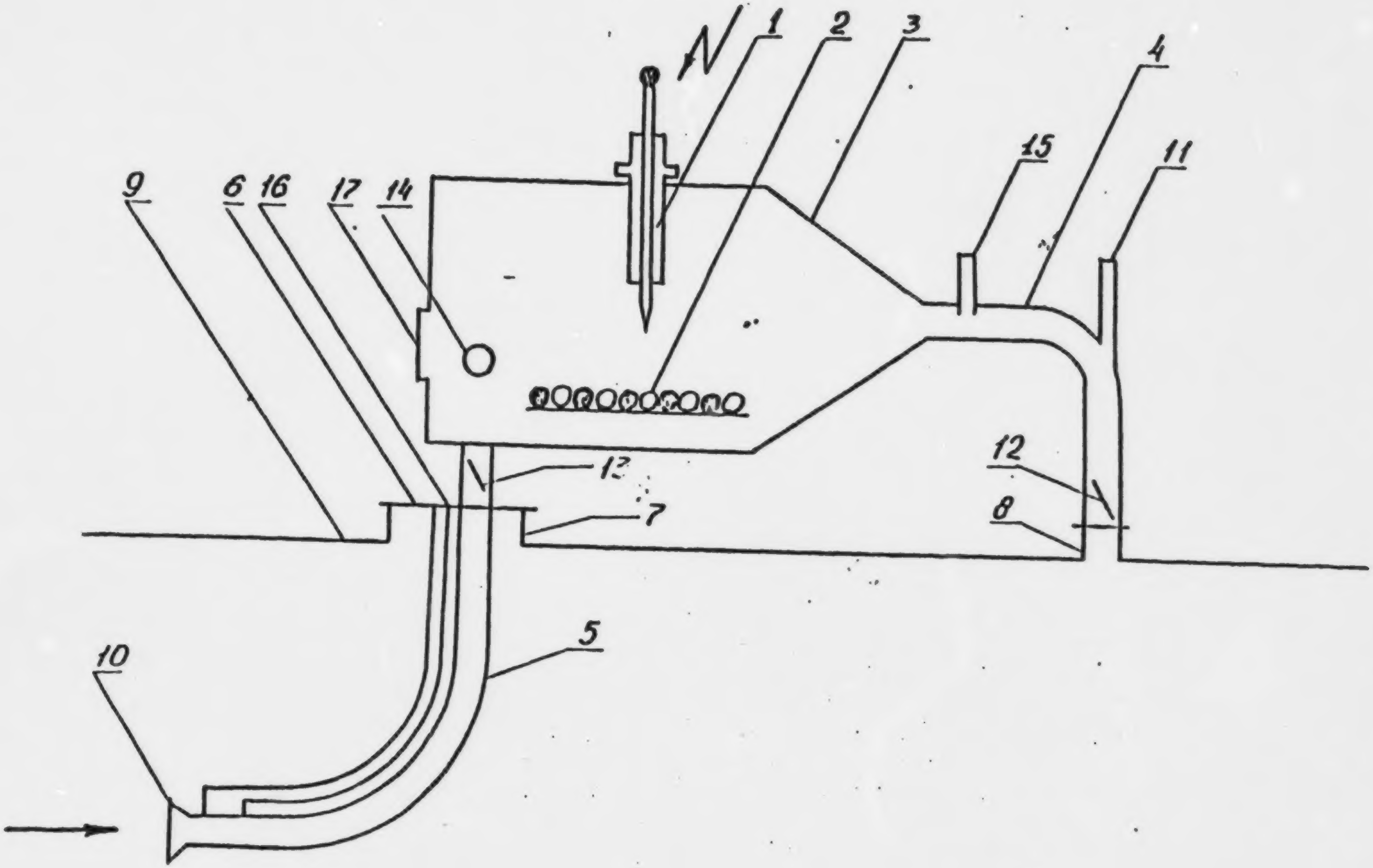

Fig.3. Back corona measurement device: 1. coronal electrode; 2. differential sensor; 3. working chamber; 4,5. gas duct outlet and inlet; 6. porthole; 7,8. connecting pipe; 9. gas duct from process. 10.- collector; ~~11.~~ ejector connecting pipe; 12,13,14. baffles; 15. thermometer connecting pipe; 16. porthole; 17. quartz window.

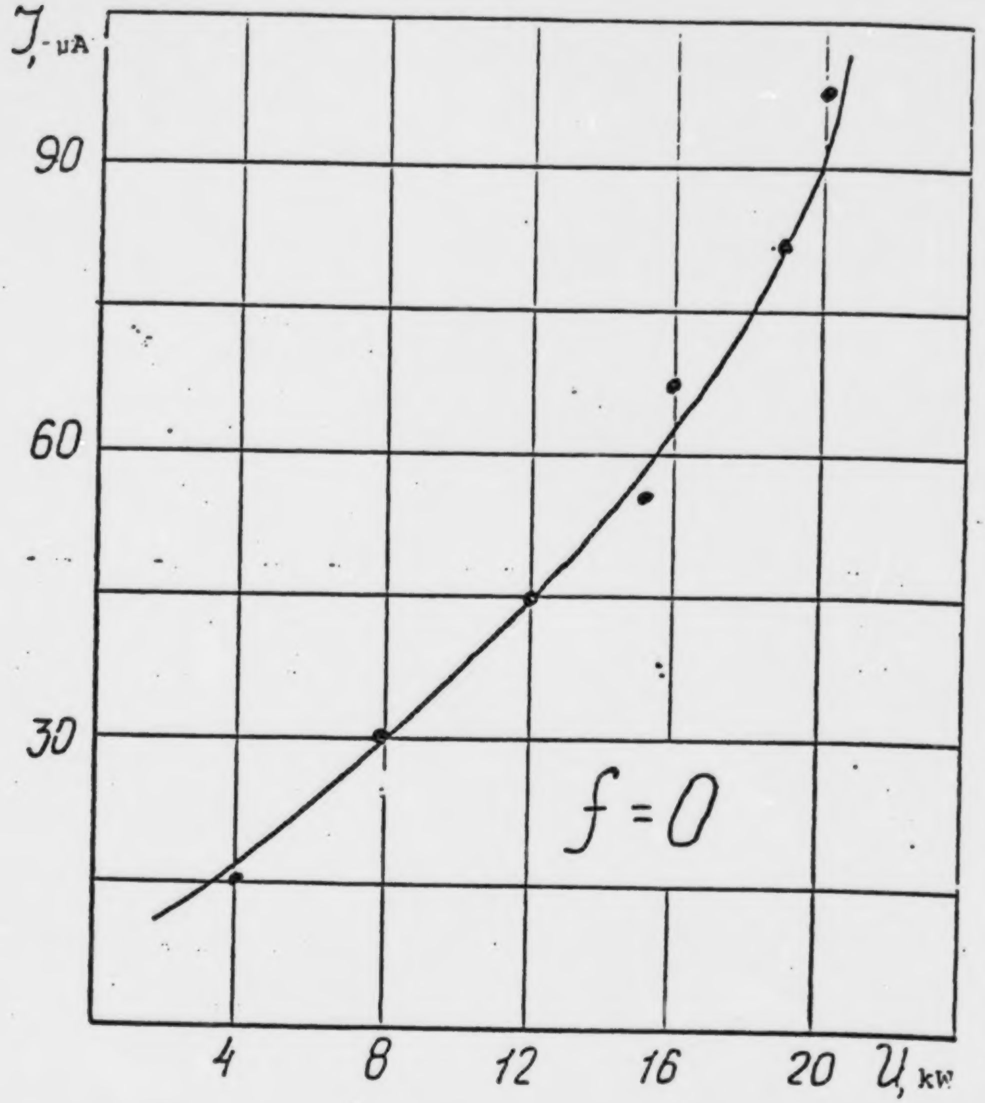

fig.4. Corona voltampere characteristics in the measurement device for aspirated air from a blast-furnace cast-house.

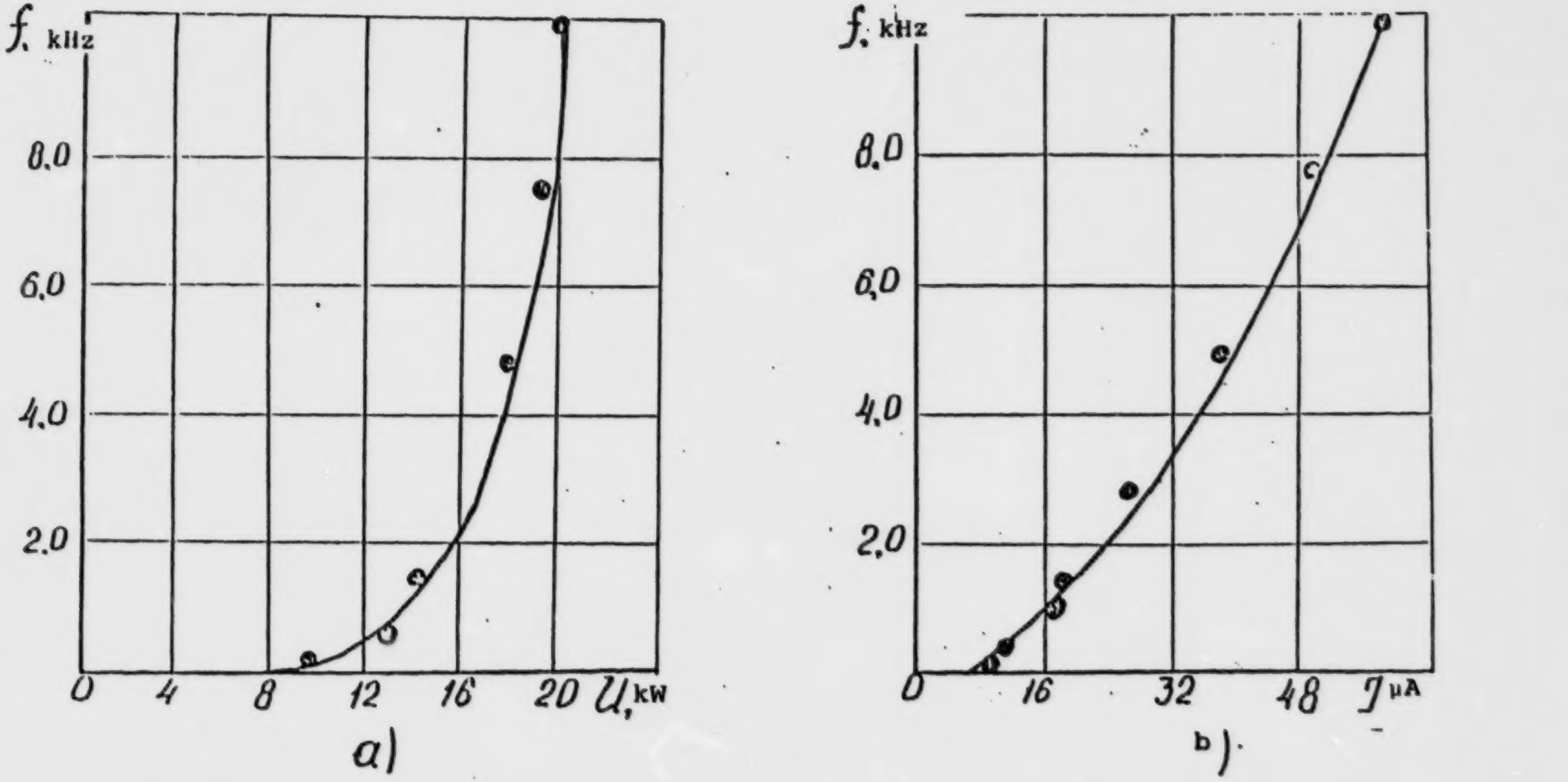

fig.5. The dependence of impulse repetition frequency of back corona on:

a. discharge voltage; b. discharge current.

Gas-dust flow feom electric-arc synthetic corundum smelting furnaces.

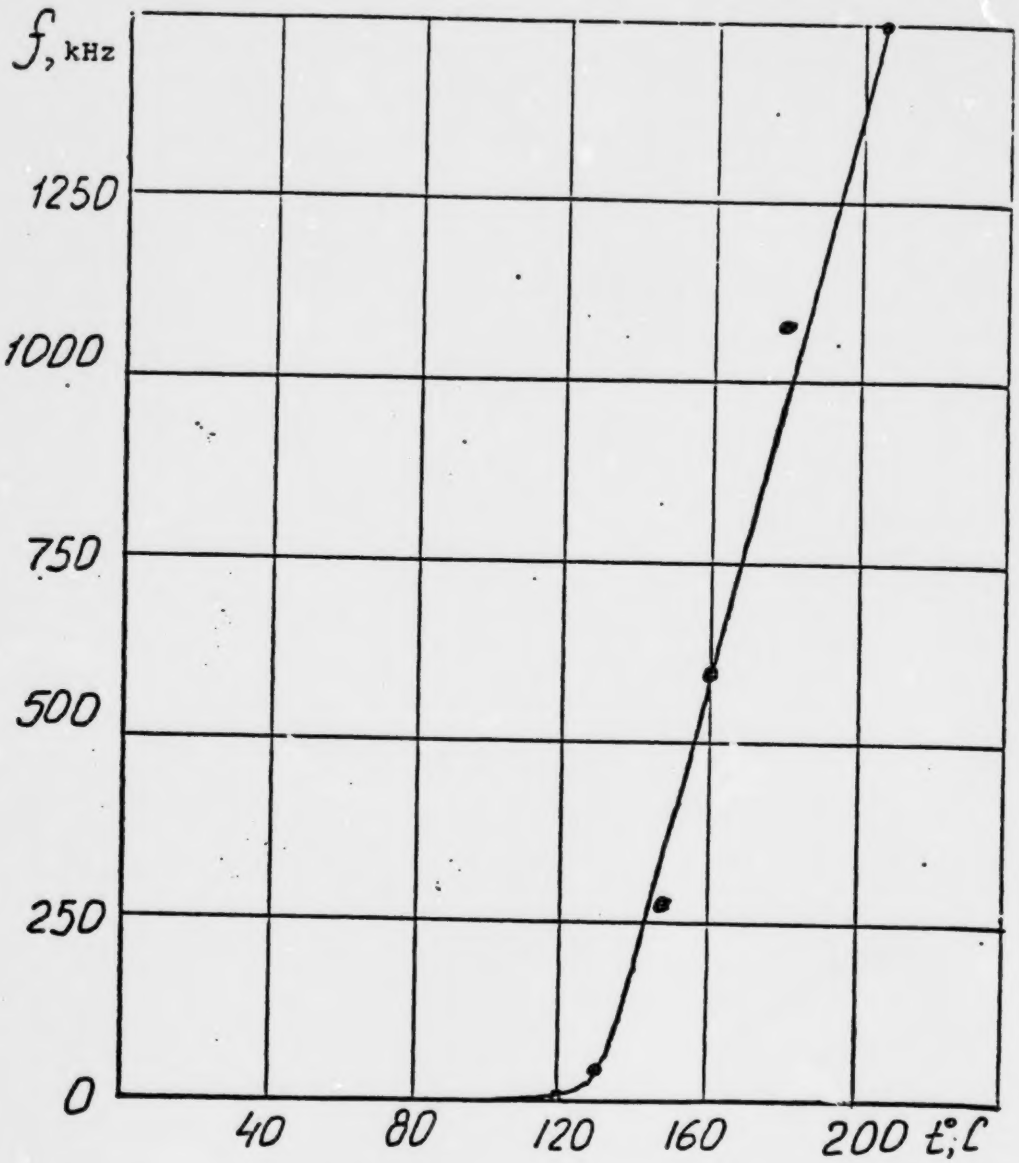

fig.6. Effect of temperature of a gas-dust stream from silicon smelting furnaces on the frequency of back corona impulse repetition.

back corona repetition frequency comprised 1500kHz. At temperatures less than 124°C, discharges from the high-resistance layer are not observed (fig.6).

Thus, the developed methods and equipment permit predicting the electrical and technological parameters under which back corona may occur in the electrostatic precipitator.

BIBLIOGRAPHY

1. Reshidov, I.K., "Back Corona Occurences in Electrostatic Precipitators", collection of reports of an inter-regional seminar on gas-cleaning, Yaroslavl, 1972.

2. Levitov, V.I., Reshidov, I.K., "On the Use of an Automated Method of Probe Characteristics in Several Electrostatic Gas-Cleaning Problems", in the collection Strong Electrical Fields in Technological Processes, Moscow, "Energy", pp.145-158, 1969.

3. Rachek, A.Y.,"A Sensor for Detection of Back Corona in Electrostatic Precipitators", in "Industrial and Sanitary Gas-Cleaning", no.4, p. 54, 1976.

4. Rachek, A.Y., Reshidov, I.K.,"Compensations of Current Shift During Impulse Electrical Discharge" in "Electronic Materials Treatment", no.2, p.36-39, 1977.

A TECHNIQUE FOR PREDICTING FLY ASH RESISTIVITY

Roy E. Bickelhaupt
Southern Research Institute
2000 Ninth Avenue South
Birmingham, Alabama 35205

Leslie E. Sparks
Industrial Environmental Research Laboratory
Environmental Protection Agency
Research Triangle Park, N.C. 27711

(This document has been reviewed and approved for publication by the U.S. EPA.)

INTRODUCTION

A research objective that has been pursued for several years is to predict fly ash resistivity as a function of temperature based on coal ash chemical analysis and a flue gas composition stoichiometrically calculated from the as-received, ultimate coal analysis. This goal has been difficult to attain because one must be reasonably certain that the laboratory resistivity data utilized in developing a predictive technique agrees with the resistivity values that the precipitator will experience. This is a difficult problem that is magnified when the sulfur oxides are introduced into the experimental environment.

EXPERIMENTAL SCOPE AND APPROACH

A large number of commercially produced fly ashes was chemically and physically characterized for this work. By having a large data base, many ranks of coal were represented, and one can assume that the effect of factors such as specific surface and ash layer porosity were minimized.

Resistivity as a function of temperature for a given set of electrical and environmental conditions was determined using all the available fly ashes. From these data, one can relate fly ash resistivity to fly ash chemical composition for one set of experimental conditions and selected temperatures. From the original group, 16 ashes were selected to investigate the effect of the variation in environmental water concentration and applied voltage gradient on resistivity. Six of these ashes were further utilized in experiments to determine the effect of sulfur trioxide on resistivity. From these experiments, expressions were developed for predicting resistivity for a given temperature, water concentration, sulfur trioxide concentration and applied electrical stress.

EXPERIMENTAL PROCEDURES

The equipment and experimental technique have been previously illustrated and discussed[1] in detail and will be only briefly mentioned here. When the effect of sulfur trioxide was not under consideration, ASME, PTC-28 test cells[2] were used in a stainless steel environmental chamber. Resistivity was determined under an applied voltage gradient of 2 kV/cm from 460°C to 85°C in an environment of nitrogen, 5% oxygen, 13% carbon dioxide, 500 ppm sulfur dioxide and 9% water by volume. In other similar experiments the water concentrations were 5% and 14%. When the effect of applied voltage gradient was of interest, the test temperature was maintained at 162°C.

A special test cell and environmental chamber were developed with which the effect of sulfur trioxide on resistivity was evaluated. The tests were conducted isothermally at several temperatures using sulfur trioxide concentrations of 2, 5 and 10 ppm in an environment of air and water vapor. A radial-flow, concentric-electrode test cell allowed the determination of resistivity for an ash layer one mm thick. This thin layer of ash can be equilibrated with the environment containing sulfuric acid vapor in a reasonable length of time.

EXPERIMENTAL RESULTS

Effect of Ash Composition

Figure 1 shows the relationship between the measured resistivity and the combined atomic concentrations of lithium and sodium for 33 fly ashes. These data were taken from resistivity versus reciprocal absolute temperature plots for the individual ashes at 1000/T(°K) = 2.4 (144°C, 291°F). Prevailing test conditions included the previously described simulated flue gas containing 9% water, applied electrical stress of 2 kV/cm, and no sulfur trioxide added.

The expressions defining the curve produced by linear regression analysis are shown. One can either calculate the resistivity for the specific set of experimental conditions prevailing using these equations or read the resistivity value from the figure. A coefficient of correlation of -0.97 was determined. This coefficient defines the degree of fit between the data and the linear regression curve, and a value of 1.00 would define perfect correlation between the two factors. Since it has been shown[3] that lithium and sodium are principal charge carriers when experimental environments excluding sulfuric acid vapor are used, the relationship shown in Figure 1 was expected.

Effect of Water Concentration

Figure 2 illustrates the effect of changes in water concentration for one of the ashes evaluated. The water concentrations used were selected based on the data sheets completed by the ash-supplying power stations which showed a range of 6 to 13 volume percent. These curves were generated using the previously defined baseline test conditions with of course the exception of water concentration and are similar to those found by other investigators.[4] The attenuation of resistivity due to increased water concentration is observable at about 230°C and becomes very significant at the lower temperatures.

One way of displaying these data in a form suitable for use in the prediction of resistivity is shown in Figure 3. In this interpretation, the resistivity data of the previous figure have been plotted as a function of water concentration for several isotherms. Expressions developed from data such as these can be used to correct the resistivity value predicted for a given set of baseline conditions to a value for some other set of conditions. For example, the average slope of the resistivity-water concentration curve at a temperature of 144°C was -0.085. This is based on the data accumulated from the selected 16 ashes used to evaluate the effect of water concentration. A simple algebraic expression can be used to convert the resistivity value for 9% water shown in Figure 1 to the value for some other water concentration.

$$\log \rho_{c,w} = \log \rho_c + (W_w - W_c)S_w \qquad (1)$$

$\log\rho_{c,w}$: logarithm of resistivity for a specific lithium plus sodium concentration, c, and water concentration, W_w.

$\log\rho_c$: logarithm of resistivity for a specific lithium plus sodium concentration, c, and a water concentration of 9 volume percent. Value obtained from Figure 1.

W_w: volume percent water concentration to which the resistivity is to be corrected.

W_c: water concentration used in establishing Figure 1, nine volume percent.

S_w: $\Delta \log \rho/\Delta\% \; H_2O$; -0.085 for 144°C and water concentrations between 5% and 15%.

Effect of Applied Electrical Stress

Increasing the electrical stress on an ash layer causes a decrease in the measured resistivity. A variation in the magnitude of the effect of applied voltage gradient on resistivity has been observed during *in situ* testing as well as in laboratory tests by other investigators.[5] ASME PTC-28 suggests determining resistivity just prior to dielectric breakdown. A research program involving dozens of ashes and a multiplicity of test conditions cannot afford to do this. Therefore tests are conducted on a few ashes to establish a relationship between resistivity and applied voltage gradient. Data for other conditions and ashes are then calculated from this relationship using an expression such as:

$$\log \rho_{c,w,e} = \log \rho_{c,w} + (E_e - E_c)S_e \qquad (2)$$

$\log\rho_{c,w,e}$: logarithm of resistivity for a specific lithium plus sodium concentration, c, a water concentration W_w, and an applied voltage gradient E_e.

$\log\rho_{c,w}$: previously defined.

E_e: applied voltage gradient to which $\log \rho_{c,w}$ is to be corrected.

E_c: applied voltage gradient used in establishing Figure 1, 2 kV/cm.

S_e: $\Delta \log \rho/\Delta E$; -0.030 for 144°C and an applied voltage gradient range of 2 to 10 kV/cm.

Effect of Sulfur Trioxide

The effect of sulfur trioxide on resistivity in an environment of water and air was examined using a limited number of ashes and tests. The procedures and results for individual tests are detailed in reference 1. Figure 4 shows the results for six tests conducted on one ash to demonstrate the combined effect of sulfur trioxide concentration and temperature on resistivity.

All data thus far obtained at ∿ 147°C using 2 kV/cm voltage gradient and a baseline environment of air containing 9 volume percent water are shown in Figure 5. Six ashes were used in conjunction with sulfur trioxide concentrations of nominally 2, 5 and 10 ppm. At this time, it is believed that the data base is too small to make other than guarded statements regarding the quantitative effect of sulfur trioxide on resistivity. It is obvious that the effect can be dramatic in that the presence of 10 ppm of sulfuric acid can reduce the resistivity two or more orders of magnitude.

The initial evidence suggests that the presence of sulfuric acid in the environment provides an alternate conduction mechanism. Therefore, other than the fact that specific ashes have different affinities for sulfuric acid vapor, there would seem to be no relationship between the acid and the ash composition with respect to conduction. Presently it is suggested that the effect of sulfuric acid can be combined with the other factors that influence resistivity by considering them as two conduction mechanisms and determining a resultant resistivity from the equation for parallel resistances.

$$\rho_r = \frac{\rho_s \times \rho_{c,w,e}}{\rho_s + \rho_{c,w,e}} \tag{3}$$

ρ_r: resultant resistivity combining the effects of composition, water concentration, applied voltage gradient, and sulfuric acid concentration.

ρ_s: resistivity resulting from the effect of environmental sulfuric acid concentration taken from Figure 5.

$\rho_{c,w,e}$: previously defined, equation (2).

ILLUSTRATION OF RESISTIVITY PREDICTION

The information required to predict resistivity in the described manner is the as-received, ultimate coal analysis and the chemical composition of the coal ash. A stoichiometric calculation of the combustion products is made using 30% excess air to determine the concentration of sulfur trioxide and water. The sulfur trioxide value is taken as 0.3% of the calculated sulfur dioxide value. The coal ash is prepared by first igniting the coal at 750°C in air, passing the ash through a 100-mesh screen, and then igniting the ash a second time at 1050°C ± 10°C in air for a period of 16 hours. Good agreement in chemical analysis has been obtained between coal ashes produced in this manner and their respective fly ashes. The usual chemical analysis of the coal ash in weight percent expressed as oxides is performed. The analysis is converted from weight percent as oxides to molecular percent as oxides. The atomic percentage of the lithium and sodium is taken as 66.6% of the molecular percentage of the oxides.

The sum of the atomic percentages of lithium and sodium is used to determine the resistivity value, ρ_c, graphically from Figure 1 or by computation. Using the concentration of water determined from the combustion products calculation and equation (1), the predicted resistivity in terms of ash composition and water concentration, $\rho_{c,w}$, is determined. For the 5 mm ash layer thickness used, it was found that dielectric breakdown generally occurred at applied voltage gradients of 8 to 12 kV/cm. Therefore, it was arbitrarily decided to use 10 kV/cm as the electrical stress at which the resistivity is predicted. Using equation (2) and E_e = 10 kV/cm, the predicted resistivity is put in terms of ash composition, water concentration and dielectric breakdown stress, $\rho_{c,w,e}$. This value then is the predicted resistivity exclusive of the effect of sulfuric acid.

Eastern ashes are generally defined as those containing low concentrations of alkaline earth elements ($<\sim 5$ w/o expressed as oxides) and moderate to high iron concentration (5 to 30 w/o). Western ashes normally contain low amounts of iron and moderate to high concentrations of alkaline earths. If one defines the coal ash as an "Eastern" and the calculated sulfur trioxide concentration is 6 ppm, a ρ_s value of about 8×10^{10} ohm·cm would be selected from Figure 5. This value would then be combined with the $\rho_{c,w,e}$ value using equation (3) to calculate the resultant predicted resistivity.

REFERENCES

1. Bickelhaupt, R.E., "Measurement of Fly Ash Resistivity Using Simulated Flue Gas Environments", Environmental Protection Agency, Research Triangle Park, N.C. Report EPA 600/7-78-035, March 1978, 29 pages.
2. ASME PTC-28, "Determining the Properties of Fine Particulate Matter, Section 4.05, Method for Determination of Bulk Electrical Resistivity, pp 15-17, 1965.
3. a) Bickelhaupt, R.E., "Surface Resistivity and the Chemical Composition of Fly Ash", APCA Journal 25 (2) 148-152, 1975.

   b) Selle, S.J., et al, "A Study of Electrical Resistivity of Fly Ash from Low-Sulfur Western Coals Using Various Methods", Paper 72-107 presented at the 65th Annual Meeting of the APCA, Miami Beach, Fla. 1972.
4. Maartmann, Sten, "The Effect of Gas Temperature and Dew Point on Dust Resistivity - and Thus the Collecting Efficiency of Electrostatic Precipitators", Second International Clean Air Congress of the International Union of Air Pollution Prevention Association, December 6-11, 1970, Washington, D.C.
5. Baker, J.W. and K.M. Sullivan, "Reproducibility of Ash Resistivity Determinations", presented at the Joint Power Generation Conference, Long Beach, California, September 18-21, 1977.

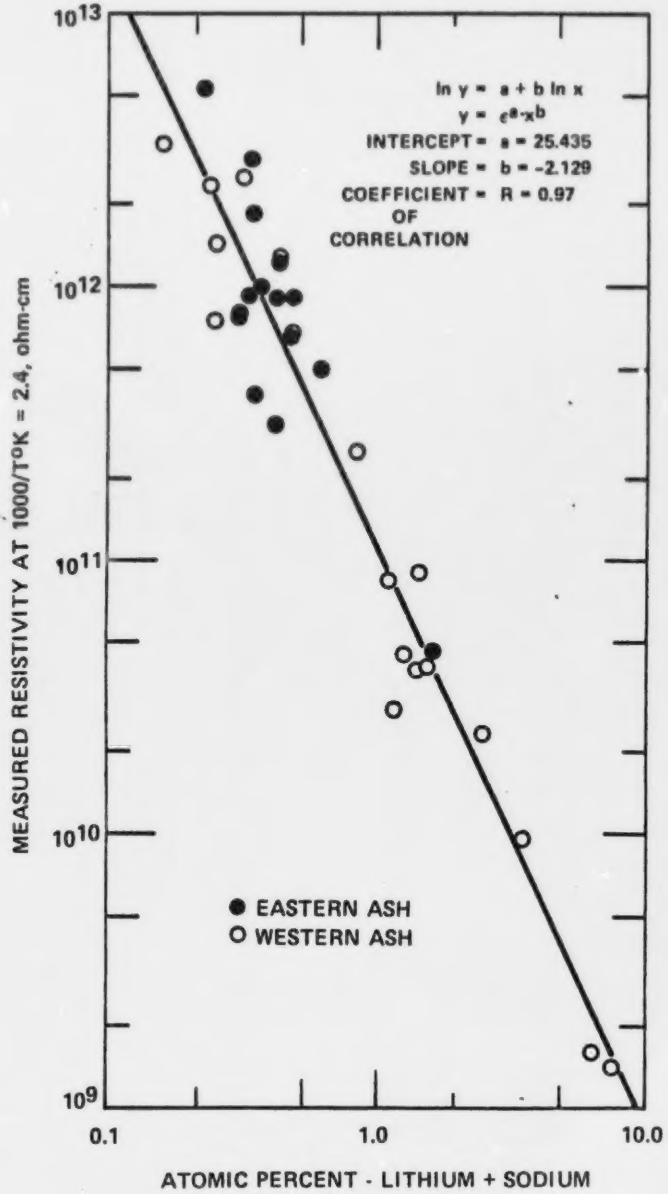

Figure 1. Resistivity as a function of combined lithium and sodium concentrations for a specific set of test conditions.

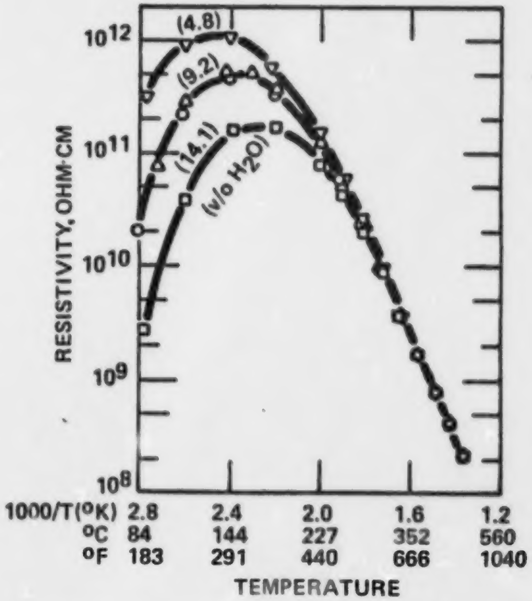

Figure 2. Typical resistivity-temperature data showing the influence of environmental water concentration.

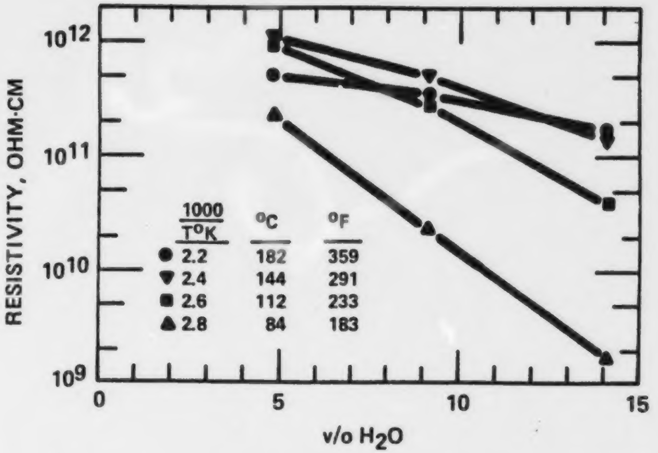

Figure 3. Resistivity as a function of environmental water concentration for various test temperatures.

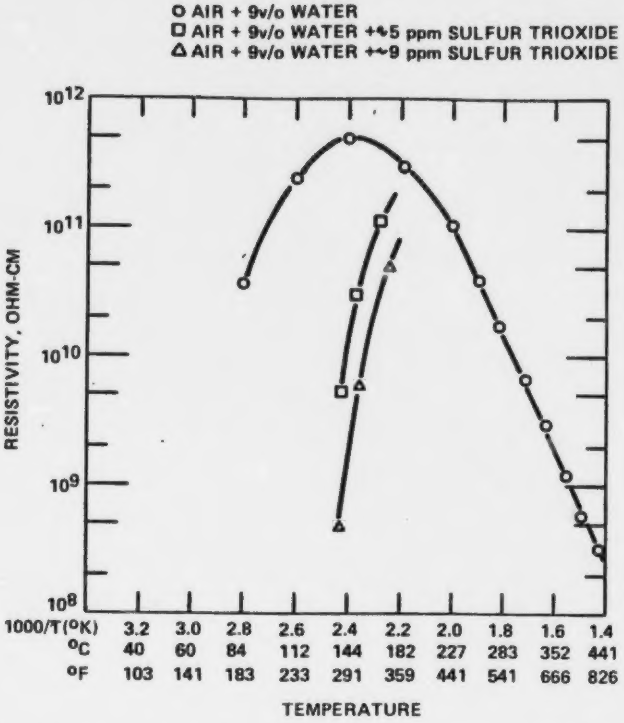

Figure 4. Typical resistivity versus reciprocal absolute temperature data showing the effect of injected sulfur trioxide.

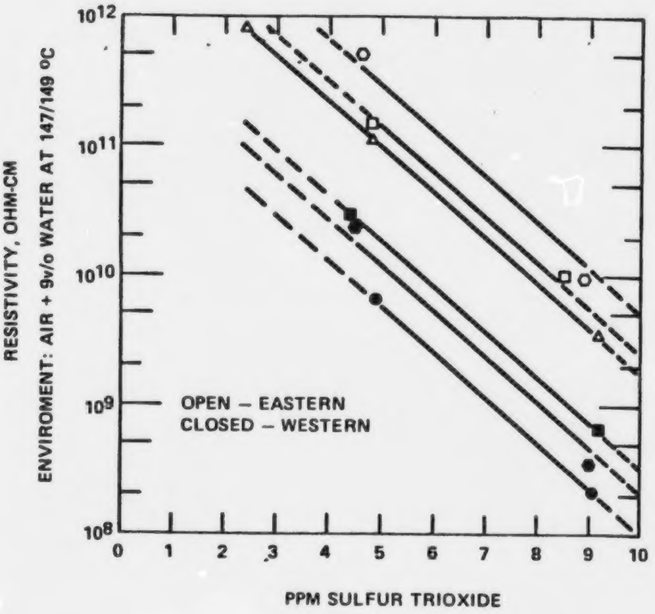

Figure 5. Resistivity as a function of environmental sulfur trioxide concentration for six fly ashes.

I.V. ERMILOV, T.I. DMITRIEVA, Y.M. MOROZOV

AN ADVANCED MATHEMATICAL MODEL FOR ELECTROSTATIC PRECIPITATOR CALCULATING

At the present time, a mathematical model has been developed in the USSR for calculating the efficiency of dry, plate-type electrostatic precipitators trapping non-high-resistance dusts under known initial data about the electrical conditions, gas-dust stream parameters, and the equipment's geometrical characteristics (1,2,3). The model was developed on the basis of research on basic dust precipitation processes in the ESP: kinetic charge and particle drift velocity (4,5), distribution of dust concentration profiles (6), and dust entrainment during electrode rapping (7). Latest achievements in the area of calculating fields with a volume charge (8), were used in the model. The correctness of this usage is asserted by field intensity measurements taken by the probe characteristic method (9). Calculated values for efficiency satisfactorily agree with experimental figures taken in industrial equipment (3).

However, calculating efficiencies according to this model is is somewhat time-consuming and in large-scale computations, use of a computer is required. This makes analysis of several factors of dust-trapping and selection of the optimal variant of the gas-cleaning set-up difficult. In connection with this, it is necessary to create a simplified, engineering method of calculation that has acceptable accuracy and exactitude in its computations. Moreover, in developement, computation of re-entrainment is needed, which was considered in preceding works as being dependent only on rapping conditions of the electrodes (1,2). Developement of methodologies for dicting the level of working voltages and corona ignition voltages in industrial precipitators is also necessary. This data is used in the model during calculation of field intensity in the unit and influence the accuracy of determining particle drift speed.

Solving these problems permits creating a finished mathematical model for calculating precipitators, where only the equipment's geometrical characteristics and the gas-dust stream's parameters are used as starting data. Prognosing the gas-dust stream's parameters in relation to production technology is a problem of more removed perspective.

Therefore, the problem of developement of of an improved mathematecal model of calculating precipitators occurs, in which the problems listed above are reflected. Such a model for calculating precipitators of thermal electric power stations is introduced in this work. One may hope that the approach used will turn out to be acceptable even for calculating precipitators of other industries.

In no.10 of the bibliography, a simplified methodology for calculating precipitator efficiency has been introduced, that was developed with use of the moment method.. However, calculations according to this methodology do not always satisfactorily agree with experimental data. This is connected with the fact that in the simplified methodology, active factors are considered less than they are in the methodology from no.1 (see bibl.).

It is therefore advisable to develop a simplified calculation methodology on the basis of the methodology from no.1 (see bibl.). For this it is necessary to to analize the significance of numerous factors entering into the calculation, in order to choose the main ones.

Calculation of the factors' significances were conducted to fit to the two most widely used types of precipitators: 1) those with coronal electrode frame design (UG); and 2) those with free-hanging coronal electrodes (UGT). In UG-type units, the relative area of the unit's active zone, S_a^* (equal to the ratio of coronal electrode height to the height of the precipitating electrodes) is 0.91 and in UGT-type units,

Table 1 introduces results of significance calculations considered in the exact methodology of factors: non-uniformity of dust concentration profiles, particle charges at the coronal electrodes, particle passage through "semi-active" precipitator zones, non-linearity of resistance of the particle movement medium, kinetics of charge and particle entrainment during electrode rapping. The calculations were carried out to fit the electrostatic precipitators at the Ladyzhin State Regional Electric Power Station and the Slantsevskit cement plant.

Table 1

Factors	S_a^*	$\frac{1-\eta}{1-\eta_1}$
non-uniformity of concentration profiles	0.9I I.0	I.02-I.06 I.25
Particle charge at the coronal electrodes	0.9I I.0	I.04-I.07 I.6
Particle charge kinetics	0.9I I.0	0.995 0.87
Non-linearity of resistance of the medium	0.9I I.0	0.98-0.99 0.97
Particle passage through "semi-active" zones	0.9I I.0	0.2 I.0
Dust entrainment during rapping	0.9I I.0	0.I-0.2 0.0I-0.05

The values, $\frac{1-\eta}{1-\eta_1}$, introduced in table 1, represent the ratio of the values for dust re-entrainment, calculated with and without taking into consideration one of the factors. As seen from the table, the most significant factors are the particle passage through "semi-active" zones and entrainment during electrode rapping. It is necessary to consider particle charge at the coronal electrodes and concentration non-uniformity profiles only for electrodes with $S_a^* \lesssim 1.0$. This is connected with the fact that during $S_a^* \gtrsim 0.91$, dust entrainment through the precipitator is basically determined by the "semi-active zone, in which the influence of charge at the coronal electrodes and of the non-uniformity of profile concentration is relatively low. The remaining factors may be disregarded during development of the simplified method.

During these simplifications, exact formulas from 1 (in bibliography) may be taken thus:

$$\eta_\varphi = 1 - S_a^* \exp\left(-\frac{w_0 L^*}{u k_u}\right) - \left(1 - S_a^*\right) \exp\left(-\frac{w_0 L^* k_2}{u k_u}\right), \quad \text{(I)}$$

where w_0 - particle drift speed at the precipitating electrode

$L^* = \frac{L}{h_0}$ - overall relative length of precipitator fields

$2h_0$ - spacing between precipitating electrodes

u - average gas velocity

k_u - coefficient of non-uniformity of the field's gas velocities ($k_u = M_\kappa$ K.3 [II])

k_2 - coefficient, considering field weakening in the "semi-active" zone ($k_2 \simeq 0{,}5$)

Drift velocity of particles of diameter d are calculated according to the formula:

$$w_t = \frac{\varepsilon_0 E_0 \varkappa}{\mu}\left(d E_0 + 5{,}47\cdot 10^{-6} T + \frac{4{,}15\cdot 10^{-7} E_0 T}{p}\right), \tag{2}$$

where ε_0 - the dielectric constant

E_0 - field intensity at the precipitator electrode

p - gas pressure in mm hG

μ - dynamic viscosity of the gas

E_0 and χ - Cunningham correction, computed according to the formulas:

$$\varkappa = 1 + 1{,}72\,\frac{l_M}{d}, \quad l_M = 2{,}41\cdot 10^{-7}\,\frac{T}{p}, \tag{3}$$

$$E_0 = \frac{U\pi}{h_0 d_0^*}\sqrt{C_0\left(1 - \frac{1}{U^*}\right)\left(\frac{2\pi}{d_0^*} - 0{,}693\right)}, \quad \text{В/м} \tag{4}$$

$$U^* = \frac{U}{U_0}, \quad d_0^* = \frac{d_0}{h_0},$$

$$C_0 = \left(0{,}515 - 0{,}56\,\frac{1}{d_0^*}\right)\left(1 + 3{,}5\sqrt{\frac{r_0^*}{d_0^*}}\right), \quad 0{,}5 < \frac{1}{d_0^*} < 0{,}8, \tag{5}$$

$$C_0 = \left(\frac{1{,}7\cdot 10^{-2}}{\frac{1}{d_0^*} - 0{,}585} - 7\cdot 10^{-3}\right)\left(1 + 1{,}75\sqrt{\frac{r_0^*}{d_0^*}}\right), \quad 0{,}8 < \frac{1}{d_0^*} < 2{,}3, \tag{6}$$

$$r_0^* = \frac{r_c}{h_c} \quad [8],$$

where d_0 - distance between coronal elements

U - precipitator's working voltage

U_0 - corona ignition voltage

r_0 - effective radius of coronal electrode

Calculation of the overall degree of gas-cleaning during the absence entrainment of precipitated dust is done according to the expression;

$$\eta = 1 - \int_0^{\infty} (1 - \eta_{\varphi}) \, \varphi(d) \, \partial(d) \qquad (7)$$

For density of particle distribution by size φ(d), the log-normal law was taken:

$$\varphi(d) = \frac{0{,}1733}{d \lg \sigma} \exp\left(\frac{\lg^2 \frac{d}{d_{50}}}{2 \lg^2 \sigma} \right), \qquad (8)$$

where σ - average standard deviation

d_{50} - average median diameter

Trapping efficiency with regard to entrainment during electrode rapping is found according to the expression:

$$\eta_0 = 1 - \exp\left[K \ln (1 - \eta) \right], \qquad (9)$$

where K - generalized coefficient of re-entrainment.

The expression (1) may take the form:

$$\eta_o = S_a^* \exp(-\beta d^* - \beta k) - (1 - S_a^*) \exp(-\beta d^* k_\delta - \beta k k_\delta), \qquad (\text{I0})$$

where $$\beta = \frac{\varepsilon_o E_o^2 d_{50} L^*}{u k_u \mu}, \qquad (\text{II})$$

$$k = \frac{T}{d_{50}} \left(\frac{4{,}15 \cdot 10^{-7}}{P} + \frac{5{,}47 \cdot 10^{-4}}{E_o} \right), \quad d^* = \frac{d}{d_{50}} \qquad (\text{I2})$$

The parameter β is analagous according to its structure by the index of the exponent to Deutsch's formula and it may be called the parameter of precipitation of poli-dispersed dust.

The parameter k considers the effect on dust precipitation of diffusion particle charging and Cunningham's correction. This is equal to the ratio of the components of drift speed, conditioned by these factors, to the basic components of drift speed, caused by impact charging of particles when $d = d_{50}$.

In relation to the formulas (7-10) introduced above, the degree of gas-cleaning depends only on three dimensionless parameters - β, k and δ .

Result analysis on a computer of the numerical calculation of the degree of gas-cleaning according to formulas 7-10 has shown that the degree of gas-cleaning may be approximated by the following formula:

$$\eta = 1 - \exp(-K A_\beta^{0,43}) \qquad (13)$$

The value of the parameter A, dependent on σ and k, is determined from the graphs in fig. 1 and 2. The relationship β 0.42 in introduced in the same graph for convenience in calculation.

In calculating the degree of gas cleaning, it is possible to use the following approximation formulas for parameter A:

$$A = \frac{I.59 + 2.38k - I.44k^2}{(\sigma - I)^{0.33} \exp(-9.28k) + 0.I} \quad \text{for } S_a^* = 0.9I \quad 0 < k \leq 0.5 \qquad (I4)$$

$$A = \frac{2.5 + 4.96k - I.II k^2}{(\sigma - I)^{0.49I} \exp(-I3.8k) + 0.I} \quad \text{for } S_a^* = I \quad 0 < k \leq 0.05 \qquad (I5)$$

$$A = \frac{2.5 + 4.96k - I.II k^2}{(\sigma - I)^{0.22I} \exp(-I.9Ik) + 0.I} \quad \text{for } S_a^* = I \quad k > 0.05 \qquad (I6)$$

The generalized re-entrainment coefficient K is calculated according to the formulas:

$$K = I - 0.275 K_1 K_2 K_3, \text{ when } 5 \cdot I0^6 \leq \rho \leq 5 \cdot I0^9 \text{ Ohm-meters} \qquad (I7)$$

$$K = I - 0.342 K_1 K_2 K_3, \text{ wnen } 5 \cdot I0^9 < \rho \leq 5 \cdot I0^{I2} \text{ Ohm-meters} \qquad (I8)$$

where $K_1 = f(H^*)$, $K_2 = f(u^*)$, $K_3 = f(m^*)$,

$H^* = \frac{H}{Ho}$ - relative height of precipitating electrodes

$u^* = \frac{u}{u_o}$ - relative gas velocity

$\frac{{}^{o}\omega}{\omega} = {}_{*}\omega$ - relative dust mass on electrodes.

The basic parameters are equal to the following measures: Ho = 8 m., Uo = 1 m/sec., Mo = 1 kg/m.

The values of the coefficients K_1, K_2, K_3 are introduced in table 2. Formulas 17 and 18 were obtained by means of generalization by method of regression analysis of experimental data according to re-entrainment coefficients, taken from industrial equipment in the USSR.

Table 2

Range of parameter measurement H^*, u^*, m^*	$K_1 = f(H^*)$	$K_2 = f(u^*)$	$K_3 = f(m^*)$
0 - 0.I	0 - 0.3	0 - 0.4	I - 0.8
0,I÷0,5	0,3-0.7	0.4-0.8	0.8-0.4
0,5÷I,0	0,7-I.0	0.8-I.0	0.4-0.2
I,0÷I,5	I,0-I.2	I.0-I.I5	0.2-0.I
I,5÷2,0	I,2-I.4	I.I5-I,3	0.I-0.04

Comparison of the calculations according to the simplified (11-13) and exact methodologies has shown that the maximum error of calculations at $S\overset{*}{a} = 0.91$

does not exceed ± by effective drift velocity and about 50% by re-entrainment. At $S\overset{\star}{a} = 1.0$, the maximum errors may be higher and may measure in separate instances ± 15% from the effective drift velocity.

Table 3 introduces comparison results of calculation and experimental values for cleanly efficiency in industrial precipitators in the USSR and USA. The calculation was done by exact and simplified methodologies. The experimental values, necessary for calculation, and the cleaning efficiency of American precipitators were taken from no. 12 (bibliography), as well as during joint research at the Allen Steam Plant in the USA by a group of Soviet and American specialists (bibl. no. 13).

Comparison of calculated values according to the exact and simplified methodologies and experimental values for efficiency attests to their satisfactory agreement. The average error in calculating entrainment according to the exact methodology does not exceed 10% and according to the simplified methodology, no more than 20% of the experimental particle entrainment in industrial precipitators.

It is worth mentioning that the agreement occurs both in experiments when the electrode rappers are shut off (k=1), and during rapping. This attests to the fact that, in the model, basic physical processes, occuring in industrial precipitators, both during electrode rapping and without electrode rapping, are apparently reflected correctly. The circumstance is especially reassuring that the agreement between the calculated and experimental values occurs in industrial precipitators in the USA, which are essentially different from Soviet precipitators according to their design ($S\overset{\star}{a}=1$) and data according to which the advanced model was not used during the development.

Experimental data were generalized by the regression analysis method, in order to predict the working voltages and coronal ignition voltages of industrial electrostatic precipitators where these voltages are necessary for calculating drift velocity. These data were obtained for 10 industrial electrostatic precipitators of thermal electric power stations using the principal grades of coal utilized in the USSR.

A type of the regression equation was selected on the basis of the experimental relationship obtained during research on laboratory and pilot plant electrostatic precipitators. This is relative in part to the dependence of the working voltage on the distance between electrodes and on dust resistivity, etc. Six influencing factors were originally considered in the regression equation. However, after testing factor significance, it turned out to be possible to ignore the influence of incomplete combustion, sulfur content, and also the relative gas density in the equation determining working voltage, whose final form is:

$$U = 15{,}8 \exp\left(-0{,}093 \frac{F}{F_\delta}\right)\left(\frac{B}{B_\delta}\right)^{0{,}25} \exp\left[-2{,}21\left(\frac{\lg^2 \rho}{\lg^2 \rho_\delta} - 1{,}25 \frac{\lg \rho}{\lg \rho_\delta}\right)\right]\frac{h_0}{h_{0\delta}}, \kappa W \quad (19)$$

where: F - area of the precipitating field of the precipitator, fed by one unit, m^2, $F\delta = 1000 m^2$,

B - gas moisture content, %, $B\delta = 6\%$,

ρ - dust resistivity, Ohmmeters, $\rho\delta = 5 \cdot 10^9$ Ohmmeters,

h_0 - distance between coronal and precipitating electrodes, m;

$h\delta = 0.1375$ m.

These same computations were carried out for determining the voltage of corona discharge ignition. However, in this case, the relative gas density turned out to be a significant factor. The resulting equation for calculating ignition voltage has the following form:

$$U = 23{,}8 \exp\left(-0{,}085 \frac{F}{F_\delta}\right)\left(\frac{B}{B_\delta}\right)^{0{,}276}\left(\frac{\delta}{\delta_\delta}\right)^{0{,}27}\left(\frac{\lg \rho}{\lg \rho_\delta}\right)^{0{,}41}, \kappa W \quad (20)$$

Where: δ - relative gas density, δ_{δ} = 0.724.

The relationship of U_0 to the distance between electrodes was not revealed in connection with the samll range of measurement h_0 in experimental data. For considering this relationship, additional research is necessary.

Table 4 shows experimental and calculated values for corona ignition voltage and the working voltage of Soviet industrial precipitators. The average magnitude of error of calculated values for working voltages comprised 3%. Furthermore, equation 19 was tested at an pilot plant precipitator at the Cherepet State Regional Power Station during changes in temperature of gas being cleaned in the unit, from 50 to 300^{0}C. The margin of error for calculated data in comparison with experimental data was no more than 10%.

The improved mathematical model is usable for calculating precipitators trapping group II ash, $10^2 < \rho < 10^8$ Ohmmeters under moderate gas dust content (the parameter of the dispersion phase is $\frac{\mathcal{D}_{\text{вх.}}}{\mathcal{D}_{\text{зол.}}} \leq 3$, which corresponds to $Z_{\text{вх.}}$ = 30-40 g/nm^3 for thermal power station fly ash).

As seen in table 3, the methodology may be used in several cases for calculating precipitator efficiency for trapping high-resistance group III dusts $\rho < 10^8$ Ohmmeters. In this case, impairment of the trapping efficiency is considered to be the reduction of the coefficient K. Moreover, it is worth keeping in mind that during the presence of a back corona, the level of working voltages sharply drops, which is also considered in the methodology. The accuracy of effectiveness calculations during group III dust trapping in connection with approximate calculation of back corona is essentially lower than for group II dusts, and may reach 15-20% out of the effective drift velocity.

BIBLIOGRAPHY

1. Ermilov, I.V., "Calculating the Degree of Gas Cleaning in Plate-type Electrostatic Precipitators", in "Industrial and Sanitary Gas Cleaning", No. 1, 1977.

2. Ermilov, I.V., "Calculating the Efficiency of Thermal Power Station Electrostatic Precipitators", in "Reports - Symposium on Controlling Particle Emissions Into the Atmosphere and Other Related Problems, 26-28 May, 1976, Kishinev".

3. Ermilov, I.V., Dmitrieva, T.I., "Mathematical Modelling of Electrostatic Precipitators and Its Use For Industrial Units in the USSR", in "Reports of the Second Soviet-American Symposium on Technology of Solid Particle Removal, 26-29 September, 1977", vol. 1, Environmental Protection Agency, Research Triangle Park, USA.

4. Ermilov, I.V., "Calculating the Degree of Gas Cleaning in Electrostatic Precipitators", in "Electricity", no. 3, 1976.

5. Ermilov, I.V., "Experimental Research in Microparticle Charge In the Corona Discharge Field", in "Electricity", no. 2, 1974.

6. Ermilov, I.V., "The Distribution of Dust Concentration In the Precipitator Corona Discharge Field", in "Electricity", no. 7, 1974.

7. Sanaev, Y.I., Ermilov, I.V., "Experimental Research of the Processes of Dust Entrainment From the Precipitating Electrodes in Electrostatic Precipitators" in "Industrial and Sanitary Gas-Cleaning", no. 1, 1976.

8. Vasyaev, V.I., Vereshchagin, I.P., "Toward Calculating Characteristics of Unipolar Corona Discharge In An Electrode System, 'Wire Rows Between Plates'", in Electricity", no. 5, 1972.

9. Vereshchagin, I.P. et al, Bases of Dispersion-Systems Electrical and Gas Dynamics, Moscow, Energy, 1974.

10. Mirzabekyan, G.Z., Udalova, V.I., "Calculating Precipitator Work Efficiency During the Dispersion Phase's High Concentrations", in "Electricity", 1976, no. 6.

11. Idelchik, I.E., The Aerodynamics of Industrial Equipment, Moscow, Energy, 1974.

12. Particulate Collection Efficiency: Measurements on Three Electrostatic Precipitators, Environmental Protection Technology Series, EPA-600/2-75-056, October 1975.

13. MacDonald, J.R., Mathematical Modelling of Electrostatic Precipitators in the USA, Reports From the Second Soviet-American Symposium on the Technology of Solid Particle Removal, 26-29 September, 1977, vol. 1, Environmental Protection Agency, Research Triangle Park, USA.

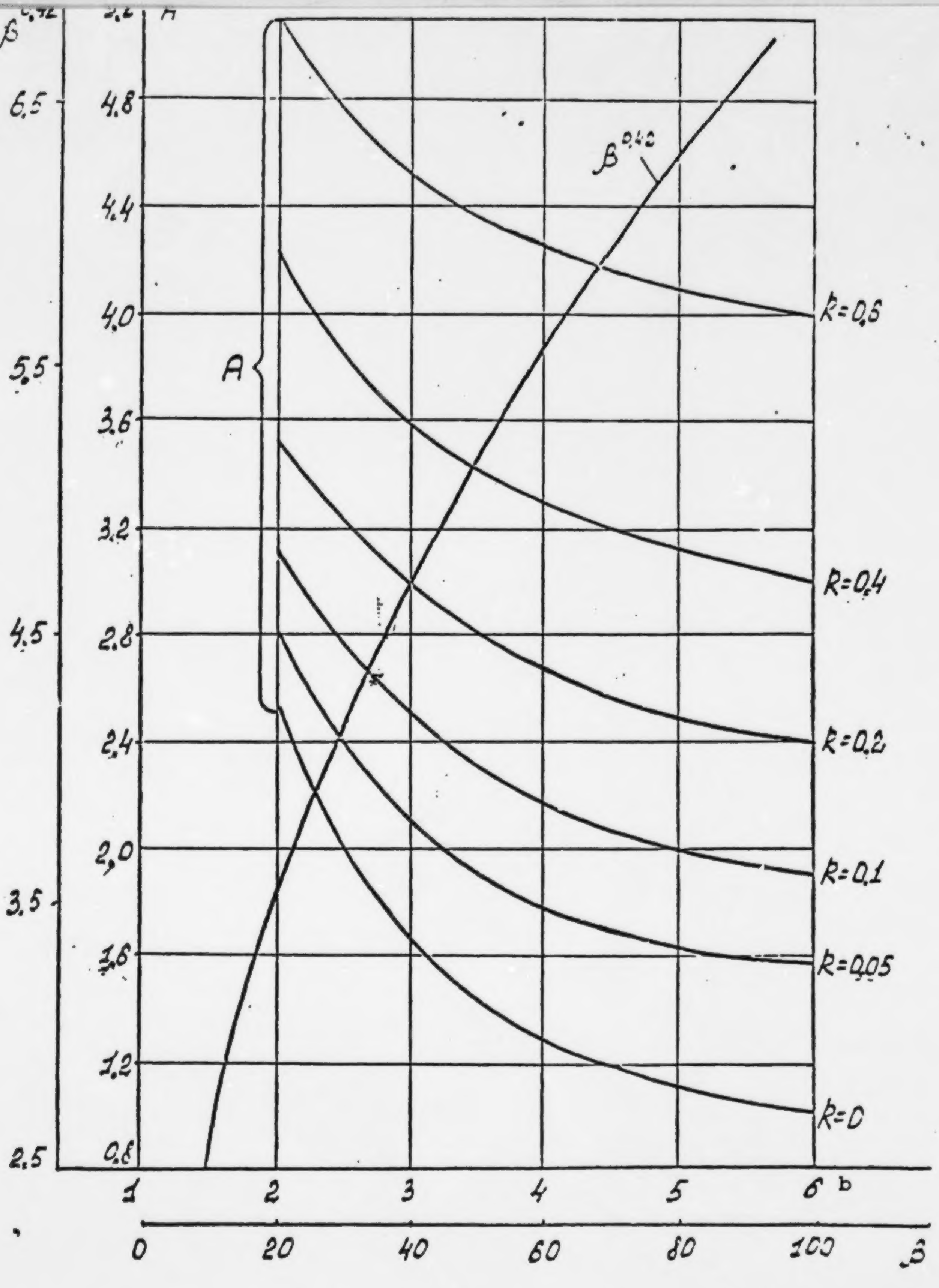

fig.1. Relationship of the coefficient A to b when $\overset{*}{Sa} = 1$, $\eta = 1-\exp(-Ka\,\beta^{0.42})$.

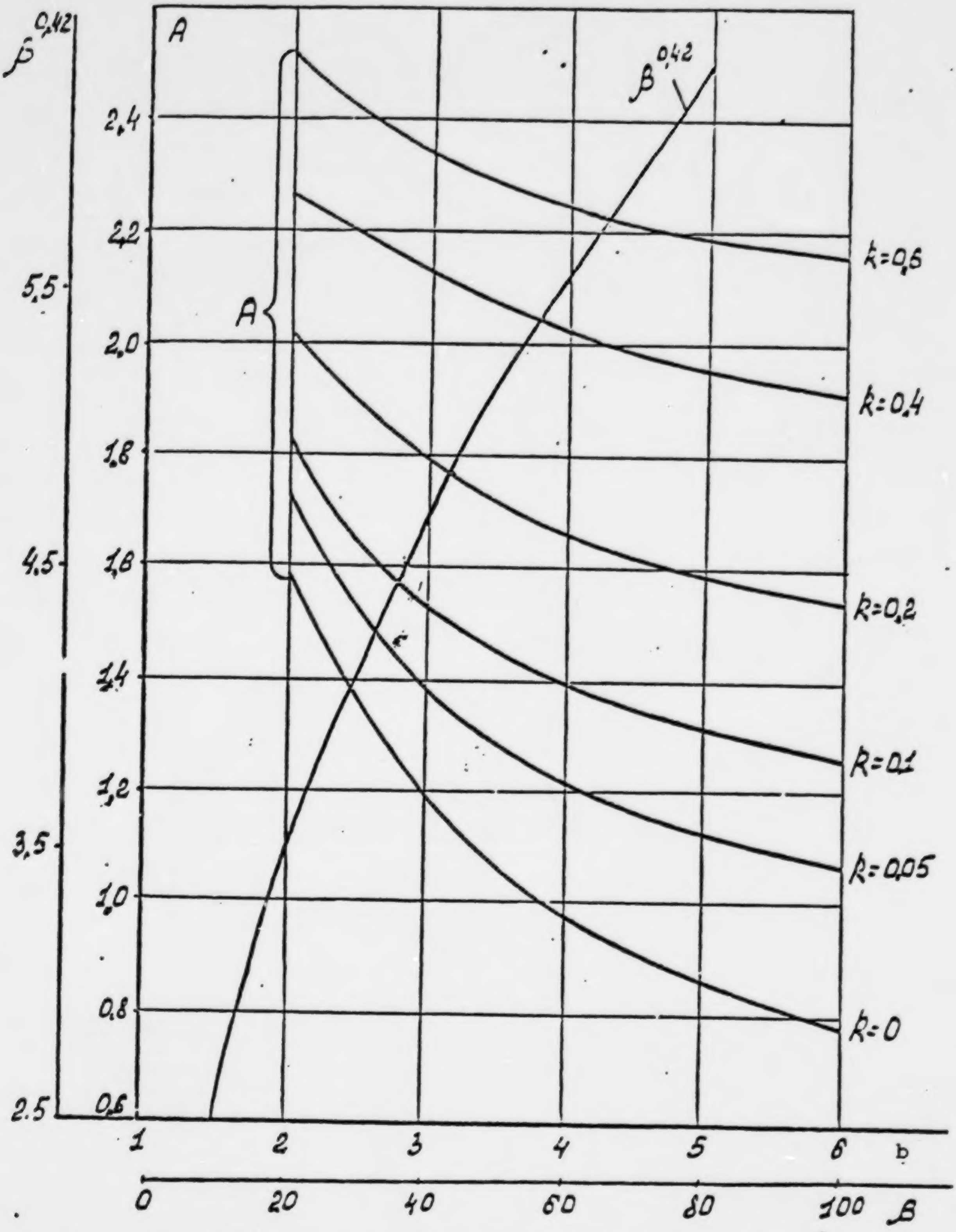

fig.2. The relationship of the coefficient A to b when $\overset{*}{Sa} = 0.91$, $\eta = 1-\exp(-KA\beta^{0.42})$.

Table 3

No.	Type of precipitator	U, kW	U_0, kW	L, m	h_0, m	d_e, m	S_0'	k_u	u, m/sec	T, °K	P, mm. Hg	μ, 10^{-4} kg/m.s.	ρ, Ohm-meters	d_{50}, 10^{-4} m	σ	K	η_0, %	η_r, %	η_e, %
I	EGZ-3-177	35,5	I9,2	I2	0,I375	0,I8	0,9I5	I,I	1.055	386,5	740	0,22I	$2\cdot10^{9}$	0,23	3,I5	0,63	98,5	98,6	98,6
2.	UG2-4-53	42,4	2I,7	I0	0,I375	0,I8	0,89	I,4	2.1	4I5	74I	0,2325	$1,5\cdot10^{8}$	0,I7	3,09	0,73	96,I	96,4	96,I
3.	DGPS-2-55	38,2	20,0	6,6	0,I625	0,I8	0,86	I,55	1.24	422	732	0,223	$7\cdot10^{9}$	0,30	3,3	I,0	96,7	97,6	97,5
4.	Experimental	40,0	22,0	5,0	0,I325	0,I8	0,9	I,05	1.5	403	740	0,2I6	$1,3\cdot10^{8}$	0,I9	3,66	I,0	98,5	98,5	98,2
5.	UG2-4-53	52,0	28,6	I0,0	0,I375	0,I8	0,89	I,4	1.711	4I8	750	0,222	$1,7\cdot10^{9}$	0,I8	3,I6	0,66	97,8	97,6	97,6
6.	PGD-3-50	45,8	22,4	7,56	0,I625	0,I9	0,88	I,4	1.122	427	750	0,238I	$1,76\cdot10^{10}$	0,207	2,88	0,68	95,6	96,0	96,3
7.	UGZ-4-265	36,3	25,0	I6,0	0,I375	0,I8	0,9I5	I,I	1.38	400	748	0,2I4	$1,1\cdot10^{11}$	0,3	3,62	0,57	97,2	97,3	97,2
8.	Experimental	32,9	23,0	I0,0	0,I375	0,I8	0,9I5	I,I	1.87	393,5	746	0,224	$7,7\cdot10^{10}$	0,3	3,62	0,58	93,4	92,2	90,5
9.		32,5	I2,0	I0,97	0,II43	0,I75	I,0	I,I5	1.8	427	745	0,2346	$2\cdot10^{8}$	0,25	5,0	0,64	99,69	99,7	99,66
I0.		23,4	I2,0	I2,2	0,II43	0,I75	I,0	I,I5	1.23	575	750	0,2832	$10^{6}-10^{8}$	0,09	4,2	0,69	99,3	99,38	99,02
II.		29,6	I6,0	I0,97	0,II43	0,229	I,0	I,I5	1.26	602	750	0,2909	$5\cdot10^{-}$	0,296	3,95	0,68	99,66	99,66	99,6I

Notes: 1) Experimental data on domestic precipitators were taken by colleagues at the Semibtatovsk Filial of NIIOGAZ under V.N. Nosin, I.P. Nosov, I.A. Kizim, I.V. Yermilov.

2) Dust resistivity ρ was measured in laboratory conditions at the gas's working temperature.

3) Data from nos. 9-11 was taken from precipitators at thb Gorgas, San Juan, and Allen Thermal Electric Stations in the USA.

Table 4

Type of precipitator	F, m²	δ	B, % gas humidity	ρ Ohmmeters	S^{r}, %	C_{r}^{w}, %	$U_{з}$, kW	U_{p}, kW	$U_{оз}$, kW	U_{op}, kW
EGZ-3-172	3046	0,743	6,9	$2 \cdot 10^{9}$	2,94	1,5	35,8	35,9	19,0	18,8
Experimental	20	0,724	4,5	$1,4 \cdot 10^{9}$	1,74	17,5	44,0	43,5	20,0	21,4
UGZ-4-53	1123	0,701	12,9	$1,8 \cdot 10^{9}$	0,43	1,0	50,0	50,6	28,6	25,9
UGZ-4-53	1123	0,693	4,7	$1,5 \cdot 10^{9}$	1,74	17,3	41,7	39,6	19,1	19,5
PGDS-3-50	1255	0,842	10,0	$7 \cdot 10^{7}$	0,76	2,2	52,3	53,0	23,3	23,4
Experimental	1247	0,706	11,7	$1,45 \cdot 10^{11}$	0,76	1,8	37,6	35,6	25,1	27,0
Experimental	1247	0,697	6,0	$1,62 \cdot 10^{11}$	0,76	1,8	28,3	29,8	22,2	22,4
PGDS-4-42	934	0,685	8,0	$7 \cdot 10^{9}$	2,71	2,2	39,8	42,1	-	22,7
DGPS-2-42	1380	0,622	8,0	$1,3 \cdot 10^{10}$	1,06	1,0	39,8	38,8	-	20,0
PGDS-3-50	1255	0,686	11,75	$2,8 \cdot 10^{10}$	0,18	1,0	42,1	40,8	-	25,9
Experimental	20	0,693	3,0	$8 \cdot 10^{10}$	0,48	5,0	35,0	35,5	22,0	20,3

1) Experimental data on domestic precipitators was taken by colleagues at NIIOGAZ's Semibratovsk Filial under the direction of I.A. Kizim, V.N. Nesin, I.P. Nosov, I.V. Yermilov, Y.M. Morozov.

2) Dust resistivity was measured in laboratory conditions at the gas's working temperature.

3) Electrical characteristics in tables 3 and 4 were recorded under varying parameters of the gas-dust stream.

CALCULATIONS OF EFFECTS OF BACK CORONA IN WIRE-DUCT ELECTROSTATIC PRECIPITATORS

by

Phil A. Lawless
Research Triangle Institute
Research Triangle Park, N.C.   27709

and

Leslie E. Sparks
U.S. Environmental Protection Agency
Research Triangle Park, N.C.   27711

(This document has been reviewed and approved for publication by the U.S. EPA.)

ABSTRACT

A model is used to calculate the effects of back corona on the voltage-current characteristic, current density distribution at the collector plate, and particle collection for five simple mechanisms describing the generation of back corona. Each mechanism is capable of simulating the V-I curves characteristic of precipitators operating in back corona, but one in particular is identified as a potential back corona mechanism on the basis of generating hysteresis in the V-I curve, in accord with limited experimental evidence.

ACKNOWLEDGMENT

This work was supported by the Industrial Environmental Research Laboratory (Research Triangle Park, N.C.), Environmental Protection Agency under Grant No. R80-58-9701. J. H. Turner is grant administrator.

CALCULATIONS OF EFFECTS OF BACK CORONA IN WIRE-DUCT ELECTROSTATIC PRECIPITATORS

Back corona in an electrostatic precipitator is a condition in which electrical breakdown in a high resistivity dust layer creates positive ions which enter the normally negative ion cloud in the duct of the precipitator.[1,2] The formation of the positive ion current leads to a characteristic increase in the slope of the voltage-current characteristic.[3,4] This increase is due to the increased numbers of positive and negative ions and can be so large as to give near-vertical or even negative slopes to the V-I curves. This voltage-current characteristic is the most common indication of the presence of back corona because direct detection of free ions of both polarities is very difficult. In this paper, we relate mechanisms for back corona formation to the calculated V-I curves produced and examine the implications for particle charging and collection.

The approach used in the calculation is a numerical solution of Maxwell's equations for the electric field. The overall approach is similar to that of McDonald, et al.,[5] and a detailed description is to be published.[6]

The equations describing the distribution of electric fields and flow of current are Maxwell's equations and the current continuity equation. In this formalism, it is more convenient to work with flux and line integrals of the electric field and the current density. These are, for the static case:

$$\oint_{s} \vec{E} \cdot d\vec{s} = \int_{V} \frac{\rho}{\varepsilon_0} \, dv \qquad (1)$$

$$\oint_{L} \vec{E} \cdot d\vec{\ell} = 0 \qquad (2)$$

$$\oint_{s} \vec{j} \cdot d\vec{s} = 0 \qquad (3)$$

In these equations, s is a surface or flux integral evaluated over the surface of a grid cell, which encloses the volume V. The line integral is the term that couples adjacent grid cells and leads to a solution for the entire region.

The relationship between the current density and electric field is given by

$$\vec{j} = \rho b \vec{E} \, , \qquad (4)$$

where ρ is the ion density and b is the ion mobility. For the present, we assume that positive and negative ions have the same mobility and that any particulate space charge has a zero mobility. It is further assumed that ion recombination or neutralization effects are negligible, so that separate current continuity equations can be written for both types of ions.

The equations are solved by an iteration procedure involving an underrelaxation of error terms. The starting values for the electric field are derived from Peek's semi-empirical relation for the electric field at the surface of the corona wire at the onset of corona,[7] and the electrostatic potential distribution of Cooperman[8] for the wire-duct geometry. The potential expression is differentiated either numerically or analytically to give initial values to all the components of E_x and E_y as a function of position. For a given negative ion current at the plate, an appropriate space charge density is calculated at the corona wire and propagated to the plate. If the local current density at the plate exceeds a threshold value, a certain density of positive ions is liberated and propagated back to the corona wire. Equation 1 is then solved to obtain new values for E_x; Equation 2 is used to calculate an error term for E_y; and a portion of the error is then used to obtain a new value for E_y. When the error terms for all E_y are adequately reduced, the equations have been solved, and the corona wire voltage can be obtained by integrating the fields from the plate to the wire.

The electric field model predicts standard clean-plate V-I curves quite well and gives excellent agreement with experimental values of the space potentials measured by Penney and Matick.[9]

BACK CORONA MECHANISMS

Although recent experimental work has begun to delineate the nature of back corona mechanisms,[10,11] revealing streamer and glow modes of propagation, the mechanisms of generating positive ions in the particulate layer are still uncertain. Electrical breakdown of the particles or the interstitial gases in the particle layer are postulated,[1,2] but detailed descriptions are lacking. The approach taken in the present work is to assume several simple model mechanisms for the generation of positive ions and to explore the consequences of each. All of these mechanisms are described in terms of a critical current density, since experimental evidence[11] indicates the sudden onset of back corona as the current density is increased. All the proposed mechanisms are assumed to be local, with back corona onset in a given location having no direct effect on adjacent locations. Finally, all the mechanisms assume a continuous generation of ions as opposed to the pulsing effects observed experimentally.[11] The five mechanisms chosen are described below.

I. Positive ions are generated in proportion to the amount that the total current density exceeds the critical current density. This can be written:

$$\rho_+ = \begin{cases} \beta(j_x - j_c)/E_x b, & j_x \geq j_c \\ 0 & , j_x < j_c , \end{cases} \tag{5}$$

where β is an adjustable dimensionless parameter and j_c is the critical current density. Since the generation of positive ions occurs in the dust layer near the plate, only the x-component of field is significant. For values of β near 1, this mechanism tends to keep the electric field at the layer constant by reducing the net space charge as the current density increases.

II. Positive ions are generated in proportion to the critical current density once the total current density exceeds the critical level:

$$\rho_+ = \begin{cases} \gamma j_c/E_x b, & j_x \geq j_c \\ 0 & , j_x < j_c , \end{cases} \tag{6}$$

where γ is an adjustable dimensionless parameter. This mechanism corresponds to a source-limited generation of ions. It can be seen to have a build-in hysteresis because the presence of the positive ions increases the total current density by a fixed amount at the threshold.

III. Positive ions are generated in proportion to the total current density once the total current density exceeds the critical level:

$$\rho_+ = \begin{cases} \delta j_x/E_x b, & j_x \geq j_c \\ 0 & , j_x < j_c , \end{cases} \tag{7}$$

where δ is an adjustable dimensionless parameter. This is similar to mechanism I for current densities far above the threshold but should exhibit a hysteresis near the threshold current density.

IV. The positive ions are generated in proportion to the square of the total current density:

$$\rho_+ = \epsilon j_x^2/j_c E_x b , \tag{8}$$

where ϵ is an adjustable dimensionless parameter. This mechanism could represent a source sensitive to heating effects. In this particular formulation, there is no sharp onset threshold, but the quadratic increase in ρ_+ is sufficiently rapid to have the appearance of threshold. In practice, the increase of ρ_+ is so rapid that numeric instabilities occur unless a maximum limit is placed on ρ_+. This roughly corresponds to the physical situation in which the rate of heating is eventually balanced by losses to the surroundings. In this work, the positive ion current density at the plate was limited to twenty-five times j_c.

V. The positive ions are generated in proportion to the negative ion current density squared:

$$\rho_+ = \kappa j_-^2/j_c E_x b \,, \tag{9}$$

where j_- is the x-component of the negative ion current density and κ is an adjustable dimensionless parameter. This mechanism describes a situation in which the positive ion current does not directly contribute to the heating effect, as would be the case if generation occurred at the surface of the layer.

In all the mechanisms except II, the adjustable parameter affects the ratio of the positive ion current to the negative ion current, and, in general, values can be found for which the ratio is nearly 1 over an extended range of currents. Mechanism II is different in that the adjustable parameter affects only the size of a step increase in positive ion density, and the positive and negative current densities will be equal at a single current only.

The effects of the resistivity of the dust layer are not considered here. The dust is assumed to have zero thickness, and effects of positive ion generation on the dust surface or within the dust layer are not considered.

EFFECTS OF BIPOLAR CHARGING

Where ions of opposite polarity impinge upon a particle of radius a, a charging equation of the following form results:

$$\frac{dq}{dt} = 3\pi a^2 \left[j_-(1-q/q_s)^2 - j_+(1+q/q_s)^2 \right], \tag{10}$$

where the sign convention chosen assumes that q_s is negative and is given by

$$q_s = 12\pi a^2 \varepsilon_0 E , \tag{11}$$

where E is the electric field magnitude far from the disturbing effects of the particle. The charge q stops changing at an equilibrium value given by

$$\begin{aligned} q_{max} &= q_s \left[(j_-/j_+ - 1)/(j_-/j_+ + 1)\right]^{1/2} . \\ , &\equiv q_s Q \end{aligned} \tag{12}$$

The factor multiplying q_s we call Q for convenience and is less than 1 (even negative) for all non-zero values of j_+. Recalling that q_s does not depend on current density, the factor Q represents the degradation in particle charge that can be expected under bipolar charging conditions, and the quantity E^2Q is proportional to the particle drift velocity under bipolar charging conditions.

After choosing a fairly standard precipitator configuration and operating conditions (wire radius = 1.34 mm, wire-wire spacing = 114.3 mm, plate-plate spacing = 228.6 mm, T = 615 K), each back corona mechanism was used to generate V-I curves. The critical current density was set at 4×10^{-5} A/m^2, and the particulate space charge, q, was chosen to be either zero or -1×10^{-5} C/m^3.

The average current density was initially set to zero and then incremented upward in steps to a maximum value, calculating the corona wire voltage at each step. The electrical conditions used as the starting values for a given step were the final solution values of the preceeding step, to mimic a real measurement of a voltage-current curve. After the maximum was reached, the current density was decremented to observe hysteresis effects, but many mechanisms showed no hysteresis effects at all. Some calculations could not be carried to completion because of numeric instabilities which were encountered, generally in cases with extreme back corona. Particular attention was paid to achieving a near-vertical V-I characteristic and to checking for hysteresis effects, since these are observed characteristics in back corona situations.

Figures 1 through 5 present the voltage-current density curves calculated for the five mechanisms. In most instances, near-vertical curves could be obtained, and in some cases hysteresis was observed. Note that hysteresis was expected in mechanisms II and III (and was calculated), but it also appeared in mechanism IV in an unusual fashion.

The particulate space charge tends to suppress the spread of back corona laterally between the wires. In Figures 2 and 3, the steps in the curve are due to the cell structure of the calculation, with each step corresponding to the formation of positive ions in one or two cells as the local current density exceeds the threshold. With q = 0, the transitions occur in all the cells over a narrow range of total current densities.

CONSEQUENCES OF BACK CORONA

In the Deutsch-Andersen theory of precipitator collection,[1,2] the drift velocity of the charged particles appears as a multiplier in the argument of an exponential term in an expression for the collection efficiency and is, therefore, especially significant. Recalling that the drift velocity is roughly proportional to E^2Q, we have plotted this quantity for the five mechanisms in Figures 6 through 10. The terms were evaluated at the place, because collection occurs at the plate, and a simple linear average over all the cells was used.

The figures illustrate that the presence of back corona has a strong effect by whatever mechanism it occurs and whether or not a particulate space charge is present. Two mechanisms are worthy of note: in mechanism II on the descending legs of the hysteresis curves, the E^2Q product average actually becomes negative; and in mechanism III, for $\gamma = 0.5$, the E^2Q product approaches zero rapidly as the current density increases. Both of these conditions are disastrous for particle collection. The other mechanisms, particularly in the presence of space charge, exhibit local E^2Q products which are zero or negative but for which the overall average is positive.

In terms of operating strategy in a precipitator suffering back corona, the E^2Q product is generally a maximum at current densities which avoid initiating back corona, i.e., low current densities.

The E^2Q curves also point out the enhanced drift velocity in the presence of a particulate space charge. Even though back corona degrades the E^2Q product, adding space charge can boost it to a significantly higher level.

COMPARISON WITH EXPERIMENT

An actual V-I curve (Figure 11) of a precipitator in back corona was obtained on an X-Y recorder, measuring the corona wire voltage and collector plate current as the voltage was slowly increased to a maximum and then decreased to zero. The particulate space charge was zero (no particulate feed).

The ascending leg of the curve exhibits both increases and decreases in the voltage as the current rises. More importantly, the X-Y recorder reveals small variations in voltages that would likely be missed in a point-to-point type of measurement. The descending leg of the curve is more regular but still has the small step-like character that the ascending leg has.

Of the five mechanisms, only mechanism II has the potential of such a pronounced hysteresis, with step-like increases and decreases in voltage. Mechanism II is incomplete, however, in that it postulates only a single threshold. In order to produce a characteristic similar to Figure 11, multiple closely spaced thresholds would be required.

A composite voltage-current characteristic consisting of the sum of five voltage-current curves from Figure 4, which were offset from each other by 100 volts, is shown in Figure 12. These offset voltages correspond to diameter variations of less than one percent, which are within the realm of feasibility for dirty corona wires. The E^2Q curves for the composite mechanism would be similar to those of Figure 7, with the more rapid variations smoothed out by an averaging process.

Other mechanisms can produce V-I characteristics similar to the ascending leg of Figure 11 with proper choice of the threshold current density and the adjustable parameters, particularly mechanism IV. The difficulty is in giving physical meaning to the parameters, which in these calculations are arbitrary. In mechanism II, the adjustable parameter controls only the size of the increase in current and can potentially be related to the properties of the dust layer. It is the superposition of many small steps, near the same threshold, which can produce the steep increase in current; and it is the sum of the increases which leads to the hysteresis of the descending leg.

CONCLUSIONS

In spite of the simplicity of the proposed back corona mechanisms, a reasonable approximation to the V-I characteristic of a precipitator operating in back corona has been obtained. Although refinements in experiment will lead to more complex models, the general effect of back corona on degrading collection efficiency in these mechanisms suggests that operation at reduced current densities will be beneficial, although not extremely so, and that an enhanced particulate space charge in the precipitator would be advantageous. Operation of a precipitator on the descending leg of a voltage hysteresis curve should be strictly avoided. The electric field model has proven to be a versatile calculational tool for diagnosing the relatively inaccessible conditions in the electrostatic precipitator and will continue to be of value as the phenomenon of back carona is investigated further.

REFERENCES

1. S. Oglesby, Jr., and G. B. Nichols. Electrostatic Precipitation (Marcel Dekker, New York, 1978).
2. H. J. White. Industrial Electrostatic Precipitation (Addison-Wesley, Reading, Mass., 1963).
3. H. W. Spencer, III. "Electrostatic Precipitators: Relationship between Resistivity, Particle Size, and Sparkover," EPA-600/2-76-144 (1976), U.S. Environmental Protection Agency.
4. H. J. White. J. Air Poll. Cont. Ass. 24, 314 (1974).
5. J. R. McDonald, W. B. Smith, H. W. Spencer, III, and L. E. Sparks, J. Appl. Phys. 48, 2231 (1977).
6. P. A. Lawless and L. E. Sparks, to be published.
7. F. W. Peek, Jr. Dielectric Phenomena in High Voltage Engineering (McGraw-Hill, New York, 1929)
8. P. Copperman. Unpublished. See Reference 5.
9. G. W. Penney and R. E. Matick. Trans. Am. Inst. Electr. Engr. 1 79, 91 (1960).
10. S. Masuda. Inst. Phys. Conf. Ser. No. 27, Ch. 3 (1975).
11. S. Masuda and A. Miguno. Proc. 4th Int. Clean Air Conference, Paper No. V-47 (Tokyo, May 1977).

FIGURE CAPTIONS

1. Voltage-current density curves for Mechanism I.
2. Voltage-current density curves for Mechanism II. Hysteresis is indicated by the dashed curves.
3. Voltage-current density curves for Mechanism III. Hysteresis is indicated by the dashed curves.
4. Voltage-current density curves for Mechanism IV. Hysteresis is indicated by the dashed curves.
5. Voltage-current desntiy curves for Mechanism V.
6. E^2Q as a function of current density for Mechanism I (β=0.5). ----(β=0).
7. E^2Q as a function of current density for Mechanism II (γ=1.0). ----(γ=0); •-•-•(current decreasing).
8. E^2Q as a function of current density for Mechanism III (δ=0.5, ■; δ=0.4, ●; δ=0.5, ▲). ---- (δ=0); •-•-•(current decreasing).
9. E^2Q as a function of current density for Mechanism IV (ε=0.020). ----(ε=0); •-•-•(current decreasing).
10. E^2Q as a function of current density for Mechanism V (κ=0.10). ----(κ=0).
11. Voltage-current curve of a precipitator section in back corona.
12. Voltage-current density curves with hysteresis for a composite Mechanism II.

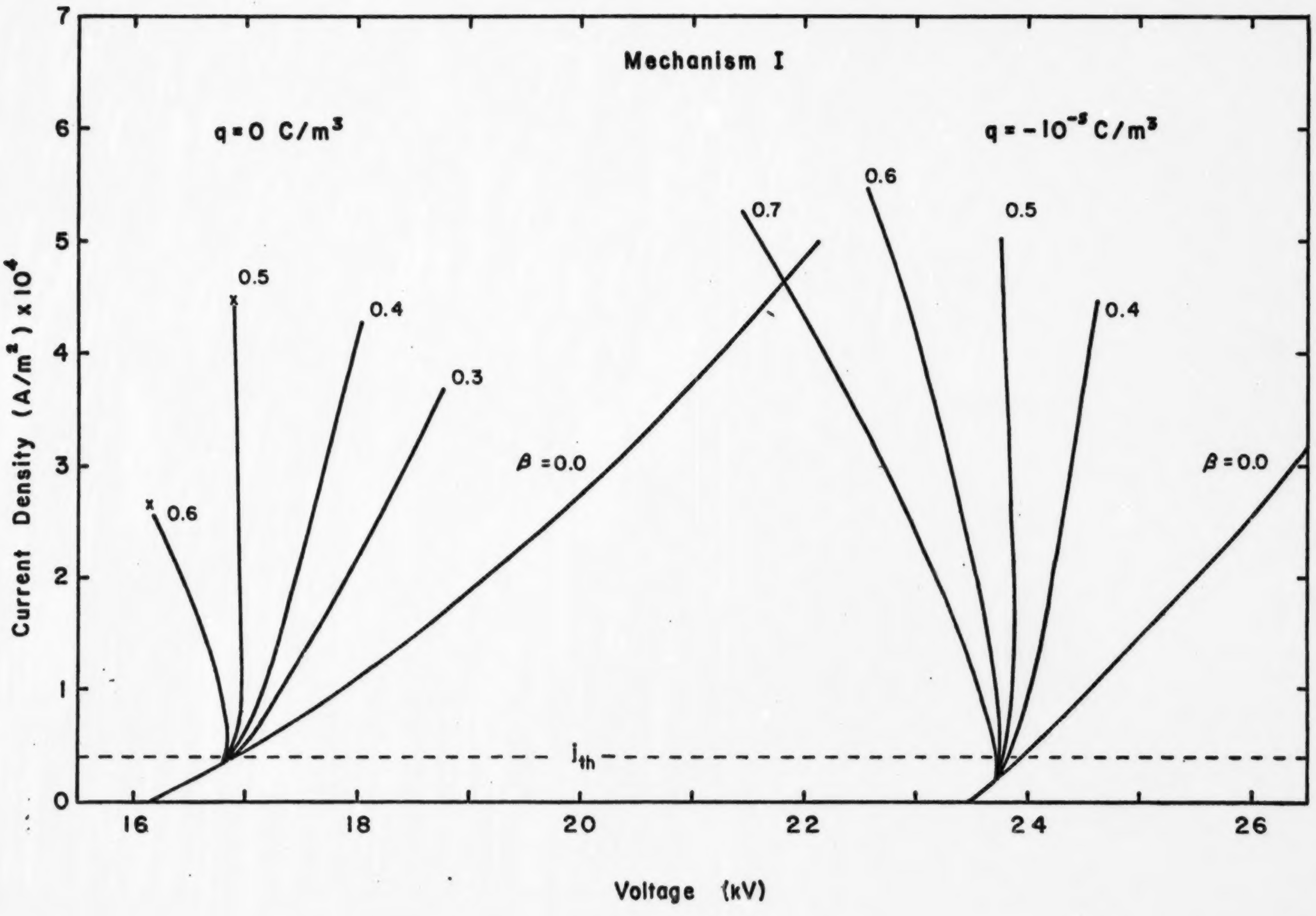
Mechanism I
q = 0 C/m^3
q = −10^{-5} C/m^3
0.6
0.5
0.4
0.3
β = 0.0
0.7
0.6
0.5
0.4
β = 0.0
j_{th}
Current Density (A/m^2) x 10^4
0
1
2
3
4
5
6
7
16
18
20
22
24
26
Voltage (kV)

Figure 1

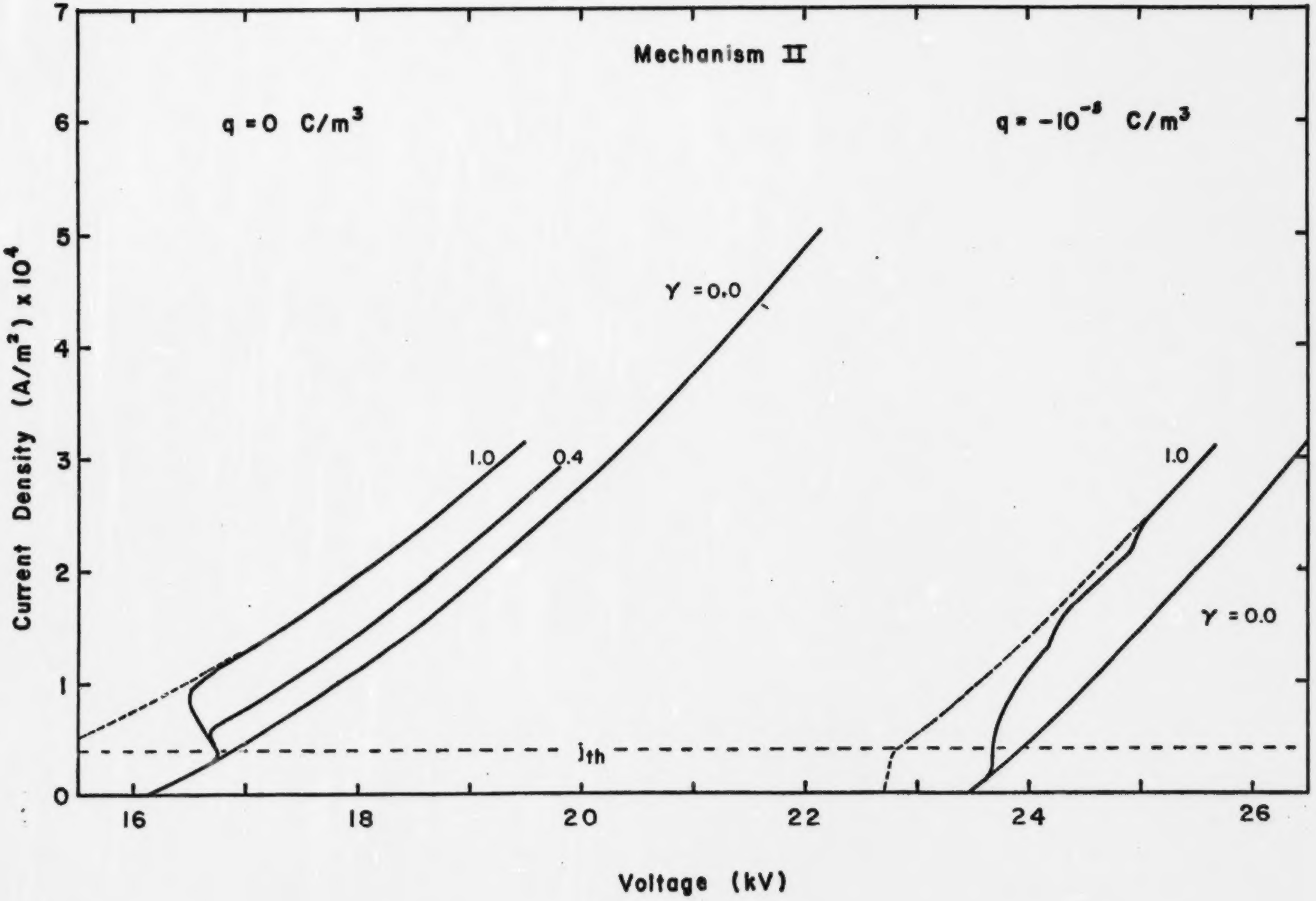
Mechanism II
q = 0 C/m^3
q = -10^-8 C/m^3
Current Density (A/m^2) x 10^4
Voltage (kV)
0
1
2
3
4
5
6
7
16
18
20
22
24
26
γ = 0.0
1.0
0.4
1.0
γ = 0.0
j_th

Figure 2

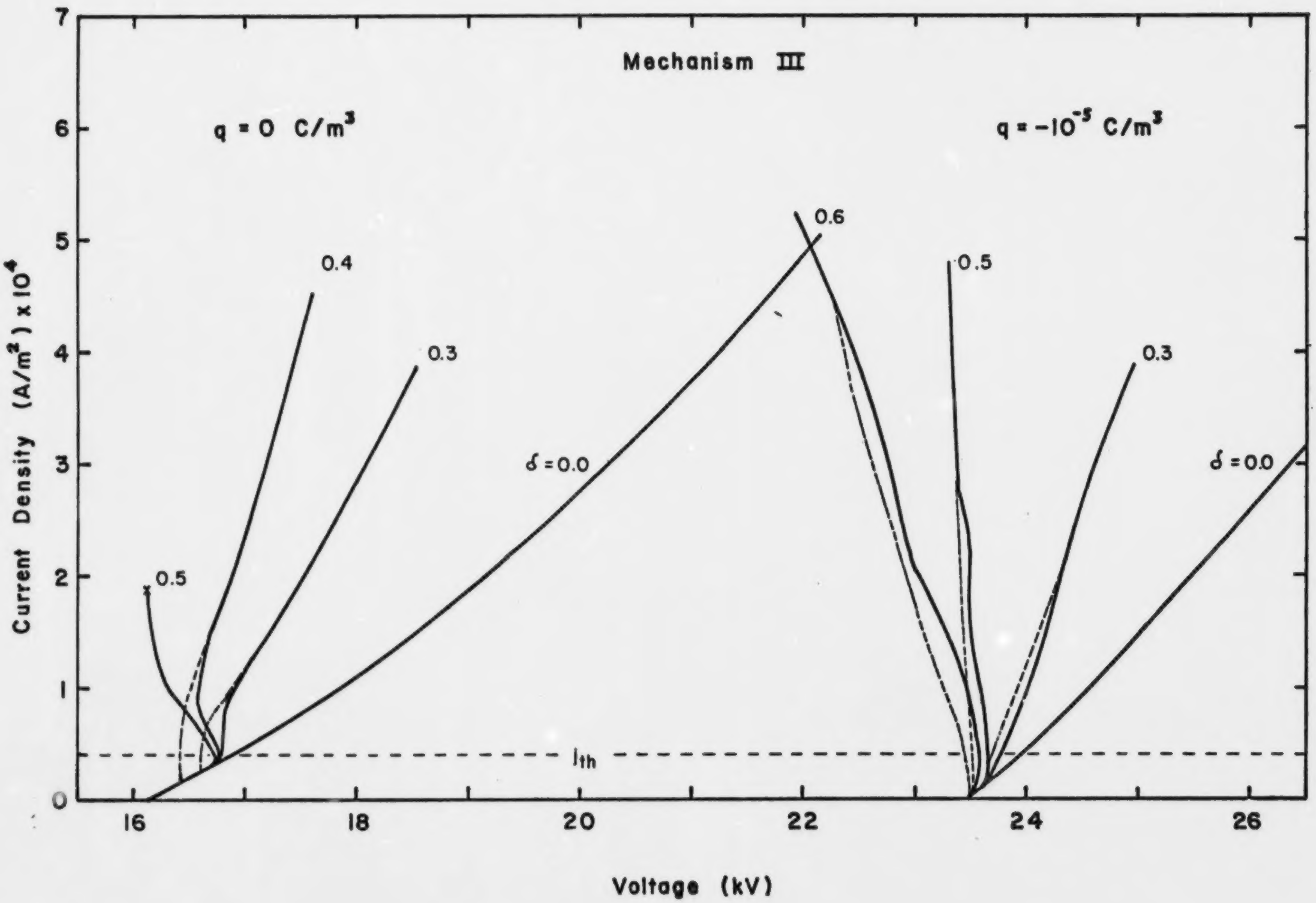
Mechanism III
q = 0 C/m^3
q = −10^{-5} C/m^3
Current Density (A/m^2) x 10^4
Voltage (kV)
0
1
2
3
4
5
6
7
16
18
20
22
24
26
0.5
0.4
0.3
δ = 0.0
0.6
0.5
0.3
δ = 0.0
I_{th}

Figure 3

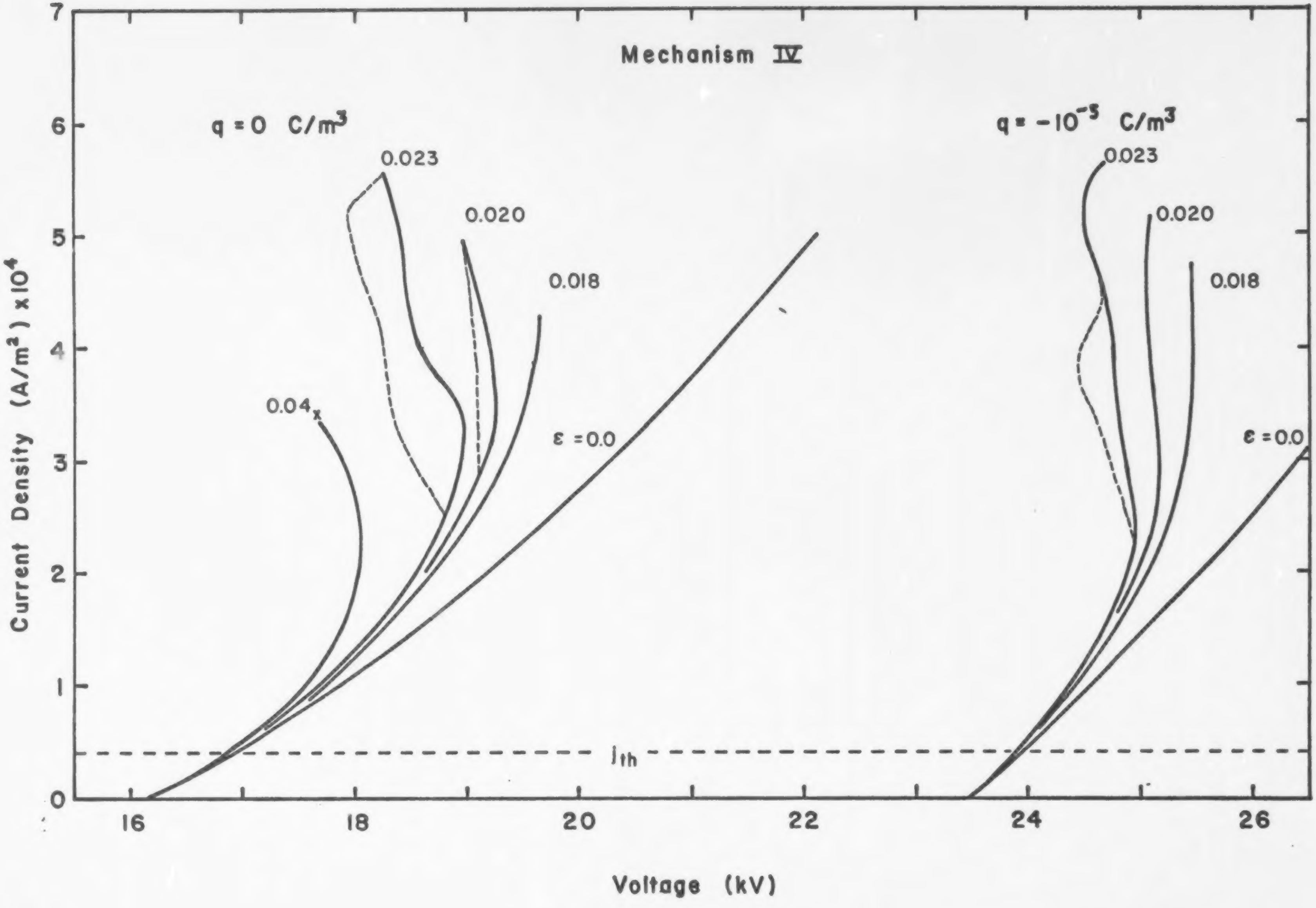
Mechanism IV
q = 0 C/m^3
q = −10^{-5} C/m^3
0.023
0.020
0.018
0.04$_x$
ε = 0.0
0.023
0.020
0.018
ε = 0.0
j_{th}
Current Density (A/m^2) x10^4
Voltage (kV)
0
1
2
3
4
5
6
7
16
18
20
22
24
26

Figure 4

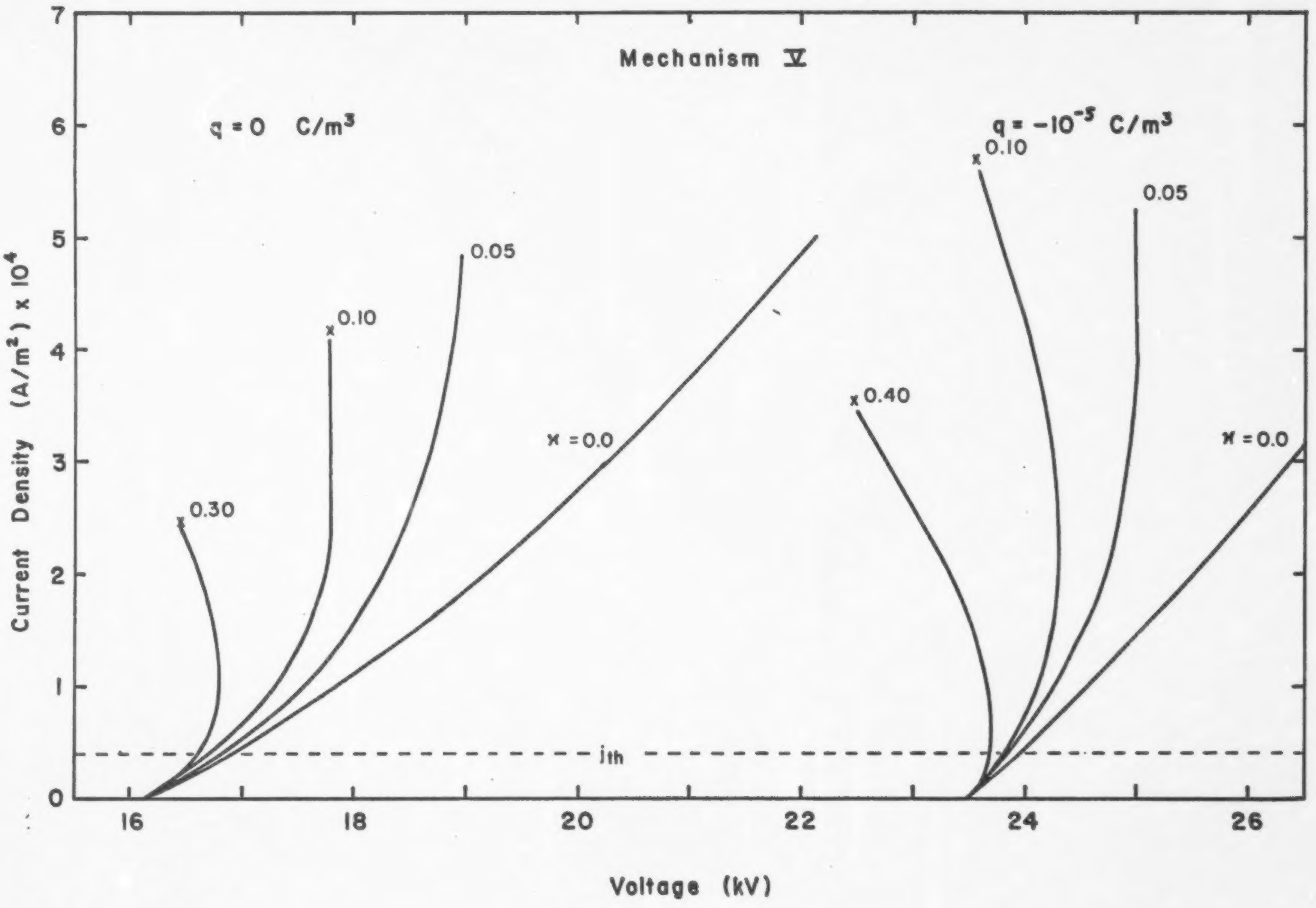
Mechanism V
q = 0 C/m³
q = −10⁻⁵ C/m³
0.30
0.10
0.05
x = 0.0
0.40
0.10
0.05
x = 0.0
j_th
Current Density (A/m²) x 10⁴
0
1
2
3
4
5
6
7
16
18
20
22
24
26
Voltage (kV)

Figure 5

Mechanism I

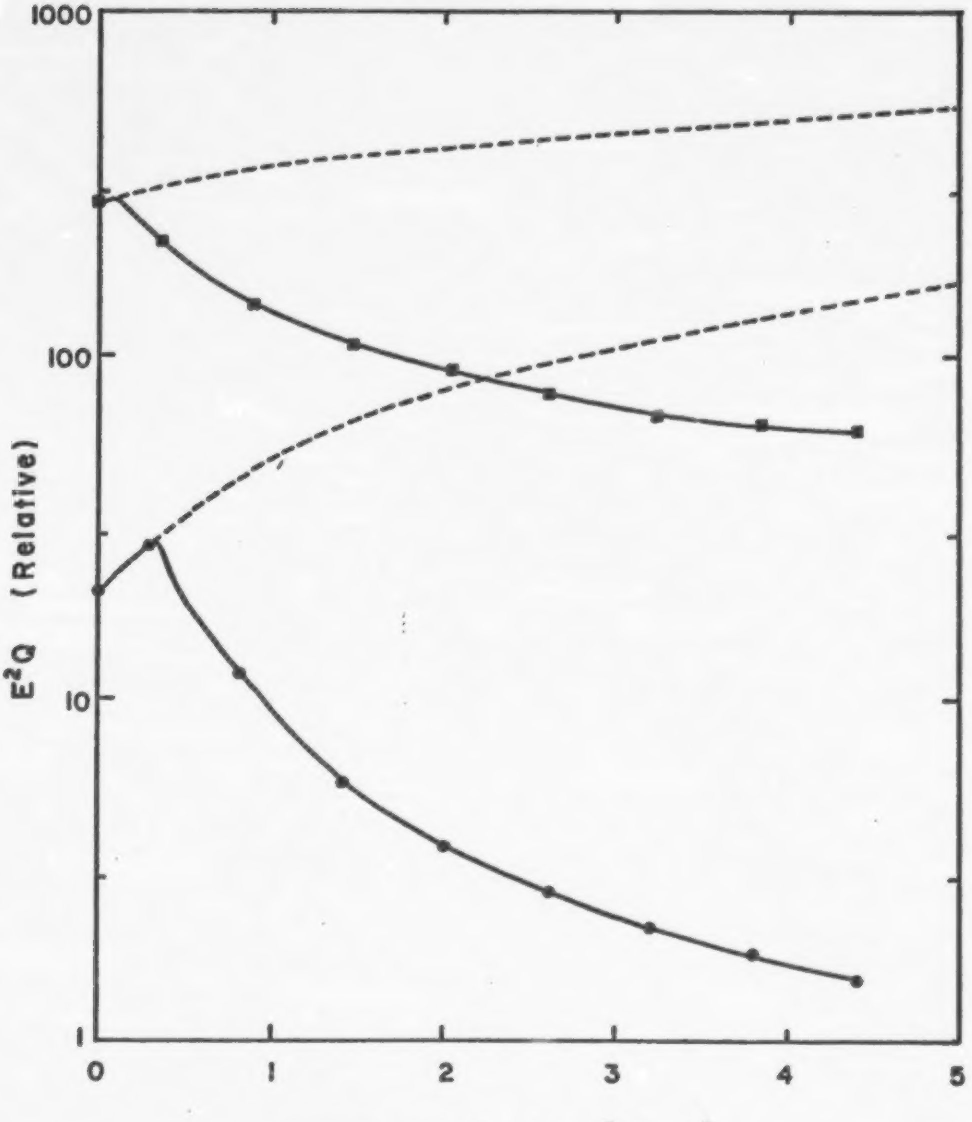

Figure 6

Mechanism II

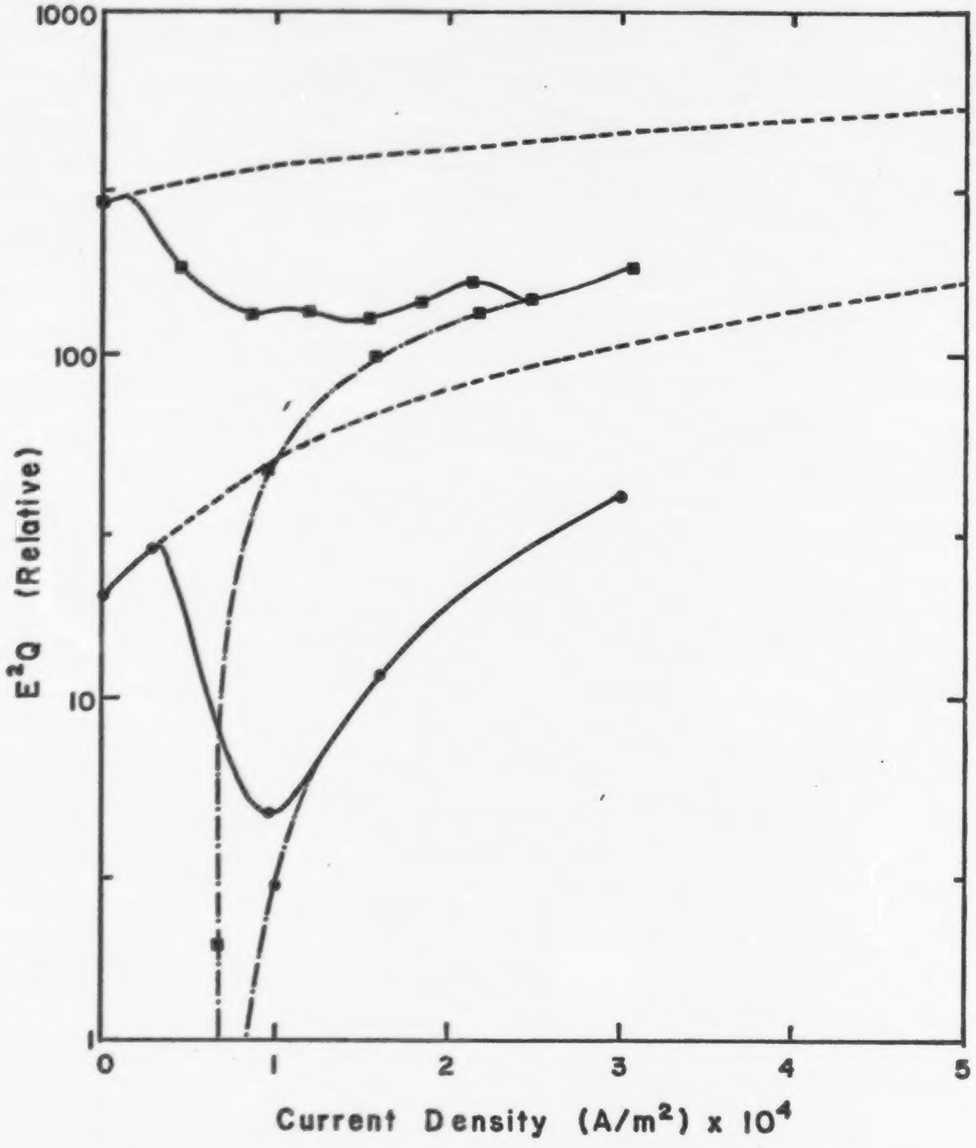

Figure 7

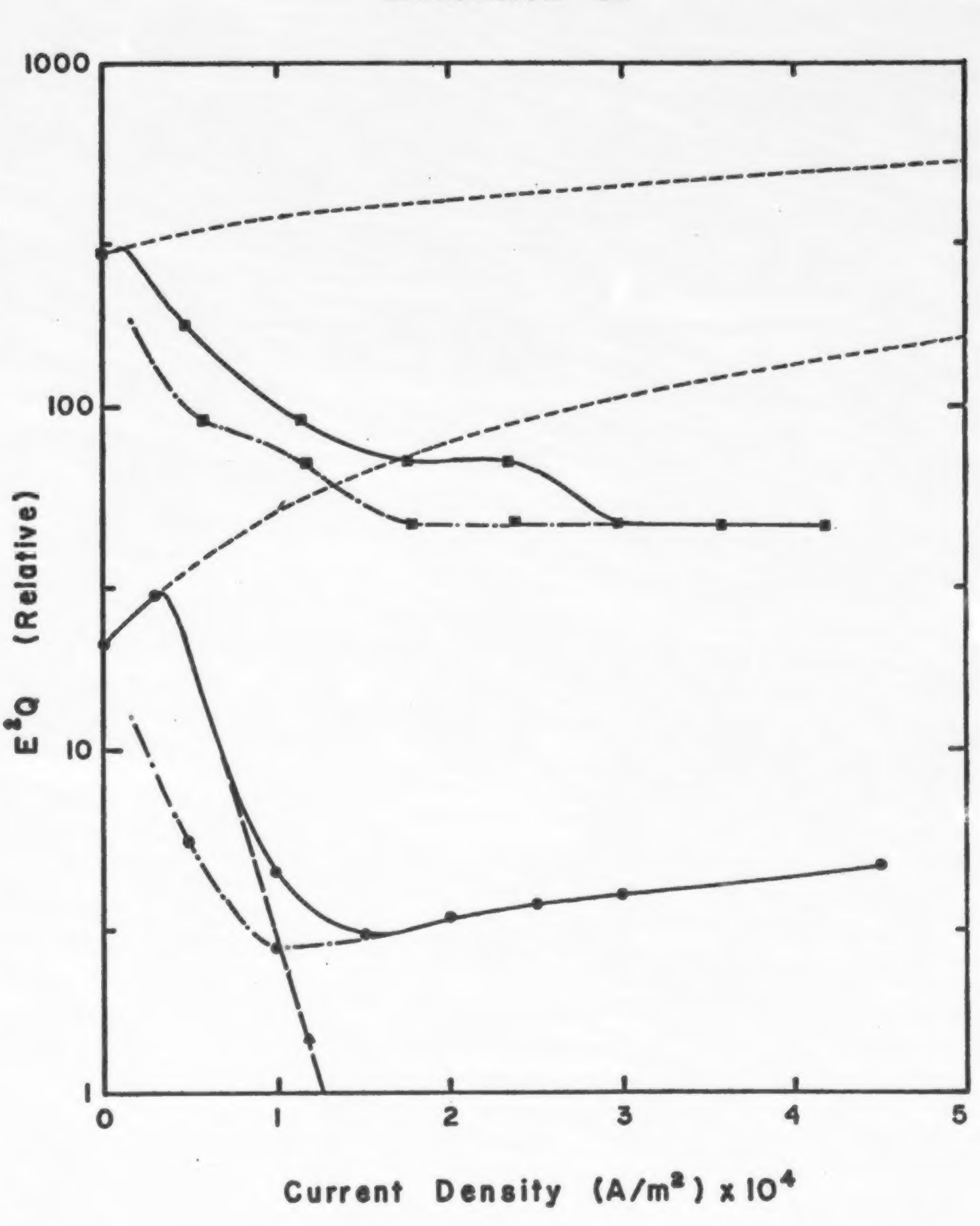
Mechanism III
1000
100
10
1
0
1
2
3
4
5
E^2Q (Relative)
Current Density (A/m²) x 10⁴

Figure 8

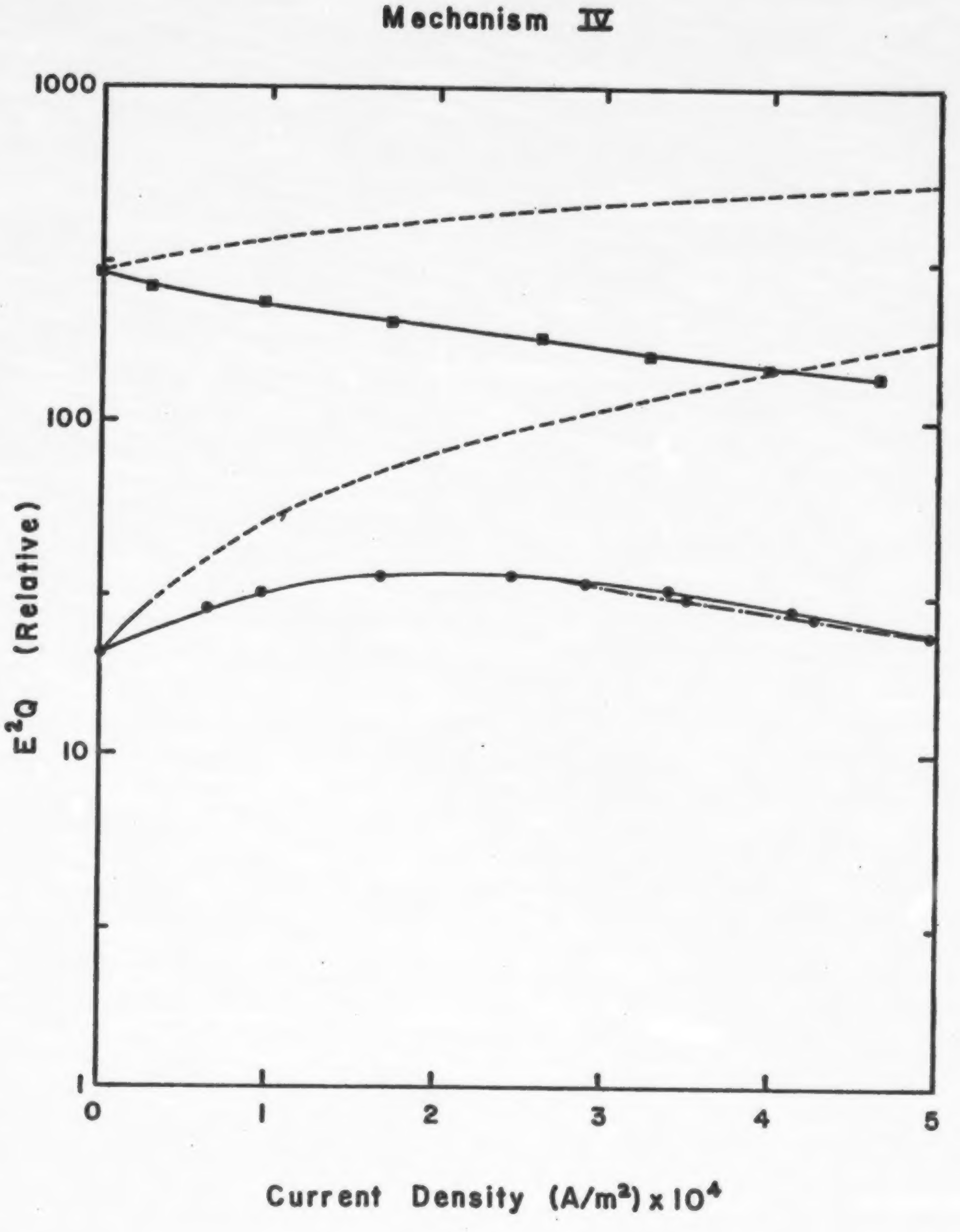
Mechanism IV
1000
100
10
1
E^2Q (Relative)
0
1
2
3
4
5
Current Density (A/m²) x 10⁴

Figure 9

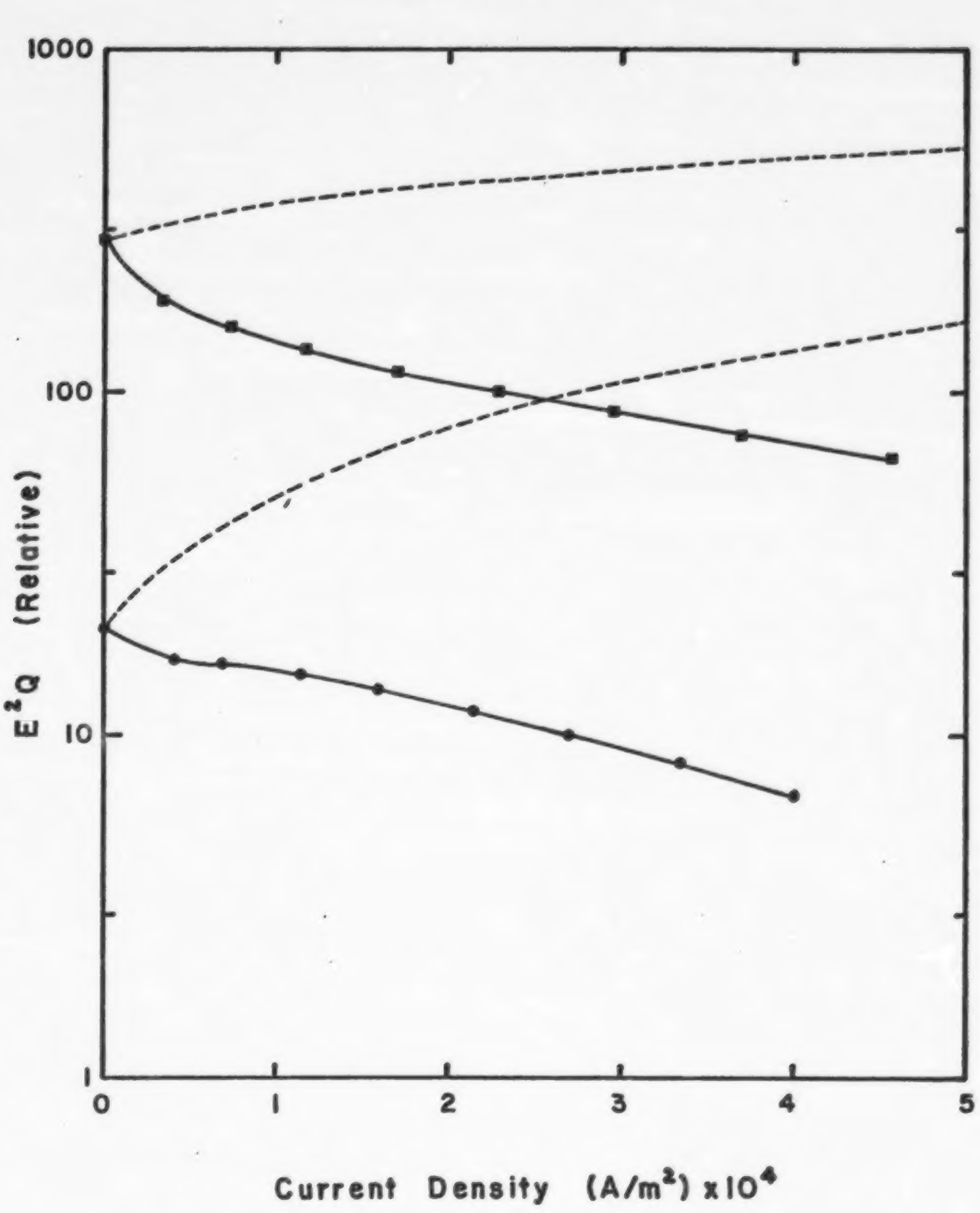
Mechanism V
1000
100
10
1
0
1
2
3
4
5
E^{2}Q (Relative)
Current Density (A/m^2) x10^4

Figure 10

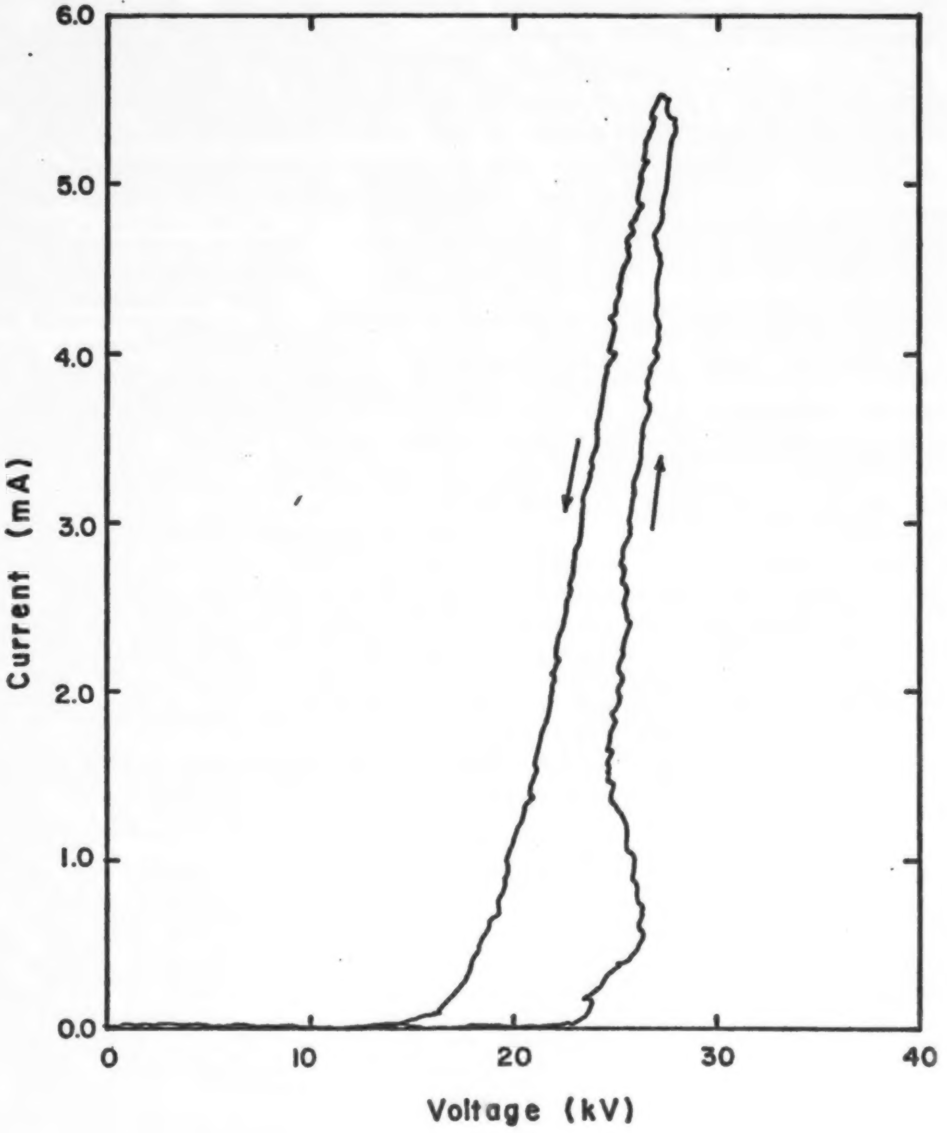

Figure 11

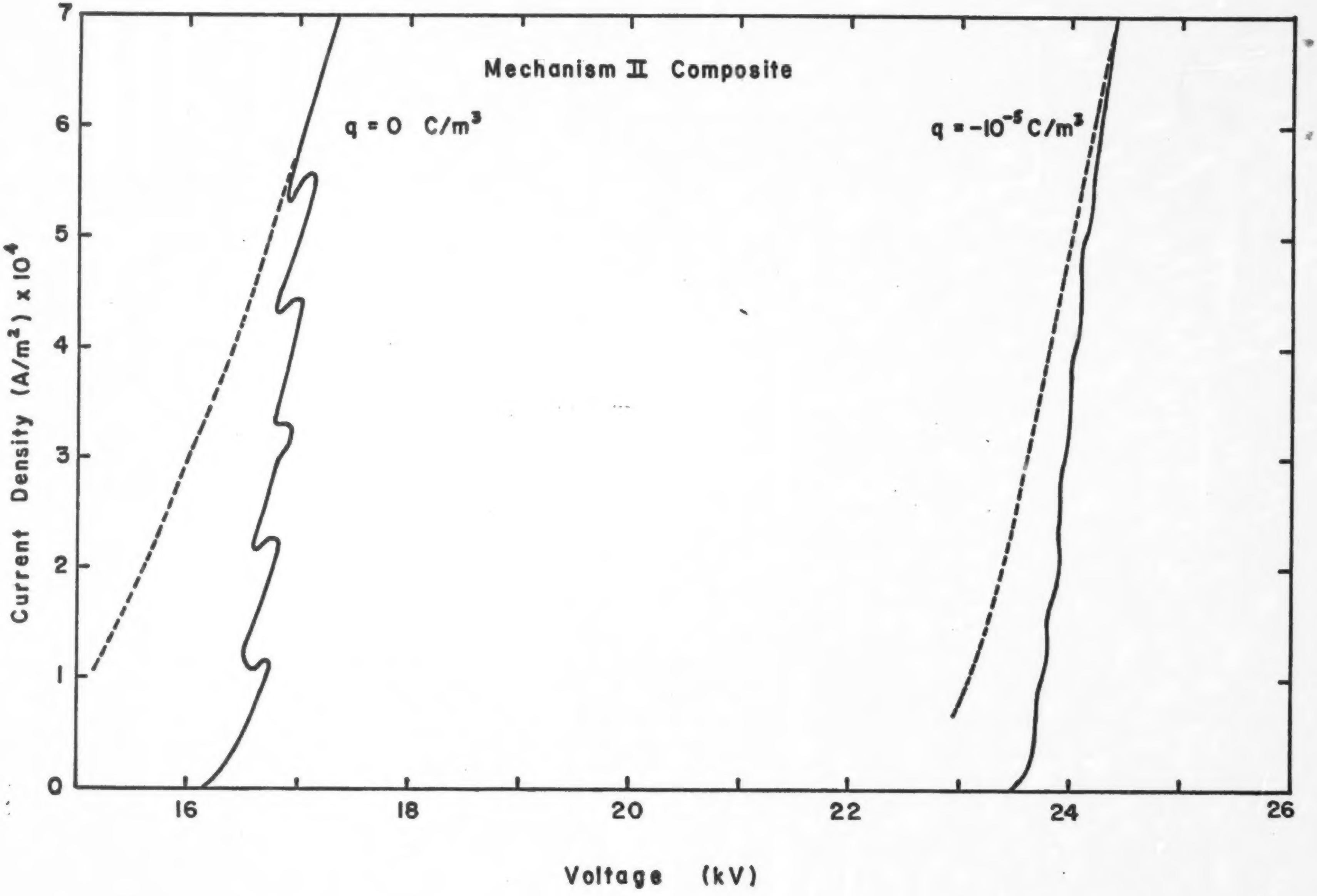
Mechanism II Composite
$q = 0\ C/m^3$
$q = -10^{-5}\ C/m^3$
Current Density $(A/m^2) \times 10^4$
0
1
2
3
4
5
6
7
16
18
20
22
24
26
Voltage (kV)

Figure 12

I.A. Kizim, B.V. Zolotarev, A.A. Troitskii, M.A. Golosov

REPORT: STUDY OF CHEMICAL CONDITIONING OF STACK GASES BEFORE ELECTROSTATIC PRECIPITATION AT A 500-MEGAWATT POWER GENERATOR

In accordance with basic directions for developement drawn up for the national economy of the USSR for 1976-1980 and long term prognoses for the coming decade, the nation's energy output will be increased chiefly through construction of large-scale thermal electric power stations and and central heating and power plants working mainly on low-grade hard fuel, primarily low-sulfur (S^P<1%) and low moisture coals from the Ekibastuz and Kuznets basins.

Combustion products of these coals includes many aluminum silicates (up to 93-94%) while the share of alkaline metals (sodium, lithium, potassium) is insignificantly small. Therefore with exhaust gas temperatures of 130-150°C, this ash has a high resistivity, comprising 10^{10}-10^{12} ohm-meters.

As practice shows, deep cleaning of combustion product fly-ash of given coals in electrostatic precipitators reaching 99-99.5% is difficult, in as much as the high resistivity in these units causes intense back corona, sharply lowering ash-trapping efficiency.

Efficient ways for solving the problems of trapping high-resistivity fly-ash are:

- precipitator installation in a gas temperature zone of 350-400°C, due to which the volume resistivity of the ash determining its resistivity sharply decreases;
- lowering exhaust gas temperature according to comparison with projected values when the ash resistivity is determined by increased surface conductiveness;
- addition to the stack gases of various chemical conditioning

substances and water steam, providing the required value of surface conductivity for the ash layer.

Each of the listed methods has its own advantages and insufficiencies. For deciding the advisability of using one of these methods, it is necessary to conduct investigation into working conditions at full-scale electrostatic precipitators.

Chemical conditioning is one of the promising directions for increasing the degree of gas-cleaning during trapping of high-resistance fly-ash.

Conditioning gas by humidifying is usable in those situations where the exhaust gases have a high temperature and lowered moisture content. Under these conditions, it has been established that the introduction of moisture has a favorable effect on increasing electrical strength and lowering gas viscosity. Water adsorption on ash particle surfaces grows proportionately to the content of moisture in the gases and inversely proportional to temperature.

With humidifying stack gases, besides lowering the ash resistance , gas cooling occurs, which in its turn, lowers the resistivity. However, introducing humidity conditioning to thermal power stations gives rise to great difficulties in as much as for these purposes, considerable input of water and steam is required. Other than this, in power station conditions, it is impossible during sufficiently low exhaust gas temperatures to produce full water evaporation because it leads to condensation in gas conduits, precipitators and exhaust fans and their surfaces become sticky, which guarantees corrosion.

SO_3 and ammonia are other conditioning reagents for stack gas conditioning.

The relationship of the degree of gas cleaning to sulfur content is known. If follows from this relationship that, upon lowering sulfur content, efficiency of ash trapping is sharply lowered. Therefore during lower-sulfur coal fly-ash trapping, SO_3 is added to stack gases to compensate for the lack of it and to raise ash-trapping efficiency. Sulfur trioxide, reacting with the ash, forms sulfates capable of raising surface conductivity of the ash particles.

Introducing ammonia to the stack gases gives a positive effect with low sulfur content, just as with high sulfur content. At the same time, ammonia may be introduced to the gas tract both after the air pre-heater and before it.

Sulfur dioxide is three times more expensive than ammonia under the same quantities of reagent and approximately the same efficiency. Therefore, ammonia was used in ekibastuz coal fly-ash trapping in industrial experimenting with chemical conditioning at the Troitskaya State Regional Power Station.

Industrial tests were conducted in 1977 on the 500 mW capacity power unit no. 8 with a flow-through boiler with a steam-production of 1650 tons/hr.

Ekibastuz coal, type SS, was the fuel used, and has the following characteristics.

ash content - $A^P = 36.9\%$
moisture - $W^P = 5.7\%$
content of combustibles in exhaust S^g_e - 1.5%
heat of fuel combustion $Q^P_h = 17.6 \ \frac{\text{Kilojoules heat}}{\text{kg}}$

Four regenerative air pre-heaters were installed at the boiler's outlet into the exhaust tract. Fly-ash trapping is done by two four-field precipitators with active sections of 265m^2 each. The precipitators are placed after the air-preheaters.

The precipitator's active zone consists of a system of C-shaped precipitating electrodes and needle-strip coronal electrodes. Rapping is done by hammers.

The precipitator fields are supplied with rectified high-voltage by ATF-1600-type step-up rectifiers. Each field consists of two electrically isolated parts (semi-fields). The high-voltage current supply circuit is the "unit-semifield".

A 14% ammonia water solution, which was fed into the gases after the air pre-heater, was used during testing.

The lay-out for ammonia conditioning consisted of an intermediate space of 5m^3 volume, equipped with a level indicator, two pumps mounted parallel to each other on one frame, distribution collectors for acqueous ammonia solution and compressed air and shut-off armature.

Ammonia enters the intermediate space from the reagent stock station. From the intermediate space, the ammonia is fed into the distribution collector, which is a pipe with branches having calibrated apertures. The compressed air system is analogously arranged. Compressed air atomizes the ammonia water solution.

During the test period, the boiler agregate worked with nominal parameters, namely:

unit's electrical load - 511 megawatts

superheated steam pressure - 23.53 - 23.73 megapaschals

boiler's steam yield - 1655-1665 tons/hr superheated steam temperature - 540-543°C

The precipitator test results are introduced in table 1.

Table 1

Precipitator parameters	without conditioning	with conditioning	
Ammonia content (parts per million)	-	30	40
Gas temperature at inlet, °C	I65	I64	I64
Gas temperature at outlet, °C	I58	I57	I57
Gas rarification, kilopaschals	3.3	3.3	3.3
Gas volume at inlet, thousands $\frac{m^3}{hr}$	I520	I535	I545
Gas dustiness, g/m^3			
at inlet	52.8	54.7	54.7
at outlet	0.99	0.30	0.20
Gas speed into precipitator, m/s	I.7I	I.74	I.75
Effective particle drift velocity, cm/s	4.93	6.85	7.3
Degree of gas cleaning,%	97.5	99.35	99.56
Average precipitator voltage, kilovolts	30.9	36.6	36.9
Average precipitator corona current, amps	0.95	0.37	0.38

Industrial precipitator test results have shown that with a velocity of 1.74m/s, the introduction of 30 parts per million of ammonia resulted in an increase of cleaning of from 97.5 to 99.35% and in a decrease of exhaust dust by 3.2 times.

The addition of 40 parts/million of ammonia, under other equal conditions makes it possible to increase ash precipitation efficiency up to 99.56% and decrease outlet dust content from 0.99g/m^3 to 0.20g/m^3 (i.e. by 5 times).

The increase in the degree of gas cleaning was due to lowering the intensity of back corona. This is supported by increasing the working voltage an average of 10-25% and lowering the magnitude of corona current along the precipitator fields by 1.7-4.6 times.

Voltampere characteristics were taken both with stack-gas conditioning and without it. With the introduction of ammonia conditioning, voltampere characteristics shift to the right, during which corona current is lessened and the loop, characterizing back corona intensity, narrows.

Measurement results of ekibastuz coal-ash resistivity give indirect confirmation of the lessening of back corona intensity during ammonia introduction. The resistivity measurement was taken both with and without ammonia stack-gas conditioning. According to measurement data, the resistivity of fly-ash at the precipitator inlet, $1.2 \cdot 10^{11}$ ohmmeters, taken during gas conditioning by a 14% ammonia water solution, was lowered by a factor of 3 and comprised $2 \cdot 10^8$ ohmmeters.

The fly-ash resistivity at the precipitator inlet was determined by use of a unit for measuring dust resistance (DRM).

The DRM unit's active principle lies in measuring dust resistance of a layer of a given thickness, formed in the corona discharge field.

Constancy of the layer's thickness is assured by dust precipitation on the comb-type precipitating electrode. Two such electrodes, arranged strictly on one plane, form the comb gap.

Other than this, studies were made of the relationship of ekibastuz and kuznets TR-type coal-ash resistivity to temperature in a range up to 350°C, when resistivity is determined by volume conductivity (fig. 1.). The ash's chemical composition strongly effects its resitivity magnitude (table 2). Silicon and aluminum dioxide with a few admixtures of iron, calcium, etc. Oxides are the basic components of fly-ash. Ekibastuz coal fly-ash contains 64% SiO_2 and 22% Al_2O_3, which determines its infusibility and abrasiveness.

Table 2

Chemical Composition of Ash

components	SiO_2	Al_2O_3	Fe_2O_3	CaO	MgO	SO_3	TiO_2	Na_2O	K_2O	calcination loss
content, % of mass	64.4	22	4.6	1.5	0.4	0.6	1.1	0.3	0.6	3.4

Ash dispersion composition (table 3) is determined in industrial conditions by the rotational separation method. Ash sampling was done at the precipitator inlet without ammonia conditioning, and at the outlet, both with and without the conditioning.

Table 3 Dispersion Composition of Ash

particle diameter d, in microns	2.5	4.0	6.3	10	16	25	40	median diameter d_{50}=21 microns
content of particles of diameter less than d, % of mass	94	84	82	70	55	37	20	standard deviation, b = 3.2
terminal velocity in air, cm/second	0.04	0.09	0.24	0.62	1.58	4.0	9.0	

It has been established experimentally, that for ash samples containing less than 10% Fe_2O_3, the magnitude of resistivity at a temperature of 356°C depends on the Na_2O content (fig. 2).

Ash resistivity, measured in industrial conditions, practically coincides with the value, determined by chemical composition with help of the given relationship. The average resistivity value at 350°C, determined by the relationship in fig. 2, comprises $7 \cdot 10^7$ ohmmeters (0.3% Na_2O) for ekibastuz coal and $2.3 \cdot 10^7$ ohmmeters (0.65% Na_2O) for kuznets coal. Therefore, as a result of studies, the relationship of resistivity to temperature was derived. It has been shown that with a gas temperature increase to 350°C, the resistivity decreases by three orders of magnitude, and its value in these conditions may be approximately determined according to its content of alkaline. oxide metals.

The effect of small quantities of ammonia introduced into stack gases is connected with particle surface conductivity in the ash precipitating layer. With the addition of ammonia, its reaction with water steam and SO_3, contained in the stack gases, occurs.

$$NH_3 + SO_3 + H_2O \rightarrow (NH_4)_2 SO_4 \rightarrow \text{[illegible]}$$

Ammonia sulfates formed during reaction increases the surface conductivity of fly-ash particles.

One of the basic characteristics of precipitators is particle drift velocity. As a result of conditioning, the effective drift velocity grew 1.44 times and measured 7.34cm/sec. under reagent consumption at 40 parts per million. In this case, the degree of gas cleaning measured 99.5%. Increasing the precipitator size 1.5 times was required to get such a degree of efficiency without gas conditioning.

Thus, industrial condition studies of ammonia stack gas conditioning during trapping of high-resistance ekibastuz coal-ash has shown that this method is an efficient means for increasing the degree of cleaning.

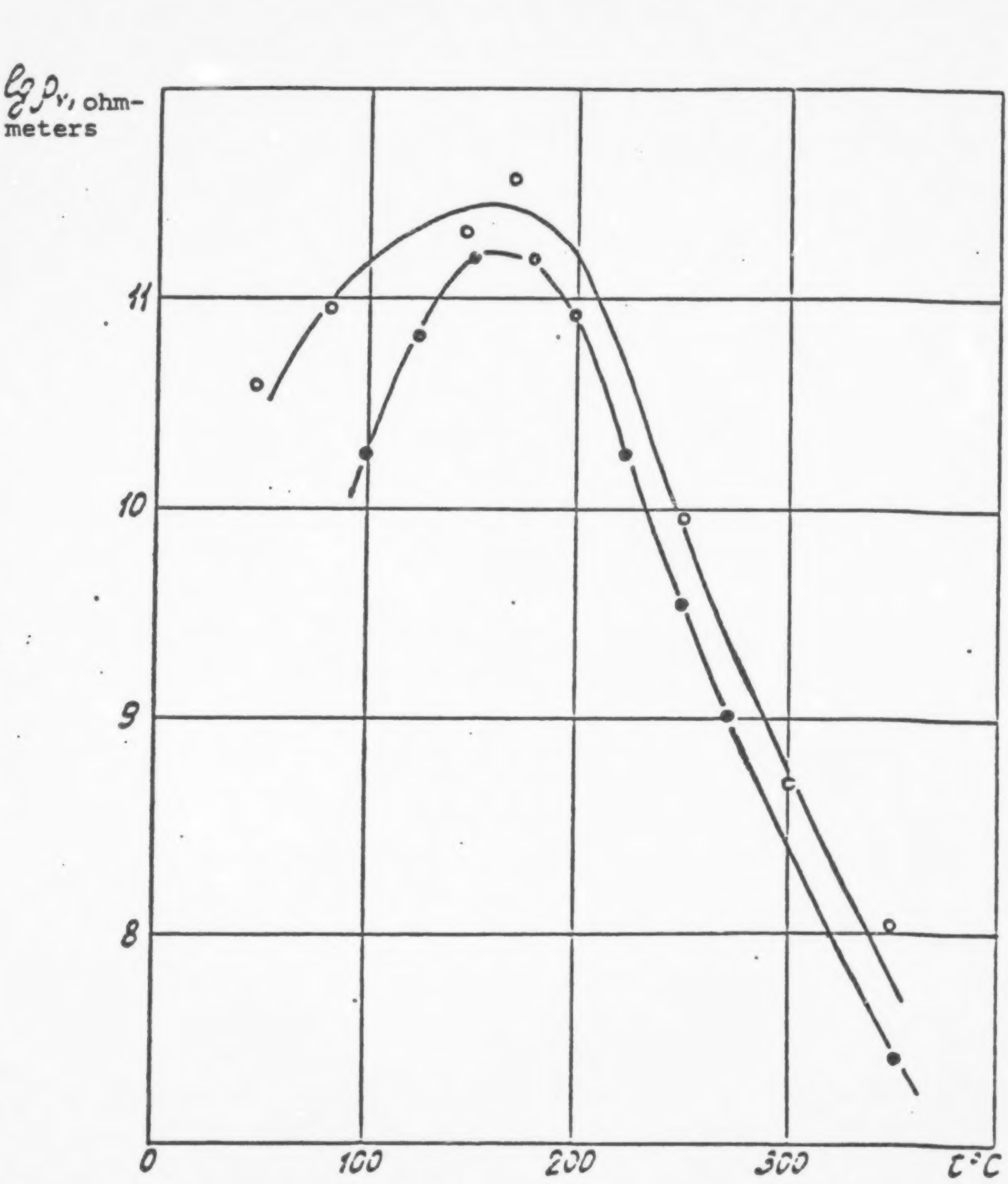

Fig.1. Dependency of kuznets and ekibastuz coal ash resistivity on temperature.

●——● kuznets coal

○——○ ekibastuz coal

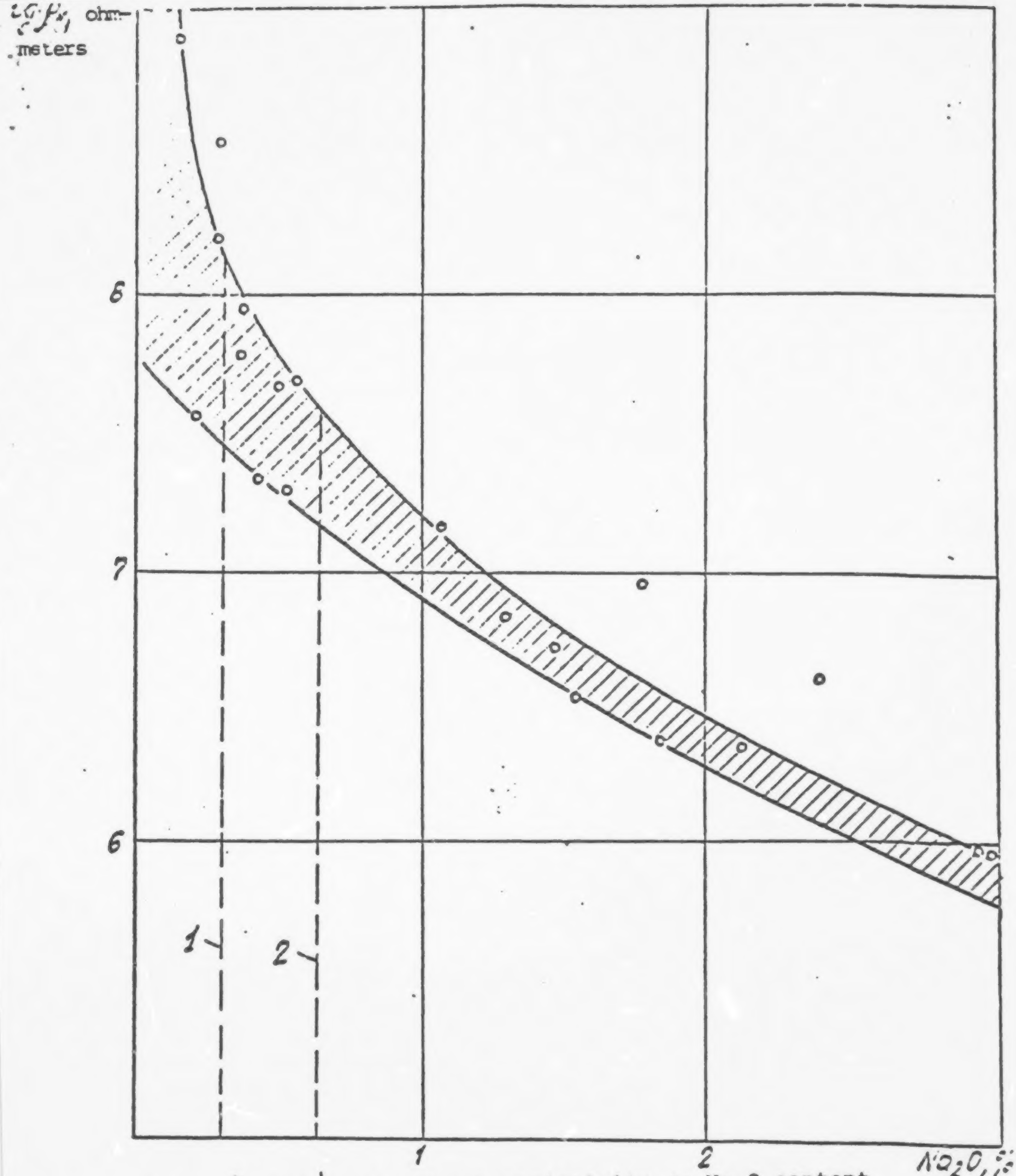

Fig.2. Dependence of ash resistivity on Na_2O content under 350°C (L.1)
(Fe_2O_3 content < 10%)

1. Ekibastuz coal
2. Kuznets coal

SODIUM CONDITIONING TEST
WITH EPA MOBILE ESP

Steven P. Schliesser
Acurex Corporation

(Although the information in this document has been funded by the U.S. EPA, it does not necessarily reflect the views of the Agency and no official endorsement should be inferred. The paper is as delivered at the meeting; Tables 2 and 4B are missing.)

1.0 SUMMARY AND CONCLUSIONS

The objective of this pilot program was to determine the conditioning effects of adding anhydrous sodium carbonate into a "cold-side" slipstream with respect to the collection performance of an electrostatic precipitator (ESP). A power plant combusting low sulfur, low sodium western coal generated the high resistivity ash (2.5×10^{12} OHM-CM @270°F) for conditioning evaluation.

A performance evaluation was conducted on a pilot scale precipitator which treated the base and sodium-conditioned flyash. The program, conducted over several weeks, consisted of twenty days of operating and testing. For each ash species, the pilot precipitator treated 28.3 m^3/min (1,000 acfm) of flue gas at an average of 110°C, maintaining a specific collection area equal to 57 m^2/m^3/sec. (290 ft^2/Kcfm).

In situ resistivity measurements, precipitator operating conditions, and particulate concentration and size distribution measurements constitute the data assembled for the comparative demonstration.

The following results reflect the effects of conditioning the base ash with a 1.0-1.5% concentration of sodium carbonate as Na_2O:

1. A sixfold reduction in specific resistivity, suppressing the base ash from 2.1×10^{12} OHM-CM to 3.7×10^{11} OHM-CM.

2. Relative improvements in achievable current densities ranging from a factor of two to six. Under steady state conditions, maximum current densities were 1-8 nA/cm^2 for the base ash, and 10-24 nA/cm^2 for the conditioned ash.

3. Enhancement of particulate collection levels, resulting in an improvement in collection efficiency from 98.19 to 99.46 percent, associated with a reduction in outlet loading from 140 to 40 mg/DSm^3.

4. Improvement in fractional efficiency characteristics, particularly in the fine particle range, as demonstrated by the following results:

FRACTIONAL EFFICIENCY@

	0.3μ	0.5μ	1.0μ	3.0μ
Base Ash	69.4	81.2	93.9	98.9
Conditioned Ash	91.8	93.7	97.4	99.7

5. On this pilot scale basis the difference in collection efficiency between the base ash and the sodium-conditioned ash was significant enough to move performance from noncompliance (0.122 lb/10^6 Btu) to compliance (0.0361 lb/10^6 Btu).

Assimilation of the test results prompt the following conclusions:

1. Conditioning by the admixture of conductive material to reduce specific resistivity of the process effluent, in quantities small enough to be potentially economical, has been demonstrated.

2. A material for such conditioning, which has the potential to be economical, commercially available, and environmentally acceptable has been identified.

3. This material can be utilized for flyash treatment without special equipment or extensive maintenance requirements by simply injecting it into a pilot scale process stream.

4. The effects of using sodium carbonate as a conditioning agent coincide with alternative methods:

    a. An increase in the operating corona points for each precipitator field.

    b. An increase in collection performance, primarily in the fine particle size range.

Note:

Federal new source performance standards for coal-fired steam electric plants of 250×10^6 Btu or greater heat input for particulate matter = 0.1 lb/10^6 Btu, 2 hour average.

2.0 INTRODUCTION

The program objective was to determine the effects on precipitator operation and collection performance of adding sodium carbonate into the exhaust of a boiler burning low sulfur low sodium western coal. The specific effects of interest were:

1. particulate resistivity level

2. precipitator operating conditions

3. particulate removal characteristics

The feasibility of utilizing conditioning agents at the test site (Montana Power Station, Colstrip, Mont.) is documented by another power facility (Montana Power/Corrette Station, Billings, Mont.) using coal from the same strip mine. Injection of proprietary conditioning material into the flue gas before it entered the precipitator dramatically affected operating corona points and improved particulate collection performance so that compliance limits were met.[1] In situ resistivity measurements at 135°C at the test site determined the flyash resistivity to be in the lower 10^{12} OHM-CM range, outside the preferred range of 10^8 to 10^{10} OHM-CM. Compositional analyses of the coal and flyash provide the basis of this excessive resistivity, i.e., low sulfur (1.01 percent) and low sodium (0.31 percent) content.

The experimental conditioning agent was anhydrous sodium carbonate (Na_2CO_3), a dry, powdery material with size distribution comparable to flyash (mean size $\triangleq$ 15 μ). Charging was achieved by metering the material with a calibrated screwfeeder, and entraining it with a compressed air supply through an injector. Identical test methodology employing a pilot-scale precipitator was implemented for a two phase program:

1. Operation with sodium carbonate addition and a 4 - 5 percent rate relative to flyash concentration.

2. Operation without conditioning additives.

The pilot scale ESP is one of three mobile field units owned by the Utilities and Industrial Power Division, Industrial Environmental Research Laboratory-U. S. Environmental Protection Agency (EPA), Research Triangle Park, North Carolina. A pilot scale scrubber and baghouse complement a fleet of conventional collection systems designed to offer:

- Comparative evaluation of removal and economic performance factors among the three conventional control systems on either traditional sources or process streams, or inadequately documented particulate-laden process streams.

- A parametric evaluation characterizing a given control device/emission source in search for optimum design criteria.

- Feasibility/demonstration programs on novel or modified processes.

- Specific problem-solving programs in control technology.

3.0 DESCRIPTION OF FACILITIES AND INSTALLATION

Power Plant

The test program was conducted at the Montana Power Company Station at Colstrip, Montana. The recently constructed facility represents current design and operating methodology for coal-fired electric-power-generating stations. Modular venturi scrubbers provide emission control for two 350 megawatt (MW) boilers. More pertinent information is available via a performance evaluation program conducted by Southern Research Institute.[2]

Design operating data from the test facility is listed in Table 1, along with power production data for several days during the test program. Table 2 presents coal and flyash analyses, as well as gas composition data.

Table 1. COLSTRIP POWER PLANT DESIGN AND OPERATING DATA

Unit 11 Operating Data As Designed	358	330	282	212
1) Coal Feed Rate, tons/hr. (appr.)	220	185	165	120
2) Steam Production, lb/hr. (design)	2,464,261	2,228,286	1,871,761	1,403,821
3) Output Steam Pressure, PSI (design)	2,520	2,400	2,400	2,400
4) Output Steam Temperture, °F (design)	1,000	1,000	1,000	1,000
5) Generation Rate, MW	358	330	282	212
6) Gas Volume, Kcfm	1,208	1,114	952	716
7) Temperature at Cold-side Air Preheater, °F	300 to 250°F (290°F Normal)			

PILOT ESP FACILITY

General Description

The mobile ESP facility consists of two separate units mounted on freight trailers 40 feet in length. Figure 1 is a floor plan of the two units. The first unit is the process trailer which houses a five-section ESP and all auxiliary equipment. This equipment consists of:

- Heat-traced, insulated 10" duct.
- Flow rectification equipment containing vaned turning elbows and diffuser sections.
- An I. D. fan with a cooling system.
- A screw conveyor and gate valve for the removal of the collected material.
- Electromagnetic vibrators for rapping the collection plates.
- Five transformer-rectifiers, with rated capacity of 50 KV and 10 MA. DC.

The system is designed to operate up to 1,000°F over a flow range of 28-35 m^3/min (1,000-3,000 acfm). Figure 2 shows an isometric of the high voltage field design.

The second unit is a control/laboratory trailer containing all process controls, monitors and recorders plus provisions for an analytical laboratory and spare equipment storage.

Pilot ESP design specifications are compared with the specifications typical of full scale precipitators in Table 3. Comparison of each design parameter between the pilot and full scale units shows that:

a. Fixed design parameters on the pilot unit lie midway in the normal range for full scale installations.

b. Operational parameters contain the flexibility to cover the spectrum typical of commercial units.

c. The single exception to conformity with commercial installations is the plate area, the inherent concession of pilot-scale methodology.

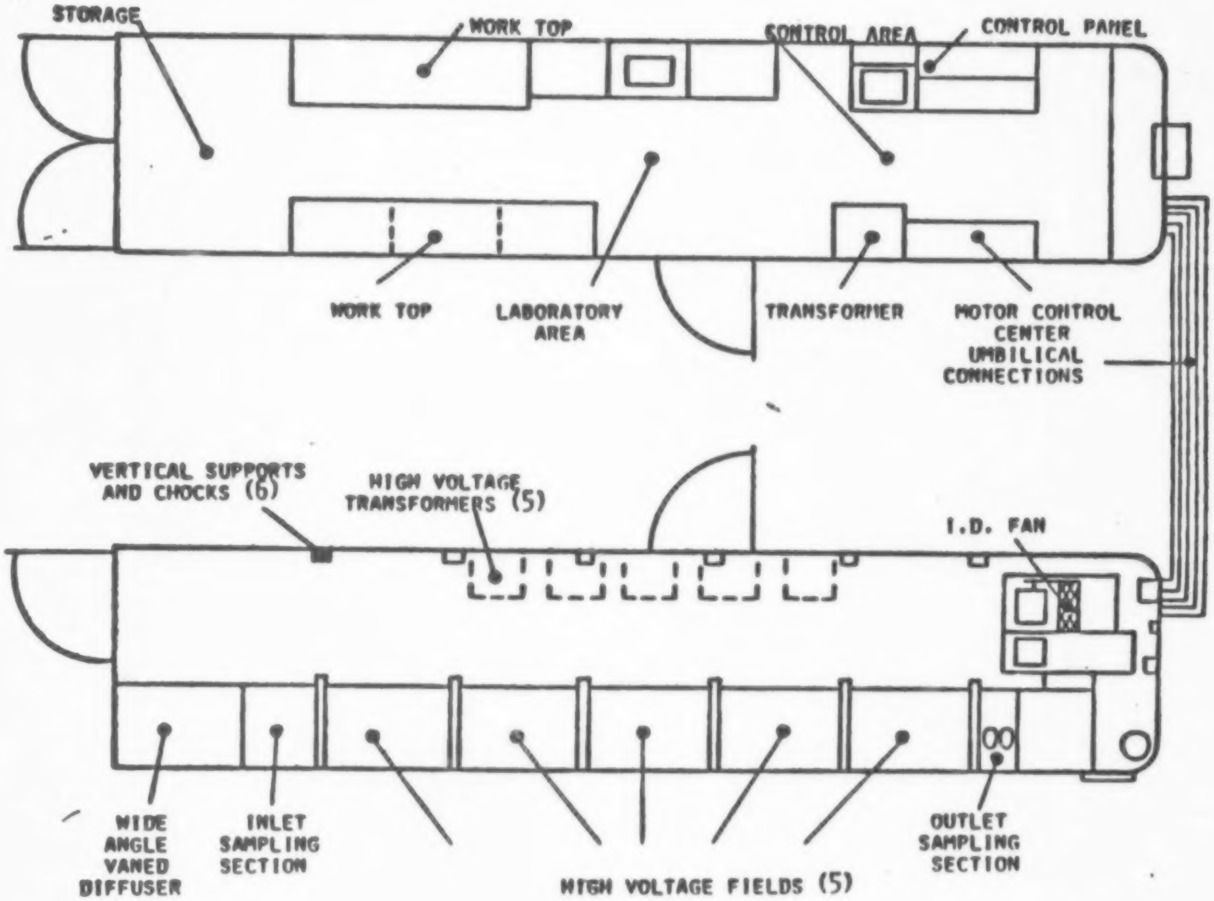
STORAGE
WORK TOP
CONTROL AREA
CONTROL PANEL
WORK TOP
LABORATORY AREA
TRANSFORMER
MOTOR CONTROL CENTER
UMBILICAL CONNECTIONS
VERTICAL SUPPORTS AND CHOCKS (6)
HIGH VOLTAGE TRANSFORMERS (5)
I.D. FAN
WIDE ANGLE VANED DIFFUSER
INLET SAMPLING SECTION
HIGH VOLTAGE FIELDS (5)
OUTLET SAMPLING SECTION

Figure 1. Plan view of mobile ESP facility

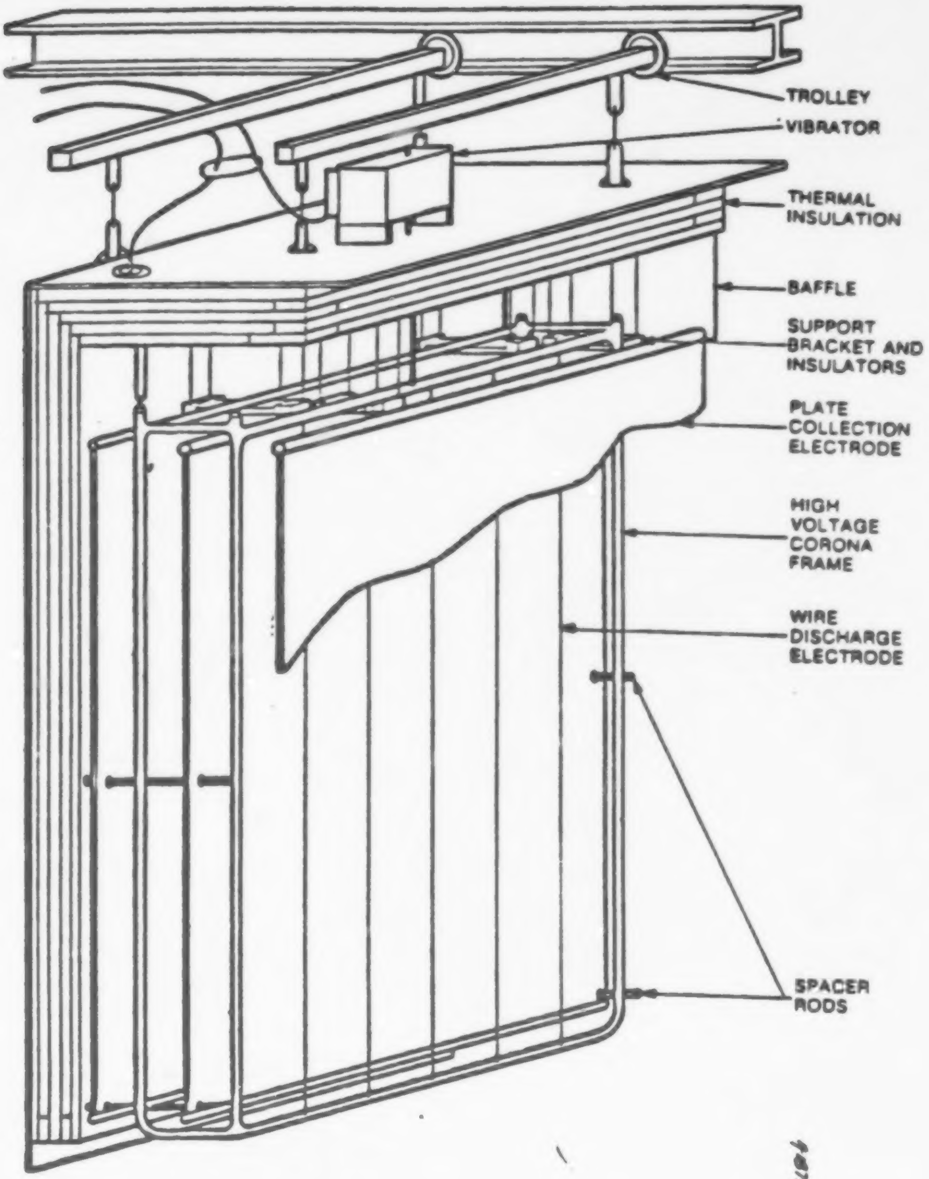
TROLLEY
VIBRATOR
THERMAL INSULATION
BAFFLE
SUPPORT BRACKET AND INSULATORS
PLATE COLLECTION ELECTRODE
HIGH VOLTAGE CORONA FRAME
WIRE DISCHARGE ELECTRODE
SPACER RODS

Figure 2. Removable high voltage field

Table 3. FULL SCALE AND PILOT ESP DESIGN SPECIFICATIONS

	Full Scale[3]	Pilot ESP
Discharge Wire Diameter, cm	0.25	0.25
Wire-Wire Spacing, cm	10-30	18
Wire-Plate Spacing, cm	10-15	13
Specific Collection Area, (m^2/m^3/sec)	20-150	20-100
Collection Area/T-R Set, m^2	50-750	9
Aspect Ratio	0.5-1.5	0.67
Specific Corona Power (watts/m^3/sec)	100-1,000	100-1,000
Current Density, nA/cm^2	5-70	5-100
Gas Velocity, m/sec	1-5	0.5-2
No. of Fields in Series	2-8	2-5

SITE INSTALLATION

A slipstream was withdrawn at a location downstream from the combustion-air preheater and upstream from the pollution control equipment. A 10" pipe located across the midpoint of the process stream served as the means of sample extraction. Sixty feet of heat-traced, insulated 10" pipe transported the slipstream to the pilot precipitator. Ambient air quality standards dictated the need for returning the particulate-abated stream to the access locations for subsequent sulfur dioxide (SO_2) removal. An access door (2½' x 4') was fitted to the stack to accommodate the extraction and return connections, along with a 4" coupling for in situ resistivity measurements. Figure 3 illustrates the positioning of the access, ducting, process unit, and sampling and injection locations.

4.0 PROGRAM METHODOLOGY

PILOT PRECIPITATOR OPERATION

To ensure that the test program was conducted on a sound basis with specific guidelines, protocol for installation, preparation, operation and data acquisition was established and is discussed below.

Installation

Considerations for locating the slipstream access point required that:

1. The conditions of the process stream be typical for those of full-scale control unit installation.
2. A representative stream could be withdrawn from the process effluent, i.e., flow disturbances are relatively absent.
3. The location and routing be appropriate for the transport and maintenance of a representative stream.

Operation

The normal operating schedule allowed for one- week test increments, starting at noon Monday and continuing until Friday evening. Operating on a continuous rather than daily start-up/shutdown basis enhanced data credibility and reliability for the following reasons:

1. Steady state conditions would be maintained rather than approached.

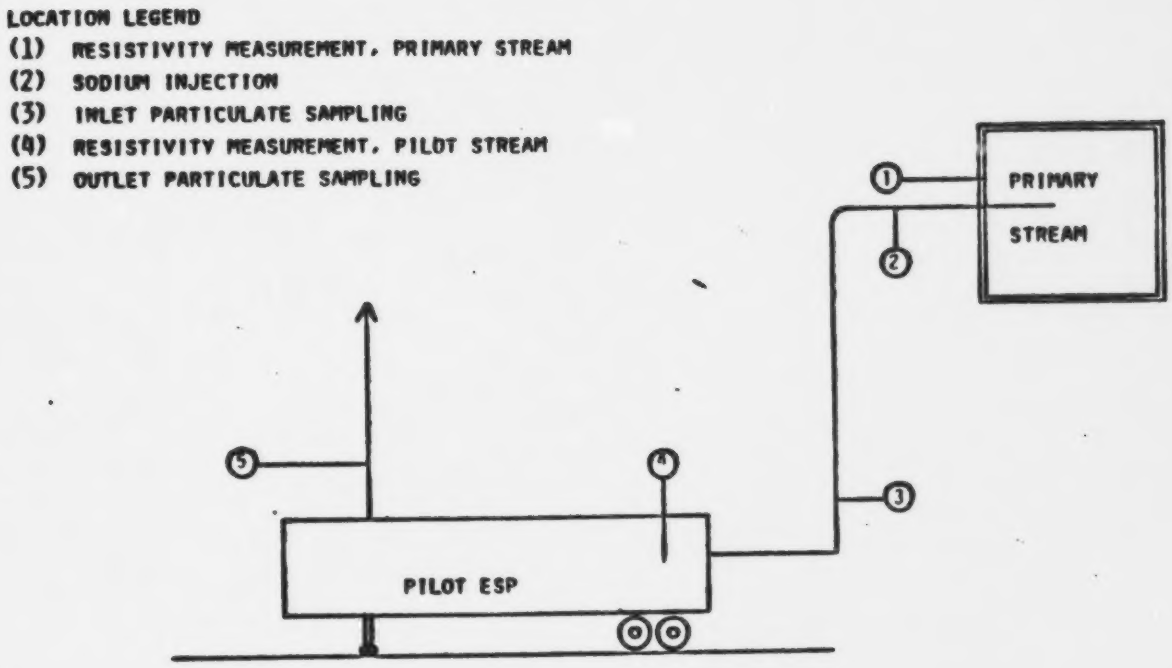
LOCATION LEGEND
(1) RESISTIVITY MEASUREMENT, PRIMARY STREAM
(2) SODIUM INJECTION
(3) INLET PARTICULATE SAMPLING
(4) RESISTIVITY MEASUREMENT, PILOT STREAM
(5) OUTLET PARTICULATE SAMPLING
PRIMARY
STREAM
①
②
③
④
⑤
PILOT ESP

Figure 3. Pilot ESP site installation

2. Extended operating time would permit clearer illustration of time-related characteristics, e.g., flyash accumulation on corona wires and collection plates.

3. Corrosive conditions due to condensation accompanying startup and shutdown periods would be minimized.

4. A uniform daily testing program could be more reliably established and maintained.

Because the reliability of the high voltage cables was limited, approximately half of the test was conducted on an interrupted rather than continuous schedule. Prior to weekly start-up, the precipitator's internal parts were cleaned in order to restore initial conditions. This process consisted of removing flyash from discharge wires and collection plates. Removal of the precipitated flyash between the base ash and sodium test increments was necessary to isolate the causal relationships of the flyash species. Since it has been shown that, due to reentrainment, rapping factors such as frequency and intensity have significant effects on effluent loading, the rapping cycles were terminated during the particulate measurement periods.[5]

Data Acquisition

The following operating data were recorded on a semi-hourly basis:

- inlet gas temperature
- outlet gas temperature
- individual voltage levels
- individual current levels

Additionally, "V-I" data (corona discharge curves) were generated before and after the daily sampling periods, and following the weekly internal cleaning. Sampling activities were conducted during normal working hours, with operating data acquisition and analytical activities being performed during the remainder of the day.

PARTICULATE MEASUREMENTS

Particulate measurements were taken using a sample train, as depicted schematically in Figure 4. Stainless steel filter holders were used with 47mm glass fiber filters to provide mass concentration data. Seven stage Brinks^{R} and U of W Mark III^{R} impactors containing greased substrates were employed to measure the inlet and outlet size distributions, respectively. A common grease mixture (20 percent Apiezon "H" with benzene) was applied to the metallic substrates used with each impactor. Quality assurance measures and procedures for conditioning, greasing, and weighing substrates were conducted in

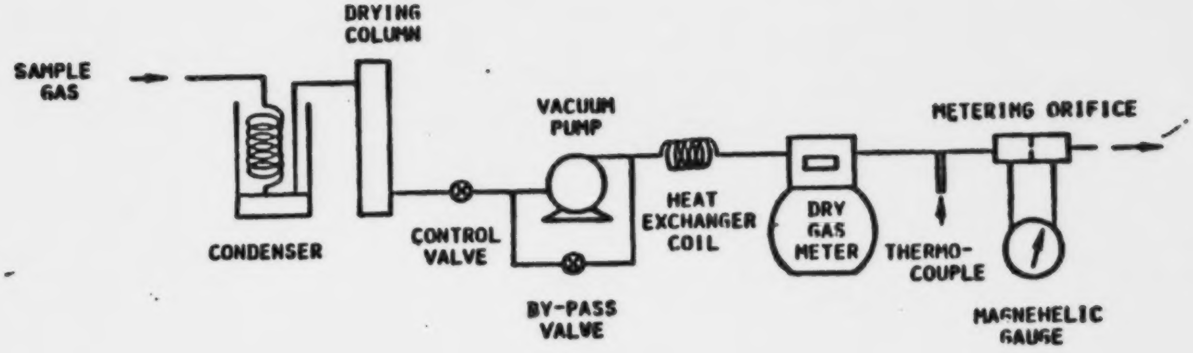
SAMPLE GAS
CONDENSER
DRYING COLUMN
CONTROL VALVE
VACUUM PUMP
BY-PASS VALVE
HEAT EXCHANGER COIL
DRY GAS METER
THERMO-COUPLE
METERING ORIFICE
MAGNEHELIC GAUGE

Figure 4. Sample train schematic

accordance with Reference 6. Sample ports, available at virtual plug-flow locations, consisted of 1" stainless steel couplings welded to the duct, 10.75" I. D.

Extractive probes (1/4" stainless tubing, 12" long) were mounted in the ports and fitted with interchangeable nozzles to allow isokinetic sample removal. The probes were positioned at average velocity locations. Particulate concentrations and size distribution determinations were conducted at inlet and outlet locations. Two determinations of each type at both locations constituted a test unit consisting of eight individual measurements. Substrate and filter weight gains were processed nightly, providing qualitative feedback on precipitator performance and data quality.

RESISTIVITY MEASUREMENTS

A point-to-plane probe was used to measure in situ resistivity. Maintenance and procedural operations were conducted in accordance with the recommended practice for resistivity measurements.[7] The primary location for these determinations was a reduced velocity area (3-5 m/sec.) immediately upstream from the first high voltage field. Longer sampling periods (1-2 hours) were required for the relaxed flow region (1-2 hours) than for the primary process (½-1 hour). Quality assurance tests were conducted in situ at the slipstream access, yielding consistently comparable resistivity levels.

Three values of resistivity are reported for each test unit, and are labeled:

- P_A (Spark Method at Breakdown Strength)
- P_B (Spark Method at Electric Field Strength = 10 kv/cm)
- P_C (Re: V-I Method).

Each resistivity value is calculated as the ratio of the electric field to current density. A complete discussion of the equipment, procedure, and significance of resistivity measurement is contained in Reference 7.

5.0 DISCUSSION OF PERFORMANCE RESULTS

The data base presented in the following sections consists of five measurement categories:

- mass balance of sodium material
- specific resistivity
- operating measurements

- particulate mass measurements

- particulate size distribution measurements

Unavoidable fluctuations in boiler load, gas temperature, and precipitator operation occurred throughout the test program, but these fluctuations did not, in the final analysis, obscure the results of the demonstration test program. The data clearly support the general conclusions that, for sodium carbonate addition:

- specific resistivity of the particulate was reduced,

- precipitator operating levels were improved, and

- particulate collection efficiency (total and fractional) was enhanced.

CONDITIONING BY SODIUM CARBONATE ADDITION

Resistivity conditioning was achieved by metering and pneumatically injecting anhydrous sodium carbonate into the slipstream immediately adjacent to the primary stream (Figure 3). Mixing was achieved by injecting the material into the center of the slipstream, and transporting the mixture through 60 feet of duct, four 90° elbows, and the flow rectification sections at the trailer entrance. A previous in-house program, in which sodium carbonate was injected 35 feet upstream from the flow rectification section, demonstrated, by analyses of samples taken from each field, that equal and consistent distribution could be achieved. Injection was accomplished through use of a screwfeeder, an air injector, and an air compressor. Figure 5 illustrates the configuration of the injection assembly. The material was metered through the calibrated screwfeeder into the injector, where compressed and induced air entrained and delivered it through a gently bending probe into the slipstream.

The amount of sodium carbonate to be injected was calculated as sodium oxide, with conversion being made on the basis of molecular weight ratio:

$$\frac{\text{Mole. Wgt, Na}_2\text{O} = 62}{\text{Mole. Wgt, Na}_2\text{O CO} = 106} = 0.585$$

Thus, under most conditions, 11.5 gm/min of sodium carbonate was added to represent 6.7 gm/min as sodium oxide, reflecting a 5.0 percent injection rate relative to a mean flyash rate of 135 gm/min.

Analysis of the collected ash from the high voltage fields (Table 4) shows an average 1.16 percent differential collection rate in sodium oxide content between the base and conditional ash. These independent determinations reveal an unaccountable portion for a mass balance of sodium material. The discrepancy between the injection and collection rates suggests two possible occurrences:

1. Deposition of the sodium material between injection and electrostatic collection, and

2. Penetration of the sodium through the ESP.

The latter contingency cannot be well supported, since the unaccountable portion of sodium carbonate is ten times the concentration of the penetrating ash. The author suggests that the unaccountable sodium material was deposited during transport to the ESP through a non-optimum injection system.

The beneficial irony of sodium conditioning is that one gram of sodium oxide caused an equal amount of flyash to be collected. Numerical analysis correlating the precipitated amounts of sodium and the causal increase in flyash shows a 1.16/1.0 relationship.

The term "conditioning" in the context of controlling particle resistivity usually implies the addition of moisture or chemicals to the carrier gas. In a broader sense, conditioning includes effectively controlling particle resistivity by any appropriate means, such as temperature or composition control.

Conditioning by sodium carbonate injection, unlike moisture and chemical conditioning, does not change the conductivity of the original flyash particles. The conditioning effect is achieved by simply injecting a conductive material into the stream, which, when collected on the plates with the original high resistivity material, provides ionic carriers or additional electrical paths for the corona current. The insulating effect of the high resistivity flyash is reduced, allowing the precipitator to treat the stream at a lower resistivity level.

The purpose of these tests was to determine the improvement in precipitator performance associated with sodium carbonate addition. To date, this approach to conditioning has several limitations:

- Some applications require large quantities of conductive material.
- Some economically viable conductive materials are unavailable.
- The material is difficult to adequately distribute into the process stream.
- Uncertainties result from selective precipitation of the conductive material.

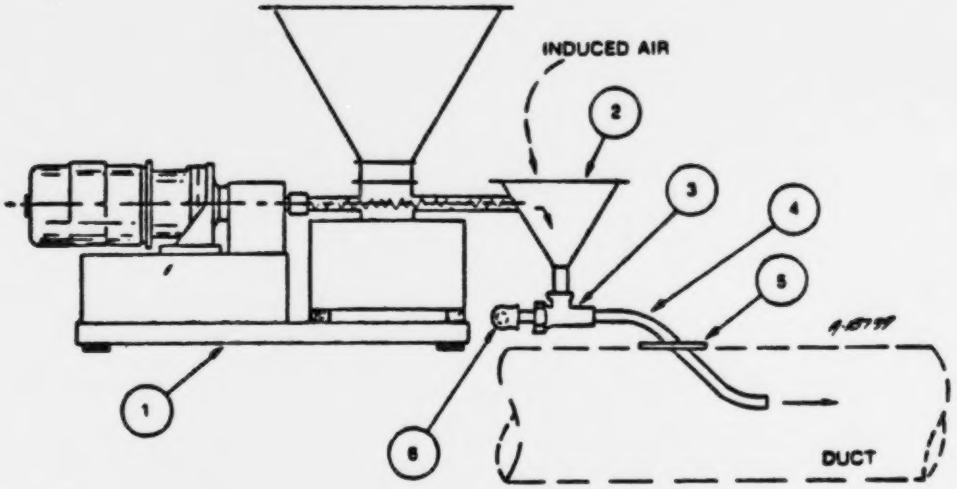

1. VIBRASCREW FEEDER SCR-20. 3/8 SCREW. 0-0.1 CFH
2. FABRICATED CONNECTION BETWEEN FEEDER AND INJECTOR
3. JET INJECTOR. McMASTER-CARR, P.O. BOX 4355, CHICAGO 60680. CAT. 4977K-11
4. FABRICATED PIPE
5. COVER PLATE APPROX. 6" DIAMETER. WELDED TO BENT PIPE
6. COMPRESSED AIR SUPPLY LINE. APPROX. 70 PSIG

Figure 5. Depiction of sodium injection equipment

Table 4A FLYASH CONSTITUENCY DATA

NO Sodium Injection

	6/24 Cell 1	6/24 Cell 2	6/24 Cell 3	6/30 Cell 1	6/30 Cell 2	6/30 Cell 5	8/23 Cell 3	8/23 Cell 4	8/23 Cell 5	8/24 Cell 3	8/24 Cell 4	8/24 Cell 5
Li_2O	0.04	0.05	0.05	0.04	0.04	0.04	0.04	0.04	0.04	0.04	0.04	0.04
Na_2O	0.60	0.58	0.56	0.56	0.74	0.75	0.61	0.61	0.71	0.59	0.59	0.61
K_2O	0.8	0.7	1.0	0.7	0.7	0.9	0.8	0.8	0.8	0.7	0.7	0.8
MgO	7.2	7.5	7.7	5.8	6.4	6.7	6.5	6.8	6.5	6.4	6.8	6.8
CaO	18.5	18.3	19.5	17.0	17.7	17.8	19.6	19.3	18.6	19.3	20.5	19.7
Fe_2O_3	4.0	3.5	3.8	3.7	3.5	3.2	3.9	3.2	3.4	3.3	3.8	3.3
Al_2O_3	23.8	23.8	-	21.4	23.3	24.2	23.7	24.4	25.0	23.3	23.6	-
SiO_2	41.5	41.1	-	44.5	43.2	41.9	41.8	40.7	40.2	42.1	39.3	-
TiO_2	1.0	1.0	0.9	0.9	1.0	0.9	0.7	0.7	0.6	0.6	0.7	-
P_2O_5	0.4	0.4	0.3	0.3	0.3	0.4	0.5	0.9	0.6	0.5	0.6	0.6
SO_3	1.1	-	-	1.3	-	-	1.2	1.4	1.7	1.2	1.5	-
LOI	0.5	0.5	0.7	0.5	0.6	0.6	0.3	0.2	0.6	0.5	0.4	-

RESISTIVITY DATA AND RESULTS

In order to quantify the resistivity suppression of sodium conditioning, resistivity measurements were taken on (1) the primary stream near the pilot stream access location, (2) the slipstream containing the base flyash, and (3) the slipstream containing the base ash plus sodium carbonate.

All determinations were made with an in situ probe designed by Southern Research Institute[7]. The design of the probe and the procedure provide the following data as presented in Table 5:

1. P_A - Resistivity value taken at the breakdown strength of the sample.
2. P_B - Resistivity value for electric field strength = 10 KV/CM.
3. P_C - Resistivity value determined by the comparison of volt-amp relationships before and after precipitation of the sample.
4. E_A - Electric field strength at breakdown.

P_A is the preferred resistivity value, because voltage is applied directly to the electrostatically precipitated sample, and determination is made at the breakdown strength of the sampled ash layer.

The other two resistivity values, P_B and P_C, are less significant to precipitator aPplications, but are offered to support the comparison between the two ash species. The last column in Table 5, EA, represents the breakdown strengths of the individual samples. Compilation of over 35 tests resulted in the following log-averaged resistivity values:

a. 2.5×10^{12} OHM-CM (on the primary stream at 130-135°C).

b. 2.1×10^{12} OHM-CM (on the slipstream at 107-115°C with the base ash).

c. 3.7×10^{11} OHM-CM (on the slipstream at 107-115°C with the base ash and 1.2 percent sodium oxide/base ash addition).

Comparison of these values indicates that:

- The characteristic resistivity of the gas and particulate stream were preserved during transport to the pilot unit.

Table 5. RESISTIVITY DATA*

Run No.	P_A	P_B	P_C	E_A
6/22/77**	2.9 E12	2.1 E12	4.5 E11	41, 22, 24
6/23/77**	2.1 E12	2.7 E12	3.8 E11	10, 17, 12, 17
4	- - -	- - -	3.6 E11	- - -
5	5.9 E11	5.2 E11	2.7 E11	19
6	1.1 E12	2.2 E12	2.1 E12	35
7	1.6 E11	- - -	4.0 E11	4
8	4.1 E11	6.8 E11	7.3 E11	32, 27
9	5.0 E11	1.0 E11	7.6 E11	26, 26, 26
10	3.2 E11	5.6 E11	7.3 E11	10, 25, 27
11	1.0 E12	1.7 E12	2.2 E12	20
12	6.0 E12	1.0 E12	2.5 E12	25
13	2.1 E12	5.0 E12	2.2 E12	8, 50
14	- - -	- - -	1.5 E12	- - -
15	- - -	- - -	6.2 E11	- - -
16	2.0 E11	3.6 E11	1.5 E12	55, 33, 73
17	- - -	- - -	2.2 E12	- - -
18	8.0 E11	1.3 E12	2.5 E12	29, 50, 40
19	4.1 E12	6.5 E12	2.6 E12	39, 26
20	2.5 E12	6.0 E12	2.8 E12	32, 37

2.17 E11 = Log Mean Resistivity for Conditioned Ash @ 107-115°C

3.70 E12 = Log Mean Resistivity for Base Ash @ 107-115°C

P_A = Resistivity Determined by Spark Method @ Breakdown Field (OHM-CM)

P_B = Resistivity Determined by Spark Method @ Electric Field Strength = 10 KV/CM

P_C = Resistivity Determined by V-I Method

E_A = Electric Field Strength @ Breakdown (KV/CM)

---

* Data Obtained at Pilot ESP Inlet

** Data Obtained on Primary Stream at the Pilot Stream Access Location

- A sixfold reduction in specific resistivity is attributable to sodium injection.

Research by Bickelhaupt has shown that, for surface resistivity of flyash, the alkali metal constituents, particulary sodium, serve as the principal charge carriers in the conduction process.[9] This observation led to two previous field tests demonstrating that sodium conditioning did reduce specific resistivity, and that the reduction was predictable by the relationship of:

$$P_1/P_2 = (W_2)^2/(W_1)^2$$

P_1 = measured resistivity in OHM-CM for W_2

P_2 = predicted resistivity in OHM-CM for W_2

W_1 = measured weight percent Na_2O in ash

W_2 = added weight percent Na_2O in ash.[10]

Demonstration of the sensitive and predictable relationship between sodium content and resistivity is shown from the test data:

For $W_1 = 0.63$, $W_2 = 1.79$, $P = 2.1 \times 10^{12}$:

$P_2 = 2.6 \times 10^{11}$ OHM-CM

The predicted value correlates with the measured resistivity value of 3.7×10^{11} OHM-CM.

OPERATIONAL DATA

Operating corona points and the associated V-I data over the allowable range were taken regularly during the program. The operating corona data reflect the electrical conditions during the sampling period for a given test. It should be noted that the control of the transformer-rectifier sets was accomplished manually, as the pilot facility was not equipped with automatic controllers customarily included in full-sized precipitators. It should also be pointed out that the operating corona points were set 4 KV lower than the maximum allowed. This was done to prevent frequent high voltage cable breakdowns responsible for delays incurred during the initial testing phase.

Table 6 and Figure 6 depict actual and comparative current densities for the base ash and ash-with-sodium conditioning tests. The above table and figure provide a histogram of the current densities related to on-line time following internal purging. The degradation rates are comparable for each species, but the base ash curves show more severe current reductions as they approach steady

Table 6 PRECIPITATOR ELECTRICAL OPERATING DATA
SECONDARY VOLTAGE (KV), CURRENT DENSITY (nA/cm^2)

Base Flyash

Cell										
1	39,11	40,4.2	40,2.3							
2	39,21	40,3.1	40,1.1							
3				38,18	39,10	40,10	40,27	38,10	36,6.0	36,4.0
4				39,24	37,16	40,21	38,21	38,11	40,7.0	38,3.0
5	41,28	39,9.0	39,6.3	39,22	36,12	40,25	38,35	36,26	32,13	32,8.0
Time[1] (days)	1	1½	2	¼	½	1	¼	1	2	3
Test No.	1	2	3	11	12	13	17	18	19	20

Base Flyash + Sodium

Cell										
1	46,36	46,13	39,8.0	42,7.8						
2	39,27	42,16	36,9.0	41,19	44,9.5					
3			35,14	37,26	40,18	42,10	42,9.0	38,23	40,14	41–19
4			39,28	37,26	40,20	41,13	41,10	40,34	40,23	39–20
5	38,31	38,30	35,41	37,23	39,24	40,21	36,5.0	38,38	40,50	
Time	½	1	1½	2	2½	3	3½	¼	1	2
Test No.	4	5	6	7	8	9	10	14	15	16

[1] Elapsed time operating since internal purge.

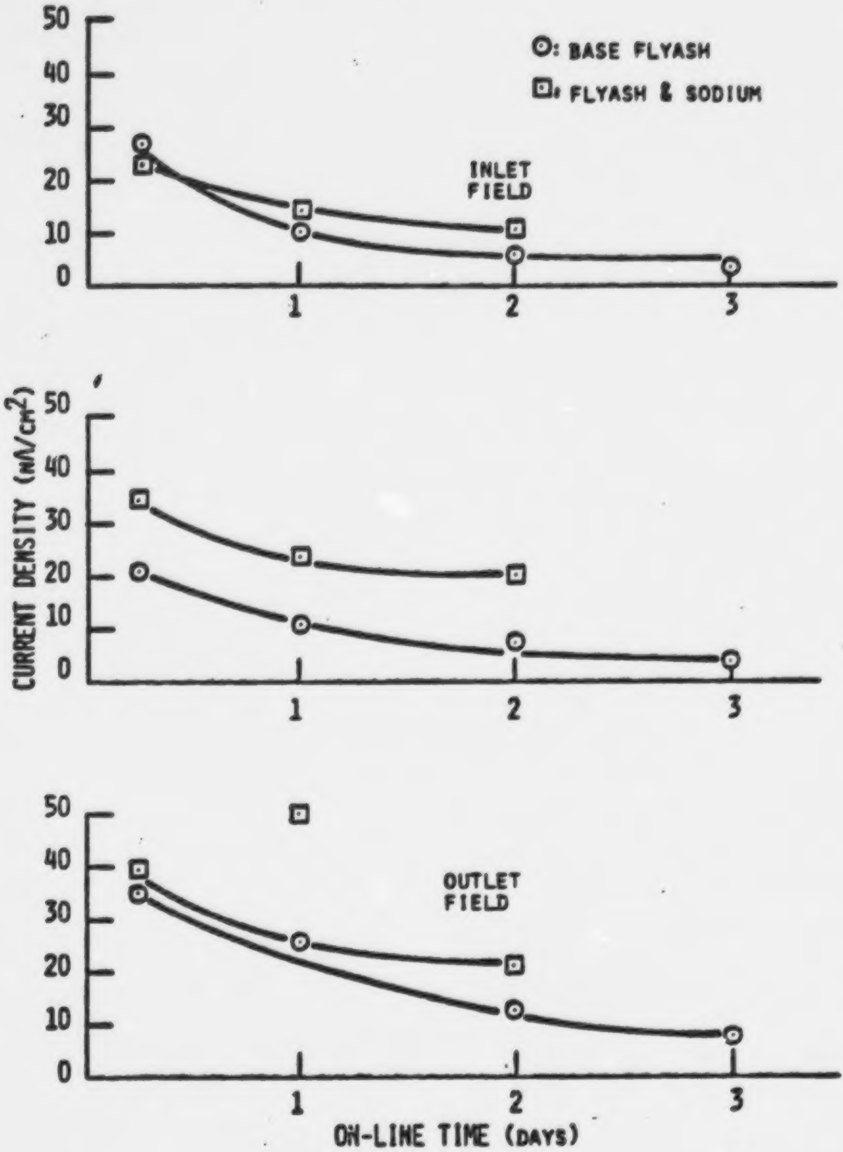

Figure 6. Current density vs. on-line time

state conditions. The inlet field histograms reflect a 2-3 factor improvement in achievable current densities for the sodium conditioning test series, having achieved a 10 nA/cm^2 level compared to a 4 nA/cm^2 level for the base ash series. A consistently comparable relationship exists for the outlet fields, with the sodium series achieving 20 nA/cm^2, relative to 7 nA/cm^2. The second or middle field histogram indicates improvement for the sodium series, achieving 20 nA/cm^2 compared to 4 nA/cm^2 for the base ash.

Reasonable correlation exists between the independent resistivity measurements and the achievable precipitator current densities approaching steady state conditions. The relationship between resistivity (P) and current density (C. D.) is defined by P=E/C. D., where E is the dielectric (breakdown) strength of the collected dust layer. Assigning the limiting breakdown strength of 10 KV/cm for each ash species, one can calculate the achievable current density from the log-averaged resistivity values. For the base ash (P=2.1 x 10^{12} OHM-CM), the calculated current density is 4.8 nA/cm^2. For sodium-conditioned ash (3.7 x 10^{11} OHM-CM the calculated value is 27 nA/cm^2. These theoretically calculated values correspond with the empirical values averaged from the operational data (5.0 and 15 nA/cm^2, respectively).

Comparison of the achievable voltage levels shown in Figure 7 for the two ashes are not as dramatic as the current density comparison but higher voltages were consistently obtained for the sodium treated ash.

The relationship of the voltage applied to each precipitation field and the resulting current (corona discharge curves) may be analyzed to gain insight into precipitator operation and performance. Figure 8 portrays the corona discharge curves for the base and conditioned ashes in graphical form. These curves show the characteristic profile of the volt-amp relationships from each field for steady state conditions. Knowledge of the meaning of the V-I curves is a fundamental tool necessary for proper operation of a precipitator. These data can characterize the following parameters/conditions:

- corona current leakage
- corona initiation voltage
- effective corona wire size
- effective wire-to-plate spacing
- alignment effects
- specific resistivity level
- specific collection area

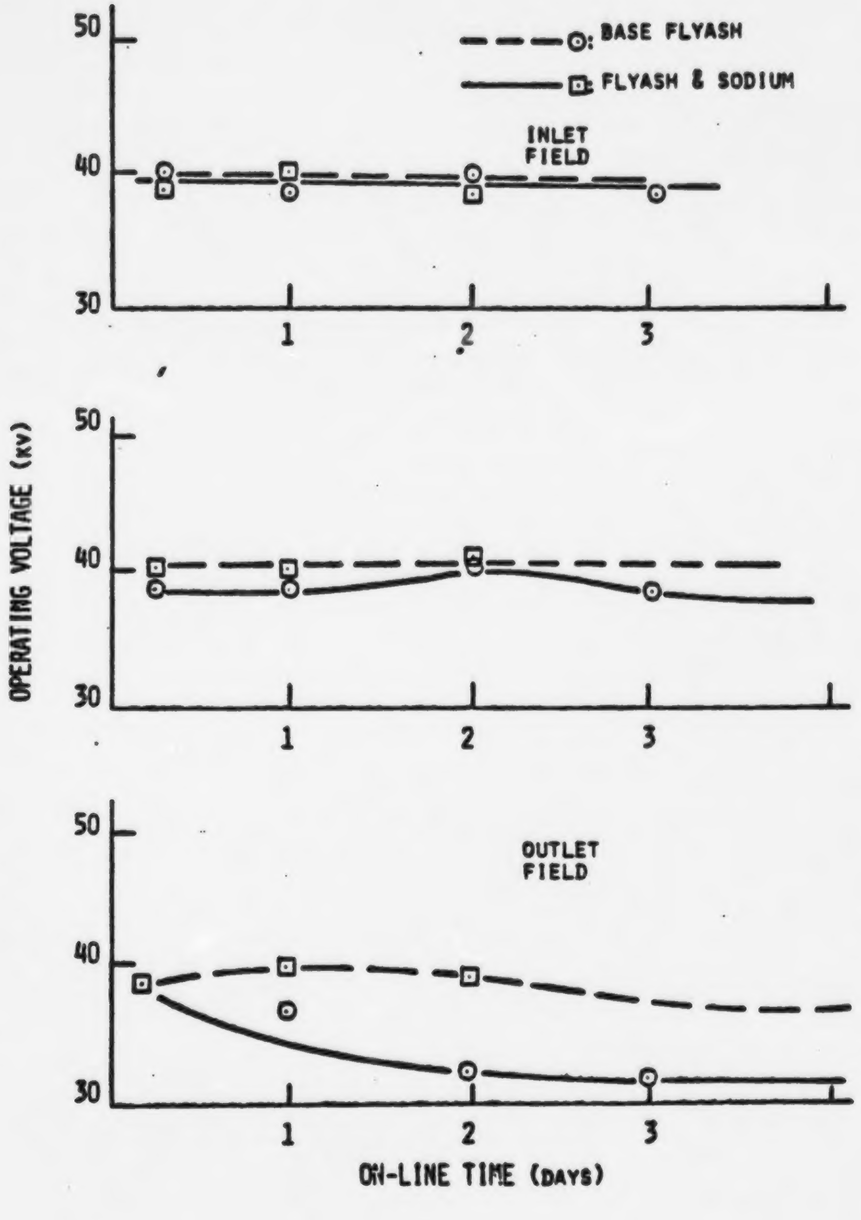

Figure 7. Operating voltage vs. on-line time

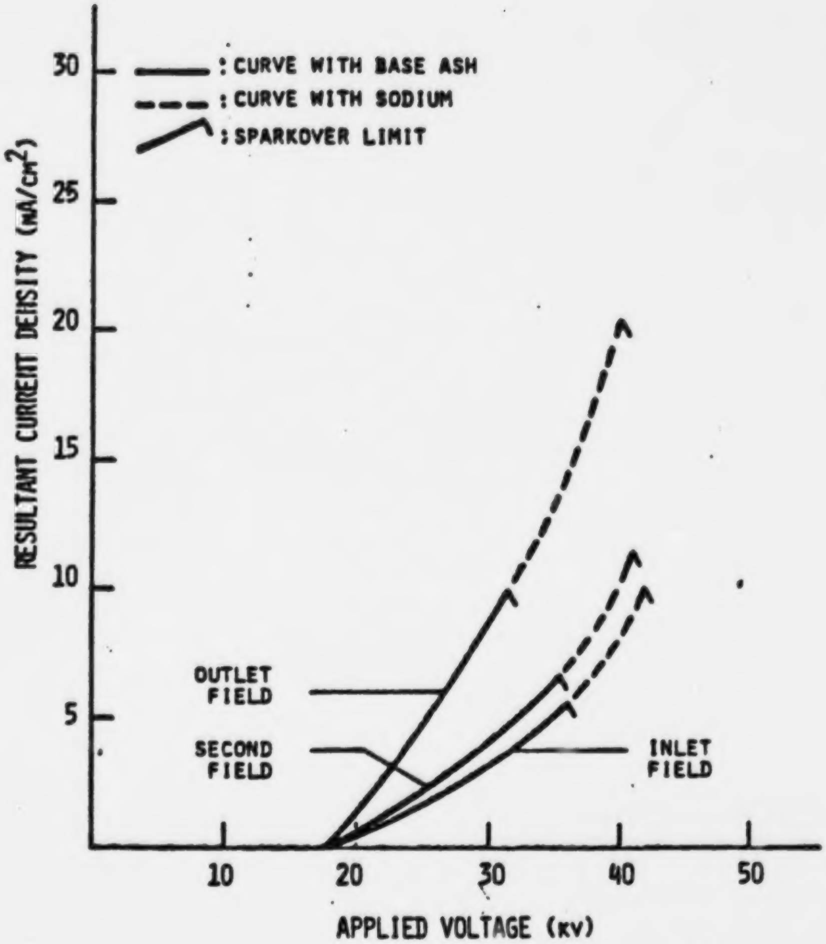

Figure 8. Corona discharge curves

- breakdown voltage
- achievable current density
- concentration of fine particulate
- relative position of each precipitation field (inlet, second ..., outlet)
- variations in emission source process

Analysis and interpretation of these curves provide the basis for the following generalities referenced in other sections of this report:

1. A reduction in specific resistivity between the base ash and sodium-plus-ash test series.
2. An improvement in achievable corona point for the sodium series.
3. An improvement in expected collection performance for the sodium series.
4. The degradation in performance related to elapsed time from internal clean-up.
5. A small increase in effective wire size due to ash build-up.[11]

PARTICULATE COLLECTION RESULTS

Particulate Concentration Results

Table 7 shows the averages of the inlet and outlet concentrations per test used to calculate the average collection efficiency values in Table 9 and Figure 9. The inlet data exhibit considerable scatter resulting from the inconsistent probe catches apparent in the raw data. Due to the reduced flyash concentration and probe catch material, the outlet data offer reasonable agreement and consistency.

The apparent scatter in the particulate data depicts an ordered trend when the elasped operating time from the precipitator "cleaning" is taken into account. As previously noted, the corona wires and collection plates were restored to a clean state between conditioning and nonconditioning test series. The degradation in performance evident particularly for the base ash was caused by the accumulation of high resistivity ash on the collection plate and the discharge electrodes. The marginal differences in performance for the tests after recent cleaning do not reflect the performance levels achievable for steady state operation. According to a best fit approach from Figure 14, sodium conditioning was responsible for reducing outlet loadings from 140 to 40 mg/Ds m^3 (0.122 lb to 0.0361 lb/10^6 Btu), resulting in an improvement in collection efficiency from 98.19 to 99.46 percent.

Table 7
Average of Particulate Data
(mg/SDm^3)

Test	Inlet	Outlet
1	8,657	182
2	11,630	133
3	14,310	394
4	5,198	29.1
5	7,076	45.6
6	19,950	40.1
7	4,259	46.3
8	8,290	47.6
9	3,824	38.2
10	5,977	36.2
11	4,642	33.2
12	4,630	30.5
13	4,649	35.3
14	8,061	17.3
15	8,633	22.9
16	7,282	34.1
17	5,587	50.4
18	3,847	44.6
19	5,908	117
20	8,610	137

Mean: 7,557

Table 8. SUMMARY OF PARTICULATE DATA AND EFFICIENCY RESULTS

Data	Base Flyash	Base Ash with Sodium
Inlet concentration (Mg/DNM^3)	7,550	7,550
Outlet concentration (Mg/DNM^3)	140	40
Inlet mean particle size (μ)	15	15
Outlet Mean particle size (μ)	2.6	2.1
Efficiency		
Total mass (% wt.)	98.2	99.5
Fractional @:		
3.0 μ	98.8	99.7
1.0 μ	94	98
0.5 μ	81	94
0.3 μ	70	92

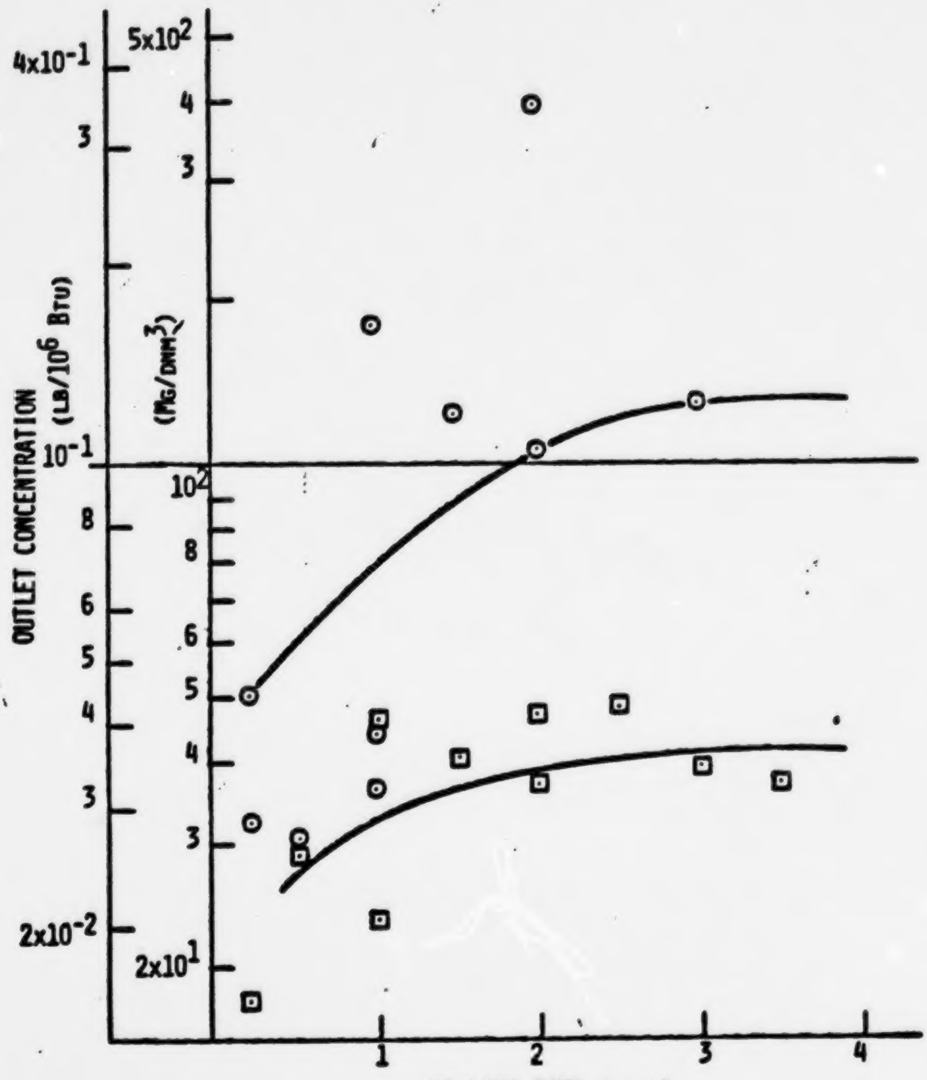

Figure 9. Precipitator collection performance

Table 9 PARTICLE SIZE DATA AND FRACTIONAL EFFICIENCY RESULTS[1]

Test No.	Mass Mean Diameter		Fractional Efficiency @			
	Inlet	Outlet				
1	8.6	1.6	29.3	42.3	90.7	89.7
2	9.7	1.7	89.7	90.9	94.9	99.2
3	26.0	3.5	87.9	90.5	87.2	96.0
4	13.5					
5	13.0	1.6	85.7	88.3	93.5	99.7
6	8.8	1.6	93.3	94.0	97.4	99.5
7	7.4	1.2	93.2	94.6	97.7	99.5
8	7.8	1.4	94.9	96.4	98.7	99.8
9	7.4	1.7	79.6	83.7	94.9	99.8
10	9.9	3.0	93.3	95.6	97.8	99.6
11	11.5	2.1	37.1	71.2	97.7	99.6
12	21.0	1.9	61.1	72.0	97.0	99.4
13	8.0	1.2	92.5	95.9	98.7	99.9
14	23.3	1.4	96.7	98.5	99.1	99.9
15	17.0	2.3	91.5	93.4	98.1	99.9
16	16.0	4.8	98.3	98.4	99.1	99.9
17	12.0	2.1	37.5	78.7	93.2	99.7
18	22.5	1.4	85.0	88.6	97.0	99.7
19	27.0	5.5	90.7	93.5	93.1	99.5
20	29.0	4.7	83.2	88.0	90.0	96.0
Base ash mean:		2.6	69.4	81.2	93.9	98.8
Sodium mean:		2.1	91.8	93.7	97.4	99.7

---

[1] Data obtained from daily averages.

PARTICLE SIZE AND FRACTIONAL EFFICIENCY RESULTS

Brink and the University of Washington (U of W) impactors were employed for obtaining size measurements on the inlet and outlet streams, respectively. Quality assurance measures and proceudres for conditioning and weighing substrates were performed in consistence with EPA/IERL specifications. Due to small weight losses on the greased substrates for the U of W, trial impactor flowrate was reduced for all subsequent tests from 189cc/S to 142cc/S. Evidence of substrate scouring was consequently eliminated with flowrate reduction.

Table 9 presents the particle size data and fractional efficiency results for all test runs. Mass mean diameter on the inlet ranged from 8-29 , with an average M.M.D. of 15 . The outlet stream contained M.M.D's from 1.2—5.5 , with 2.1 and 2.6 being the average mean size for the sodium conditioning and base ash effluents, respectively.

Figure 10 demonstrates the improved fractional collection performance associated with sodium conditioning, particularly in the submicron range.

REFERENCES

1. Private Communication with Bob Olmstead, Plant Superintendent, Montana Power Corrette Station, Billings, Montana.

2. McCain, J.D., CEA Variable Throat Venturi Scrubber Evaluation. EPA-600/7-78-094, U.S. Environmental Protection Agency, Research Triangle Park, N.C., June, 1978.

3. White, H.J., INDUSTRIAL ELECTROSTATIC PRECIPITATION, Reading, Mass., Addison-Wesley, 1963, p. 359.

4. "MOBILE ESP OPERATING MANUAL," Environmental Sciences Group, Naval Surface Weapons Center, Dahlgren, VA., October, 1976.

5. Spencer, H.W., A Study of Rapping Reentrainment in a Nearly Full-Scale Pilot Electrostatic Precipitator. EPA-600/2-76-140, U.S. Environmental Protection Agency, Research Triangle Park, NC, 1976.

6. Harris, D.B., Procedures For Cascade Impactor Calibration & Operation in Process Streams, EPA-600/2-76-144, U.S. Environmental Protection Agency, Research Triangle Park, NC.

7. Nichols, G.N., Test Methods & Apparatus For Conducting Resistivity Measurements, U.S. Environmental Protection Agency, Contract No. 68-02-1083, Final Report No. 3121-III., Sept.,1977.

8. White, H.J., Op. Cit., p. 312.

9. Bickerhaupt. R.E., Surface Resistivity & The Chemical Composition of Flyash, Proceedings From Symposium On Electrostatic Precipitators For The Control of Fine Particles, For National Environmental Research Center, PB 240 440, Jan., 1975, p. 246.

10. Bickelhaupt, R.E., SODIUM CONDITIONING TO REDUCE FLY ASH RESISTIVITY, EPA-650/2-74-092, U.S. Environmental Protection Agency, Research Triangle Park, NC.

11. Banks, S.M., McDonald, J.R., Sparks, L.E., VOLTAGE CURRENT DATA FROM ELECTROSTATIC PRECIPITATORS UNDER NORMAL AND ABNORMAL CONDITIONS, Proceedings: PARTICULATE COLLECTION PROBLEMS USING EPA'S IN THE METALLURGICAC INDUSTRY, EPA-600/2-77-208, U.S. Environmental Protection Agency, Research Triangle Park, NC, October, 1977.

ACKNOWLEDGEMENTS

This program was sponsored by EPA with participation by Montana Power Company, Southern Research Institute, Monsanto Research Corporation, and Acurex/Aerotherm. The program was initiated under EPA Contract No. 68-02-1816 with Monsanto Research Corporation, and completed under Contract No. 68-02-2646 with Aerotherm.

The author expresses sincere appreciation to the following individuals for their involvement with and contribution toward this program:

Ivan Bonnette, Ray Hoffman, and Bruce Knusten of Montana Power Company, Colstrip, Montana;

Dale Harmon and Les Sparks of EPA, Research Triangle Park, North Carolina;

Grady Nichols and Jerry Sutton of Southern Research Institute, Birmingham, Alabama;

Don Zanders, Billy Bowles, Tony Wojtowicz, and Mark Wherry of Monsanto Research Corporation, Dayton, Ohio;

Hal Buck, Mike Griffin, Randy Page, and Clyde Stanley of Acurex/Aerotherm, based at Research Triangle Park, North Carolina.

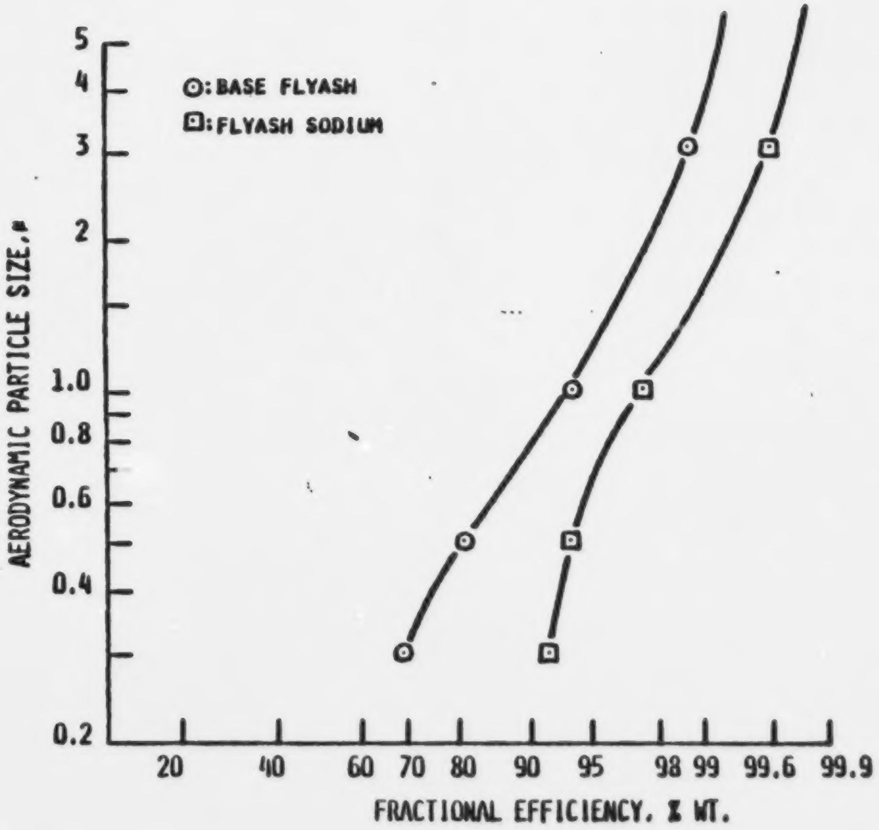

Figure 10. Comparison of mean fractional efficiency results

V.I. SIKORSKI, V.V. KUTLYASHOV

IMPROVING ELECTRICAL FEEEDING SYSTEMS FOR ELECTROSTATIC PRECIPITATORS (Thyristor Automatic Precipitator Voltage Regulator)

NIPIOTSTROM's Electrostatic Gas-Cleaning Laboratory has developed an automatic electrical-feeding parameter regulator for gas-cleaning precipitators. It is intended for use in step-up transformer-rectifier units with thyristor control of primary-power circuits. The power circuit of such a unit is illustrated in fig. 1. The automatic regulator (AR) carries out, by means of the thyristor control unit (TCU), phase regulation of tension in the primary coil of the high-voltage transformer (HVT), and consequently, in the precipitator electrodes too.

During research on the converter-electrostatic precipitator system as an object of phase regulation, basic automatic control aims were formulated:

1) Continuous electrical power supply parameter support for precipitators on a level assuring efficient gas-cleaning;

2) Increasing corona discharge stability in the precipitator's volt-ampere characteristic section corresponding to sparking and sparkover;

3) Prevention of emergency conditions arising due to electrical parameter instability of the regulated unit.

Electrostatic precipitators, examined as to their electrical load qualities, possess many characteristic features.

First of all, they show instability of the voltampere characteristic, bound with changes in many factors influencing the corona discharge intensity in the environment of an industrial stack.

Fig. 1. Functional scheme of automatic regulator and electrical scheme of power circuit of a thyristor converter unit.

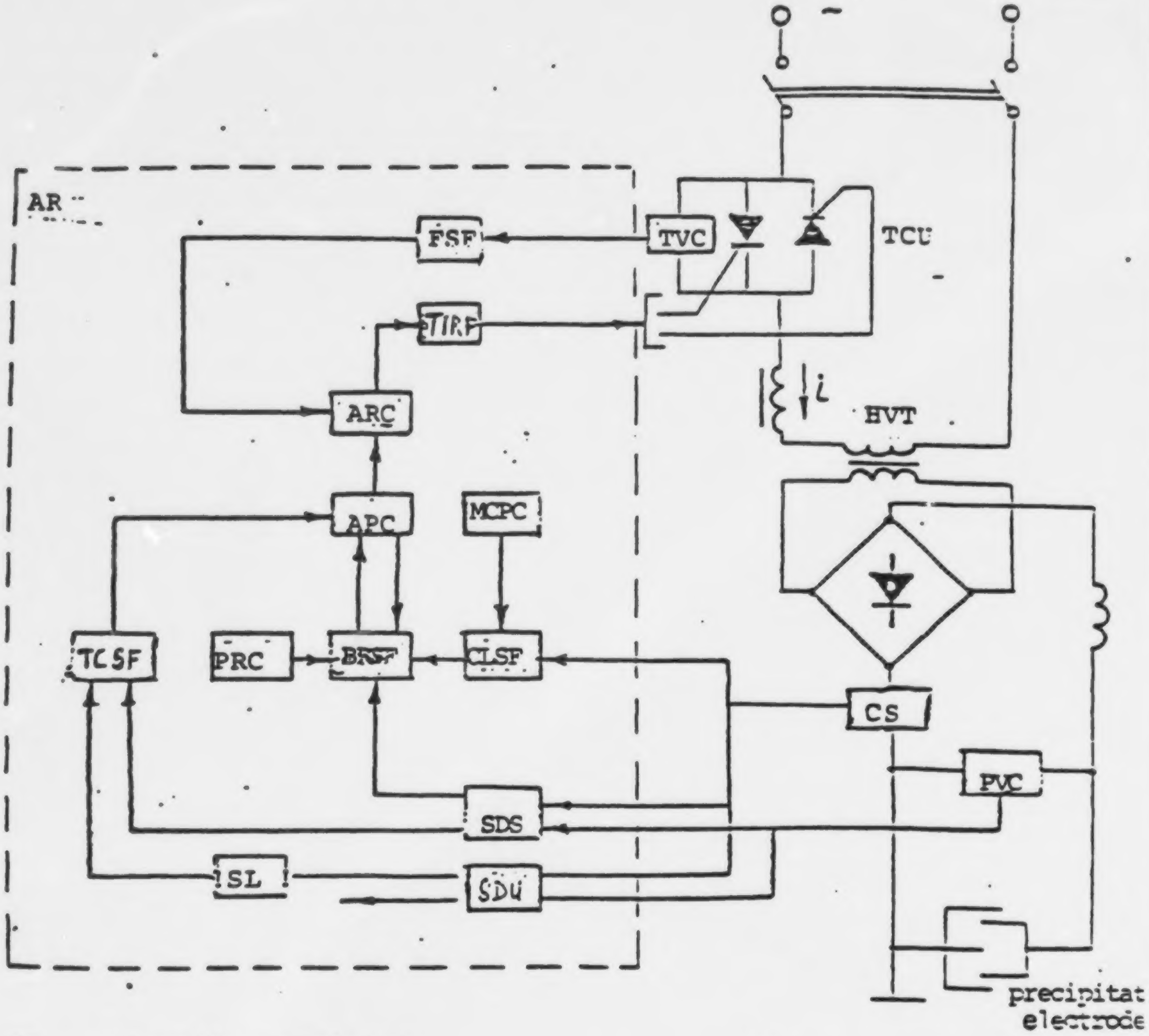
~
AR
FSF
TVC
TCU
TIRF
ARC
i
HVT
APC
MCPC
TCSF
PRC
BRSF
CLSF
CS
PVC
SDS
SL
SDU
precipitat
electrode

AR - automatic regulator
FSF - feedback signal former
TVC - thyristor voltage control
TCU - Thyristor control unit
HVT - high-voltage transformer
TIRF - Thyristor impulse regulation former
ARC - angle regulation corrector
APC - amplitude-phase converter
MCPC - maximum current power control
TCSF - transient condition signal former
PRC - program regulation control
CLSF - current limiter signal former
BRSF - basic regulator signal former

CS - current sensor
PVC - precipitator voltage controller
SDS - spark discharge selector
SDU - sensory defense ur
SL - shorting limiter

The precipitator's voltampere characteristic instability leads to frequent overloads in the power supply as a result of the latter's power limitations. An automatic regulation system should, therefore provide limits to the precipitator's working current.

The second feature is frequent sparking and spark-over in the precipitating space. They are, essentially, brief shorts in the feeding source and are accompanied by significant current impulse surges in the power circuit, and have thermal and dynamic effect upon the circuit's elements. Along with this, spark discharges are one of the basic conveyors of information about processes in the precipitating space. Spark intensity characterizes the position at a given moment of the working point in the voltampere characteristic and its degree of closeness to spark-over conditions. Using spark intensity, along with other electrical parameters, it is possible to indirectly make a judgement as to the degree of back corona intensity, dust content in the gas stream and the degree of dust contamination of the ESP electrodes.

Spark intensity is characterized by the frequency of discharge and by the energy given off by each spark.

Energy, given off by spark discharge, is proportional to the electrode system's capacity and to the voltage at the moment of discharge, squared.

The fullest characteristic of spark intensity is conversion of average frequency into average spark energy- this is the average capacity of the spark process. However, due to difficulty in measuring this parameter, upon development of a regulator serving as the spark process intensity characteristic, the relative duration of transfer elements in the precipitator current was taken, indirectly connected with spark capacity. To accomodate relative duration, it is necessary to to understand the relationship of sum duration of these processes having a space for integration period, to the integration period in relation to the expression:

$$Pu = \frac{\sum_{1}^{n} tui}{T} = \frac{n \cdot tu}{T} = fu \cdot tu,$$

where: Pu - spark intensity, μs/min;
T - integration period, min.
n - number of sparks during integration period;
t_{ui} - duration of i^{th} spark, μs;
$fu = \frac{n}{T}$ - average spark frequency, 1/ min;
$tu = \frac{\sum_{1}^{n} tui}{n}$ - average spark duration, μs

The third pecularity of precipitators is the considerable electrical capacity of its electrode system.

The precipitator capacity, together with the inductive elements of the feeding unit's power circuit, form oscillation circuits. During sparking and arc discharges, shock excitation of these circuits occurs, accompanied by high and low frequency oscillations. These oscillations cause impulse surges in the unit's circuit elements and give the essential action to the spark formation process in the precipitating space.

Specifically, excitation of the low-frequency oscillation circuit formed by the precipitator's capacity and the primary power circuit's inductiveness, having resulted due to tension reduction after spark discharge, is one of the causes of spark-over. Under these circumstances, there occurs instead of separate sparks in the precipitating area, a lengthy series of spark-overs in every half-period of line-voltage.

It is necessary to relate to precipitator peculiarities, examined in the light of electrical capacity, the increased probability of dead-end shorting and shorting through low resistance, connected basically with breaks of coronal electrodes and the jamming of dust in the precipitator hoppers.

At low angles of thyristor conductivity, caused by the preceding conditions and also due to actuation of the operating current limiting system, the average current value of short circuits may be equal to or less than the unit's nominal current, whereas its amplitude value reaches levels representing a danger to power circuit elements. Semiconductor mechanisms, thyristors and high-voltage rectifiers, are especially vulnerable in this case.

A specific feature of thyristor phase control of the power transformer's primary circuit is the possible occurence of the half-wave feeding of the primary coil. This is due to the circuits' discreteness of transmission of positive and negative half-periods, relay characteristics of the thyristors and the short duration of controlling impulses.

Half-wave conditions may subdivide into stable, caused by irreversible damage to one of the circuit's branches, and quasi-stable conditions, lasting a considerable period due to internal positive feedback, present in the process because of, for example, the occasional not switching in of single thyristors.

Positive feedback is formed in this case as a result of the presence in the circuit of non-linear induction of the power transformer's primary coil. Following transmission, the current half-cycle by-passes the non-remagnetized circuit. This induces a sharp increase of its duration and amplitude. If such a half-cycle increase prevents switching in of a thyristor in the successive half-wave, a quasi-stable half-wave occurs that is, in contrast to the stable, a reversible event.

The original omission of one of the thyristors is possible, for example, in two instances:

1) On decrease by the regulator of the angle of inclusion, α_β, of the thyristors to the measure of the least natural phase angle

of the primary circuit, upon which cureent constriction angle α_3 exceeds the angle of inclusion and the including impulse will be given to the thyristor's control electrode with lack of anode voltage;

2) On spark discharge in the precipitator, occuring in work conditions when the angle of thyristor inclusion is less than 90 degrees, the current has in this case a purely inductive character and the angle of constriction α_3 approaches, according to its value, 90 el.degrees.

Half-wave feeding conditions are, according to their consequences, close to short circuits. Therefor an automatic regulator should contain a device, preventing their development during the occasional switch-off of thyristors.

On the basis of the preceding, the observation can be made that stable and efficient work by unit systems and precipitators may be assured under the condition that the automatic regulator will carry out multipurpose control according to the following directions:

1) That it contunuously mauntain in the precipitator a given relationship between spark intensity and electrode voltage, with the purpose of optimizing gas cleaning;

2) That it extinguish spark-overs and prevent occurence of secondary spark discharges, thus increasing the coronal discharges stability.

3) Automatically limit in the precipitator the critical average current value, in relation to the given unit;

4) Prevent occurence of half-wave conditions in primary power circuit feeding;

5) During shorting in the precipitator, to disconnect the unit after the necessary time lag;

6) Limit the average short circuit current during the protective time lag to a value, not exceeding 10% of the unit's nominal current.

The automatic regulator, fulfilling these functions, consists of the following functional circuits and units (fig. 1):

1) The basic control signal former circuit, forming, along with the precipitator unit system, the basic automatic regulating circuit; this contains the spark discharge selecter (SDS), basic regulator signal former (BRSF) with the program regulation control (PRC), the amplitude-phase converter (APC), and the thyristor impulse regulation former (TIRF);

2) The transient condition signal former circuit, consisting of the spark discharge selector (SDS), the transient condition signal former (TCSF) and the remaining elements of the basic circuit, except for the regulator signal former (BRSF);

3) A circuit, correcting the basic signal according to the value of the working current, which consists of a current limiting signal former (CLSF) and the maximum current force control (MCFC);

4)A circuit for basic signal correction according to the allowed value of the angle of inclusion for power thyristors, consisting of a feedback signal former according to inclusion angle former (RCSF) and an angle regulation corrector unit (ARC);

5) A system for protection against precipitator short circuits, including a sensory defense unit (SDU) and a shorting current limiter (SL).

Signals enter the regulator's input from the current sensor (CS), from the precipitator voltage control (PVC) and the thyristor voltage control (TVC).

The control angle of power thyristors, represented by the phase angle of of transmission of the current's short-term inclusion impulses, fed into the thyristor control junctions of the thyristor control unit (TCU), represent the regulator input signal.

The automatic regulator works in the manner described below. After the unit is switched on, the basic signal former circuit provides a smooth increase of the thyristors' control angle in relation to the regulator's basic booster characteristic, thus the precipitator's voltage and current steadily rise. With spark discharge in the precipitator, the spark discharge selector divides transient elements in the current and rectified voltage and forms right-angle impulses, whose duration is equal to the duration of the spark current. The succesion of these impulses is subjected to sticking non-linear integration into the basic regulator signal former unit. At the same time, each impulse induces intermittent output-signal decrease in the regulator to the value, proportional to the selctor's impulse duration, in relation to the function:

$$\Delta\alpha_y = \frac{Kn}{K_3} \cdot \alpha\upsilon,$$

where $\Delta\alpha y$ - decrease in cogtrol angle of individual sparks, el. degrees

$Kn = 0.65$; $K_3 = 18.6$ - regulator constants

αu - selector impulse duration, el. degrees.

In intervals between spark discharges, the control angle steadily grows, with proportionately decreasing speed. Such a regulator output signal provides intermittent voltage reduction for the precipitator during discharges and smooth current build-up until the next spark-over. This improves to a considerable degree the coronal discharge's stability.

The succession of drops and increases in control signals forms a somewhat dynamic level of thyristor angle control, determined by spark discharge intensity.

The dependence of averaged angle control on sparking intensity represents the static characteristic of the basic signal regulator former circuit.

The approximate formula of the static characteristic takes the form:

$$Pu = 3.33 \cdot 10^3 \cdot \frac{k_3}{k_n} \cdot \alpha' y,$$

where $Pu = fu \cdot tu$ - sparking intensity, μs/min.

$\alpha' y$ - rate of change of control angle, el. degrees/μs

Automatic control of feeding parameters, carried out by the basic circuit, is directed at the system's retention on the basic signal former's static characteristic which is in the given case the regulator's programm.

The basic regulator signal former's circuit can be considered an astatic regulator of a set relation between sparking intensity and the power thyristors' control angle.

The quality of the control process can be characterized by dynamic error, the static error being equal to zero.

The automatic regulator has five fixed control programs to which correspond five static characteristics, distinguished by their slope toward the Pu axis. Program switching is produced with the help of the program regulation control (PRC), which changes the value to K_p.

With each spark-over the transient condition signal former is triggered by the spark discharge selector's (SDS) forward front. The action of the basic regulation program is temporarily terminated and the transient condition program is activated, which determines thyristor control angle for the next few half-periods of network voltage.

In accordance with this program, the control signal is removed in entirety, at the moment of discharge, and is absent during two half-cycles of network voltage. Then exponential signal build-up follows with a time constant of 20 μs up to its discharge at the level of the basic signal.

The described process provides quick-acting spark extinguishing (spark current does not last more than 0.01 seconds) and entirely precludes a lengthy series of spark discharges in the precipitator. Thus, coronal discharge stability is raised and erosion of precipitator electrodes is lessened to a considerable degree.

The prevention of developing half-wave conditions is done by correction of the value of the regulator-produced thyristor control angle.

The basic condition for occurence of half-wave conditions, as shown above, is the exceeding by the angle of current constriction α_3 of the angle of thyristor connection αB, given by the regulator.

The feedback signal former (FSF) fixes in each half-cycle of circuit voltage the closing of current constriction according to the moment of anode voltage restoration in the thyristor unit and generates the signal, equal according to its value to the current maximum allowable thyristor control angle (fig.1).

This signal is compared in the angle regulation corrector (ARC) with the signal produced by the basic regulator circuit. The least of the angles, compared in the ARC, enters the thyristor impulse regulation former.

In this way, during occasional current constriction, the thyristor inclusion angle increases according to the degree of this constriction and development of half-wave conditions does not occur.

Unit protection from possible current overloads is provided by automatic limitation of the working current's average value.

A signal is continuously formed in the current limiter signal former (CLSF, fig.1), proportionate to scale set by the maximum current power control (CFC) to the average precipitator current. The value of this signal is compared with some fixed level laid in the regulator. During a current overload of the unit, the average current signal exceeds the indicated level and at the signal regulator former (BSRF) input a negative feedback signal will appear. The basic regulating circuit, acting to extinguish this signal, lowers the precipitator's current to the given value.

In this manner, the current limiting circuit, along with elements of the basic regulating circuit form a static stabilizor for current of one-way action. Acceptable accuracy in supporting the set current value is provided by high coefficients of amplification of the regulating tract and of the thyristor control unit.

Selection of direct short circuit conditions in the precipitator for purposes of their elimination, is devised on the principle of current protection with voltometric blocking. In the sensory defense unit (SDU), the device for defense against short circuits is continuously compared with precipitator average current values and voltage. If due to a lack of voltage the current value exceeds the sensitivity threshhold, the device switches on an element independent of time lag (not shown in fig.1) and also switches on the short circuit current limiting unit (SCL). The latter, acting through the transient condition signal former, instantaneously limits the power thyristors control angle to a value, providing short circuit average current (nearly 10% of the unit's nominal current) defense sensitivity minimally necessary. According to the time lag lapse, the unit cuts off.

The automatic regulator is a contactless device using semiconductors. This established its high working reliability and durability.

FLY ASH DIELECTRIC PROPERTIES AND CRITICAL CURRENT DENSITY

by

John P. Gooch
Jack R. McDonald
Southern Research Institute
2000 Ninth Avenue South
Birmingham, Alabama 35205

and

Leslie E. Sparks
Industrial Environmental Research Laboratory
U.S. Environmental Protection Agency
Research Triangle Park, N.C. 27711

(This document has been reviewed and approved for publication by the U.S. EPA.)

1. Introduction

A critical factor in the design of an electrostatic precipitator for a given application is the prediction of the operating values of applied voltage and current density which can be achieved under the design conditions. For example, if the electrical resistivity of the collected dust and the particulate space charge are not limiting factors, it is expected that an average current density of ∿ 50 to 60 nA/cm^2 at average applied voltages of ∿ 45 kV will be achieved with conventional parallel plate electrode geometry. The practical significance of such operating parameters is that collection efficiencies exceeding 99.5% for coal fly ash can be obtained with a specific collecting area of 50 m^2/(m^3/sec). In contrast, if the current density and voltage are limited by the dust properties to 5 nA/cm^2 and 35 kV, specific collecting areas exceeding 100 m^2/(m^3/sec) are required to achieve 99.5% collection efficiency with all other conditions equal. Empirical methods are generally used to estimate electrical operating points from properties of the collected dust layer. The precision and applicability of these methods require improvement in view of the high level of performance needed for most electrostatic precipitator applications.

As a result of the importance of understanding the processes involved in predicting electrical operating conditions, the Environmental Protection Agency is sponsoring research concerning the physical processes by which charge transport occurs across the interelectrode space and through the dust layer on the collection electrodes. The overall objective of this research effort is the development of a methodology which will allow a more precise prediction of the optimum electrical operating point for a specific application given the following: (a) the properties of the fuel undergoing combustion (in the case of coal) or the properties of the particulate undergoing collection, (b) the temperature, pressure and composition of the gas in the precipitator, (c) the electrode geometry, and (d) the type of electrical energization.

2. Description of Field Measurements

A study of the parameters influencing operating values of secondary voltage and current density is in progress at Southern Research Institute. The study has been initiated with a measurement program conducted at several coal-fired power boilers. Measurements which were performed included the following:

- Secondary voltage-current data were obtained from the precipitator power supplies under normal operating conditions.
- In-situ determinations of ash resistivity and breakdown strength were conducted with a point-plane probe.
- In-situ determinations of particle size distribution were performed with inertial impactors at the precipitator inlets.
- Effective flue gas ion mobilities were determined with a wire-cylinder probe.
- Chemical analyses were performed on collected samples of coal, fly ash, and flue gas.

The particle size distribution data and the effective ion mobilities are used in the theoretical calculation of voltage-current relationships and electric field profiles between electrodes with a mathematical procedure described by McDonald, et al[1] and discussed elsewhere.[2] This paper is limited to an examination of the relationship between fly ash dielectric properties and apparent values of critical current density observed for full-scale precipitator transformer rectifier sets.

Table 1 contains data obtained at precipitator installations collecting fly ash with high to moderate electrical resistivity. Comparisons are made between apparent and measured dust breakdown strengths. The "selected" operating points were subjectively chosen based on an indication of incipient electrical breakdown in the dust layer. The selection is based on either an apparent deviation from the expected form of the voltage-current relationship in which

$$j = k(V-V_s)^n \tag{1}$$

where: j = current density, amps/m^2

k and n = constants

V_s = corona starting potential, volts

V = potential, volts,

or an obvious onset of sparking. The actual observed operating points were not chosen because of the complications introduced by the response of various automatic control systems to sparking or back corona.

The "apparent" breakdown strength of the dust layer is calculated by using the relationship

$$E_B' = j_{avg}\,\rho \tag{2}$$

where: E_B' = apparent breakdown strength, volts/m

j = average current density, amps/m^2, at selected operating point

ρ = measured resistivity, ohm-m

The measured breakdown strengths given in Table 1 were obtained from a point-plane device in the flue gas at a voltage immediately prior to dielectric failure. The estimated operating points were obtained from the measured values of in-situ dust resistivity and the assumed breakdown strengths of 1 and 5 kV/cm suggested by Hall.[3]

Similar data are given in Table 2 for two precipitators collecting low resistivity fly ash. Figures 1 and 2 display the voltage-current density relationships for Plants A and F representing the high and low resistivity cases, respectively. The secondary voltages were obtained with calibrated voltage divider assemblies which were attached to the high voltage output of the transformer rectifier sets under study.

3. Discussion

It is generally recognized that factors other than dust dielectric properties can influence the allowable electrical operating parameters in full scale precipitators. Specifically, electrode design, electrode alignment, voltage waveforms and control system response, collection area per transformer-rectifier set, flue gas composition, temperature and pressure, and electrode cleaning system effectiveness are considerations which can significantly alter precipitator electrical conditions for a given application. However, the comparisons of measured and apparent breakdown strengths given in Tables 1 and 2 are of interest in that the deficiencies of the existing empirical approach and the complexity of the task of predicting operating points are illustrated.

Plants A and B are typical of large specific collecting area units which have been constructed to collect high resistivity fly ash. The ratio of measured to apparent E_B values are within the range which can be expected due to dust layer non uniformity, and the useful input power is clearly limited by the fly ash dielectric properties. The increase in apparent E_B' from inlet to outlet is hypothesized to result at least in part from the variation of fly ash breakdown strength with layer thickness. It has been observed in both field and laboratory environments that the breakdown strength of fly ash decreases with increasing layer thickness. Therefore, the thinner dust layers which usually are present in outlet fields may be able to tolerate higher average electric fields. Another possible contributing factor is the variation of resistivity due to particle size distribution variations which occur from inlet to outlet.

Plant C exhibits an unusual variation in inlet to outlet operating points, and electrode cleaning system ineffectiveness is a probable cause. The ratio of actual to apparent E_B decreases to less than unity for the outlet fields, which suggests that either; (1) the point-plane probe collected a dust sample not representative of the collected dust layer in fields 7 and 8, or (2) a back corona discharge exists which is not detectable from the V-I curves.

The low values of current density achieved at Plant D are difficult to explain in terms of the measured properties of the fly ash. However, the sparking threshold is clearly influenced by dust or flue gas properties, as the data in Figure 3 illustrate. These voltage-current curves were obtained with and without SO_3 conditioning for the indicated TR set. Plant D has a relatively ineffective rapping system, and it is probable that residual dust layers which were present on the collecting electrodes possessed a higher resistivity than that measured with the point-plane probe during the test series. If a residual layer with a resistivity of 2.7×10^{12} ohm-cm were present, the apparent E_B' values would fall within the expected range of 5 to 10 kV/cm. These circumstances illustrate both the difficulty of estimating the limitation imposed by high resistivity and the value of flue gas conditioning as a means of alleviating the problem. Note that the assumption of 1 to 5 kV/cm as an apparent breakdown strength interval failed to bracket the selected operating points for the four plants described in Table 1.

Plants E and F represent precipitator installations which are not performance-limited by dust resistivity. The low apparent values of E_B' suggest that the sparkover voltages are determined by factors other than dielectric failure in collected dust layers. Although the current densities achieved at Plant E were relatively low, the collection efficiency was relatively good because of the high operating voltages. For both plants E and F, it is apparent that electric field intensity in the dust deposits does not provide a basis for estimating operating points. For these circumstances, however, high levels of performance can be achieved without excessive plate area requirements, and the accurate prediction of achievable current density is less critical than for the plants listed in Table 1.

The variations in measured and apparent breakdown strength in Tables 1 and 2 illustrate the need for a thorough understanding of the electrical properties of collected dust layers. McDonald and Mosely[4] have proposed an approach for describing the electrical characteristics of such layers based on coupling the current transport equation and Poisson's Equation. In this method, the electrical breakdown of the dust layer is attributed to enhanced values of the local electric field (defined as the electric field at a point between particles) due to the combined effects of polarization of the particles in the dielectric layer and the contribution to the electric field from the space charge distribution in the solid phase of the dust layer. The average value of the electric field for which breakdown will occur can be computed as a function of dielectric constant of the particles by specifying a breakdown strength for the trapped gas. Table 3 shows the results of calculations for several cases of interest. This approach implies that the operating current density limit could be predicted from measurements of resistivity and dielectric constant in an appropriate environment. Other factors may require consideration, however, such as charge carrier density gradients which may develop in collected dust layers over extended time periods.

In order to construct appropriate charge transport models for collected dust layers, certain experimental studies need to be performed to determine appropriate values of the parameters and boundary conditions that must be utilized in modeling the electrical phenomena. These studies include measurements to determine the following:

- whether electrical breakdown is due to gas breakdown or particle breakdown
- electric potential distribution and concentration profiles of charge carrying species in the dust layer
- values for transference numbers, activation energies, conductivities, diffusion coefficients, and mobilities of the different charge carrying species
- values of the dielectric constants for different dusts in simulated flue gas environments.

4. Summary

The actual and apparent breakdown strengths of electrostatically collected dust layers exhibit large variations which are not adequately represented by existing concepts. Physical models of the charge transport process across the interelectrode space and through the collected dust layers have the potential of providing a methodology for accurate prediction of optimum electrical operating conditions utilizing dust and flue gas properties and the design parameters of the electrostatic precipitator. Fundamental studies of dust layer properties are continuing with the objective of developing the required predictive methods.

References

1. McDonald, J.R., W.B. Smith, H.W. Spencer, and L.E. Sparks. A Mathematical Model for Calculating Electrical Conditions in Wire-Duct Electrostatic Precipitation Devices. J. Appl. Phys., 48(6):2231-2246 (1977).

2. McDonald, J.R. A Mathematical Model of Electrostatic Precipitation: Revision 1. Volume 1, Modeling and Programming. EPA-600/7-78-111a, U.S. Environmental Protection Agency, Research Triangle Park, North Carolina, 1978.

3. Hall, Herbert J., "Trends in Electrical Energization of Electrostatic Precipitator. Proceedings of the Electrostatic Precipitator Symposium, Feb 23-25, 1971, Birmingham, Ala.

4. McDonald, J.R., R.B. Mosley, and L.E. Sparks. An Approach for Describing Electrical Characteristics of Precipitated Dust Layers. Submitted for publication in JAPCA, March, 1979.

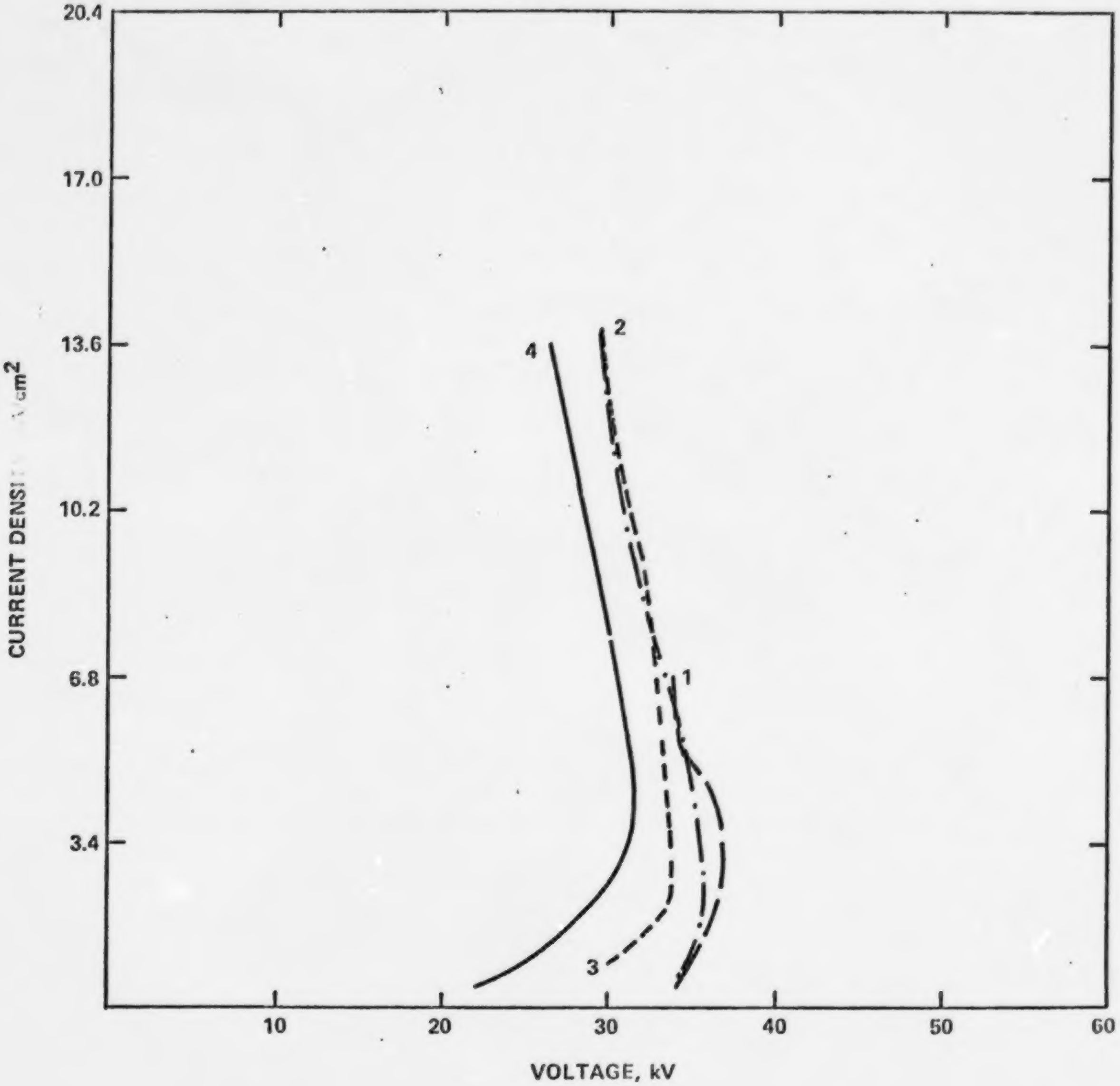

Figure 1. Voltage-current curves for plant A.

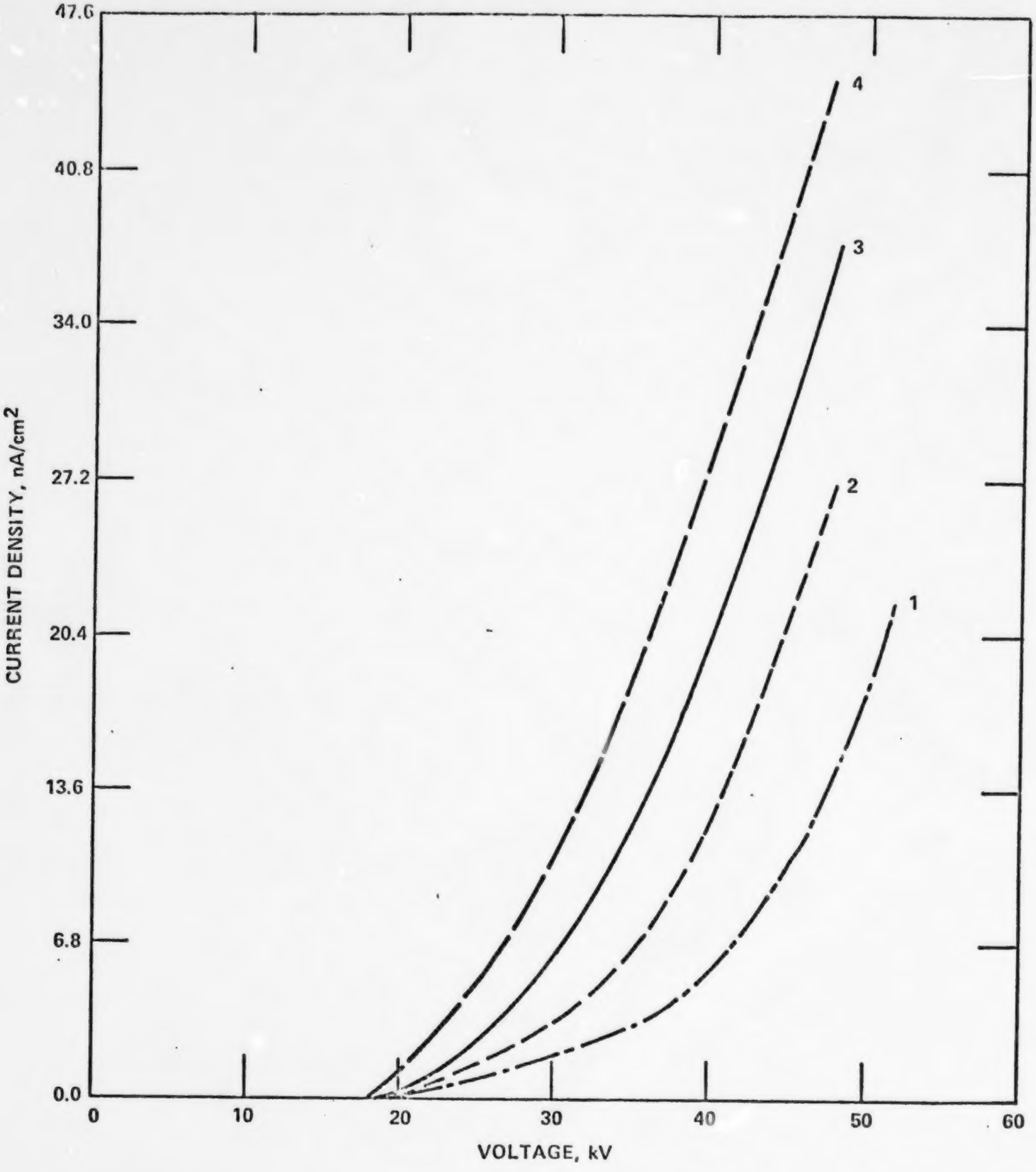

Figure 2. Voltage-Current Curves for Plant F.

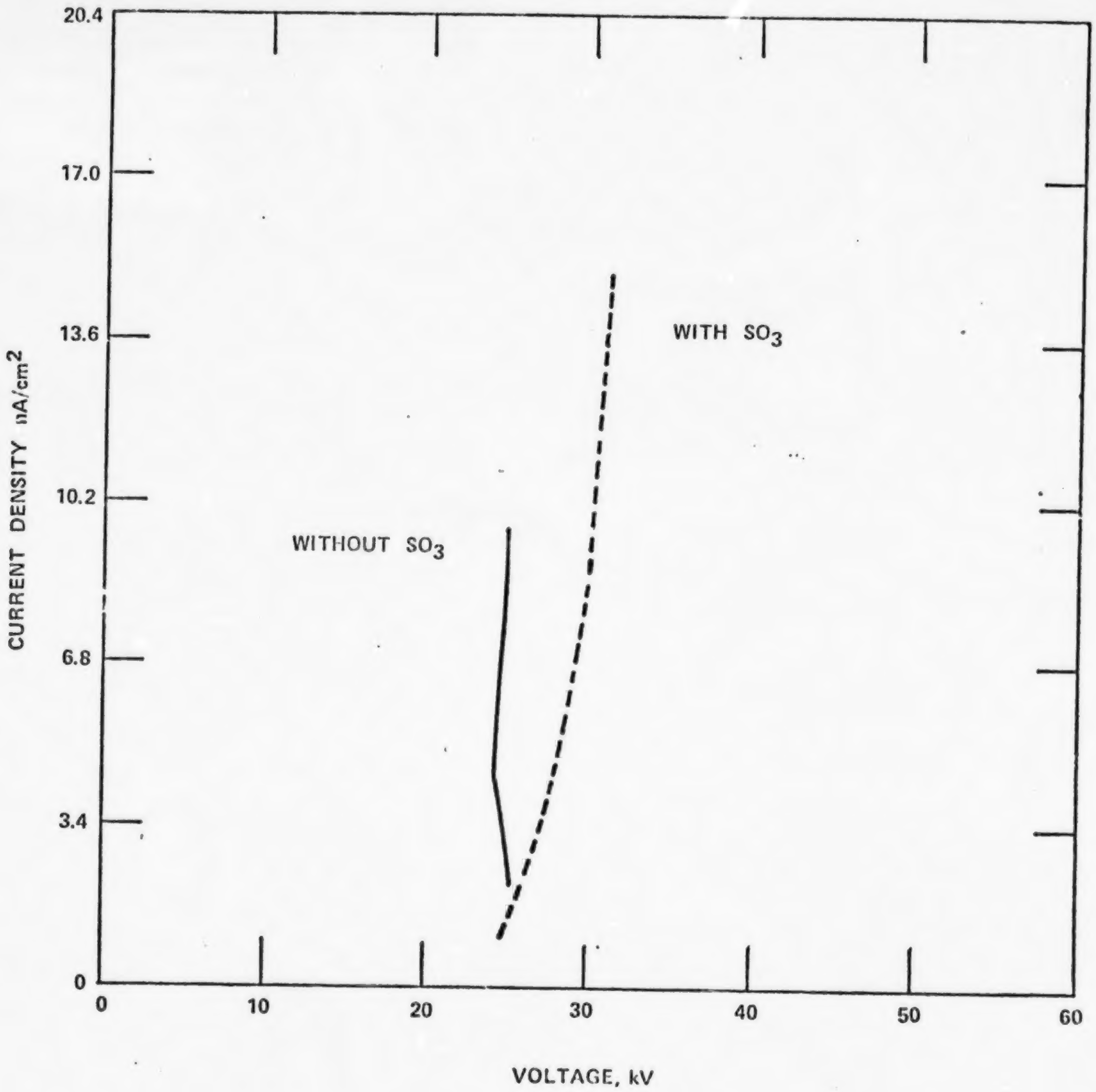

Figure 3. Voltage - current curves for Plant D, Fourth Field

Table 1
Selected Operating Points and Apparent Breakdown Strengths
High to Moderate Resistivity

Plant	Field in Direction of Gas Flow	Selected Operating Point kV	Selected Operating Point nA/cm^2	Electrode Geometry	Temperature °C	Resistivity ohm-cm	Area/TR set m^2	Apparent E_B' kV/cm	Measured E_B kV/cm	$\frac{E_B \text{ Measured}}{E_B \text{ Apparent}}$	Estimated Operating Point nA/cm^2 1kV/cm	Estimated Operating Point nA/cm^2 5kV/cm
A	1	37.0	2.0	30.48 cm plate spacing, discharge electrodes are 4.26 mm square, fluted & twisted held in a rigid mast.	138	3×10^{12}	2675.5[a]	5.8	27.2	4.7	0.33	1.7
	2	36.0	2.0				2675.5[a]	5.8		4.7		
	3	33.5	2.0				2675.5[a]	5.8		4.7		
	4	32.0	3.0				2676.5[a]	8.7		3.1		
B	1	34.0	4.0	25 cm plate spacing, discharge electrodes are spiraled, 2.5 mm in diameter & held in a rigid frame.	135	2×10^{12}	3518.6	7.2	26.6	3.7	0.50	2.5
	2	36.0	5.3				3518.6	9.5		2.8		
	3	36.0	5.5				3518.6	9.9		2.7		
	4	33.0	10.0				3518.6	18.0		1.5		
	5	33.0	12.0				3518.6	22.0		1.2		
C	2	36.0	2.5	22.86 cm plate spacing, discharge electrodes are round(2.68 mm diameter) & weighted.	144	5×10^{11}	1424.2	1.25	10.5	8.4	2.0	10.0
	7	28.0	44.0				1424.2	22.0		0.48		
	8	29.0	48.0				1424.2	24.0		0.48		
D	1	32.0	2.0	22.86 cm plate spacing, discharge electrodes are round(2.68 mm diameter) and weighted.	164	3×10^{11}	961.5[a]	0.54	13.8	25.5	3.7	18.5
	2	32.0	2.0				961.5[a]	0.54		25.5		
	3	27.0	2.0				961.5[a]	0.54		25.5		
	4	25.0	2.0				961.5[a]	0.54		25.5		

---

a. collection area per bushing

Table 2
Selected Operating Points and Apparent Breakdown Strength
Low Resistivity

Plant	Field in Direction of Gas Flow	Selected Operating Point kV	Selected Operating Point nA/cm²	Electrode Geometry	Temperature °C	Resistivity ohm-cm	Area/TR set m²	Apparent E_B' kV/cm	Measured E_B kV/cm	$\frac{E_B \text{ Measured}}{E_B \text{ Apparent}}$	Estimated Operating Point nA/cm² 1kV/cm	Estimated Operating Point nA/cm² 5kV/cm
E	1	46.0	8.0	27.9 cm plate spacing, 4.2 mm square twisted discharge electrodes held in a rigid mast.	153	2×10^{10}	2458.1[a]	0.16	14.0	88.0	50.0	250.0
	2	45.0	8.0				2458.1[a]	0.16		88.0		
	3	45.0	24.5				2458.1[a]	0.54		26.0		
F	1	55.6	20.0	25.4 cm plate spacing, discharge electrodes are rigid tubular barbed electrodes	160	2×10^{10}	1475.2[a]	0.40	17.0	42.0	50.0	250.0
	2	51.7	27.3				1475.2[a]	0.55		31.0		
	3	48.9	36.0				737.6[a]	0.72		24.0		
	4	48.5	46.0				737.6[a]	0.92		18.0		

---

[a] collection area per bushing

Table 3. Average electric field at breakdown for various dielectric constants, temperatures, and pressures

	E_B = 30 kV/cm at 293°K, 760 mm Hg		E_B = 20.8 kV/cm at 422°K, 760 mm Hg		E_B = 11.4 kV/cm at 616°K, 608 mm Hg	
K	E_{loc}/E_{Ave}	E_{Ave} for Breakdown (kV/cm)	E_{loc}/E_{Ave}	E_{Ave} for Breakdown (kV/cm)	E_{loc}/E_{Ave}	E_{Ave} for Breakdown (kV/cm)
1	1.50	20.00	1.50	13.90	1.50	7.60
2	3.38	8.88	3.38	6.15	3.38	3.37
3	5.25	5.71	5.25	3.96	5.25	2.17
4	7.13	4.20	7.13	2.92	7.13	1.60
5	9.00	3.33	9.00	2.31	9.00	1.27
6	10.88	2.76	10.88	1.91	10.88	1.05
7	12.75	2.35	12.75	1.63	12.75	0.89
8	14.63	2.05	14.63	1.42	14.63	0.78
9	16.50	1.82	16.50	1.26	16.50	0.69
10	18.38	1.63	18.38	1.13	18.38	0.62

A.I. Zavialov, V.B. Meshcheriakov

RESEARCH, DEVELOPMENT AND INTRODUCTION OF ADVANCED PRECIPITATING ELECTRODE DESIGNS OF INDUSTRIAL PURPOSE ELECTROSTATIC PRECIPITATORS

In connection with the growth in volumes of dusts removed from stack gases with the aid of industrial ESP's, special attention is being paid to the problem of the reliability and durability of their mechanical components. In the course of the last ten years, NIIOGAZ's Semibratovsk branch and the Moscow Institute of Transport Engineeers have conducted complex experimental-theoretical research into the dynamics of precipitating electrodes of industrial purpose ESP's. During the course of research, a science-based experimental procedure (1) was developed along with methodology for the computational evaluation of precipitator electrode rapping efficiency where the rapping was carried out by the impact method (2).

As a result of research, reasons for the unsatisfactory degree of cleaning the electrodes from accumulated fly-ash were established, as well as the causes for the breakdown of rapping band and rapping mechanisms. The basic research results are published in various articles and have also been presented in symposiums (3,4).

Related to the number of basic factors causing unsatisfactory electrode performance are rapping blow energy losses at the junctures of the electrodes with the rapping band and the dampening of the disturbance with great element length. Density of contact in the areas of energy transmission plays a large role. Specially set experiments have shown that the presence of a gap to the magnitude of 0.1mm may lower the magnitude of the transmitted impulse by two or more times. With fly-ash falling into this gap, the lowering of the magnitude of impulse becomes more substantial (5).

New design variants are being developed for improving the work of precipitating electrodes. The main direction of this development is increase of element width and raising the contact reliability of the elements with the rapping band. Widely distributed electrode designs may be operatively redesigned with the aim of increasing their rapping efficiency and raisng their operating reliability and endurance. Design variants developed in NIIOGAZ's Semibratovsk branch may be used for this.

0.35m-wide precipitating elements are doubled and hung excentrically. This measures increases the excentricity, lowers the number of places of energy transmission and increases the contact reliability.

The precipitating elements in the electrode are combined into two groups (6). The first groups elements are hung excentrically for taking the blow from the rapping mechanism's hammer. Elements of the second group are also hung excentrically but are drawn against the rapping band for taking the rapping blow against the supports. Such design (see fig.2) gives an opportunity for considerably raising the average level of maximum accelerations on the electrode. The element' solid contact with the rapping band is also provided by the precipitating electrode with vertical alignment of the elements to the rapping band. A precipitator element variant is proposed with vertical element support against the rapping band and with a mechanism for element rapping (7) in order to eliminate differences in acceleration at the first and last elements from the place of impact (due to non-uniform pulse distribution). Such design provides uniform distribution of the shock impulse according to the electrode's height and width and also a sufficient degree of cleaning with a smaller number of impact loads. The low level of vibration of neighboring unrappable elements during the drop from a specified height of one (in this case, the fourth) element (see fig.3) and the opportunity for regulated rapping speed make it possible to decrease re-entrainment, but a decrease of the number of impacts make it possible to increase electrode reliability.

All of the suggested design variations on precipitating electrodes passed a stage of stand and industrial testing and accounted well for themselves. Thus, for example, testing of advanced designs (fig.1 and 2) at the Troitskaya State Regional Electric Power Plant have shown that these designs possess great advantages in comparison with earlier-used designs.

At the Sredneuralsk copper-smelting works, nine-month testing of the precipitating electrode with vertical element support and element-by-element rapping system was conducted (7). These tests showed that a high degree of rapping efficiency (90-95%) is obtained through one-two "raise and drop" cycles.

Precipitating electrodes with two groups of elements (fig.2) are recommended for introduction in serially produced and redesigned precipitators of various types.

Precipitating electrodes with vertical element-by-element rapping are advisable for use in precipitators removing strongly-aglutinating dusts (cement dust, etc.) and for high-resistivity dusts.

BIBLIOGRAPHY

1. Zavialov, A.I., Methods and Research in Dynamics of Precipitating Electrodes, "Tsement", 1975, No.3.

2. Meshcheriakov, V.B., Numerical Evaluation of Precipitating Electrode Rapping Efficiency in Industrial Precipitators, in the collection "Industrial and Sanitary Gas Cleaning", TsINTIKhIMNEFTEMASh, 1977, No.1.

3. Meshcheriakov, V.B. et al, Results of Theoretical and Experimental Study of Dynamics of Precipitator Electrodes : Report Abstracts of the Symposium "Electrical Gas Cleaning Methods", Moscow, 1973.

4. Meshcheriakov, V.B., Zavialov, A.I., Dynamics of Precipitator Electrodes and Predicting Effectiveness of their Regeneration : Report to the Second Soviet-American Symposium on Particulate Control, Washington, 1977.

5. Zavialov, A.I., Meshcheriakov, V.B., Research in the Dynamics of Advanced Precipitator Electrodes, in the collection "Industrial and Sanitary Gas Cleaning", TsINTIKhIMNEFTEMASh, 1977, No.6.

6. Zavialov, A.I., Sobchuk, S.I., Smirnov, L.P., Nagornyi, V.V., The Precipitator Electrode, author's certificate, patent no. 472690, bulletin "Discoveries, Inventions, Industrial Models, Trade Marks", 1975, No.21.

7. Zavialov, A.I., Nagornyi, V.V., Panasenko, V.I., Sobchuk, S.I., The Electrostatic Precipitator, author's certificate, patent no. 523712 letin "Discoveries, Inventions, Industrial Models, Trademarks", 1975, No.29.

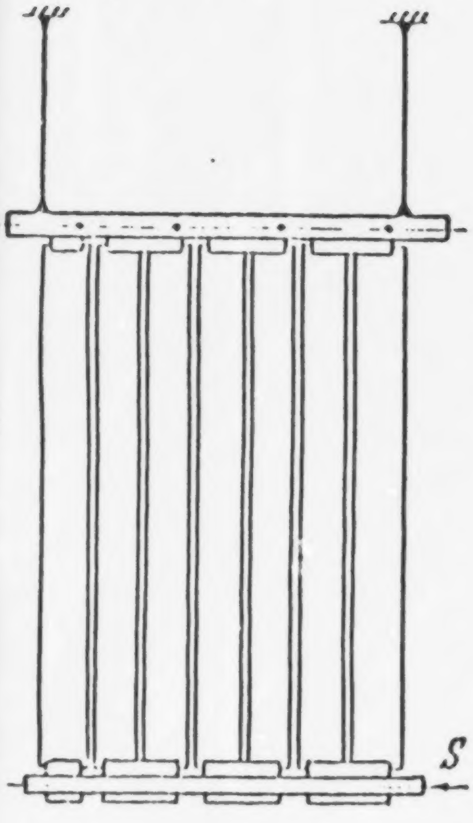

fig.1.

Precipitating electrode with paired elements.

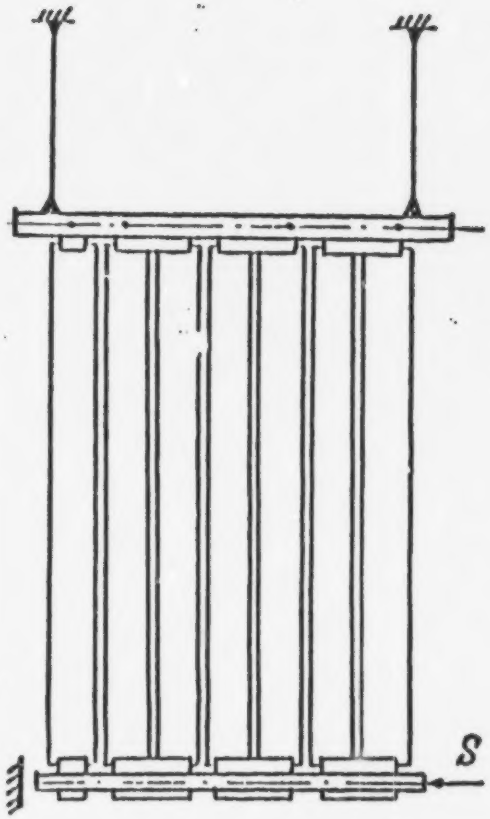

fig.2

Precipitating electrode with two groups of elements

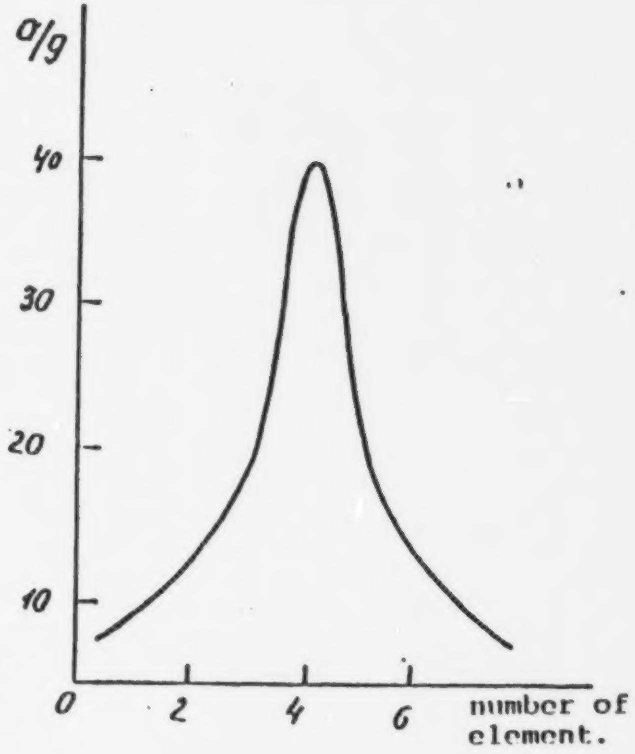

-fig.3.

Acceleration distribution in precipitating electrode with elemen by-element rapping.

PERFORMANCE OF A HOT-SIDE ELECTROSTATIC PRECIPITATOR

G.H. Marchant, Jr.
John P. Gooch
Southern Research Institute
2000 Ninth Avenue South
Birmingham, Alabama 35205

Leslie E. Sparks
Industrial Environmental Research Laboratory
Environmental Protection Agency
Research Triangle Park, N.C. 27711

(This document has been reviewed and approved for publication by the U.S. EPA.)

INTRODUCTION

The performance of a hot-side electrostatic precipitator installed on a large power plant boiler was investigated. The tests were made on Unit 3 of the Navajo Generating Station of the Salt River Project in Arizona. Overall and fractional collection efficiencies were measured across one chamber of the unit, and fractional collection efficiency was measured for the entire precipitator. Voltage-current characteristics of the power supplies were measured. An engineering analysis for the installation included estimates of the specific collecting areas required for improving performance of the hot-side precipitator and for replacing it with a cold-side precipitator.

The electrostatic precipitator has two levels (Figure 1), each with eight isolable chambers (Figure 2), and was designed to operate with a total volume flow rate of 1860 m^3/sec at 350°C with 99.5% collection efficiency. Each chamber contains 6 electrical fields in the direction of gas flow and 35 gas passages spaced 22.9 cm apart. A total of 48 transformer-rectifier sets power parallel fields in parallel chambers. The collection electrodes are 1.83 m in depth and 9.14 m high. The discharge electrodes have diameters of 2.68 mm and the average spacing between each wire is 22.9 cm. Each precipitator has a total collecting area of 112,372 m^2, which results in a design specific collection area of 60.4 $m^2/(m^3/sec)$.

TEST RESULTS

The overall fly ash collection efficiency (by mass) of one isolated chamber (Chamber 8) of the electrostatic precipitator was found to be 99.22%, based on mass train measurements at the inlet and outlet of the chamber. Test data are shown in Table 1. In these tests, average secondary voltage was 22 kV, average secondary current density 40 nA/cm^2, specific collection area 52.6 $m^2/(m^3/sec)$, and fly ash resistivity (determined in situ) $5x10^9$ ohm-cm at 350°C. Plant operating problems prevented the measurement of collection efficiency for the entire precipitator by a mass train. However, a limited number of measurements were made by impactor traverses in the stack and at the precipitator inlet, producing the results in Table 2. The stack data indicated a mass emission rate of 31 ng/J, of which 9 ng/J consisted of particles with diameters < 2 μm. The gas volume flow rate in the stack was consistent with that at the outlet of Chamber 8. Oxygen contents, determined simultaneously at the inlet and in the stack, indicated that air in-leakage across the precipitator and air preheater was about 11%.

Figure 3 compares the particle-size distributions measured with impactors at the inlet to the electrostatic precipitator and to Chamber 8. The bimodal particle-size distributions are typical of those produced by pulverized coal-fired boilers, with one mode a maximum at about 2 μm, and the other at a diameter > 10 μm. The mass median diameter of the fly ash, based on impactor data, is about 13 μm. If it is assumed that the difference in mass loadings measured by the impactor and the mass train sampling system is due to inefficient capture of particles > 20 μm by the impactor, the corrected mass median diameter is 16 μm.

Concern about the effects of soot blowing on the particulate loading of the flue gas entering a hot-side electrostatic precipitator led to comparative tests which showed that there were significant (at the 90% confidence level) increases in loading at the inlet of Chamber 8 during soot blowing, as measured with a mass train. However, no significant differences were observed at the chamber outlet as the result of soot blowing. Figure 4 shows the particle size distributions obtained with impactors at the inlet to Chamber 8 with and without soot blowing. Most of the increase in loading during soot blowing was due to particles > 8 μm.

Figure 5 compares the differential particle-size distributions in the stack and at the outlet of Chamber 8. The stack data exhibit substantially higher loadings of particles with diameters from 0.8 to > 10 μm. These differences are also reflected in the fractional collection efficiency results shown in Figure 6. The fractional collection efficiency curve showed a minimum value of 92% at a particle diameter of about 0.50 μm. The disagreement between the impactor and ultrafine results in the 0.5 μm region is partly due to experimental error.

Values of electrical resistivity of the fly ash measured at 350°C _in situ_ and in the laboratory are in reasonable agreement with those measured for other fly ashes of similar chemical composition. The resistivities remained relatively constant during the test program.

Coal and ash analyses indicated constant quality of the coal supply. Attempts to measure sulfur dioxide in the flue gas indicated that concentrations were never above the detection limit of ∿ 0.5 ppm at the inlet or either of the two outlet sampling locations.

The voltage waveforms and secondary voltage-current relationships observed during the tests appeared to show the effects of back corona. Figure 7 presents voltage-current curves obtained for Chambers 7 and 8 (secondary voltages were determined from voltage divider readings). The operating voltages were lower than anticipated, especially for the outlet fields. Several observations indicated that fly ash deposits on the collection electrodes affected the functional relationship between applied voltage and corona current:

The V-I curves do not respond to changes in discharge electrode diameter to the extent theoretically predicted (Figure 8). The curves from the outlet field show some hysteresis. The shapes of the curves are affected by electrode cleaning (Figure 9). Voltage-current waveforms (Figure 10) suggest a back corona discharge at high current levels.

Although the precipitator has not maintained design efficiency, it has operated reliably. The most significant maintenance problems have been air infiltration and ash build-up in hoppers.

ENGINEERING ANALYSIS

The estimated cost of the electrostatic precipitator installation is given in Table 3. These costs were calculated from the 1973 and later contract costs, plus a 20% distributable cost, plus 9% of the contract and distributable cost for engineering costs, and escalation of each cost element to 1977 at 7.5%/year.

Table 4 shows the annual operating cost, including maintenance cost assigned to the electrostatic precipitator.

The performance tests indicated that the two principal causes of poor performance of the precipitator were the relatively low operating voltage and the relatively low value of specific collecting area. To indicate changes in precipitator design that should overcome these deficiencies, values of design parameters listed in Table 5 were calculated for an improved hot-side unit. The basic geometrical configurations of the existing unit were arbitrarily retained. A mathematical model was used to extrapolate the apparent collection efficiency of the existing unit (98.6% at a specific collecting area of 53.15 $m^2/(m^3/sec)$) to give a specific collecting area of 78.74 $m^2/(m^3/sec)$

required for 99.5% collection efficiency. To reliably attain a 99.5% collection efficiency in the presence of the unfavorable electrical operating conditions requires a design specific collecting area of 93.90 $m^2/(m^3/sec)$, which provides a safety margin of about 20%. The design parameters for the improved precipitator are listed in Table 5. The new design has an increase in collection surface of 83% over the existing unit. The estimated capital cost for this design is \$60,440,000, or \$75.5/kW, based on 800 MW generating capacity. No retrofit charges are included in the estimate.

Table 5 also includes data on two cold-side designs for 99.5% minimum collection efficiency, for which the estimated capital costs are \$52.4/kW and \$65.1/kW, for collecting fly ash with electrical resistivities of 9×10^{10} and 7×10^{11} ohm-cm, respectively.

TABLE 1

AVERAGE INLET AND OUTLET PARAMETERS, ISOLATED CHAMBER 8

	Inlet	Outlet	Collection Efficiency, %
Temperature, °C	361	330	
Gas Volume Flow Rate, dsm^3/sec	44.4	51.5	
Mass Loading, g/dsm^3			
Impactor	5.19	0.0384	99.26
Mass Train	6.77	0.0529	99.22
Number of Tests			
Impactor	27	32	
Mass Train	16	16	

TABLE 2

AVERAGE INLET AND STACK PARAMETERS

	Inlet	Stack
Temperature, °C	368	161
Gas Volume Flow Rate, dsm^3/sec	-	860
O_2, % dry basis	3.90	5.55
Mass Loading, g/dsm^3	5.40	0.0776
Number of Tests	12	10
Apparent Collection Efficiency, %	98.56	

TABLE 3

COST OF PRESENT INSTALLATION

Item	Estimated Cost in 1977 dollars	$/kW[a]	$/m²
Electrostatic precipitator and labor	$ 9,863,673	12.33	87.73
Electrostatic precipitator ductwork and insulation	5,460,345	6.83	48.55
Ash collection system	8,915,691	11.14	79.33
Accessory electrical equipment	7,637,144	9.55	67.92
Miscellaneous	3,059,186	3.82	27.23
TOTAL	$34,940,000	$43.67	$310.76

---

[a] Based on 800 MW.

TABLE 4

OPERATING COSTS
July 1, 1976 to July 1, 1977

	$/yr	mills/kWh	% of Total Annual Operating Costs
Energy cost[a]	$ 534,300	0.0953	8.2
Normal operating and maintenance cost	276,000	0.0492	4.2
Ash handling cost	460,900	0.0822	7.07
Sub-total	1,271,200	0.227	19.5
Capital charges $34,940,000x0.15 =	5,240,000	0.935	80.5
TOTAL	$6,511,000	1.162	100.0

---

[a] Based on 7008 hr/yr at full load (800 MW), 80% load factor

TABLE 5

RECOMMENDED DESIGN PARAMETERS FOR IMPROVED PERFORMANCE[a]

Condition	Hot-Side Peabody Coal	Cold-Side Peabody Coal	Cold-Side Utah Coal
Gas flow, m^3/sec	2,194	1,571	1,571
Temperature, °C	350	150	150
Electrical fields in direction of gas flow	8	8	8
Number of chambers	22	22	28
Total collection area, m^2	2.062×10^5	2.062×10^5	2.623×10^5
Specific collecting area, $m^2/(m^3/sec)$	93.9	131.1	166.9
Collection efficiency, %			
Design minimum	99.50	99.50	99.50
Expected	99.70	99.77	99.75
Dust resistivity, ohm-cm	5×10^9	8.5×10^{10}	7.0×10^{11}

---

[a] Based on indicated dust resistivity values.

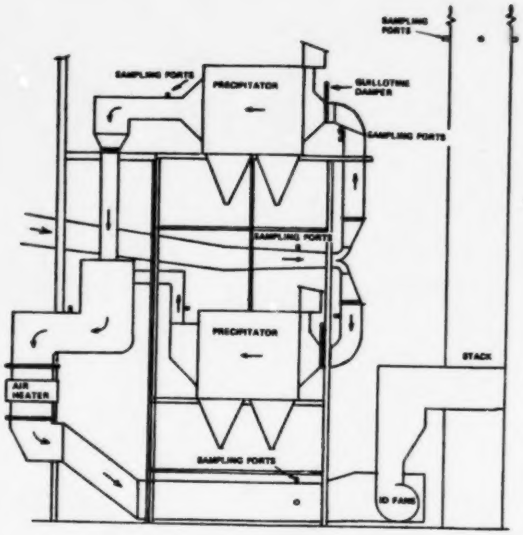
SAMPLING PORTS
SAMPLING PORTS
PRECIPITATOR
GUILLOTINE DAMPER
SAMPLING PORTS
SAMPLING PORTS
PRECIPITATOR
AIR HEATER
STACK
SAMPLING PORTS
ID FANS

Figure 1. Ductwork and precipitator arrangement for Navajo Station, Unit 3.

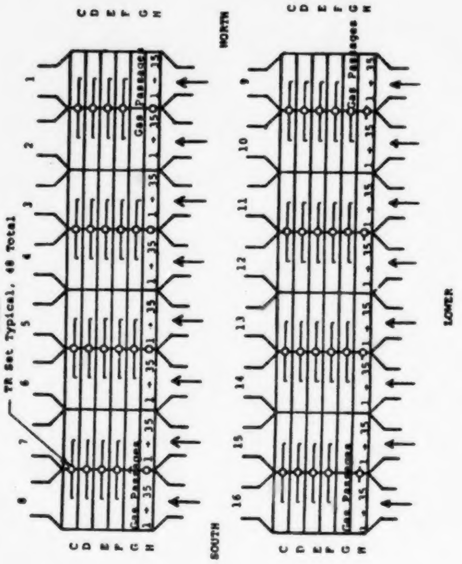
NORTH
SOUTH
UPPER
LOWER
TR Set Typical, 48 Total
Gas Passages
1 → 35
1
2
3
4
5
6
7
8
9
10
11
12
13
14
15
16

Figure 2. Precipitator chamber arrangement.

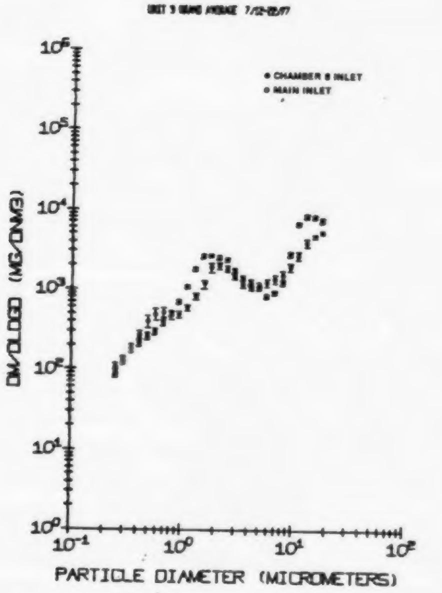

Figure 3. Average inlet differential size distribution.

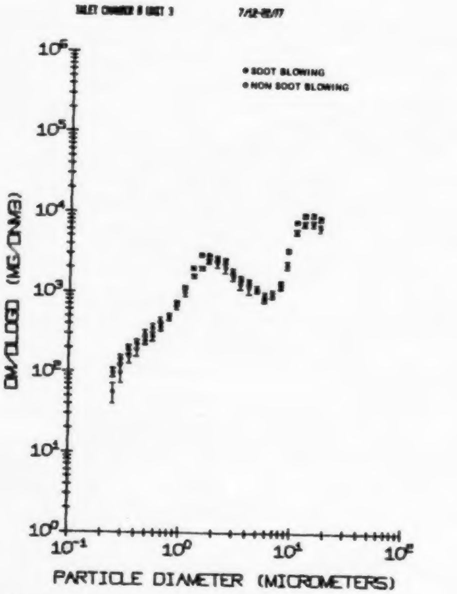

Figure 4. Differential size distributions, Chamber 8 inlet.

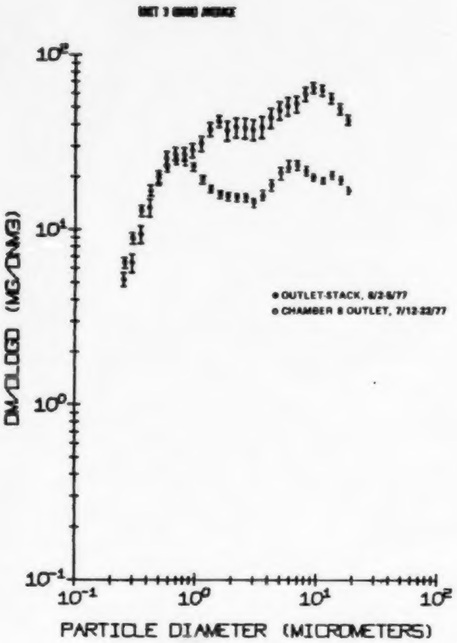

Figure 5. Outlet differential size distribution.

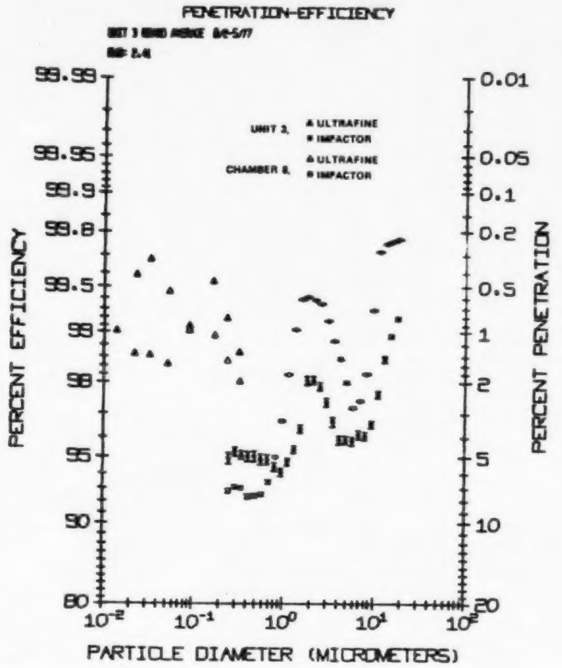

Figure 6. Fractional efficiency for Chamber 8 and total ESP.

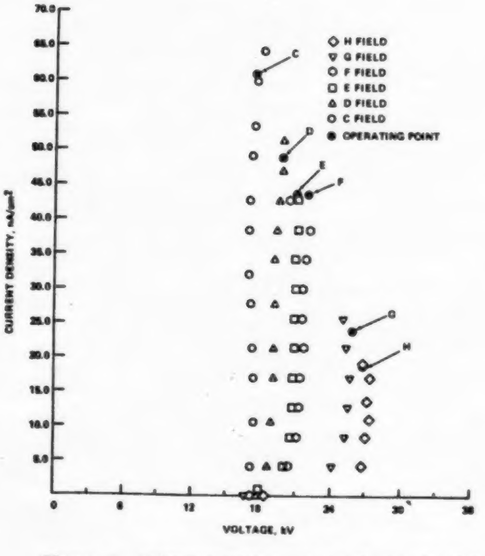

Figure 7. Voltage-current curves for Chamber 7 and 8, July 12-13, 1977.

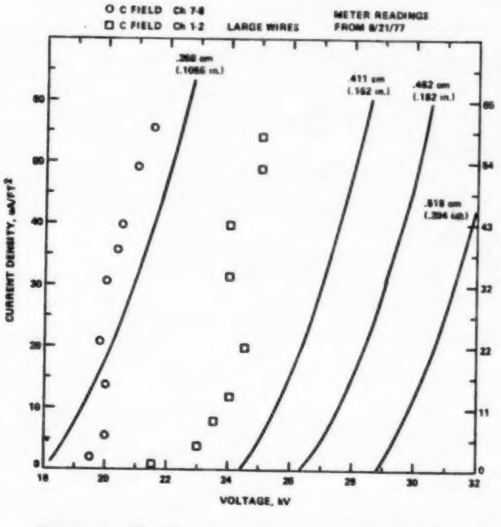

Figure 8. Theoretical and experimental voltage-current relationships for various wire diameters.

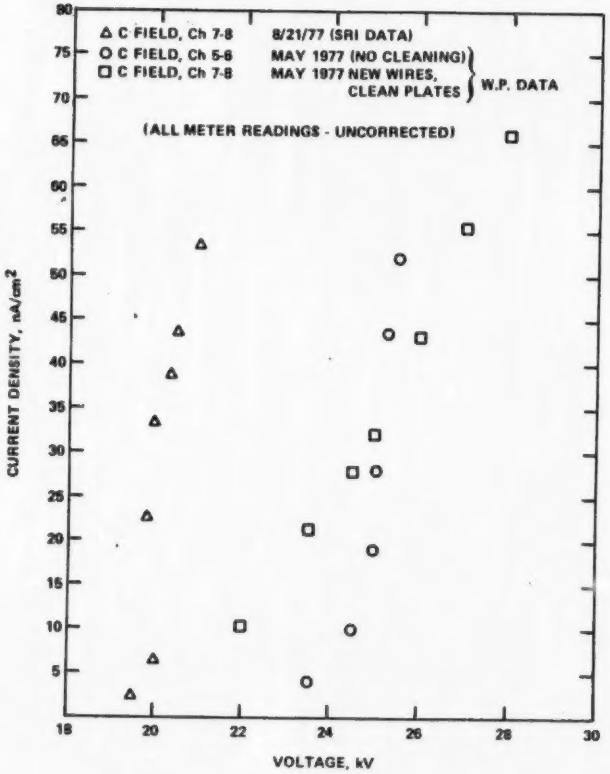

Figure 9. Voltage-current relationships for C Fields, Ch. 7 & 8 and Ch. 5 & 6.

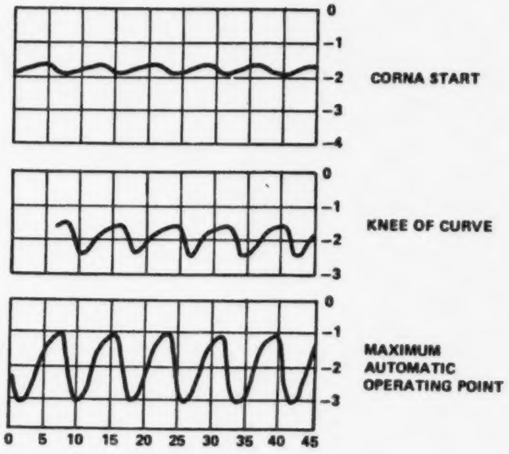

Figure 10. Voltage waveforms for C Field, Chambers 7 and 8.

E.N. Kurbatskii, V.B. Meshcheriakov, E.N. N[illegible]metov.

STUDY OF THE DYNAMICS AND STRENGTH OF CORONAL ELECTRODES IN ELECTROSTATIC PRECIPITATORS

Existing systems of coronal electrodes in industrial electrostatic precipitators do not to the full degree meet the requirements presented them in their section where settling fly-ash is removed, and in their reliability and durability.

This report elucidates study results from the work of the two most widely distributed in practice coronal electrodes: those with elements hung from support beams and those with frame-construction electrodes. A complex experimental-theoretical study was conducted for the obtaining reliable reults during investigation of the electrodes' dynamic work.

In the course of theoretical study, integral and differential equations were compiled describing processes of formation of contact forces and the transmission of disturbances in the system's units (1). Approximate methods for calculating maximal accelerations and stresses in the units of coronal electrodes under pulsed loads have been developed. In these calculations, all physical-geometric electrode characteristics and conditions of the formation of inlet effect are considered. Means of rigid and hanged hanging of the elements to the support beam were separately considered.

Contact force during transverse impact to the support beam is determined by the following non-linear integral equation:

$$\left(\frac{P(t)}{K_0}\right)^{2/3} = V_0 t - \frac{1}{m}\int_0^t P(\tau)(t-\tau)\,d\tau - \frac{1}{2\rho F_1 C_1}\int_0^t P(\tau)\,d\tau. \qquad (1)$$

where: $P(t)$ - sought contact force

t - time

V_0 - initial impact velocity

m - mass of the striking body

ρ - density of the material

F_1 - transverse area of beam section

C_1 - propagation of the dis- waves in the beam

K_0 - coefficient, related t physical-geometric c teristics of the e

As a result of the impact to the beam, flexible elements hung to the beam are subject to a loss of stability in a small portion of length by the value ℓ with a maximal deviation of y_0 (these parameters depend upon intensity of the impact and upon the character of attachment of the elements to the beam). The disturbance taken by the element is propagated along its length and as a result all points of the element are subject to the acceleration.

Maximal acceleration at the points of the coronal elements during rigid attachment to the support beam is determined by the approximate formula:

$$a = \frac{2\pi^2 P_0 y_0 c}{\rho F_1 c_1 \ell^2} \exp\left[-\frac{\pi}{t_0}\left(\frac{\gamma z}{c} + \frac{\gamma_1 x}{c_2}\right)\right]$$

where: P_0, t_0 - maximal value of contact force and duration of contact

c, c_2 - velocity of propagation of longitudinal and transverse waves in flexible coronal elements.

γ, γ_1 - coefficients of internal friction in support beam material and in the element, determined experimentally

z, x - distance from the point of the impact to the point of attachment of the element and coordinates of the point of the element.

Maximum stress in coronal elements is determined according to the formula:

$$\sigma_{max} = \frac{P_0 c}{F_1 c_1} + \frac{Q}{F_2} ,$$

where: Q - force of element stress, F_2 - area of its transverse section.

During developement of a method of experimental study of the dynamics and durability of coronizing electrodes with flexible elements, specific features of the studied system were considered. The impulse character of charging, great element flexibility and small driven mass impose essential limitations on the choice of monitors and methods for measuring dynamic characteristics.

Inertial-type monitors based on resistor, capacity, electromagnetic and piezoelectrical converters have received the greatest distribution for measurement of the parameters of movement (2). For measuring acceleration occuring in coronizing electrodes, piezoelectric accelerometer-sensors which possess wide ranges of measurement for amplitude and frequency and small dimensions and mass were used.

The method of fastening the sensor and its mass have an effect on the measurement results when the measurement sensor is fixed directly to the surface of the object. In this case, the error, caused by the means of attachment, did not exceed 10%. For determining the effects of the monitor's mass, special experiments were carried out and the problem of flexible element oscillation with concentrated mass was theoretically solved. The calculated dependence of measured accelerations on the mass of the sensor and experimental data for a frequency of 2.08 kilohertz is introduced in fig.1. The obtained relationship allows either selection of sensor mass providing desired accuracy of measurement, or calculating the true value of acceleration with respect to the figure for measured accelerations with a known sensor mass. Relative measurement error of accelerations as taken by the described method did not exceed 19%.

As a result of experimental investigation of dynamic characteristics, the effect of a whole series of factors on the level and character of the distribution of maximum accelerations (those normal to coronal electrode surfaces) were established. These factors are: method of fixing of the elements to the support beam; element length and their stretching strength; mass of the rapping mechanism's hammer and initial velocity of the impact.

Fig. 2 introduces basic results of dynamics studies for coronal electrodes with hanging elements. The results are relative to cases of rigid element mounting to the support beams.

The contact force from a blow to the coronal electrode unit frame (see fig. 3) is determined using a non-linear integral equation similar to equation 1, with the only difference being the last term in the right part of the equation before the integral - a factor of the following type:

$$\frac{1}{2\rho F_1 c_1 + \rho F_3 c}$$

where F_1 - area of transverse section of frame rod taking the blow.

F_3 - Area of transverse section of frame rod, taking the longitudinal blow.

As a result of the impact to the frame assembly, a disturbance is propagated through all of the rods. Wave reflection and refraction occurs in the frame assemblies, and as a result of this, the amplitude of the disturbance steadily diminishes. Fig. 3 is a diagrammatic calculation of the distribution of maximum accelerations through the frame with regard to the transmission of impact energy to all coronal elements.

A section of the distribution of the level of maximum accelerations lengthwise along rod A-A, taking the longitudinal blow, is shown in fig. 4. Experimental results are shown for comparison. Discrepancy of the calculations with the experimental data is explained by the fact that in experiments, sufficiently close contact of the coronal elements with the frame rod A-A was not provided. In support of this, a dotted line in fig. 4 shows the result of calculation with the complete absence of coronal electrodes.

The experimental-theoretical study of dynamic characteristics undertaken allows calculation of coronal electrode dust-removal efficiency still at the electrostatic precipitator's planning stage, it allows choosing optimal variants of their design , and also evaluation of the reliability and durability of their work.

On the basis of results from the research conducted in NIIOGAZ's Semibratovsk branch, improved coronal electrode design variants have been developed. At present, these are being studied as laboratory bench-scale models.

BIBLIOGRAPHY

1. Goldsmit, V., Shock: Theory and Physical Properties of Colliding Bodies, Moscow, Stroizdat, 1965.

2. Iorish, Y.I., Vibrometrics, Moscow, Mashinostroenie, 1963.

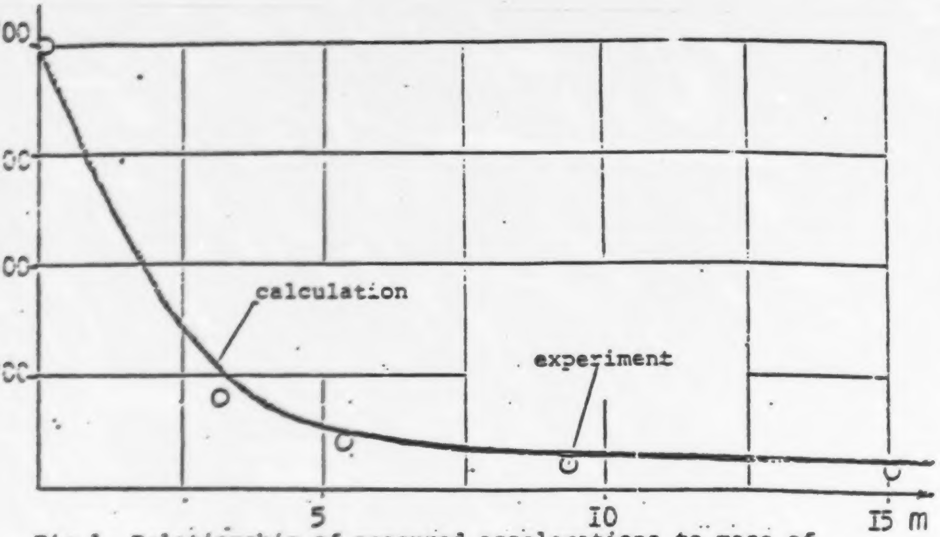

Fig.1. Relationship of measured accelerations to mass of of the sensor.

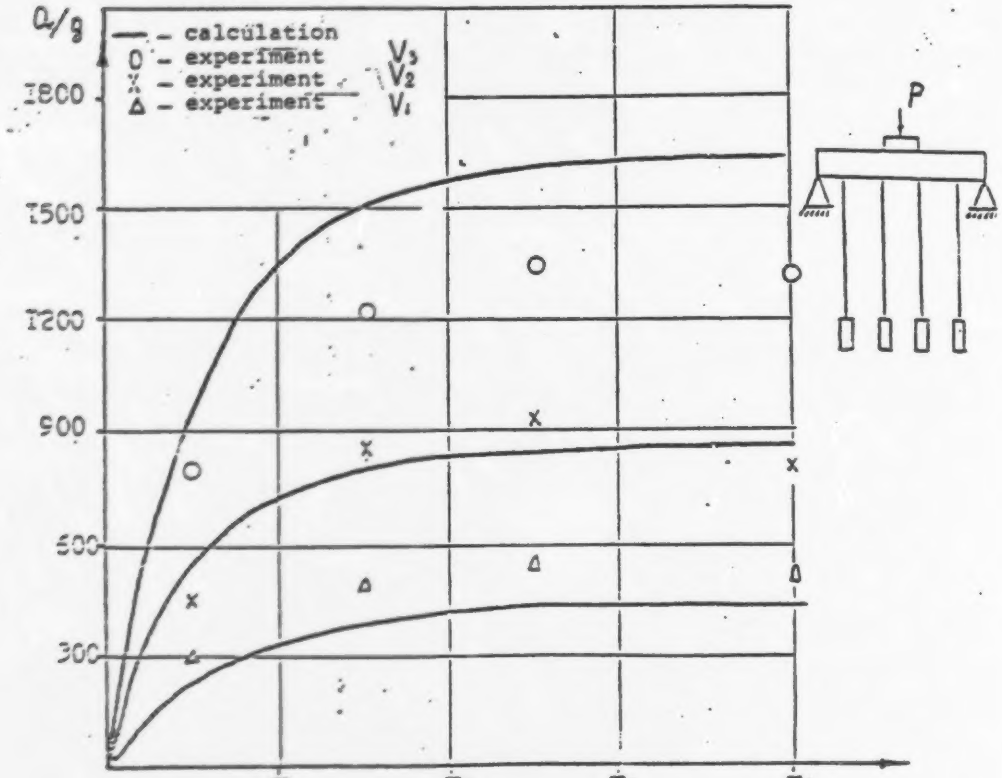

Fig.2. Relationship of mean level of maximum accelerations

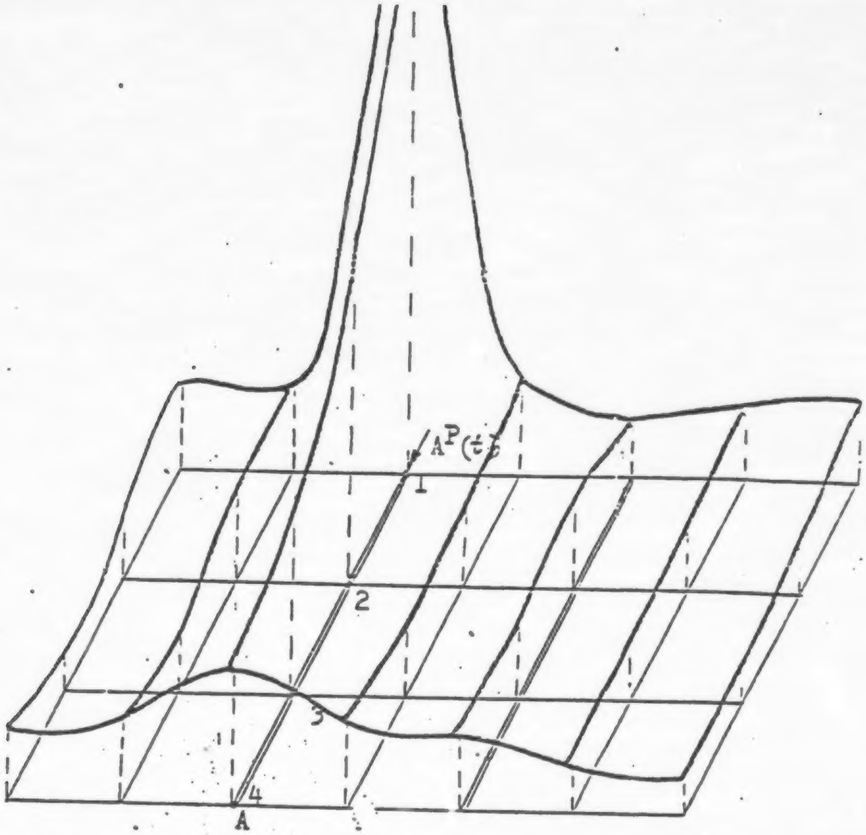

Fig.3. Calculated distribution of level of accelerations along frame-design coronal electrode.

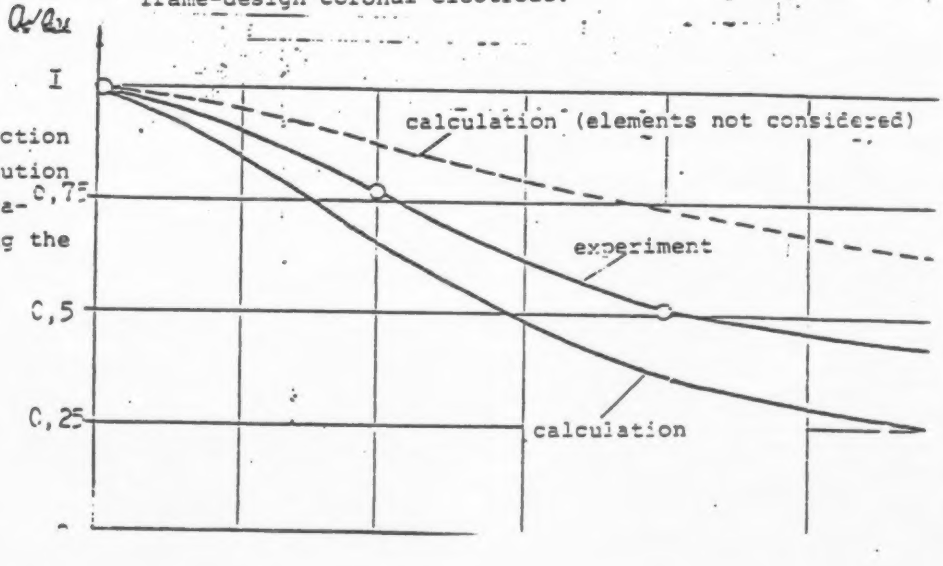

Fig.4. Section of distribution of accelerations along the line A-A.

PROGRESS ON ELECTROSTATIC PRECIPITATORS FOR USE AT HIGH TEMPERATURE AND HIGH PRESSURE

by

George Rinard, Donald Rugg
Robert Gyepes, James Armstrong
Denver Research Institute

and

Dennis Drehmel
Particulate Technology Branch
Industrial Environmental Reseach Laboratory
Environmental Protection Agency
Research Triangle Park, N. C. 27711

(This document has been reviewed and approved for publication by the U.S. EPA.)

INTRODUCTION

The electrostatic precipitator (ESP) is one candidate apparatus for use as the tertiary collector in a pressurized fluidized-bed combustion (PFBC), combined-cycle power plant. This application would require operation of the ESP at temperatures on the order of 1000°C and pressures of 1 MPa. ESP's in this range of temperature and pressure may also find application in coal gasification and magnetohydrodynamic (MHD) power generation. While some work has been done on ESP's operating under these conditions, the feasibility of commercial application of ESP's for use with PFBC is yet to be demonstrated.

Presently work* is being conducted to determine the feasibility of ESP operation under these extreme conditions. The project is to design and build a high temperature pressure vessel and test ESP operations under flow conditions. Many of the technical problems to be overcome relate to the materials that can be used for extended periods of time at the high temperature involved. Under the present schedule, initial testing will start about December 1979.

BACKGROUND

All work to date on ESP's at high temperature and pressure has utilized cylindrical electrode geometry. Some of the earlier work on on high temperature, high pressure (HTHP) ESP's was done at General Electric[1] In this work the negative corona characteristics of air and methyl chloride were determined over a temperature range of 20 to 500°C and pressures from 100 to 500 kPa. This work concluded that, for a range of current densities of 68 to 680 nA/cm^2, the temperature and pressure had no effect on the corona discharge other than on the density of the gas. Thus, the characteristics were uniquely determined by the relative density of the gas between the electrodes.

---

*This work was supported under EPA Research Grant R805939(010) through EPA's Industrial Environmental Research Laboratory, Research Triangle Park, N.C.

Several years later corona characteristics were measured at Princeton for both positive and negative corona for air and nitrogen at temperatures from 65 to 825°C and with pressures from 10 to 800 kPa.[2] At this time it was reported that positive corona characteristics were a function of gas density only. However negative corona characteristics were found to depend on gas temperature as well as gas density. In addition, pressure dependent instabilities were observed at high temperature for both polarities.

Shale's work[3] at the Bureau of Mines in 1963 also showed that negative corona depended on gas temperature as well as gas density. This work was done in a 5 cm diameter cylindrical ESP for temperatures of 315°C to 815°C and pressures of 100 to 640 kPA, using negative discharge corona. The results indicate stable precipitator operation for the full range of pressure and temperature up to 730°C. Above 730°C, operation was limited to pressures above atmospheric, because sparking occurred before corona could be generated at lower pressures. The length of the corona wire was 107 cm' the 5 cm diameter pipe section was 61 cm long. The current densities were in the range of approximately 3-5 nA/cm^2. This is considerably higher than normally encountered in low-temperature, atmospheric-pressure ESP's. An effective ion mobility was calculated from the experimental data: with all else constant, it was found to decrease with gas density, to increase with both temperature and field strength. The higher effective mobility, at higher temperatures and field strengths, was attributed to larger components of electron current since the mobility of ions changes very little with these parameters.

Cooperman[4] predicts high thermal ionization rates at high temperatures. Trace quantities of alkali metals could serously effect ESP operation at temperatures above 800°C. However, Shale's[3] conclusion concerning thermal ionization is that this should not be a problem over the range of temperatures and pressures considered.

A year later Shale repeated his earlier experiments,[5] using positive discharge corona. The same procedure that was used for negative corona was used, with the polarity reversed. This work showed essentially the same corona-start voltage for positive or negative corona, except that, at above 650°C, the negative corona-start voltage was considerably lower than for positive corona. Sparkover voltage was considerably higher for negative corona below 200°C, at which temperature it was equal to that for positive corona. Above 200°C, sparkover voltage for negative corona was lower than for positive corona, becoming about equal to the corona onset voltage at 800°C. The positive corona sparkover voltage, however, remianed high at higher temperatures. From this result, Shale predicted that positive corona would be more efficient at high temperatures. He calculated that at 650°C a positive-corona ESP would have to be four times as large as a negative-corona ESP to achieve the same collection efficiency.

In 1969 Shale reported on a multitube, high-temperature, high-pressure ESP operating at 800°C and 640 kPa.[6] The equipment utilized a modified atmospheric gas/air combustor. The ESP, designed and constructed under contract with Research Cottrell, was 1.5 m in diameter and 9.1 m high. There were 16 tube-type collecting electrodes each 15.2 cm in inside diameter and 1.8 m long. Its SCA was 19.7 $m^2/(m^3/sec)$, with all tubes parallel with the gas flow. The power supply was 45 kV unfiltered dc (70 kV peak) at 250 mA. This supply would allow about 1 nA/cm^2, which, although lower than used in his earlier experiments, is high compared to atmospheric ESP's.

Shale found that he obtained higher collection efficiencies using negative corona. He obtained much higher currents with negative corona and operation was spark-limited. On the other hand positive current amplitudes were about 20 percent of those obtained with negative corona even though the voltage was considerably higher. He did not get sparking at the maximum positive voltages, which would indicate that the maximum voltage was still too low. With the equipment available, he was not able to operate in the high voltage positive corona range where he predicted that collection efficiencies would be higher. The apparent reason for this is that he increased the size of the tubes from 5.1 to 15.2 cm but did not increase the power supply voltage sufficiently to be able to operate in the range where higher efficiency was expected for positive corona. The average measured efficiencies were 75 to 77 percent for positive corona. The average measured efficiencies were 75 to 77 percent for positive corona and 91 to 96 percent for negative corona.

In 1971 a larger scale HTHP ESP was tested[7] by Brown at Research Cottrell: the temperature was as high as 940°C at pressures up to 1.05 MPa. The ESP was a 20.3 cm diameter, 4.6 m long pipe. The corona V-I characteristics and collection efficiencies agreed well with those obtained by Shale. Negative corona currents were much higher for a given voltage than positive corona currents, and negative corona collection efficiencies were much higher. Collection efficiencies for negative corona were as high as 91 percent; the SCA was about 37.4 $m^2/(m^{3/sec)}$.

Recent work on HTHp ESP's was also done at Research Cottrell by Feldman.[8,9] This work presents clean plate V-I corona curves for both polarities at temperatures up to 1093°C and pressures up to 3.5 MPa. The collector eletrode was a 7.6 cm diameter tube. In this work negative corona appeared to provide higher sparkover voltages than positive corona even in the range of temperature and pressure used by Shale and Brown.

A recent review of HTHP ESP work in the Soviet Union is given by Val'dberg.[10] This work covers the temperature range to 400°C and pressures of 100 to 600 KPa. Cylindrical and point-plane ESP's were used. The cylindrical ESP's used tubes 6.4, 9.9, and 14 cm in diameter and 49.8 cm long. The corona electrode was a strip-needle configuration, unlike the smooth round wire or twisted wires utilized by U. S. investigators. Their conclusions indicate once again that negative corona provides more efficient collection than positive corona. Another cylindrical ESP (with a 15.2 cm diameter tube, 2.4 m long) was tested on a blast furnace exhaust at 99.9 percent efficiency. The SCA was 19.7 $m^2/(m^3/sec)$. This ESP operated at a temperature of 250°C and a pressure of 300 kPa. The corona wire was operated at a negative voltage of 85 to 90 KV.

An HTHP ESP experiment is being conducted in Essen, Germany.[11] The apparatus consists of a recirculating pressure chamber, with provision for dust entrainment; it too is cylindrical.

The importance of hot gas cleaning is summarized in a recent EPA report.[12] The importance of fluidized-bed technology and hot gas cleaning to the power industry is summarized in the 1977 FBC workshop proceedings.[13] A theoretical review of important parameters relating to dust collection at HTHP is given in another EPA report.[14] This report emphasizes that the behavior of these parameters in the range of temperature and pressure are only partially understood.

A review of HTHP ESP work is given by Robinson[15] who indicates that as pressure is increased a critical pressure may be reached where the sparkover voltage is lower than the corona onset voltage. The critical pressure is a function of corona electrode size and relative gas density. A range of operation suitable for PFBC ESP's is given.

The results of this past work indicate stable operating regions for HTHP ESP's suitable for use with PFBC. There appears to be agreement that ESP's can be operated effectively at HTHP. The high temperature has a degrading effect on performance, but these effects are countered by increased pressure. If the corona characteristics are very nearly depending on density only, at the pressures and temperatures under consideration, one could expect two to three times the operating voltage that is normally found in a typical cold-side precipitator. There are many questions. How will gas density affect its viscosity and, in turn, particle migration velocity? What SCA's will be needed? How should the sections be subdivided mechanically and electrically? What about ash resistivity and consistency at high temperature? What about thermal ionization, particularly those trace compounds with low ionization potentials that may occur in stack gas? The object of the present project is to test HTHP ESP performance in the laboratory, using reentrained fly ash, and to determine answers to these questions.

LABORATORY MODEL HTHP ESP

A laboratory model HTHP ESP system is presently being designed and is shown pictorially in Figure 1. The air compressor will supply 27.2 kg-mol/hr at 1 MPa to the burner package. The burner is a specially designed high pressure unit capable of burning either methanol or No. 2 fuel oil. The burner has a maximum heating capacity of 244 J/s and a maximum turndown ratio of 4:1. Gases at temperatures up to 1000°C leaving the ESP will be cooled to 260°C before the outlet sampling port. Cooling will involve an air cooled jacket and cooling fins.

The planned pressure vessel is shown in Figure 2. It has a cool outside pressure shell. The hot gases enter near the bottom and exit near the top of this shell. The inside of the shell is lined with castable refractory. The chamber will be capable of accommodating collecting tubes up to 30 cm in diameter. The collecting tube will be supported by three rapping rods which will extend through the top of the pressure vessel.

The corona wire will be supported by an air cooled, one piece, high density alumina feedthrough. Cooling will be provided by cooling fins inside the pressure shell and a water jacket outside. Radiation shields on the corona wire will help prevent radiant heat from reaching the high voltage feedthrough. The maximum design temperature for the high voltage feedthrough is 260°C.

The shell and flanges will be carbon steel. The shell will be rolled plate stock, with butt-welded ASA flanges. Sufficient insulation will be provided to maintain a maximum temperature of 110°C on all carbon steel components and welds. The collector tube will be 18 BWG (1.25 mm) 310 stainless steel or equivalent. The corona wire will be Hastelloy X, and the radiation shields will be 310 stainless steel. Other materials considered were Iconel, tungsten, and Incoloy. Inconel and Incoloy alloys do not have the creep strength required at 980°C and tungsten oxidizes at temperatures above 425°C. The cooling section of the outlet will be 316 stainless steel or Hastelloy X.

A cooling water system will cool the top and bottom of the precipitator vessel to a temperature where the high voltage feedthrough can operate at a maximum temperature of 260°C. The system will consist of a cooling water jacket around the top of the vessel, a circulation pump, and air cooled heat exchanger, and associated piping and controls.

Laboratory tests were conducted to simulate the air flow and electrical conditions of the HTHP ESP. For air flow modeling, the following was assumed: the main gas velocity through the ESP is 1 m/sec, the collector tube diameter is 29.2 cm, and the gas pressure is 1 MPa. The Reynolds number was calculated to be,

$$Re = 1.4 \times 10^4$$

To obtain the same Reynolds number of the half scale model at an ambient temperature of 21°C at Denver's altitude of 1.6 km required an average velocity of

$$\bar{v}_{scale} = 1.8 \text{ m/sec}$$

Air velocity traverses were made at 13 points along the length of the model including the hopper and high voltage feedthrough area. The velocity distribution had a normalized standard deviation of less than 10 percent in the collector tube between 3 tube diameters from the inlet to 1 tube diameter before the outlet.

Smoke tests in the model indicated that essentially stagnant conditions existed in the hopper and high voltage feedthrough areas.

The results of the air flow modeling indicates that good quality air flow should exist in the HTHP ESP.

The electrical modeling was done in a 23 cm diameter tube to determine if a lower corona wire guide would be required and to examine potential sparking problems at the inlet and outlet ports. The tests were performed at ambient conditions and the results extrapolated to indicate what could be expected at the relative gas densities of the HTHP ESP.

The results of these tests indicate that a lower corona guide will be required to prevent pendulum action of the corona wire. To ensure good electrical insulation of the guide, the hopper area, where the guide is located, will be water cooled.

The tests also show that sparking should not occur with clean conditions below 200 kV. For a corona wire diameter of 0.635 cm, the calculated negative corona onset voltage is 130 kV. It is expected to be possible to obtain corona current densities as high as 1 a/cm^2.

While the electrical tests at ambient conditions should not be used to predict actual performance of the HTHP ESP, they were done to help indicate practical parameters for the working unit.

REFERENCES

1. Koller, L. R. and Fremont, H. A., "Negative Wire Corona at High Temperature and Pressure," Journal of Applied Physics, Vol. 21, pp. 741-4, August 1950.

2. Thomas, J. B. and Wong, E., "Experimental Study of dc Corona at High Temperatures and Pressures," Journal of Applied Physics, Vol. 29, No. 8, pp. 1226-30, August 1958.

3. Shale, C. C., Bowie, W. S., and Holden, J. H., "Feasibility of Electrical Precipitation at High Temperatures and Pressures," Bureau of Mines Report of Investigations RI 6325, 1963.

4. Cooperman, P., Commun. Electron., 75, 792, 1964.

5. Shale, C. C., Bowie, W. S., Holden, J. H., and Strimbeck, G. R., "Characteristics of Positive Corona for Electrical Precipitation at High Temperatures and Pressures," Bureau of Mines Report of Investigations RI 6397, 1964.

6. Shale, C. C. and Fasching, G. E., "Operating Characteristics of a High-Temperature Electrostatic Precipitator," Bureau of Mines Report of Investigations RI 7276, 1969.

7. Brown, R. F. and Walker, A. B., "Feasibility Demonstration of Electrostatic Precipitation at 1700°F, "Journal of the Air Pollution Control Association, Vol. 21, No. 10, pp. 617-20, October 1971.

8. Feldman, P. L., "Development of a High Temperature Electrostatic Precipitator," Progress Report, EPA Contract 68-02-2104, Cottrell Environmental Sciences to EPA, Research Triangle Park, N. C., June 1975.

9. Feldman, P. L., "High Temperature, High Pressure Electrostatic Precipitator," in EPA/DOE Symposium on High Temperature/High Pressure Particulate Control, EPA-600/9-78-004 (NTIS No. CONF-770970, 3/78, Washington, D. C., September 20-21, 1977.

10. Val'dberg, A. Y., Danilin, V. V., Lyapin, A. G., and Tkachenko, V. M., "Electrical Gas Cleaning at Higher Pressures," in Second US/USSR Symposium on Particulate Control, EPA-600/7-78-037 (NTIS No. PB 279-625, 3/78, Research Triangle Park, N. C., September 2629, 1977.

11. Weber, I.E., "Problems for Gas Purification Occurring in the Use of New Technologies for Power Generation," EPA/DOE Symposium on High Temperature/ High Pressure Particulate Control, EPA-600/9-78-004 (NTIS No. CONF-770970, 3/78, Washington, D. C., September 20-21, 1977.

12. Parker, R., Calvert, S., and Drehmel, D. C., "High-Temperature and High-Pressure Particulate Control Requirements, EPA-600/7-77-071 (NTIS No. PB 271-699) July 1977.

13. "Proceedings on the Fluidized Bed Combustion Technology Exchange Workshop, Vol. 1 and 2," sponsored by ERDA and EPRI, CONF-770447-P-1, April 13-15, 1977.

14. Calvert, S., Parker, R., and Drehmel, D. C. "Effects of Temperature and Pressure on Particle Collection Mechanisms: Theoretical Review," EPA-600/7-77-002 (NTIS No. PB 264-203), January 1977.

15. "Air Pollution Control, Part 1", edited by Werner Strauss, John Wiley, New York, pages 283 to 298.

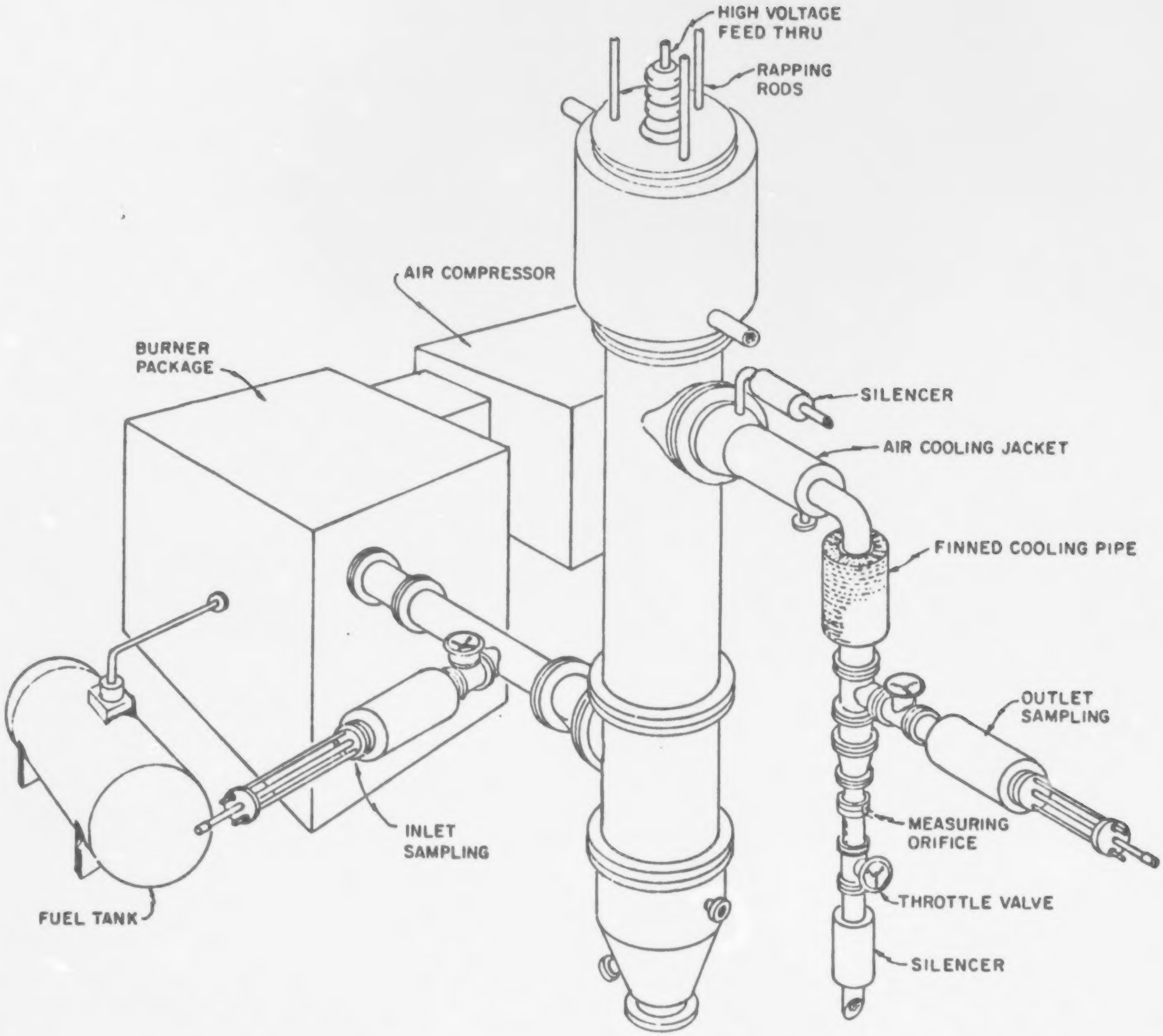
HIGH VOLTAGE FEED THRU
RAPPING RODS
AIR COMPRESSOR
BURNER PACKAGE
SILENCER
AIR COOLING JACKET
FINNED COOLING PIPE
OUTLET SAMPLING
INLET SAMPLING
MEASURING ORIFICE
THROTTLE VALVE
FUEL TANK
SILENCER

FIGURE 1. HTHP-ESP SYSTEM

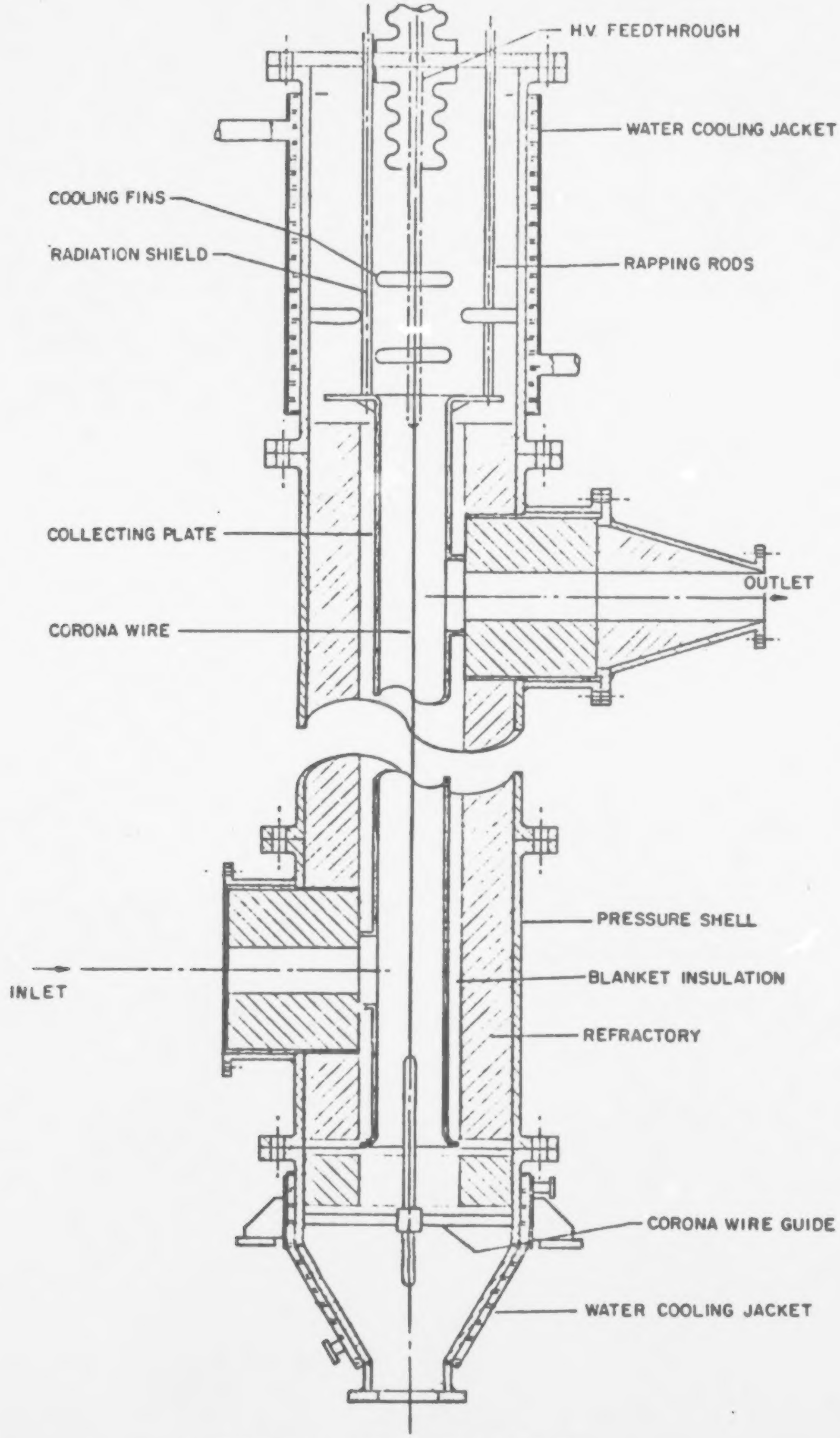
H.V. FEEDTHROUGH
WATER COOLING JACKET
COOLING FINS
RADIATION SHIELD
RAPPING RODS
COLLECTING PLATE
OUTLET
CORONA WIRE
PRESSURE SHELL
INLET
BLANKET INSULATION
REFRACTORY
CORONA WIRE GUIDE
WATER COOLING JACKET

FIGURE 2. HTHP-ESP VESSEL

V.M. Tkachenko, V.A. Rodionov, A.D. Malgin

PURIFICATION OF HOT ASPIRATED AIR FROM SINTERING MACHINES AND CLINKER COOLERS

Presently in the USSR, dry electrostatic precipitators have been accepted as the basic unit in planning the purification of aspirated air in iron industry sintering plants.

With an increase in aspirated air temperature, the resistivity of dust caught in the precipitators rises and this may cause back corona in the precipitator's electrodes. It is known that the back corona considerably lowers the precipitators' work efficiency.

Therefore, one of the basic research problems of electrostatic precipitation of aspirated air from sintering machines is in determining maximum temperature and other parameters of the aspirated air, under which precipitators can efficiently work without back corona.

Such research has been conducted by the State Scientific Research Institute for Gas Purification in Industry and Sanitation (NIIOGAZ) in the sintering plant of a metallurgical factory where aspirated air from AKM-312 sintering machines was cleaned on installment of 8 DVPNI-4x20 electrostatic precipitators. Before passing the precipitators, the aspirated air at this site was mixed in a common collector. This air was from various sources: sites where charge was loaded into compacters, from hammer mills, sifters, conveyer sinter overfills, covering of front and rear portions of line coolers, and others. Cleansed aspirated air enters an exhaust fan from each precipitator and is then expelled through a common flue into the atmosphere.

The electrostatic precipitator DVPNI-4x20 is a dry gas, vertical, plate-type unit with coronal needle electrodes and has the following technical characteristics:

1. Number of sections	4
2. Active sectional area of sections, m^2	20
3. Number of precipitating electrodes in one section	18
4. Precipitating electrode dimensions, m	7.9x4

Each precipitator section is fed by a separate unit, the ATF-250, with nominal rectified current of 250mA and a maximal voltage value of 80kv.

During research on precipitators, sintering machine technological condition was characterized by the following indices: sinter basicity (the relationship $\frac{CaO}{SiO_2}$) ran 1.16-1.30, and iron content in sinter was 57.9-58.7%.

From the eight operating precipitators, one was chosen for research at whose intake the temperature was maximal and ranged from 107-115°C. The air's moisture content had a value of 7.5-13g/m^3 with an mean value of 11.1g/m^3 (of moist air). Under these conditions, the cleansed air's dust resistivity changed in the range of (1-8) 10^{10} ohm.cm. (i.e. on a critical value level). Average particle size at the intake, as determined by liquid sedimentation, was 19 microns.

Under the indicated moisture-temperature conditions of aspirated air, dust resistivity values, and the tested current density (up to 0.23mA/m^2), the precipitator operated without back corona. Coinciding corona volt-ampere characteristics, measured under voltage rise and drop attests to the lack of back corona. A sample of such characteristics is introduced in table 1. It is known, that with the presence of back corona in precipitators, the volt-ampere characteristic runs higher at a drop in voltage than with a voltage increase.

With air entering the precipitator at an operational velocity of 0.75m/s, the degree of cleaning's mean value comprised 99.38% when the residual dust content was 13mg/m^3(n), and with an increase in the velocity up to 1.15 m/s, the degree of purification was lowered to 96.8% and the mean value of residual dust after electrostatic precipitation rose to 87mg/m^3(n).

The indicated precipitator work efficiency was obtained with feeding the units under conditions of periodical spark-overs and optimized electrode rapping the interval between precipitator electrode rappings were 125 minutes, and its duration was for five minutes, with 40 and 20 minutes correspondingly for coronal electrodes.

Thus, at temperatures of sintering machine aspirated air reaching 110°C, and a moisture content of 7.5-13g/m^3 (of moist air), the DVPNI-4x20 vertical precipitator works efficiently without back corona under a current density of 0.23mA/m^2, which conforms well with results, predicted for back corona occurence with use of NIIOGAZ equipment (fig.1.).

Aspirated air from clinker coolers contains a large amount of coarse dust fractions, whose median particle diameter is 30-40 microns with a dispersion of 4.5-5. The dust is noted for its abrasiveness and high resistance which usually ranges 10^9 to 10^{10} ohm.m.

Aspirated dust temperature depends on processing conditions and may change from 120°C to 280°C.

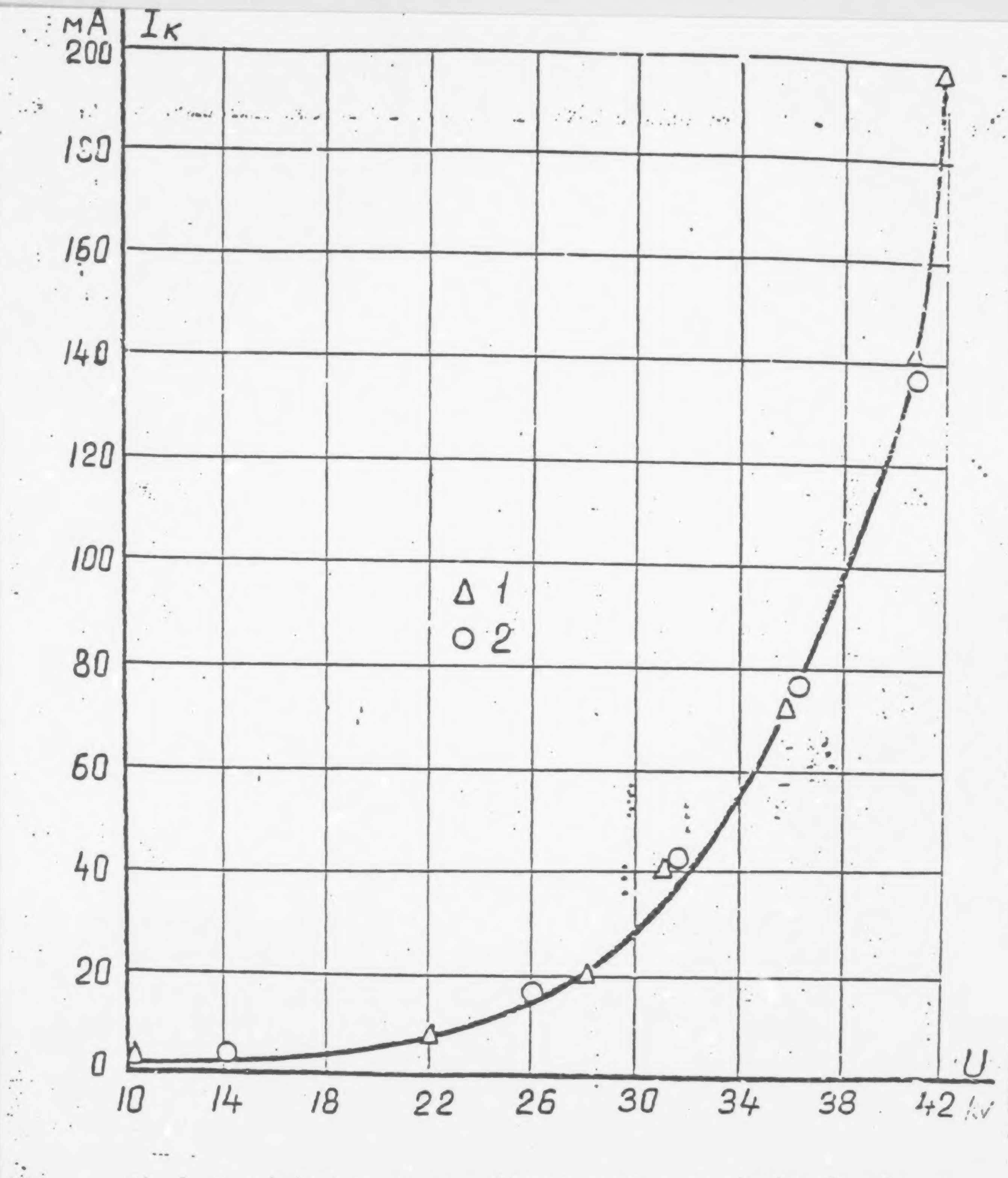

Fig.1. Precipitator corona volt-ampere characteristics for the DVPNI-4x20: 1. at a rise in voltage 2. at a drop in voltage; air temperature in precipitator, 107°C, 11.2g/m^3 air moisture.

In using electrostatic precipitators for cleaning aspirated gases, troubles occur, connected with the dust's high resistance. To efficiently purify the gas, it is necessary to condition the dust-gas mixture entering the cleaning process. It will, otherwise, complicate and raise the expense of cleaning to a considerable degree.

Using cyclone dust-removal equipment will not meet sanitary requirements set for cleaning aspirated air. The abrasiveness of coarse dust particles rapidly erodes cyclone elements.

The high temperatures of aspirated gases impede the use of filter bags equipped with inexpensive filtering materials made from synthetic fibers.

As test results from NIIOGAZ's Semibratovsk branch show, using gravel filter-cyclones has been shown to be highly-promising for cleaning clinker cooler gases. The filter-cyclone's distinctive feature is its three-stage cleaning process. A precipitation chamber, spread between the two rows of cyclone elements, is the first step in the process. The third step is a filled layer made up of 2-4mm gravel.

A significant characteristic of the unit is the double layer positioning of the filled layer and its regeneration by agitation and reverse blowing with air. The blown air which passes through the filter layer from below upwards attracts dust particles and carries them to the cyclone, where the large particles of sinter material settle out. The fine sinter particles together with the blown air stream enter other sections which operate as filters and settle out in the gravel layer.

Agitation has the main significance of separating dust from the filled layer granules. Moving relative to each other during granule agitation, the dusts, which cannot be blown out by an air-jet stream, are conducive to separation.

The filter-cyclone FTGN-120, with a 120m^2 filter surface, is used to clean aspirated air from a "Volga 35" clinker cooler in one cement plant. The unit is estimated to clean gas at a rate of 100-120 thousand m^3/hour. Experience with filter-cyclones in industrial conditions has shown that dust concentration at the unit's outlet is

40-50mg/m^3, and the degree of purification about 99%. The unit's hydraulic resistance is 2500-3000 Pascals. Studies have shown that 80% of the dust settles in the cyclone and dust chamber and only 20% enters the filled layer.

Uniform distribution of the granules in the layers in one and the same section has the essential effect on the operation of the unit. In those trays where the gravel layer is lower, the hydraulic resistance is less, the stream of dust and gas passes through it with great speed, and the degree of purification is reduced. In connection with a build-up of a considerable dust layer, regeneration in these trays passes less intensively.

Filter-cyclone operation in cement factories has shown the unit's sufficient reliability.

A MODEL OF ELECTROSTATIC PRECIPITATION FOR TI-59 CALCULATOR

by

L. E. Sparks
Particulate Technology Branch
Utilities and Industrial Power Division
Industrial Environmental Research Laboratory
Research Triangle Park, N. C.

ABSTRACT

A mathematical model of electrostatic precipitation has been developed for the Texas Instruments TI-59 calculator. The equations used in the model are presented. The calculated results of the model are shown to be in good agreement with the results of the EPA-Southern Research Institute Computer Model for Electrostatic Precipitation.

(This document has been reviewed and approved for publication by the U.S. EPA.)

INTRODUCTION

Recent advances in calculator technology have made available calculators with tremendous computing capability. This computing capability can be used to model electrostatic precipitation without a large computer. This paper describes such a model for the Texas Instruments TI-59 Calculator.

THE MODEL

The ESP Model for the TI-59 Calculator is based on the EPA-Southern Research Institute (EPA-SoRI) ESP Computer Model Revision I by McDonald.[1] A brief discussion of the theory behind the model and the assumptions in the model are given here. The reader interested in more detail should consult the referenced reports.

Steps in Electrostatic Precipitation Process

The electrostatic precipitation process can be divided into 4 steps:

1. Corona generation and establishment of electric field.
2. Particle charging.
3. Particle collection.
4. Removal of the collected material.

A complete model of the process would handle all four steps. However, Step 4 is too complex to be modeled at this time and is neglected by both the EPA-SoRI Model and the TI-59 Model. Step 1 is modeled in detail by the EPA-SoRI Model but is neglected in the TI-59 Model. The TI-59 Calculator does not have sufficient power to handle the computation used in the computer program. Work is underway to develop approximations for use in the TI-59. When these approximations are developed they will be incorporated into the model. Until then the user must supply as input data the applied voltage and current density.

Particle Charging

Particle charging generally takes place by two mechanisms--field charging and diffusion charging. For large particles field charging is by far the dominant mechanism. Diffusion charging dominates for very small particles. Particles of major interest in air pollution (those with $0.1 \le d \lesssim 2$ μm) are charged by both mechanisms. Pontius et al^2 have shown that the following approximation for the charge on a particle agrees with experimental data and detailed theory fairly well.

$$\eta p = \frac{\Pi d}{2} C_1 \left\{ \frac{b\ d/aE_{Av}Nt}{b\ Nt + C_1} \left[1 + 2\left(\frac{K-1}{K+2}\right)\right] + C_2 T \ln\left(\frac{dvNt}{2C_1C_2T} + 1\right) \right\} \qquad (1)$$

ηp = number of charges
C_1 = $4\ \varepsilon_o/e$
C_2 = k/e
ε_o = permitivity of free space
e = charge on electron
k = Boltzman's constant
b = ion mobility
E_{Av} = average electric field
N = free in density
t = residence time for charging
K = particle dielectric constant
v = mean thermal speed of ions
d = particle diameter

The charge on a particle, q, in coulumbs is given by

$$q = \eta_p e$$

This equation is used in the TI-59 program and in the approximation procedure in the EPA-SoRI Model.

The average electric field used in the calculation is given by

$$E_{Av} = U/H \qquad (2)$$

where U = the applied voltage qv
H = wire to plate spacing, m

The free ion density, N, is given by

$$N = bE_{Av}/j$$

where b = average ion mobility,
j = current density a/m^2

Particle Collection

Particle collection in an ESP is given by the Deutsch Andersen equation

$$Pt(d) = \exp\left[- \omega(d)\, A/V \right] \tag{3}$$

where $\omega(d)$ = electrical migration velocity of particles with diameter d, m/s

A = collector plate area m^2

V = volumetric flow rate of gas m^3/s

The ratio A/V is called the specific collector area (SCA).

The electrical migration velocity near the collector plate for small particles is given by Stokes' law as

$$\omega(d) = q\, EpC'/3\pi\mu d \tag{4}$$

where q = the particle charge, coul. ($q = e n$)

Ep = the electric field at the plate, v/m

C' = the Cunningham correction factor

$= 1 + 2A\frac{\lambda}{d}$

$A = 1.246 + 0.42 \text{ esp } (-0.87\, d/2\lambda)$

λ = mean free path of gas

$= \lambda_o\left(\frac{76}{p}\right)\left(\frac{T}{296.2}\right)$

λ_o = mean free path at 23°C and 76 cm Hq pressure

P = barometric pressure, cmHg

T = temperature, °K

μ = viscosity of gas kg/m-s (10 poise = 1 Kg/m-s)

McDonald[1] reported that for ESP collecting flyash

$$E_p \approx E_{Av}/1.75 \tag{5}$$

This estimate of E_p is used in the TI-59 Model.

McDonald also reported that equation (4) underpredicts the migration velocity for real ESP. He recommends that the migration velocity be corrected by an emperical factor to improve agreement between predictions and theory. The corrected migration velocity is given by

$$\omega(d) = \omega(d)_{\mu} \text{ X } (1.7 - 0.45d) \qquad (5)$$

where $\omega(d)_{\mu}$ is the uncorrected migration velocity Equation (5) applies for $0.2 < d < 4.5$. Outside this range equation (4) applies.

Non-Ideal Factors

The Deutsch Andersen equation applies to an ideal situation. Certain non-ideal factors exist in real ESP which result in higher penetrations than those predicted by Equation (3). Chief among these non-ideal factors are non-unform gas flow, sneakage, and reentrainment. Gooch et al.[3] have shown that the effects of these non-ideal factors can be estimated from

$$Pt'(d) = \exp\left[\frac{-\omega(d)A}{BF\ V}\right] \qquad (6)$$

where $Pt'(d)$ = the corrected penetration,
B = the correction factor for sneakage and reentrainment
F = the correction factor for non-uniform gas flow

$$B = \frac{\ln P + (d)}{N_s \ln\left[S + (1 - S)Pt(d)^{1/N_s}\right]} \qquad (7)$$

N_s = number of baffled sections
S = the fraction of particles that are reentrained and that bypass electrified region per section.

$$F = 1 + 0.766\ [1 - Pt(d)]\,\sigma^{1.786} + 0.0755\ \sigma \ln[1/Pt(d)] \qquad (8)$$

σ = the normalized standard deviation of the gas flow ($\sigma = 0.25$ is generally considered good)

Note that both B and F are particle size dependent.

The overall penetration, Pt_o, is given by

$$Pt_o = \int_0^\infty Pt(d) f(d) dd \qquad (9)$$

and the corrected overall penetration, Pt_o', is given by

$$Pt_o' = \int_0^\infty Pt(d)' f(d) dd \qquad (10)$$

where f(d) is the fraction of particles with diameters between d and d + dd.

TI-59 ESP Model

A mathematical model based on the above equations has been programmed for the Texas Instruments TI-59 Calculator. In the TI-59 Model the ESP is divided into user specified time increments. The division of the ESP into time increments is necessary to account for the time dependent nature of the particle charging and particle collection process. For each time increment the calculator calculates particle charge, particle migration velocity, and particle penetration through the increment. All these calculations are performed for each particle diameter in the user specified particle size distribution. The penetration of a given particle diameter through the ESP is given by

$$Pt(d) = \prod_{i=1}^{n} Pt(d)_i \qquad (11)$$

where $Pt(d)_i$ = penetration of particles of diameter d through the i^{th} increment.

An effective migration velocity for each diameter for the entire ESP is calculated from

$$\omega(d)_e = \frac{-\ln Pt(d)}{A/V} \qquad (12)$$

The penetration corrected for non-ideal factors Pt(d)' is calculated from

$$Pt(d)' = \exp - \left(\frac{\omega(d)_e \, A/V}{B \times F}\right) \qquad (13)$$

These calculations are performed for each of the m particle diameter in the user specified particle size distribution. The overall penetration is given by

$$Pt_o = \sum_{i=1}^{m} Pt(d)_i \, f_i \qquad (14)$$

and the corrected penetration

$$Pt_o' = \sum_{i=1}^{m} Pt(d)_i \, f_i \qquad (15)$$

The results of the TI-59 Model are in good agreement with results of the computer Model as shown in Table I.

CONCLUSION

The TI-59 Model provides a useful tool for examining the performance of an ESP. The answers are obtained quickly and without a large expensive computer.

REFERENCES

1. McDonald, J., A Mathematical Model of Electrostatic Precipitation (Revision 1) in two volumes. EPA-600/7-78-111a and EPA-600/7-78-11b.

2. Pontius, D. H., L. G. Felix, J. R. McDonald and W. B. Smith, Fine Particle Charging Development. EPA-600/2-77-173, August 1977.

3. Gooch, J. P., J. R. McDonald, and S. Oglesby, Jr., "A Mathematical Model of Electrostatic Precipitation." EPA-650/2-75-037, 1975.

Table I. Comparison of TI-59 and EPA-SoRI Computer Model Results

Diameter	Pt(d) Computer	Pt(d) TI-59
0.30	0.15	0.13
0.40	0.16	0.15
0.525	0.16	0.15
0.7	0.16	0.15
0.95	0.15	0.14
1.25	0.13	0.13
1.6	0.11	0.12
2.05	0.10	0.10
3.15	0.086	0.074
4.0	0.073	0.060
5.25	0.049	0.042
7.0	0.024	0.021
9.0	0.012	0.010
13	0.0037	0.0036

Conditions: U = 26.7 KV j = 13.3 na/cm^2 SCA = 56.81 m^2/m^3/s

Urgent Ash-Trapping Problems at Thermal Power Stations.

L.I. Kropp, G.S. Chekanov

Thermal power engineering's basic orientation to the use of solid fuels, including its inexpensive types, increases the urgency of protecting the atmosphere from stack gas solid contaminants. The extraordinary diversity of domestic fuels is responsible for the substantial variety in emission of harmful contaminants in combustion products. Table 1 includes data on several fuels and their usage in large-scale condensation-type thermal power stations.

Table 1

Fuel	gas discharge (brought to normal conditions) – m^3/1000 KW hrs.	ash discharge g/1000 KW hrs
		fly-ash
Berezov lignite	4,35	29
Kuznetz SS	4,I	82
Donetz low-grade coal	4,0	97
Ekibastuz coal	4,05	253
Estonian shale	5,2	320
Moscow lignite	4,8	242
Mazut (S^p =3%)	4,0	0,4

In the hygienic evaluation of the harmfulness of fly-ash from thermal power stations, at the present time, it is accepted that its charactersitics most nearly correspond to non-toxic dusts raised, for example, from road surfaces by wind or traffic. In reality, it is known however that there are harmful substances in the composition of fly-ash, such as free calcium oxide and silicon oxide, incompletely-burnt fuel particles and small quantities of still more harmful substances such as lead, arsenic, mercury compounds, and from some fuels, radioactive elements (1). The content of these contaminants found in ash is significantly higher than their average content in the earth's crust. Therefore, only some fuel ash can be equated with non-toxic dusts. At the present time, detailed analyses of the various fuel ashes are still lacking and the full measure of their toxicity has not been determined. In connection with this, it has not been excluded that, subsequently, maximum concentration standards (MPC) for ash in the atmosphere will be established differentially with respect to peculiarities of the various fuels' compositions.

In addition to this, MPC values established by sanitary institutions only indicate that dust concentration in the air by weight should not exceed the given value. With this, dust dispersion composition is not specified. Meanwhile, it is known that dust with a particle size over 10 microns doesn't penetrate human lungs but is arrested in the upper respiratory track where it is comparatively easily expelled from the organism. On the other hand, dust particles that are around 1 micron in size do penetrate the lungs, remain there and cause many illnesses. From that point of view, fly-ash released into the atmosphere past thermal power station fly-ash control equipment is dangerous, since it has a nearly 30% composition of particles less than 5 microns.

It should also be noted that the atmosphere's ability to cleansing itself of dust particles is in a very large degree dependent on the dispersion composition of the dusts. Thus, particles of a size larger than 10 microns subside relatively quickly to the earth's surface, 4-10 micron particles rise another km. with the smoke current and are spread along thousands of kilometers of the earth's surface. Particles less than 4 microns precipitate poorly in rain, but slowly subside, reaching the surface from the height of a kilometer in the course of a year. Particles that are less than a micron in size are involved in Brownian motion and are spread like atmospheric gas molecules, settling to the surface only under special conditions, namely, with moisture condensation around them. Thus, highly dispersed fly-ash is capable of accumulating in the atmosphere, which can lead to undesirable consequences (2).

In this connection, gaseous stack gas contaminants, such as sulfuric and nitrous oxides are less dangerous since their presence in the atmosphere is limited to approximately five days, during which they are removed from the air, dissolving into open water and precipitation, reacting with ammonnia secreted by microorganisms, and absorbed by soil and vegetation.

It should also be considered that atmospheric dust disperses solar radiation and reflects part of the energy reaching earth back into space. Measurements show a significant loss of solar radiation intensity in large cities and industrial centers, especially the ultra-violet region of the spectrum, which is the most active biologically. Light dispersion by one and the same amount by weight of dust is inversely proportional to particle size to the sixth degree. The intensity of light dispersion depends not only on particle concentration, but also on the thickness of the dusty air layer.

Taking all sanitary and ecological considerations into account together, it is necessary for power generating units of the new large-scale thermal power stations burning solid fuel to provide the maximum technologically attainable degree of ash removal from stack gases, independent of stack height. For lower capacity thermal power stations, and also for those burning fuels with lower ash content, the regulated degree of ash-cleaning may be lowered somewhat. Indices based on such an approach are presented in table 2 (3). In the following, these indices may be more rigid, according to the degree of completion of the dust-trapping equipment.

Table 2

Type and capacity of power generating station burning solid fuel.	Necessary degree of stack gas cleaning for fly-ash, no lower than.		
	Given ash content of fuel %kg/1000 kcal $A^{np} < 3$	A^{np} = 3-5	$A^{np} > 5$
1. SREPS*, 2400 MW output TETS**, 500 MW output	98.5-99.0	99.0	99.5
2. SREPS, from 1000 to 2400 MW TETS, from 300 to 500 MW	98.0	98.5	99.0
3. SREPS, less than 1000 MW TETS, less than 300 MW	94.0	96.0	98.0

* SREPS - State Regional Electric Power Station
** TETS - Central Heat and Electric Power Plant

For meeting the requirements introduced in table 2, large-scale coal-burning power generators are equipped with electrostatic precipitators. For low-capacity power stations and boiler generators, scrubbers and inertial action dry dust-catching equipment is used.

Technically feasible adaptation of parameters of exit gases (temperature and sometimes moisture content) is of major significance to conditions for efficient ash-trapping by electrostatic precipitators, and it is especially urgent with large-scale generating units burning berezov, ekibastuz, of kuznetz coal. In connection with this, it is advisable in some instances to re-examine norm definitions for exit gas temperatures and judge this index on the basis of a summary minimum outlay of steam generators and ash-trapping equipment.

A complex approach based on close interrelationship of electrostatic precipitators and convective parts of the steam generator may be, as experience shows, widely used not only in designing new thermal power stations, but in those already operative, that are burning solid fuels. Thus lowering discharged gases' temperatures by 15-20° C within allowable limits before they reach the precipitators may in many cases cut fly-ash emission by 30-40% with a simultaneous increase in ash-trapping reliability. An analogous effect is also attained by introducing measures to lower the excess coefficient of air in discharge gases to the value $\Delta\alpha = 0.2$-0.25. Such an approach, along with cutting fly-ash emission, assures perceptible fuel and electrical economy.

With many coal-burning thermal power stations equipped during a period of less demand for atmospheric purity, modernizing active electrostatic precipitators to increase their efficiency and working reliablity, the basic resource for cutting fly-ash emission from energy production, is a complex problem. Considering here industrial site limitations and thermal power station working conditions, it is especially important to find methods of intensifying processes in electrostatic precipitators, to find layout methods and techno-economic expediencies in a variety of cases where there is some increase of hydraulic resistance in modernized ash-trapping installations, in order to attain the necessary indices. Solving these problems demands considerably widening the typical dimensions of precipitators installed in power stations according to the height of precipitating electrodes, width of the units, etc.

One of the problems with electrostatically cleaning stack gases is in providing stable and efficient precipitation while burning a quantity of mazut at the same time hard fuel is being burned. In connection with the insolvability of the above problem, electrostatic precipitators are in many instances shut off while hard fuel and mazut are simultaneously burned, which is impermissible. Meanwhile, in connection with present fuel-supply conditions, simultaneous burning of both of these fuels will be practiced at many power stations.

A considerable share of energy production in thermal power plants will be based on using low-sulfur, low-moisture coals, especially ekibastuz and kuznetz coal, whose combustion products possess unfavorable electrophysical properties and therefore, solid contaminants are porrly removed by electrostatic precipitators, due to the so-called back corona.

Relative to this, criteria can be used for predicting ash behavior in precipitators in burning diverse fuels whose numerical value is related to factors determining volumetric and surface resistivity of the ash layer precipitators during cleaning of combustion products of a given fuel (4).

The proposed criterion has the form:

$$K = \frac{(Al_2O_3^p + SiO_2^p) \cdot A^p}{(W^p + 9H^p)\, S^p}$$

Here all designations are commonly accepted. The criterion is a dimensionless value. During its derivation, the following circumstances were considered. Aluminum and silicon oxides have the highest volumetric resistivity in ash composition. The higher the content of these oxides in the ash, the more likely will the ash layer in the precipitator have a high volumetric resistivity. Therefor, the value representing the sum of these oxides is placed at the root of the criterion.

It is known that calcium oxide also has a high resistivity value, however, from chemical analysis of ash under calcium oxide it is understood that not only free calcium oxide is contained in the ash, but also all other calcium compounds, among them sulfate having a significantly lower resistivity value and always present in ash. Thus, calcium oxide is not included among the oxides determining high volumetric resistivity of ash.

In order to reflect the effect of processes determining surface layer resistance, the value representing fuel ash content relationship to sulfur content has been in the criterion. with this, it is proposed that the amount of sulfur oxides formed in the boiler is proportionate to fuel sulfur content, but dust layer surface resistivity changes correspondingly to the amount of ash per unit of forming sulfur trioxide.

In actuality, the amount of sulfur trioxide found in stack gases entering electrostatic precipitators depends on the content of alkaline compounds in the ash. However, considering that the result of chemical reaction of sulfur trioxide alkaline compounds forms sulfates also having a measure of volumetric resistivity, adjustment for sulfur trioxide binding with ash is not introduced in the criterion.

With the increase in fuel combustion products of the content of water vapor formed from burning fuel hydrocarbons and from moisture eveaporation, the temperature rises, upon which sulfuric acid steam condensation begins on ash particle surfaces and the probability of an ash layer with a high volumetric resistivity at 130-150°C lessens. Therefore, the value characterizing combustion product moisture, W^p+9H^p, is brought into the criterion.

Given in table 3 are the value K's compilation results for the majority of the USSR's energy fuels, which are arranged in order of the value's decrease. The greatest values for K were received for several coals from Kuznetz basin open pits and ekibastuz deposits. Electrostatic stack gas cleaning practice shows that in the actual burning of these fuels, difficulties are observed in obtaining high cleaning indices in electrostatic precipitators. This attests to the possibility for adapting the proposed criterion for predicting ash behavior in precipitators under normal operating temperatures of discharged steam boiler gases.

Recent research experience shows that the most perspective direction in solving the back corona problem is in technological treatment of the stack gases before they enter the precipitators. This can be done primarily on the basis of using and improving various control devices for humidity and temperature conditioning of the gases, thus assuring acceptable values of gas temperature and moisture content in fly ash electrodeposition. Considering along with this the scale of the scale of the given problem, it is advisable to widen research and testing of electrostatic technical processes for overcoming the harmful effects of back corona in precipitators in the burning of such fuels. In this regard, works on optimization of pulsed supply presnt interest. Moscow Power Engineering Institute has suggested a method of feeding precipitators by square - wave alternating voltage (5) and also, in the USA, there has been recent development of systems for preparatory ionization of stack gases entering the precipitators. Advisable as well are non-electric methods of dry ash-trapping, applicable according to efficiency, but in a greater measure satisfying working conditions of thermal power stations. These are more applicable than electrostatic precipitators, that are, for example, less sensitive to increase in stack gas temperatures encountered in steam generator operation.

To achieve all-out cutting out of fly-ash emission, it will also be necessary in coming years to study the increasing efficiency and operative reliability of a large stock of dust control equipment used in operating electric power plants and also at new low and medium capacity thermal electric power plants burning fuels with a low calcium oxide content in the ash.

Relatively inexpensive scrubbers with Venturi coagulators have been developed and are being used in many thermal power stations ecipped with reverse scrubber systems cleaning stack gases at 96% with a hydraulic resistance near 100mm Hg (6).

Completed research results show that the means of optimizing Venturi tube scrubbing and estimating physical-chemical reaction properties of gas-forming and liquid phases is the completely practicle construction of economically adaptable equipment assuring reliable gas scrubbing at 97.5-98.5% efficiency with burning of the majority of solid fuel types under condition of reverse water supply.

Reliable performance of the scrubber system is the necessary condition for highly effective work by scrubber units. The mechanisms intended for ash-removal from dust control equipment hoppers should also exclude the suction of air into the equipment. This should also eliminate dust spilling into the scrubber building due to single instances of loading of considerable amounts of ash into the hoppers, such as, for example, when the precipitator electrodes are rapped after lengthy shut-offs of the rapping mechanism, and ensure sufficiently rapid emptying of hoppers full of ash as need arises.

All of these demands are met by ash-removal systems, adapted for use in high-capacity power stations equipped with electrostatic precipitators. Beneath every precipitator bin in these systems is placed a pneumatic-layer seal batcher or a pneumatic-layer seal batcher switcher. Pneumatic layer seals are analogous by active principle to hydroseals, in which aerated ash takes the role of fluid (7).

Seals are combined with a system of jets by which ash enters the mixing unit where it is mixed with water and later pumped to an ash dump. If there is a need for use of dry ash, then part or all of the ash gathered by the jets, is pumped pneumatically to a special ash deposit, from which it is taken as needed.

Work experience with such ash removal systems asserts their reliability and economy. Furthermore, pneumatic layer seal batchers placed under precipitator bunkers allow the precipitating electrodes to be rapped after maximally lengthy periods, based only on the thickness of the ash layer on the electrodes and its effect on the precipitator's electrical condition. This practically implies that rapping intervals of the first-field electrodes may be increased as much as 1-2 hours, the second field, by 4-8 hours, and those of other fields by as much as a day or more.

Such a method of electrode rapping, aside from increasing dust-trapping efficiency, assures an increase of essential work reliability by the mechanical part of precipitators, as well as considerable cut in energy expenditure in rapper and ash removal drive mechanisms.

The work of wet scrubbers is still dependent in a large degree on ash removal systems. For preventing water-table pollution, water ash removal systems are made reverseable. Due to frequent ash contacts with stack gases, the salinity of water circulating in reverse water ash removal systems increases to 10g/l and more, and the pH indicator reaches 11.5-12.0 and at higher ash calcium oxide content, pH reaches 12.6. Using such water for irrigating scrubbers is connected with difficulties coming from carbonate and calcium sulfate deposits forming in pipelines, jets, nozzles, on the walls of intake pipes and demisters.

On the basis of research and work experience with scrubbers irrigated with back-water, it has been established that, as a means of preventing carbonate deposits, it is necessary to change irrigation water's pH to 10.5, and then sulfate deposits will not form if the production of Ca^{2+} and SO_4^{2-} ion concentration does not exceed a value, equal to 1500. The last condition may be maintained if the reverse water ash removal system's work is provided a set regime including a sufficiently lengthy period for water to clarify at the ash dump and also an insignificant addition of industrial water to the system.

With concern to lowering alkalinity, this may be done by adding a corresponding amount of acid.

At the present time industrial testing is being carried out on a method of neutralizing alkaline clarified water by use of stack gases, which other than cutting expenditure on reagents, allows for lowering Ca^{2+} ion concentration in the water, which is important for preventing sulfate deposits.

Table 3

Fuel Deposit	K	Fuel Deposit	K
I	2	3	4
Kuuchekin	230	Donetz ARSh	35.0
Ekibastuz	I77	Raichikhin	33.7
Tomusin open-pit Nos. 7-8 Kuzbass	I75	Kharanor	3I.0
Kemerov	I43	Irsha-Borodinsk	30.0
Tomusin open-pit Nos. 3-4 Kuzbass	I60	Estonian shale	20.0
Karagandin Promprodukt	94.8	Intin	22.0
Kedrov open-pit Kuzbass	84	Donetz G Promprodukt	2I.0
Osinnikugol	79	Badaevsk open-pit Kuzbass	20.0
Krasnogorsk open-pit Kuzbass	63.5	Cheliabinsk	I7.4
Gusinozersk	48.5	Berezovsk	I6.0
Listviansk open-pit Kuzbass	46.7	Podmoskovnoe	I5.4
Donetz A-Sh	46.0	Lvovsko-Volynsk	I5.0
Vakhrushi open-pit Kuzbass	44.0	Donetz	I4.3
Novosergievsk open-pit Kuzbass	43.0	Itatsk	I2.7
Krasnoborodsk open-pit Kuzbass	4I.0	Donetz D	I2.57
Kolmogorsk open-pit Kuzbass	35.7	Donetz G	I2.4
		Donetz T	II.5
		Kizelovsk	I0.4
		Angrensk	I0.0

BIBLIOGRAPHY

1. Zalogin, N.G., Kropp, L.I., "The Work of Electric Power Stations and Protection of the Environment", in "Thermal Power Engineering", 1975, no.4, p.5-7.

2. Zalogin, N.G., Kropp, L.I., "On the Necessary Degree of Cleaning Fly-Ash From Stack Gases At New Large-Scale Thermal Power Stations", in "Electric Power Stations", 1977, no.6, p.2-3.

3. Kropp, L.I., "Ways of Abatting Harmful Emissions From Thermal Power Stations", in "Thermal Power Engineering", 1978, no.11, p.2-7.

4. Zalogin, N.G., Kropp, L.I., Shmigol', I.N., "Criteria for Evaluating the Behavior of Fly-Ash in Electrostatic Precipitators", in "Electric Power Stations", 1978, no.6, p.15-16.

5. Mirzabekyan, G.Z., Rudenko, V.M., Shevalenko, I.S., "Study of Electrostatic Precipitator Feed Conditions, Assuring the Absence of Back Corona Discharge", in "Electron Treatment of Materials", Academy of Sciences of the Moldavian SSR, 1978, no.2, p.70-73.

6. Kropp, L.I., Akbrut, A.I., Ash-Control Equipment With Venturi Tubes at Thermal Power Stations, Moscow, "Energy", 1977, 159pp.

7. Chekanov, G.S., "The Use of Pneumolayer Mechanisms for Ash-Removal from Control Equipment Hoppers" in "Industrial and Sanitary Gas-Cleaning", 1978, no.1, p.9

PARTICLE COLLECTION BY GRANULAR BED FILTERS AND DRY SCRUBBERS

by

D. C. Drehmel
Particulate Technology Branch
Industrial Environmental Research Laboratory
U. S. Environmental Protection Agency
Research Triangle Park, N. C. 27711

and

R. Parker and S. Calvert
Air Pollution Technology, Inc.
4901 Morena Blvd.
San Diego, California 92117

(This document has been reviewed and approved for publication by the U.S. EPA.)

To Be Presented at the
Third US/USSR Symposium on
Particulate Control
Moscow, USSR
September 1979

Introduction

Granular bed filters and dry scrubbers may be defined as any collection system comprised of stationary or moving discrete, relatively closely packed granules as the collection medium. With respect to motion of the granules, granular bed filters may be classified as moving or fixed bed filters. Dry scrubbers may be very similar to moving bed filters except that the gas stream may be accelerated before contacting the granules in order to maximize collection from impaction.

A moving bed filter is usually arranged in a cross-flow configuration. The bed is a vertical layer of granular material held in place by louvered walls. The gas passes horizontally through the granular layer while the granules and collected dust move continuously downward and are removed from the bottom. The dust is separated from the granules by mechanical vibration. The cleaned granules are then returned to the overhead hopper and the panel by a granule recirculation system.

CPC Dry Scrubber

The Combustion Power Company's "dry scrubber" is an example of a continuously moving bed filter. The granular bed material flows downward between two concentric cylinders. The gas passes through the bed and is filtered by the granules. The granules are recycled pneumatically and the collected dust particles are disengaged from the granules and sent to a conventional baghouse.

The performance of this device has been reported by Wade, et al. (1978). They conducted extensive cold flow tests to investigate the effects of bed depth, granule diameter, and other parameters on the collection efficiency. Particulate loadings ranged from 0.46 to 4.6 g/Nm^3 (0.2 to 2.0 gr/scf). The superficial gas velocity was varied from

20 to 80 cm/s (40 to 160 ft/min). The medium flow rate was varied from 0.4 to 1.6 kg medium/kg air. Pressure drop ranged from 1.2 to 5.7 kPa (5 to 23 in. W.C.).

Unfortunately, the fractional efficiency can be low for submicron size particles. However, the CPC moving bed filter is capable of particulate removal efficiencies in excess of 98% for particles larger than 1 μmA in diameter. Submicron particles can be collected at an efficiency in excess of 90% only in cases with high velocities, high loadings, and low collection media recirculation rates. Beds with larger thickness-to-granule-diameter ratios were most effective in the capture and retention of particles in the 2 to 5 μmA diameter range. Also, intermittent media movement was shown to improve efficiency by a few percent. However, the economics of this operational technique have not been analyzed.

High temperature tests of the moving bed filter are planned. No high temperature data are available at this time.

The major advantage of the moving bed filter design is that the bed granules are removed and cleaned out of the primary gas stream. This enables efficient cleaning and a relatively steady collection efficiency. Also, it is not necessary to isolate filter units during cleaning so that the total filter area open to gas flow is available for filtration at any time.

The moving bed design also has some limiting operating characteristics. The granule recirculation system adds significantly to the operating cost. Particle reentrainment caused by the relative motion of the granules limits the granule flow rate and affects the overall collection efficiency. Erosion of the retaining grids, louvers, and transport system components may be a problem, especially in high temperature and pressure systems. The collected dust particles cannot form a filter cake so that the operating efficiency will be essentially that of a clean bed. Temperature losses may be large and will be proportional to the heat capacity and temperature of the recirculated granules.

It may be possible to resolve most, if not all, of these problems through further development and testing. Performance data at high temperatures and pressures will be important in identifying the most serious operational problems.

APT Dry Scrubber

EPA is developing through its contractor, Air Pollution Technology, Inc., a dry scrubber system which can be used for high temperature and pressure gas cleaning. This system has been reported by Calvert et al. (1977) and Patterson, et al. (1978).

This system is somewhat similar to a venturi scrubber system in that it uses relatively large particles as collection centers for the fine particles in the gas stream. The principal advantage with this system is that it maximizes the collection efficiency of individual collector particles and thereby reduces the number of collectors that need to be cleaned and recycled.

The collector particles introduced to the gas stream collect fine particles by mechanisms such as diffusion, inertial impaction, interception, and electrophoresis. The larger size of the collector particles allows easy separation from the gas stream by methods such as cyclones and gravitational settling.

The first step in the particle collection process involves introducing the collectors to the gas stream. This can involve pneumatic or mechanical injection. The second step involves contacting the collectors with the gas in such a way as to encourage the movement of the fine particles toward the collectors. A venturi device can be used for the contactor, in which case the system would be analogous to a venturi scrubber (with solid collectors instead of liquid drops).

The next process step is to remove the collector particles after they have captured the fine particles initially present in the gas. This is accomplished by using the large size and mass of the collector particles to separate them from the gas. A cyclone separator, gravity settler, or virtual impactor could be used for this step. Two streams leave the separator: 1) the cleaned gas stream; and 2) the flow of collector particles to the next step. The final process involves either discarding the collector particles or cleaning them for recycle and disposing of the particulate matter collected from the gas stream.

The particle collection efficiency and pressure drop for an APT dry scrubber with co-current flow can be predicted with the same relationships that define co-current wet scrubber performance. The theoretical performance of the APT dry scrubber has been determined based on the venturi scrubber performance model of Yung, et al. (1977). The predicted efficiencies at 20°C and 820°C are similar but slightly lower at 820°C. Efficiencies will be somewhat lower at high pressure for the same pressure drop.

Experimental work has been done to determine fine particle collection efficiency in an APT dry scrubber in order to confirm the predictions obtained from available mathematical models. A dibutylphthalate (DBP) aerosol was used in collection efficiency experiments with 100 μm mean diameter sand as collector particles. The DBP aerosol had a mass median aerodynamic diameter of 1.3 μmA and a geometric standard deviation of 2.0.

The prediction compares well with the experimental curve. Higher collection efficiencies can be achieved using denser collector particles.

For this reason experiments were also conducted with 125 μm nickel beads.

Particle penetration data for all runs with nickel and sand collectors were calculated in terms of the 50% cut diameter as a function of gas pressure drop. These data were found to fall on the line which represents the best available relationship for industrial scale wet venturi scrubbers. Therefore, the APT dry scrubber follows the same primary collection efficiency/power relationship as wet venturi scrubbers.

The overall efficiency of the APT dry scrubber will depend on the reentrainment characteristics of the specific system configuration in addition to the primary collection efficiency. Particle and collector properties, system geometry, flow rates, and other parameters will influence reentrainment.

APT has built an atmospheric fluidized bed coal combustor which will be used for testing a pilot plant dry scrubber at high temperature. Electrostatic augmentation is also being investigated as a means of increasing the collection efficiency independently of pressure drop, and possibly improving the adhesion of fine particles to collector particles.

Fixed Bed Filters

Fixed bed filters operate in two modes: filtration and cleaning. During filtration the bed is stationary. The gas passes through the bed and collected particles are deposited within the bed and on the bed surface. During cleaning the bed is isolated from the main flow and agitated mechanically or pneumatically by a reverse flow of gas.

Currently two fixed bed devices are being developed: the Rexnord gravel bed filter and the Ducon granular bed filter. The Rexnord filter uses a rake-shaped stirring device to agitate the bed during cleaning. This loosens the filter cake which is then removed by a reverse flow of clean air.

The Ducon granular bed filter cleans the bed by a reverse flow of gas which fluidizes the bed and elutriates the fine collected particles.

The Ducon filter was tested on the effluent from a fluid bed catalytic cracking unit regenerator at an oil refinery (Kalen and Zeng, 1973). The gas was at 370°C to 480°C and 1 to 1.5 atm. The dust loading ranged from 0.34 to 1.94 g/m^3 (0.15 to 0.85 gr/acf). A collection efficiency of 85-98% was obtained on dust with a mass median diameter of 35 μm and a geometric standard deviation of about 4.

A high temperature and pressure design of the Ducon filter was tested at the Exxon Miniplant (Hoke, et al., 1978). Initially severe plugging of the bed retaining grids was encountered. This problem was resolved by eliminating the grids and redesigning the bed housing to provide sufficient freeboard above the bed to allow cleaning of the bed without loss of bed material.

A number of operating problems were encountered during the Exxon tests of the modified Ducon filter. The lowest demonstrated particulate outlet concentration was 68.6 mg/Nm^3 (0.03 gr/scf) which was considered to be too high to protect a gas turbine and borderline for meeting current emissions regulations. The use of smaller filter media could improve efficiency. However, at times the filtration efficiency was very poor and the outlet particulate concentrations were as high as 700 to 1,200 mg/Nm^3 (0.3 to 0.5 gr/scf).

It was also observed that the efficiency decreased with time in the longer runs, dropping from 90% initially to about 50% later in the run.

Loss of filter medium during blowback was another recurring problem. Further attempts were made to use 50 mesh retaining screens, but they failed because of plugging. Additional tests with 10 mesh screens also resulted in significant screen plugging.

A significant buildup of particles in the filter beds was also observed amounting to about 30% of the weight of the filter medium. A possible steady long term increase in filter pressure drop may result because of this. However, no significant increase in filter pressure drop was noted during any of the shakedown runs.

It was also observed that the particles were not only building up in the beds, but were uniformly mixed with the filter medium. It is possible that the buildup and mixing of particles in the bed could be responsible for the increase in the particle concentration in the outlet gas with time.

Another potential problem with the current design was its vulnerability to upsets. When upsets occurred, such as bed plugging or loss of filter medium, the operating problems caused by such upsets required shutdown of the system. Another problem which may be unique to the Mini-plant was the interaction of the granular bed filter with the rest of the FBC system during the blowback cycle. An increase in system pressure was noted during blowback, resulting in problems with the coal feed system which is controlled by the differential pressure between the coal feed vessel and combustor. This required modifications to the coal feed control system to minimize the effects.

Granular bed filter performance data for all runs give a range of efficiency from 31 to 97%. The efficiencies are based on an inlet concentration of 2.3 g/Nm^3 (1.0 gr/scf) which is the average for the emissions from the secondary cyclone. The fractional efficiency decreased rapidly with decreasing particle size below 1 μm.

The granular bed filter test program was suspended in November 1977. In all runs in which more than one outlet concentration was measured, it was observed that the outlet concentration increased with time. Exxon was not able to demonstrate that the current EPA emission standard (0.1 lb/10^6 Btu or 0.05 gr/scf) could be met for more than a few hours of operation. In no run was the anticipated new standard (0.05 lb/10^6 Btu or approximately 0.025 gr/scf) satisfied.

Discussion

The three devices discussed in this paper give a range of design features available for collection of particulate on hard granules (see Table 1). At one end of the spectrum are fixed granular bed filters which rely on collection throughout the bed material until a layer or cake is formed. The cake provides greater filtration efficiencies especially for submicron particles. Optimizing the performance of the fixed granular bed filter requires a cleaning system which preserves some of the cake while preventing unacceptably high pressure drops. Moreover, it is essential that the cleaning systems not allow particulate to work its way through the bed either by insufficient cleaning or by motion of the granules.

At the other end of the spectrum is the dry scrubber which relies only on impaction for collection and a cake is never formed. In this case, the gas velocity is high to optimize impaction. Collection of submicron particles may be augmented by charging particles and granules with different signs.

Table 1. Summary of Performance Information

	Device		
	CPC Dry Scrubber	APT Dry Scrubber	Ducon Filter
Superficial gas velocity, cm/s	20-80	3,000-6,000	45
Pressure drop, KPa	1.2-5.7	2-7	8(from prediction)
Bed depth, cm	20-40	NA	3.8
Granule diameter, cm	0.08-0.2	0.01	0.04
Efficiency at 1 μm, %	78	96	82
Efficiency at 6 μm, %	93	99	96

In the middle is the dry scrubber in which the granules move slowly enough to form a bed which acts like a filter. This device works partially by impaction and partially by filtration but cannot be optimized for either since the gas velocities are low and the bed is removed before a cake is formed. However, some designs using intermittently moving granular beds do establish and preserve a cake for better filtration.

The information in Table 1 is a quick comparison of the points in the spectrum discussed above. Pressure drops for all three devices tend to be the same. The APT dry scrubber has a very high gas velocity and no bed. The CPC dry scrubber has a low gas velocity and a thick bed. The Ducon filter has a low gas velocity and a thin bed. The thick bed is used with the CPC dry scrubber to ensure good filtration in the absence of cake filtration or high gas velocity for impaction collection. Based on these data, the APT dry scrubber gave the best performance.

Conclusions

A spectrum of particulate collecting devices has been discussed in terms of three examples under development. Advantages of these differing approaches are:

APT Dry Scrubber (dry scrubber)

High collection efficiency possible from impaction and electrostatic attraction.

Collecting granules are removed from the system for easy cleaning.

Ducon Filter (fixed bed filter)

High collection efficiency possible from cake filtration.

Low attrition rates of bed material.

Minimum energy requirement because of low heat loss and no bed recirculation power.

CPC Dry Scrubber (moving bed filter)

Collecting granules are removed from the system for easy cleaning.

Electrostatic augmentation may provide high collection efficiencies.

Choosing between these alternatives important considerations include cost, the adhesiveness of the particulate, and the importance of energy conservation. For example, if the particulate is sticky, a system which removes granules for easy cleaning will be necessary. On the other hand, if a fixed bed filter can be cleaned and removal of granules implies a high energy loss, cost considerations may favor the fixed bed filter.

References

Calvert, S. et al., Paper #III-5, in EPA/DOE Symposium on High Temperature, High Pressure Particulate Control (September 1977), EPA-600/9-78-004 (NTIS CONF-770970), March 1978.

Hoke, R. C. et al., Miniplant Studies of Pressurized Fluidized-Bed Coal Combustion: Third Annual Report, EPA 600/7-78-069 (NTIS PB 284534), April 1978.

Kalen, B. and Zeng, F. A., CEP 69 #5, pg. 67, June 1973.

Patterson, R.G. et al., APT Dry Scrubber for Particulate Collection at High Temperature and Pressure, Symposium on the Transfer and Utilization of Particulate Control Technology, Denver, Colorado, July 1978.

Wade, G. et al., Granular Bed Filter Development Program, Report to DOE, FE-2579-19, April 1978.

Yung et al., Venturi Scrubber Performance Model, EPA 600/2-77-172, NTIS PB 271-515/9BE, August 1977.

I.K. Goryachev, Y.V. Abrosimov

FILTERING MATERIAL FOR GAS-CLEANING AND POSSIBLE AREAS FOR ITS USE

The ever-greater distribution of dust removal of industrial and exhaust gases from chemical, metallurgical, construction industries and others takes in use of bag houses supplied with high-effectiveness filtering materials.

From the assortment of filtering material serially produced in the USSR, approval can be given to material possessing features for withstanding the extended effects of high temperatures, corrosive action of dusts and gases with preservation of highly filtrational, durable and regenerative features.

For cleaning aspirated air in the ventilation systems of work areas, and air sucked out from transfer operations, transport and packing of fine particulates, inexpensive synthetic materials having a high dust-trapping coefficient under relatively low hydraulic resistance are widely used. These materials efficiently trap such high-dispersion dusts as industrial-grade carbon, zinc oxide, etc., assuring sanitary norms for dust emission from exhaust systems (1).

For cleaning industrial gases at temperatures reaching 130° C, filtering fabrics and non-woven materials made from Lawson (trans. note: Soviet equivalent of Dacron) fibers are receiving ever wider use

Lawson fabrics possess high indices for dust-separation, strength and regenerative properties. The warp and woof of these fabrics are made from staple fiber. Experimental work at NIOGAZ's Semibratovsk Branch, conducted on an industrial filter FRKDI-1100 during the cleaning of gases from electric-arc steel-smelting furnaces has shown that the staple Lawson fabric L-3 has a dust-removing efficiency of 99% and a high regeneration capacity (2).

Non-woven needled Lawson materials have wide use in scrim filters with impulse blowers. They are relatively simple to manufacture, inexpensive and possess high filtering and strength characteristics. Thus, for example, in removing lead monoxide dust with a 3 micron median particle diameter, FRKI-type bag houses, furnished with needled non-woven material, had an operational effectiveness for dust removal of 99.8% during the course of a year and a half, and the dust content of the expelled gases during this time did not exceed 4-6mg/m^3.

Materials made from poliacrylnitryl nitron fibers are used in many industries. Nitron filter bags have withstood temperatures up to 130°C for extended periods. They possess a relatively high chemical stability and sufficient durability against wear and bending. At non-ferrous metallurgy sites, nitron fabrics comprise nearly 40% of the total amount of all used filtering materials.

Using increased thermal-resistant synthetic fiber filtering materials (oxalon, sulphon) makes possible an increase in filter efficiency by means of reducing air inflow for the cooling of the gases. The determined heat resistance limit of such fabrics is 180-200°C.

In cleaning rotary kiln gases in zinc plants, oxalon fabric provides dust-removal efficiency at 99.5% with the temperature of the gas being cleaned at 200-210°C (3).

Glass filtering fabrics are widely used for cleaning gases with temperatures reaching 250°C in technical-grade carbon production, cement plants and in ferrous and non-ferrous metallurgy. Glass fabrics possess a complex of physico-technological and chemical properties not characteristic to any fabric of organic fibers. The basic advantage of glass fabric over other filtering materials is its high thermal resistance and maintenance of its mechanical strength. Glass fabric works efficiently for a period of 1.5-2 years in FR-5000 type filters with fabric regeneration by back-blowing in technical-grade carbon plants. Glass fabric possesses however a relatively weak resistance to frequent bending and abrasion. Accordingly, glass fabric is not used in scrim-design filters.

In the USSR a special anti-static filtering material has been developed for bag-houses working in dangerously-explosive surroundings for removal of dusts that are capable of building up static electricity.

Testing this antistatic material in industrial working conditions in a chemical-metallurgic plant for a long period showed its high dust-removal efficiency and reliability in providing secure filter work.

Asbestos fabrics are sometimes used with filtering fabric-corrosive high-temperature gases. Asbestos fabrics are sufficiently resistant to acids and alkali and withstand high temperature. However, due to their low strength, they are used only in low pressure drop conditions.

Different fiber materials are added to asbestos fabrics to raise their strength. Endurance indices are raised in this case, but the resistance to increased temperatures is lowered somewhat.

Fabric and non- woven material prepared from needling methods is used as filtering partitions for cleaning hot gases with a temperature higher than 220°C.

Thus, for example, serially-manufactured metallic fabric sieves (4) are widely used for removal of chemical regeants and particularly pure chemical substances (potassium carbonate, nickle, cadmium, and the oxides of zirconium, silver, vanadium, molibdenum, tungsten, etc.) at exhaust gas temperatures up to 500°C. Basically, fabric nets made from Kh18N10T-grade steel wire and NMZhMts-2.5-1.5 grade nickle-copper alloy (monel) are being used. Kh18N10T-grade austenite chrome-nickle steel is characterized by higher heat resistance, full non-magnetization and good weldability.

For fibers of 0.12 to 0.18mm diameter, intermittent resistance is $5_{\beta} = 95 \text{mg/mm}^2$, and relative elongation is $\delta = 20\%$.

NMZhMts28-2.5-1.5-grade nickle-copper alloy (monel) is distinguished by its high corrosion resistance to acids, alkalis and gas media.

This alloy is distinguished by its high mechanical properties, considerable heat resistance, and weak magnetic properties.

It is necessary to note that fabric fiber screen made by interweaving wire warp with woof without mesh formation in the beginning of the filtration process is inferior in dust-trapping efficiency to natural-fiber fabrics.

However, metallic woven net is distinguished by high heat-resistance and corrosion resitance, and provides the very same degree of trapping after an elementary dust layer has formed on its surface as natural fiber fabrics.

On the basis of experience in industrial operation of filters furnished with metallic net fabric for trapping potassium superoxide, and the oxides of molibdenum and tungsten, a type-dimensional series of filters for cleaning gases up to a temperature of 500°C was developed.

These filters regenerate themselves by section by compressed air blasts (from 1.5 to 2 kg/cm^2).

non-woven filtering materials lacking a scrim base are currently being developed and tested in the USSR. These materials are, by their strength charactersistics, slightly inferior to needled materials with scrim bases but in their filtering characteristics, are not inferior to the best foreign models. The cost of producing needled filtering materials lacking scrims is several times lower than scrim material.

New technology in producing non-woven filter material lacking scrims simultaneously allowed solving the problem of producing high-temperature filtering materials from oxalon fibers with thermal resistance up to 230°C and production of material from metallic fibers with thermal resistance up to 500°C. By its mechanical properties, felting without scrim from oxalon fibers is not inferior to analogous materials on a scrim.

Residual dustiness in cement and quartz dusts (d_{50}=8microns) at a specific gas load of $4m^3/m^2$min. and an intake dust content of $8g/nm^3$ for felting without scrim did not exceed $7.5mg/nm^3$. Felting regeneration efficiently worked with compressed air back blowing ($P=1.2kg/cm^2$).

Needled felting was manufactured in the USSR from metallic fiber with the aim of making filtering material with a heat-resistance up to 500°C. Microfiber made from 1Kh18N9T-grade steel was used as the raw material.

Comparative stand testing of a sample of metallic fiber and of S120-12Kh18N10T State Standard 3187-76 woven wire filter screen in removing quartz and cement dust (d_{50}=8 microns) has shown that use of non-woven material instead of nets allows an increase of gas filter performance by 1.5-2.0 times.

1. Goryachev, I.K., Kazakov, A.K., "Experience in Using Small Dimension Cellular-Design fabric Filters in Exhaust Lines", in the book Industrial Gas Cleaning and Aerodynamics of Dust-Trapping Equipment , Yaroslavl, 1975. pp.118-119.

2. Pozin, L.M., Istomin, V.S., Malgin, A.D., "Cleaning Arc Steel-Smelting Furnace Gases by FRKDN-1100-Type Bag Houses" in"Industrial and Sanitary Gas Cleaning", 1977, no.5, p.2.

3. Gordon, G.M., Kaplan, V.G., Luk, V.I., "Study in Filtering Fabric Made From Highly Thermal-Resistant Synthetic Oxalon Fiber", in "Industrial and Sanitary Gas-Cleaning",1978, no.4, pp.4-5.

4. Abrosimov, Y.V., NIIOGAZ's Scrim Glass Fabric Filters, Mashinostroenie, 1972.

Translation by Carl Gruber, IERL, RTP, N.C., July 1979.

HIGH TEMPERATURE CERAMIC FILTERS

by

D. C. Drehmel
Particulate Technology Branch
Industrial Environmental Research Laboratory
U. S. Environmental Protection Agency
Research Triangle Park, N. C. 27711

and

R. Parker and S. Calvert, APT, Inc.
4901 Morena Blvd.
San Diego, California 92117

(This document has been reviewed and approved
for publication by the U.S. EPA.)

To Be Presented at the
Third US/USSR Symposium on
Particulate Control
Moscow, USSR
September, 1979

INTRODUCTION

Conventional fabric filters are limited to operating temperatures below 250°C. The maximum temperature varies with the specific fabric and is the temperature at which accelerated fabric deterioration or abrasion occurs.

Glass fiber bags are the most common type used for higher temperature applications and are limited to about 300°C. The glass fibers are coated with a silicone, silicone-graphite, or equivalent finish in order to provide lubrication between the fibers. Unfinished glass fibers experience extreme abrasion and unsatisfactory bag life. The temperature limit of glass fiber fabrics is directly related to the temperature limit of the finish.

In fact, it is generally true that in practice the effect of temperature and pressure on filtration mechanisms was not a determining factor in the application of high efficiency filters. The main problems are the physical and chemical effects of a high temperature environment on the filter materials. These effects may appear as reduced mechanical strength and resilience or loss of adhesion, leading to mechanical leakage and decrease in efficiency.

PREVIOUS WORK

Filtration media for extreme temperatures and pressures have been investigated by many authors (see Table 1). Silverman and Davidson (1956) suggested the use of ceramic fibers sandwiched between layers of woven metallic or ceramic fabrics for filtration at temperatures to 1,100°C and higher. Billings et al. (1955) and Silverman (1962) discussed the use of metallic fiber "slag/wool" filters for high temperature

Table 1. High Temperature Filtration

Investigators	Temperature Range, C°	Media	Efficiency Range, %
Silverman (1956) Davidson	to 1100	woven metallic or ceramic	NA
Billings (1955) Silverman (1962)	300-650	"slag/wool"	75-98
First (1956) Kane (1960)	760	ceramic fiber	82-91
Drehmel (1977) Shackleton	815	ceramic felt	99
Drehmel (1977) Ciliberti	360-815	ceramic membrane	81-99

filtration of open-hearth furnace fume. They found that efficiencies ranged from 75 to 98% for the slag-wool filter at temperatures from 300 to 650°C and dust loadings from 0.1 to 1.1 g/Nm^3. A continuous slag-wool filter was designed and tested at 300-400°C. The efficiency ranged from 10 to 80% for Fe_2O_3 particles with a mass median diameter of 0.65 μm.

First et al. (1956) and Kane et al. (1960) reported on the use of ceramic fiber filters capable of withstanding temperatures up to 1,100°C. First et al. (1956) measured collection efficiencies at 21°C and 760°C. The mass median particle diameter was 8.5 μm with a particle density of 6.4 g/cm^3.

A composite filter comprised of fibers from 4 to 20 μm in diameter gave over 99% collection for all temperatures. The fractional efficiency for the composite tests is greater than 95% for particles larger than 1 μm.

THEORETICAL PREDICTIONS

Filtration theory has been reviewed by many authors including Davies (1973) and Pich (1966). Using the theory presented by Davies to predict the collection efficiency of a clean fiber filter at high temperature and high pressure, the following parameters were assumed:

Filter weight = 0.026 g/cm^2
Fiber density = 2.53 g/cm^3
Fiber diameter = 5.0 μm
Superficial velocity = 12 cm/s
Particle density = 2.5 g/cm^3
Air properties at:
Temperature = 20 and 1,100°C
Pressure = 1 and 15 atm

These parameters simulate a typical aluminum-silicate ceramic paper.

At high temperature and low pressure the Brownian diffusion regime becomes very significant and the collection efficiency of particles smaller than approximately 0.5 μm increases dramatically. At high temperature and high pressure this effect is less apparent.

In the inertial impaction regime, high temperature and high pressure reduce the collection efficiency from that obtained at standard conditions. Even at high temperature and pressure, however, the predicted collection efficiency is effectively 100% for particles larger than 2 μm. This is consistent with the data reported earlier from the work by First et al. (1956).

RECENT DEVELOPMENT WORK ON BAG FILTRATION

Recent development work on high temperature and pressure ceramic fiber filters involves three groups of materials:

1. Woven structures - Cloth woven from long-filament yarns of ceramic fibers.
2. Papers - Ceramic structures produced from short lengths of fibers, generally held together with binders.
3. Felts - Structures produced to form mats of relatively long fibers. These materials are known as blankets in the insulation industry. They tend to be less tightly packed than conventional felt materials.

Ceramic fiber filters have two major drawbacks at high temperature and pressure. First, they must be very durable. Conventional filter bags are expected to last at least 1 year (see Billings and Wilder, 1970). Bag life at the Nucla Power Plant was estimated to be 5 ±1.3 years. For typical cleaning pulse frequencies, a bag may have to withstand a few million pulses in its lifetime. For this reason, blanket or felted ceramic fiber materials are expected to be the most promising. They combine good filtration properties with relatively high strength.

The second drawback is the size of typical fabric filter installations. Most conventional fabric filters operate at superficial velocities in the range of 1 to 3 cm/s. Slightly higher velocities (up to 10 or 20 cm/s) are possible with some felted fabrics although bag life will be shortened.

In comparison, granular bed filters (GBF) operate at superficial velocities from 40 to 80 cm/s. For a given gas flow rate, fabric filters will require from 4 to 20 times the surface area required by granular bed filters. This is especially important at high pressure where the cost of the pressure vessel can be a significant fraction of the capital cost. For greater efficiency, both baghouses and GBF's should be designed to maximize the surface to volume ratio.

These problems are being considered. Preliminary experience at high temperature and pressure indicates that at least three configurations show promise, having survived 50,000 cleaning pulses at 815°C and 9 atm. Test conditions were:

Temperature - 815°C
Pressure - 930 kPa (9 atm)
Air-to-cloth-ratio - 5 to 1 (2.54 cm/s)
Cleaning pulse pressure - 1,100 kPa
Cleaning pulse interval - 10 s
Cleaning pulse duration - 100 m/s
Dust - redispersed.

The three filter media configurations tested were:

1. Saffil* alumina mat contained between an inside and an outside layer of 304 stainless steel knit wire screen.

---

*ICI United States, Inc., Concord Pike and New Murphy Road, Wilmington, DE 19803

2. Woven Fiberfrax* cloth with Nichrome** wire scrim insert.
3. Fiberfrax blanket contained between an inside and an outside cylinder of 304 SS square mesh screen similar to common window screen. The ceramic fiber blanket was held in position between the screens with 302 SS wire sewn between the screens.

Pressure drop during the tests was controlled by the rapid cleaning pulses and in general remained less than about 5 kPa (20 in. W.C.). Formation and removal of the filter cake for these configurations and test conditions presented no problems.

The average outlet loading during the Fiberfrax blanket test was 0.0055 g/Nm^3 (0.0024 gr/scf). The fly ash dust dispersion apparatus used was suitable for filter loading tests but may not be representative of the dust characteristics and size distribution to be encountered in a real-life application.

To obtain test data in a real pressurized, fluidized-bed combustion application, a ceramic baghouse was tested at the Exxon Miniplant. The test program has shown that the bags will survive pressure drops as high as 10 kPa and can be kept clean at air-to-cloth ratios as high as 10 to 1 (5 cm/sec).

WORK ON MEMBRANE FILTRATION

Several available ceramic materials in many configurations have been evaluated as possible high-temperature filters. One of the most promising materials tested was the ceramic cross flow monolith, Thermacomb.***

---

*Carborundum Co., P. O. Box 808, Niagara Falls, NY 14302
**Driver-Harris Co., Harrison, NJ 07029
***3M, 3M Center, St. Paul, MN 55101

This material is composed of alternate layers of corrugations separated by thin filtering barriers. This type of configuration affords a large amount of filter surface in a very small volume.

The Thermacomb cross flow structure is made up of several layers in the following pattern: a thin (0.25 - 1.5 mm) porous cordierite sheet, a layer of cordierite corrugations similar in appearance to those used in cardboard, another flat sheet of cordierite followed by another layer of corrugations oriented 90% from the corrugations below. Now available forms of the material have 1.97, 3.15, or 4.72 corrugations per cm. A similar material is manufactured by W. R. Grace & Company.* This material has perpendicular dividers with rectangular holes, rather than the triangular holes of Thermacomb. The Grace material tested had approximately 8.5 holes per cm and an equal number of layers per cm.

These materials have many properties that make them attractive as filters. Among these are (1) working temperature to 1,200°C, (2) very good mechanical strength despite thin separators, (3) excellent resistance to thermal shock, (4) excellent resistance to corrosive atmospheres and, (5) very high surface area to volume ratios.

Efficiency of filtration was determined with a limestone test dust. The mass median diameter was typically 1.4 μm and the geometric standard deviation was 3.0.

Results of the high temperature Thermacomb tests show that the overall collection efficiency averaged 96.4%. No problems were encountered in cleaning the filter media by reverse pulses of compressed air. It was possible to clean the filter and return to a stable pressure drop even with relatively heavy dust loadings.

---

*W. R. Grace and Co., 1114 Avenue of the Americas, New York, NY 10036

Similar results were obtained in a limited number of tests on the W. R. Grace material.

CONCLUSIONS

A number of investigators have shown that high collection efficiencies are possible with ceramic filtration at high temperature (greater than 800°C) and/or high pressure (greater than 900 kPa). The recent work has tested both ceramic bags and rigid ceramic filters. Advantages of these differing approaches are:

Ceramic Bag	Rigid Ceramic Filter
High collection efficiency	High collection efficiency
Easy to clean	Compact
Resists failure because of thermal shock	Resists failure because of high pressure drop

The endurance of both media is unknown. If the rigid ceramic filter can be used without clogging or thermal shock, it could be maintained in service for many years. However, ceramic bags are expected to have a limited life because of the less durable nature of the bag structure. Tests to date indicate that ceramic bags will easily survive up to 50,000 cleaning pulses or the equivalent of 1 year's light service.

REFERENCES

Billings, C.E. and Wilder, J. E., Handbook of Fabric Filter Technology, Volume I, EPA No. APTD 0690, NTIS No. PB 200-648, December 1970.

Billings, C. E., et al., JAPCA 5 #3 p. 159, November 1955.

Davies, C. N., Air Filtration, Academic Press, New York, 1973.

Drehmel, D. C. and Ciliberti, D. F., Paper #77-32.4, APCA Annual Meeting, Toronto, June 1977.

Drehmel, D. C. and Shackleton, M.S., Paper #17, Third Symposium on Fabric Filters for Particulate Control, Tucson, December 1977.

First, et al., I&EC Chem 48 #4, p. 696, 1956.

Kane, L. J. et al., Bureau of Mines Report 5672, 1960.

Pich, J., In Aerosol Science, C. N. Davies, ed., Academic Press, New York 1966.

Silverman, L. and Davidson, R. A., U. S. Patent # 2,758,671, August 1956.

Silverman, L., U. S. Patent #3, 063,216, November 1962.

N.G. Bulgakova, D.L. Zelikson

METHODS AND EQUIPMENT FOR MEASURING OF FINELY DISPERSED PARTICLE SIZE LESS THAN 0.3 MICRONS FOR INDUSTRIAL GASES

The task of measuring size of finely-dispersed particles less than 0.3 microns is at the present time very urgent. This is in connection with the fact that such particles are usually poorly removed by dust-cleaning equipment and are emitted into the atmosphere along with exhaust gases. For example, in gases from electric power stations that burn coal, particle content after precipitators reaches 20% for particles less than a micron in diameter and as much as 5-10% of those less than 0.3 microns, while in ferrol alloy production, content of such particles is 70% after cleaning by wet scrubbers. As recent research has shown, it is namely these particle-fractions that are a serious source of air pollution in connection with their peculiar toxicity. Therefore from the point of view of increasing the effeciency finely-dispersed particle removal, abating their emission into the atmosphere, and selection and evaluation of the work of dust-control equipment, the development of methods and equipment for measuring sub-micron particles provides further technical progress in the area of protection and renewal of the environment.

In as much as the indicated sub-micron diameter range of particles is close to the operative limits of pitical, acoustical, aeromechanical, etc. measuring equipment, choosing the method of measurement presents known difficulties.

Out of the methods known for sizing sub-micron particles, the following should be noted.

Electron microscope method. Based on the visual study of individual particles. The measurement process is time-consuming, and requires use of high-cost and operationally complex equipment. The method does not ensure automation of the measurement process.

Electrical methods. Based on registering the electrical charge of the particles and their separation in electrical, magnetic or electromagnetic fields. The methods are sufficiently simple and allow quickly obtaining results and automation of the measurement process. The basic shortcoming of these methods lies in the necessity of preliminarily preparing the gas sample in the majority of industrial discharges, i.e. to cool and dilute ~~rari~~fy the gas. The equipment for sample preparation is often more complex than the measuring unit.

This method has been fulfilled in the USA in the particle electrical mobility analyzer unit.

Diffusion methods. Based on particle separation under the influence of diffusion forces with aerosol movement in a laminar flow. This method is implemented in a unit-incorporating diffusion batteries of various design with condensation nuclei counters. This method may be used during variation in particle size distribution in air aerosol flow, but requires preliminary sample preparation.

Inertial methods. Based on particle separation from aerosol stream by the latter's flow around the settling surfaces. This method is the simplest and most operative. It allows chemical sample analysis when needed. Direct removal of the sample in the gas conduit excludes the need of preliminary sample preparation.

The method is accomplished by a cascade-impactor, which is widely used for dispersion analysis of particles of 0.3-30 microns.

Theoretical and experimental research (1) has shown the possibility of using cascade impactors for analysis of sub-micron particles in a size range of 0.01-0.3 microns. For this, it is necessary in the unit's last stages to form a sufficiently low absolute pressure of 10-100mm Hg (10^3-10^4 pascals) to assure sub-micronic particle settling through an adjusted Cunningham coefficient (1).

Cascade impactor calculation is based on known theoretical premises (2).

The main calculation formula links diameter d_{50} of the particles (with 50% settling efficiency in each stage of the impactor) with nozzle diameter D; gas flow rate and viscosity V, μ; particle density ρ, and with Cunningham's correction also $C_{(P)}$.

$$d_{50} = \left[\frac{2{,}61\,\mu\,D}{C_{(P)}\,\rho\,V}\right]^{1/2}$$

The latter is described by the following expression:

$$C_{(P)} = 1 + \frac{2\lambda}{d_{50}}\left[1.257 + 6.4\exp\left(-1.1\,\frac{d_{50}}{\lambda}\right)\right]$$

where: λ is the average length of the free run of gas molecules, which is determined by gas pressure.

It follows from considering these expressions, that by reducing the range of analyzed particles to the sub-micron level is accomplished by varying the three parameters, v, D and $C_{(f)}$.

The increase of gas velocity ( ) is limited to the speed of sound. Nozzle diameter reduction is limited by the technological capability of producing aperture smaller than 0.1mm in diameter. Aside from this, the theory of inertial particle settling derives from the viscosity condition of the gas flow in the nozzle, but with a decrease in the nozzle diameter and increase in the Cunningham correction, i.e. reduction in pressure, the length of free run becomes commensurable with the diameter of the flow and the flow regime crosses into the molecular.

Increasing the Cunningham correction is possible increasing the average molecule run length, i.e. decreasing absolute pressure. With 7.6mm Hg pressure, the correction C(p) comprises more than 2000 for particles less than 0.01 microns.

In this manner the possibility in principle for the use of cascade impactors for analyzing sub-micronic particles is obtained. Several such impactors are known, such as, for example, that developed in the USA (1).

At NIIOGAZ a eight-stage sub-micron cascade impactor model (fig.1) has been produced with the following characteristics:

- least nozzle diameter - 0.2mm.
- greatest flow velocity in nozzles - 200m/s
- lowest pressure in final stages - 20mm Hg
- gas flow - 5 lit./min.
- unit dimensions - Ø 65mm; 150mm length

Parameters of the sub-micron cascade impactor are given in table 1.

Table 1

№ of stages	nozzle - aperture diameters in mm's	number of apertures	gas exhaust velocity, m / sec.	static pressure in the stages ΔP, mm Hg	value of d_{50}, micron
I	IO	I	6,4	760	5
2	0,8	4	40	750	0,950
3	0.8	4	40	740	0.950
4	0.8	4	40	730	0.950
5	0.2	I8	I50	620	0.250
6	0.2	I5	200	420	0,I25
7	0,2	23	200	220	0.050
8	0,2	44	200	20	0.0I0

The table shows values for particle diameter with regard to the Cunningham correction.

By design, the impactor is made in the form of diaphragm-stages with 60mm diameter by 7mm thick and are connected by four pins. The nozzles are made in the form of aperture in a stainless steel plate of a thickness of 0.3mm and a diameter of 8mm. The plates are hermetically glued-in to the diaphragm. Filtering material or lubricant serves as the precipitating surface in the first four stages, and in the rest of the stages, pieces of optical glass K-8 (Ø 10x5), are placed at a distance of 1mm from the nozzles. An exterior view of a separate diaghragm-stage is presented in fig. 2. The glass precipitation surface may be covered by a special lubricant or may be used for measuring settlement by microscopic methods.

The cascade impactor was tested on a laboratory stand, the scheme of which is shown in fig. 3a and 3. The stand consists of an aerosol generator 1,2, drying system 3,4, and measuring and regulating units 5-

9. Air was bubbled through a solution of methylene blue with subsequent drying of the aerosol in the air stream served as the aerosol generator. The compressed air is fed into the atomizer (1), at the end of which there is a thin-walled head-piece with 0.5mm apertures. The aerosol formed, bubbling through the methylene blue solution, enters the drying column (3,4), filled with silica jel impregnated with calcium chloride, where it is dryed and leaves the measuring system. Under these conditions, the aerosol contains solid methylene blue particles.

An AFA filter was used for measuring the discharged aerosol's concentration. The particle dispersion composition was controlled with the aid of a diffusion battery (7). A submicron impactor (6) measured particle size. Control and measurement of the air flow rate was done by the valves (9) and rheometers (8).

Aerosol with an average methylene blue particle size of 0.3-0.8 microns was produced on the stand. Table 2 shows results of one of the analyses conducted by the eight-stage cascade impactor. The number of particles settled on the diaphagm-stages was determined by weight. The flow rate of air through the impactor was 5 lit./min.

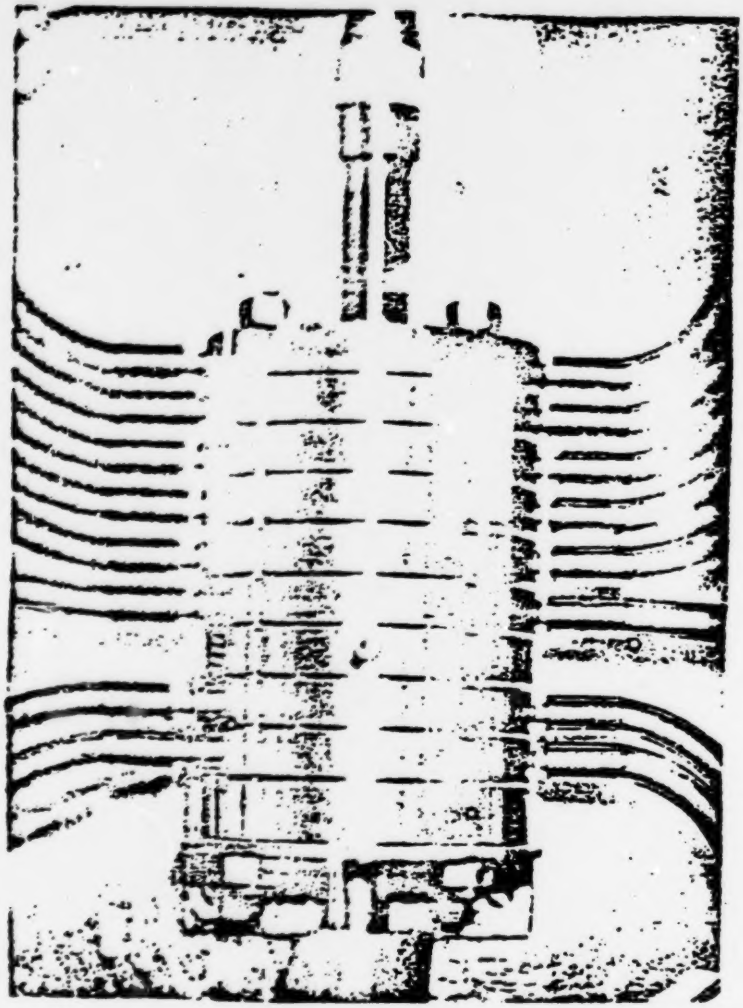

Fig.1. General view of a submicron cascade impacter

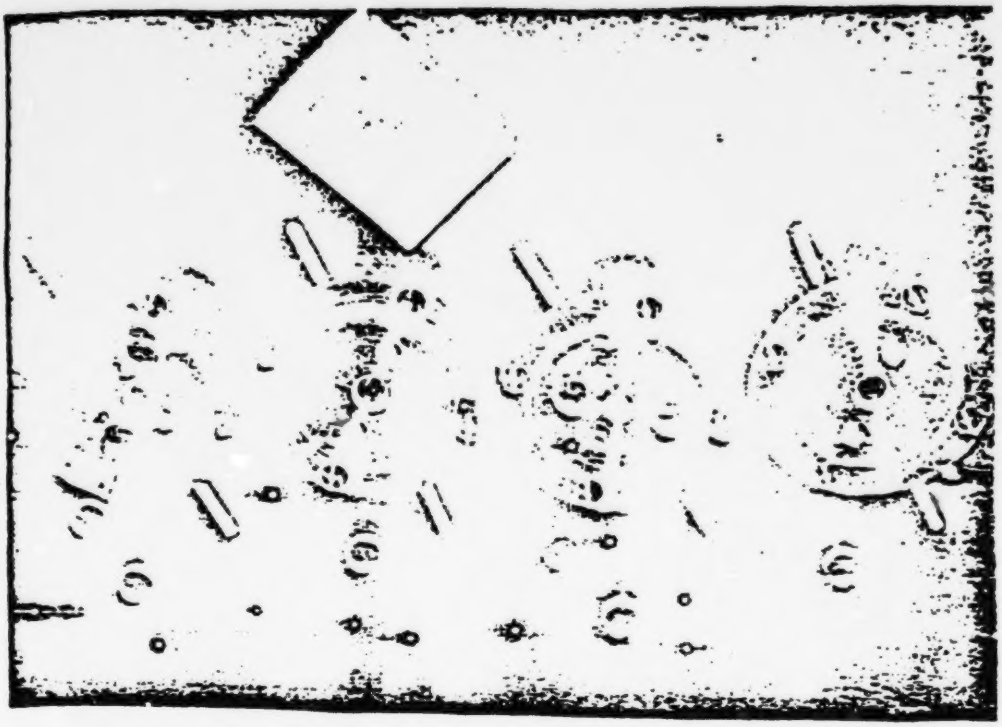

Fig.2. Diaphragm-stages (matchbox shows scales)

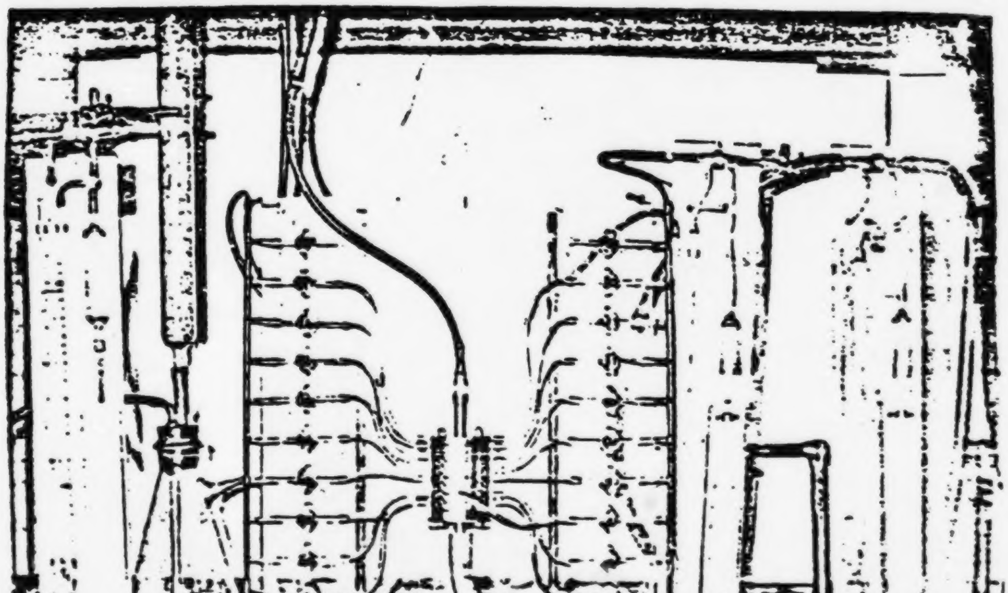

Fig.3a. General view of the laboratory stand.

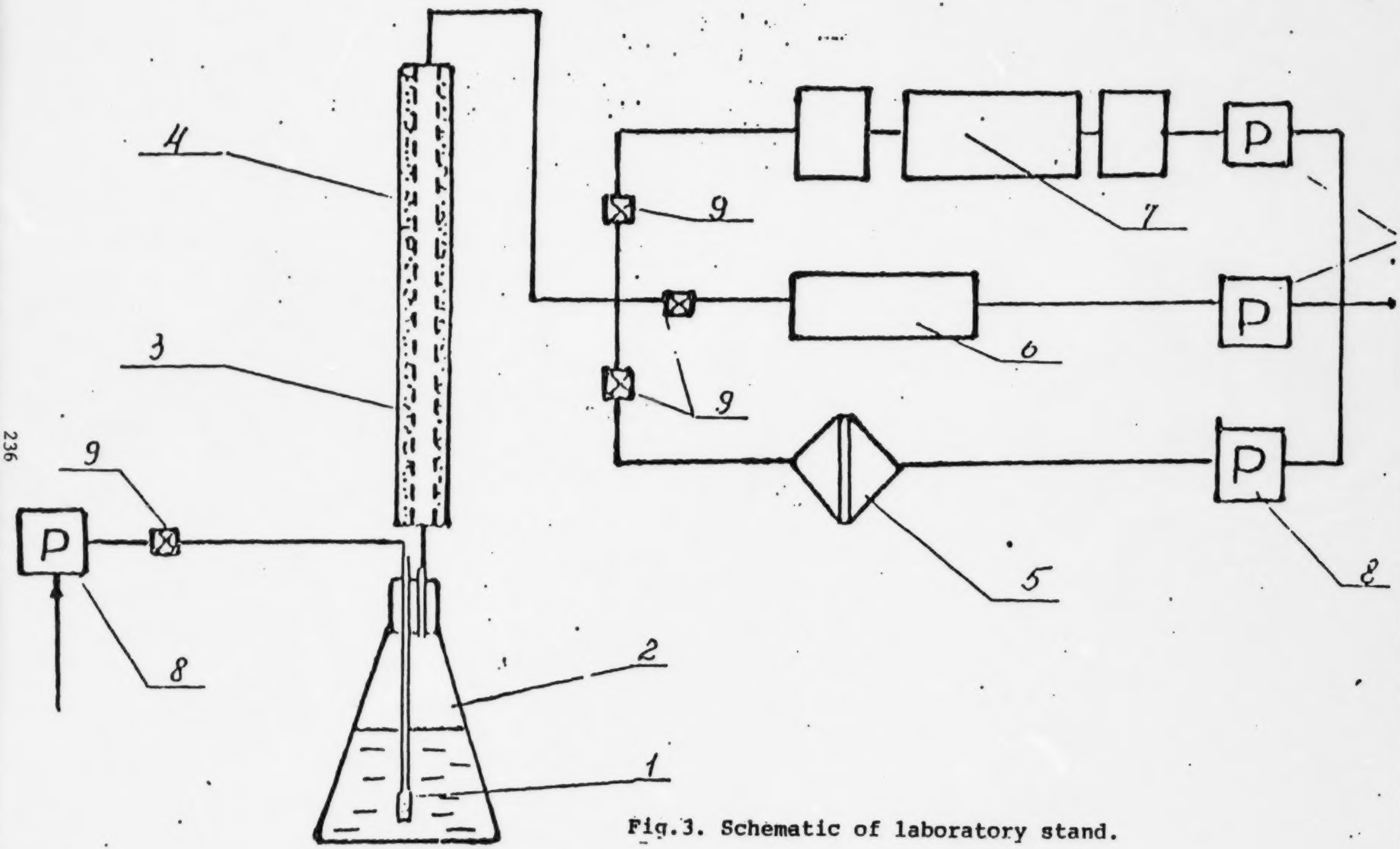
4
3
9
P
8
2
1
9
9
7
6
5
P
P
P
8

Fig.3. Schematic of laboratory stand.

Table 2.

No. of stages	amount of gained, mg.	% share	total content %	d_{50}, micr
I	-	-	-	5
2	0.25	I7.86	I7.86	0.95
3	0.I5	I0.7I	28.57	0.95
4	0.25	I7.86	46.43	0.95
5	0.40	28.58	75.0I	0.25
6	0.I5	I0.7I	85.72	0.I25
7	0.I0	7.I4	92.86	0.05
8	0.I0	7.I4	I00	0.0I
filter	-	-		
	I.40			

According to this table's data, the distribution of methylene blue particles by size is plotted in a probability-logarithmic coordinate grid (fig. 4). As can be seen from the figure, the average particle size 0.71 microns.

In analyzing the results taken here, it can be concluded that cascade impactors may be used to analyze submicron particles down to 0.01 microns.

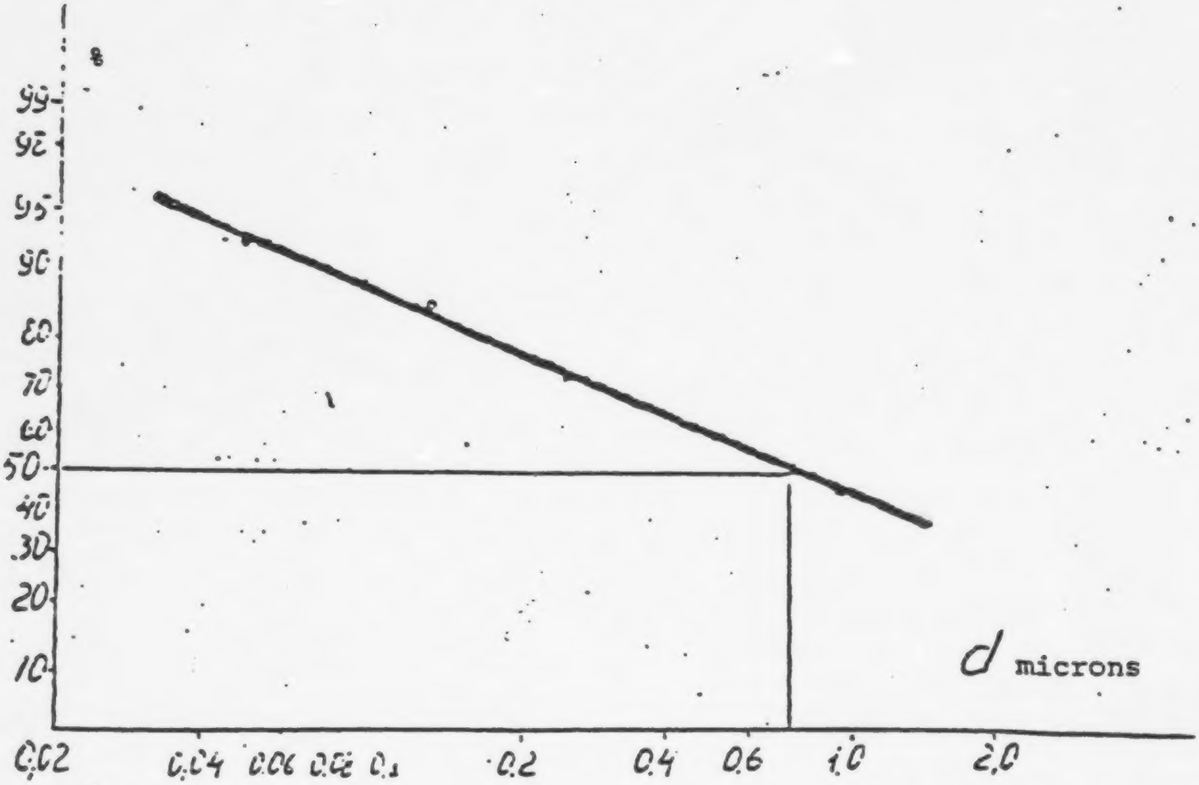

Fig.4. Methylene blue dispersion composition, as taken by the submicron impactor.

PARTICLE MEASUREMENT IN THE U.S.A.

W. B. Smith
K. M. Cushing
Southern Research Institute
2000 Ninth Avenue South
Birmingham, Alabama 35205

D. B. Harris
Industrial Environmental Research Laboratory
Environmental Protection Agency
Research Triangle Park, N.C. 27711

(This document has been reviewed and approved for publication by the U.S. EPA.)

PARTICLE MEASUREMENT IN THE USA

INTRODUCTION

Measurements are made to characterize the emissions from sources in order to obtain the data needed to assess the impact on health and the environment, to develop and enforce emission regulations, and to develop control strategies. For airborne particulate emissions, the required data include the size distribution, concentration, and composition of the particles.

Methods are described in this paper for measuring the particulate emissions from stationary sources. Measurements made inside ducts or stacks are referred to as instack or in situ measurements. The fraction of the particles emitted from a process that escape directly into the atmosphere (unducted) are called "fugitive" emissions and must also be measured. If measurements are made in the atmosphere around an industrialized area where more than one source contributes to the atmospheric burden, the measurements are termed "ambient" measurements. Methods used in the USA to measure particle size and mass in situ, in fugitive emissions, and in the ambient are listed in Table 1.

Manual methods for sampling in situ, fugitive, and ambient aerosols are discussed in this paper. A second paper includes a discussion of automatic systems for particle sizing.

SAMPLING IN PROCESS STREAMS - IN SITU SAMPLING

MASS CONCENTRATION AND MASS EMISSION RATE

Gravimetric methods using filtration for obtaining samples are used for determinations of mass concentration and mass emission rates. Samples are obtained by withdrawing measured gas volumes from the process stream for equal

TABLE 1. METHODS AVAILABLE FOR MEASURING PARTICULATE SIZE AND MASS

MASS	SIZE
AMBIENT	
Filters	Impactors
Hi-Vol	Hi-Vol
Others	Mega Vol
Piezoelectric	Others
Nephelometer	Dichotomous Sampler
β-gauge	Diffusion Batteries
	Electrical Mobility Analyzers
	Optical Counter
	Piezoelectric
	Impactor
	Centrifuge
	Cyclones
	Centrifuge
FUGITIVE	
Filters	Filters
Hi-Vol	Hi-Vol
Others	Mega Vol
Piezoelectric	Others
Nephelometer	Dichotomous Sampler
β-gauge	Diffusion Batteries
Lidar	Electrical Mobility Analyzers
	Optical Counter
	Piezoelectric
	Impactor
	Centrifuge
	Cyclones
	Fugitive Assessment Sampling Train (FAST)
	Centrifuge
	Elutriators
STACK SAMPLING	
Filters	Impactors
Charge transfer	Cyclones
β-gauge	Optical
Peizoelectric	Electrical Mobility Analyzers
Optical	Diffusion Batteries
Transmissometers	Surface Ionization
Lidar	

time intervals at a series of points across the duct. These traverse points are located at the centers of zones which divide the duct into a number of zones of equal area. The number of zones into which the duct is divided depends on the distances to upstream and downstream flow disturbances and the duct dimensions. All samples are taken under isokinetic conditions.

One of two general types of sampling systems is used for these determinations depending on the test conditions and the purposes for which the data are being acquired. The simpler system, illustrated in Figure 1, utilizes a filter holder and attached sampling nozzle which are introduced directly into the gas stream. The filtration medium may be a flat glass fiber filter, a glass fiber thimble or an alundum (ceramic) thimble. The choice depends on gas temperature, the concentration of the particulate matter, and the intended use of the data. A pitot tube and thermocouple located adjacent to the sampling nozzle make it possible to continuously monitor the gas velocity and permit correction of the sample flowrate as required to maintain isokinetic sampling conditons. On those occasions when the velocity field within the duct is stable over long periods of time separate traverses may be made for determination of velocity and dust sampling, in which case the pitot tube on the sampling probe may be omitted.

Testing for compliance with air pollution regulations is generally done with the system shown in Figure 2. This system, known as the U.S. Environmental Protection Agency's Method 5 sampling train, uses a nozzle and heated probe to withdraw the sample from the duct to a filter located within a temperature controlled oven.

The filter may be followed by either a condenser and moisture absorbent or by a series of impingers and an absorbent. A leakless pump is used to provide the necessary suction downstream of which are located a dry gas meter and an orifice-type flow meter. The latter is used for monitoring and setting the sampling rate during a test. This system provides for simultaneous determinations of volumetric gas flows within the duct being tested, mass emission rate, mass concentration, and moisture content. The use of appropriate reagents in

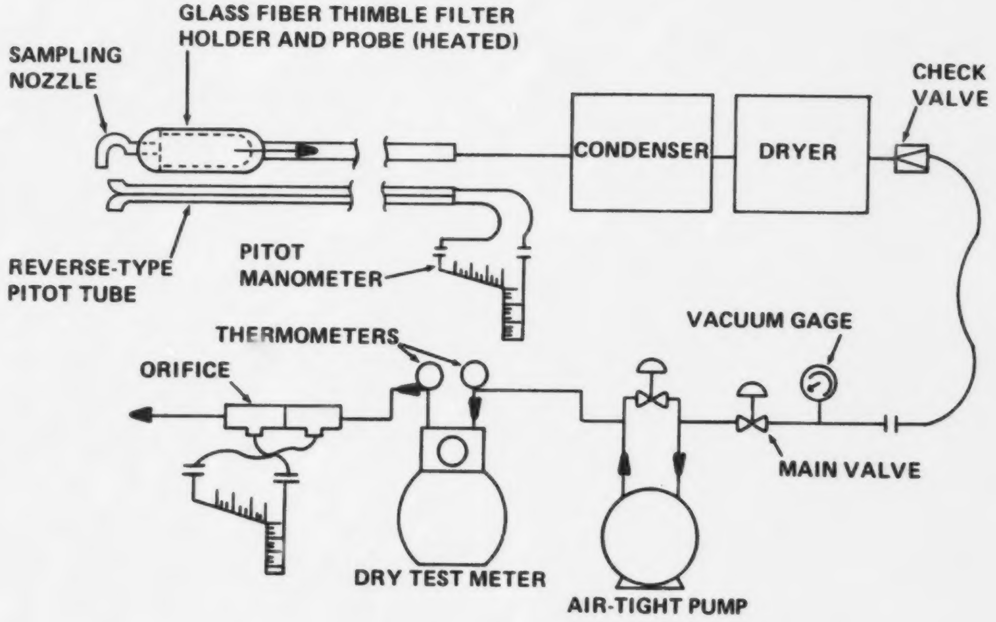
GLASS FIBER THIMBLE FILTER HOLDER AND PROBE (HEATED)
SAMPLING NOZZLE
CHECK VALVE
CONDENSER
DRYER
REVERSE-TYPE PITOT TUBE
PITOT MANOMETER
VACUUM GAGE
THERMOMETERS
ORIFICE
MAIN VALVE
DRY TEST METER
AIR-TIGHT PUMP

Figure 1. American Society For Testing and Materials' Particulate Sampling Train.

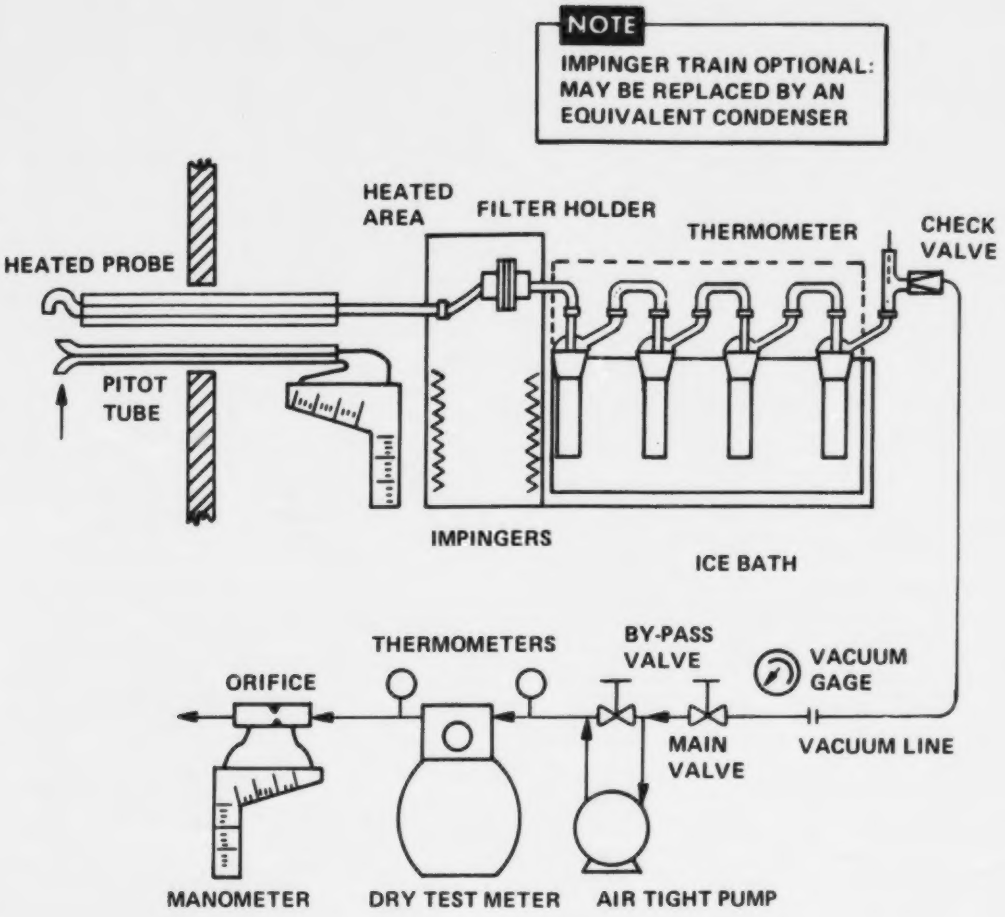
NOTE
IMPINGER TRAIN OPTIONAL: MAY BE REPLACED BY AN EQUIVALENT CONDENSER
HEATED AREA
FILTER HOLDER
THERMOMETER
CHECK VALVE
HEATED PROBE
PITOT TUBE
IMPINGERS
ICE BATH
THERMOMETERS
BY-PASS VALVE
VACUUM GAGE
ORIFICE
MAIN VALVE
VACUUM LINE
MANOMETER
DRY TEST METER
AIR TIGHT PUMP

Figure 2. U.S. Environmental Protection Agency's Method 5 Particulate Sampling Train.

the impinger portion of the train permits simultaneous determination of one or more vapor phase components of the flue gas as well (e.g., SO_3, SO_2). The probe connecting the nozzle and filter housing must be glass lined or, if longer than 2.5m, may be stainless steel or Incalloy. With the exception of tests of fossil fuel utility boilers the temperatures may be raised to 165°C to prevent or minimize the addition of sulfuric acid condensate to the particulate catch. Sampling rates range from 20 ℓpm to 200 ℓpm.

PARTICLE SIZE DISTRIBUTIONS

The methods most widely used in the U.S.A. for the determination of particle size distributions of industrial flue gas particulate matter are based on inertial separation. The separators include cascade impactors, cyclone separators, and other forms of air elutriators, including the Bahco "microparticle classifier." Because of the lack of resolution in the fine particle end of the size spectrum and the problems inherent in the redispersion of collected aerosols, the use of laboratory devices such as the Bahco are generally being discarded in favor of other devices which perform the size separation during the sampling operation.

The cascade impactor is the device most commonly used at this time for determining particle size distributions. In the devices, an aerosol sample is withdrawn isokinetically from the gas stream and passed sequentially through a series of impingement stages. Each succeeding stage operates at higher jet velocities than the previous stage thereby removing successively smaller particles at each stage. Determinations of the amount of particulate matter collected on each stage is then made either by gravimetric or chemical analysis. The particles size range spanned by an impactor is usually from about 0.50 μm to 10 μm. The number of stages ranges from about 6 to 13 and flowrates range from about 0.6 ℓpm to 30 ℓpm. Prototypes of impactors providing size distribution information to diameters as small as 0.02 μm have been constructed and successfully tested at industrial sites. Figures 3 and 4 show two of the more popular conventional (0.5 μm to 10 μm) impactors used in the U.S.A.

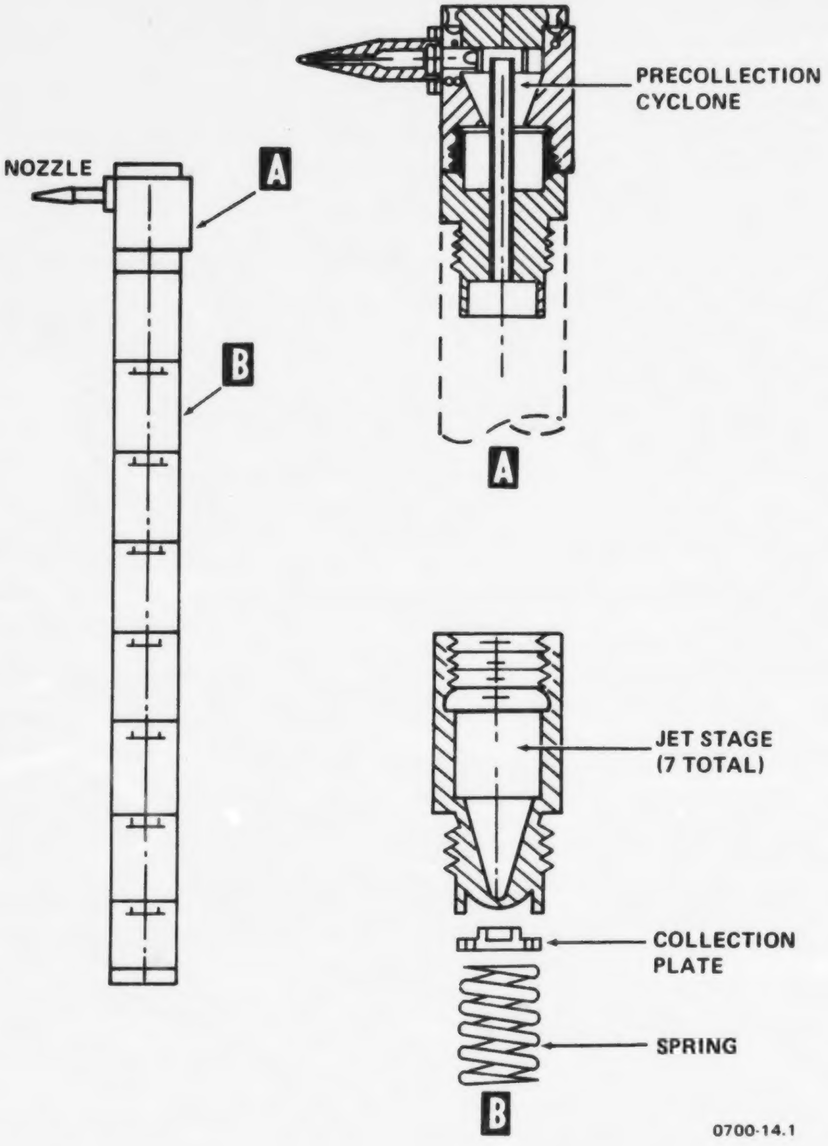
PRECOLLECTION
CYCLONE
NOZZLE
A
B
A
JET STAGE
(7 TOTAL)
COLLECTION
PLATE
SPRING
B
0700-14.1

Figure 3. Modified Brink Model BMS-11 Cascade Impactor.

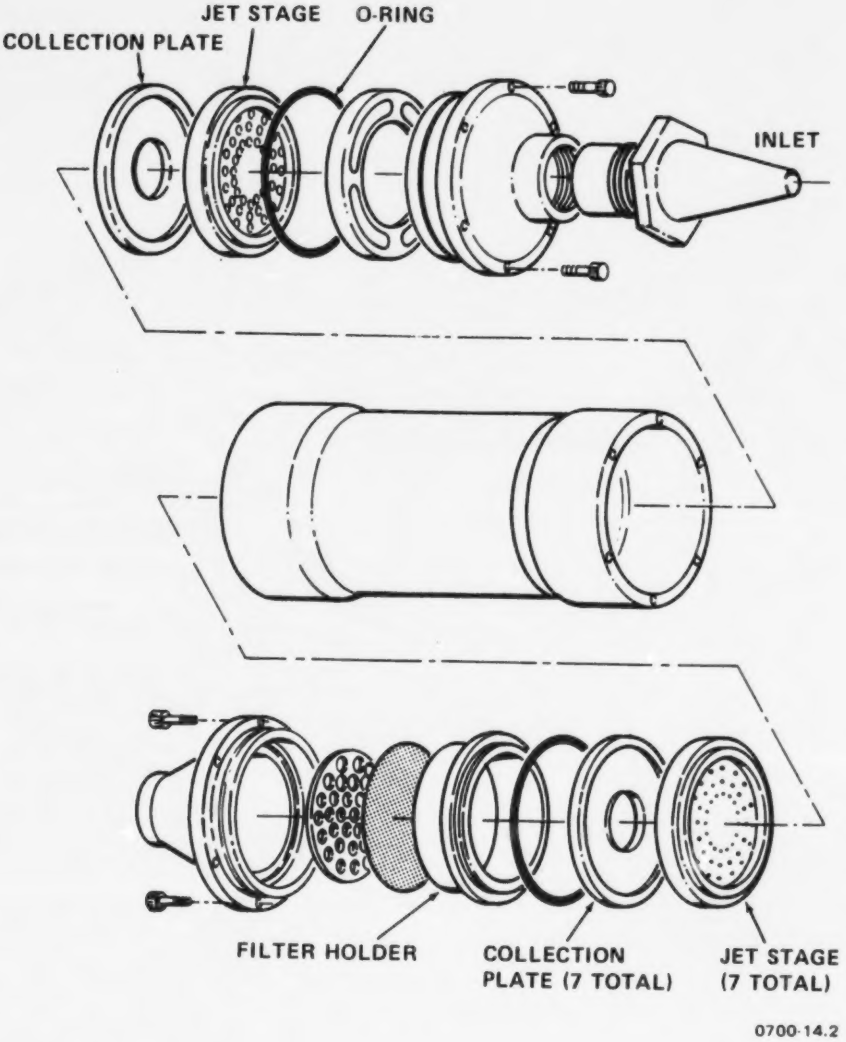
JET STAGE
O-RING
COLLECTION PLATE
INLET
FILTER HOLDER
COLLECTION PLATE (7 TOTAL)
JET STAGE (7 TOTAL)
0700-14.2

Figure 4. University of Washington Mark III Source Test Cascade Impactor.

The cyclone separator is a second type of inertial separator which is in fairly wide use at the present time. Small cyclones have been demonstrated to provide rather sharp particle size selection characteristics as illustrated in Figure 5. This shows calibration data obtained using monodisperse aerosols for a "cascade cyclone" designed and constructed by Southern Research Institute for the U.S. Environmental Protection Agency. The system operates at a nominal flowrate of 28 ℓpm and provides particle size information from about 0.3 μm to 7.0 μm. Figure 6 illustrates the cyclone system. Cyclonic type collectors are particularly useful when sampling gas streams having high dust concentrations, which tend to lead to rapid overloading of impactors, and when large samples are needed for chemical or toxicological studies. They may also be a valuable tool for determining size distributions in high temperature process streams (600°C to 1100°C) such as those associated with coal gasifiers and fluidized bed combustors for combined cycle electrical generating stations. Cascade impactors may not be suitable for high temperature studies because of a lack of a suitable substrate on which to collect the particles. Small cyclonic separators are also frequently used as precollectors upstream of cascade impactors to eliminate rapid overloading of the first impaction stage. Figure 3 shows one application of a cyclone precollector.

A three-stage "cascade cyclone" operating at a flowrate of 140 sℓpm is in routine use today as a part of the Source Assessment Sampling System (SASS). The SASS, illustrated in Figure 7, is used for providing semiquantitative information on the form, nature, and composition of pollutants emitted from industrial processes for the purpose of assessing their potential impact on the environment. The system provides size segregated samples of particulate matter in four size ranges (greater than 10 μm, 3 μm to 10 μm, 1 μm to 3 μm, and smaller than 1 μm), usually in sufficient quantities for chemical analysis and for toxicological studies to determine their potential impact on human health and terrestrial and aquatic ecosystems. In addition to the particulate samples, the system also provides samples of organic and inorganic vapors for similar analyses.

Optical and electron microscopy are also used occasionally for determining particle size distributions, but difficulties in obtaining unagglomerated

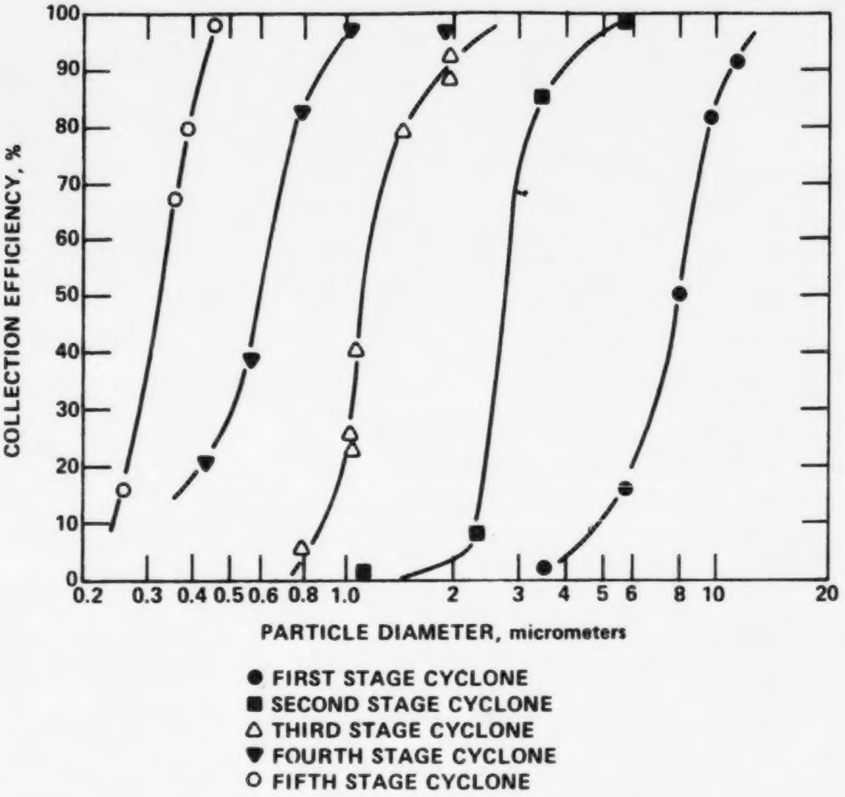

Figure 5. Laboratory Calibration for the Five Stage Series Cyclone System. (472 cm^3/sec, particle density--1.0 gm/cm^3).

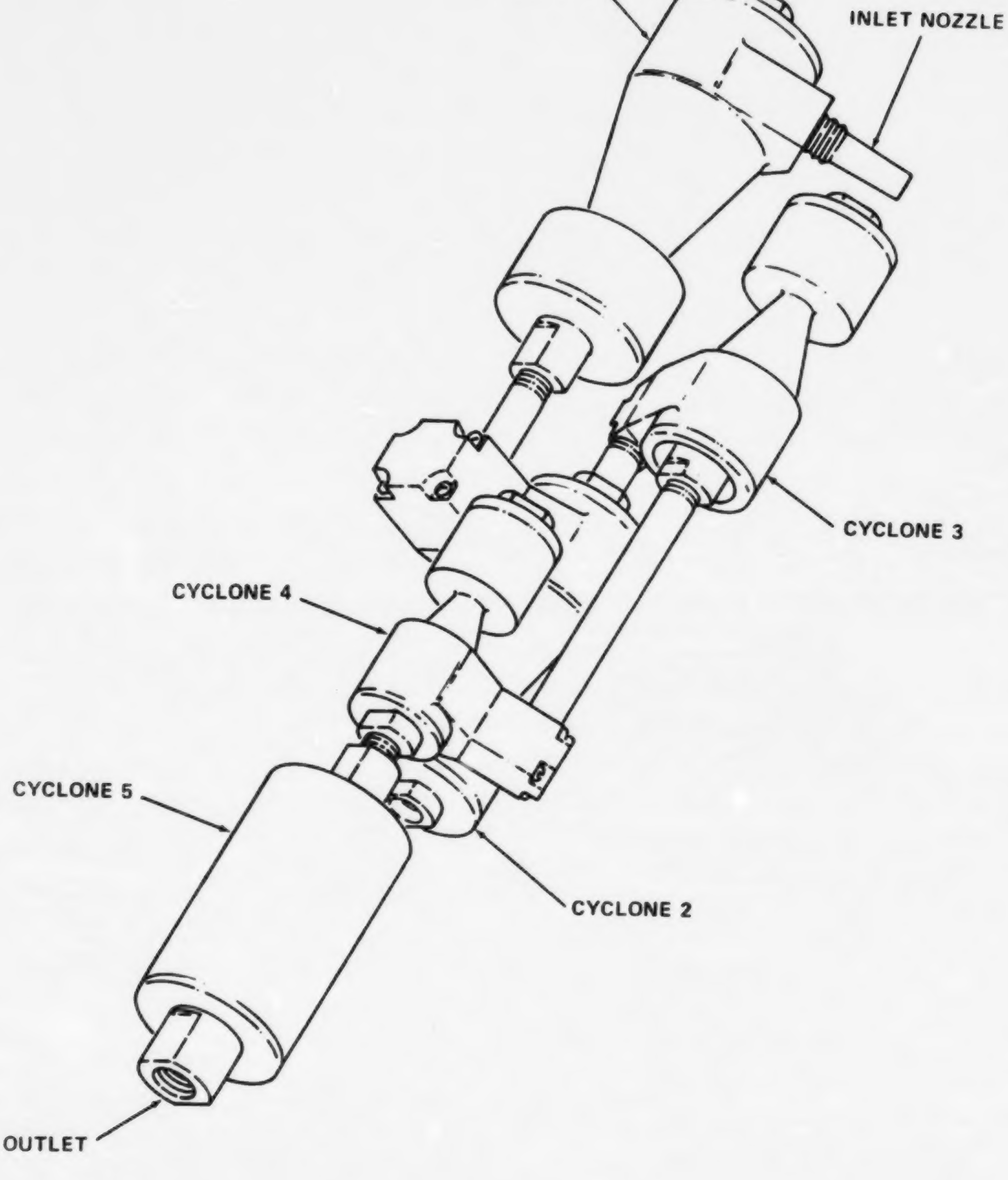
CYCLONE 1
INLET NOZZLE
CYCLONE 3
CYCLONE 4
CYCLONE 5
CYCLONE 2
OUTLET

Figure 6. Five Stage Series Cyclone System.[3]

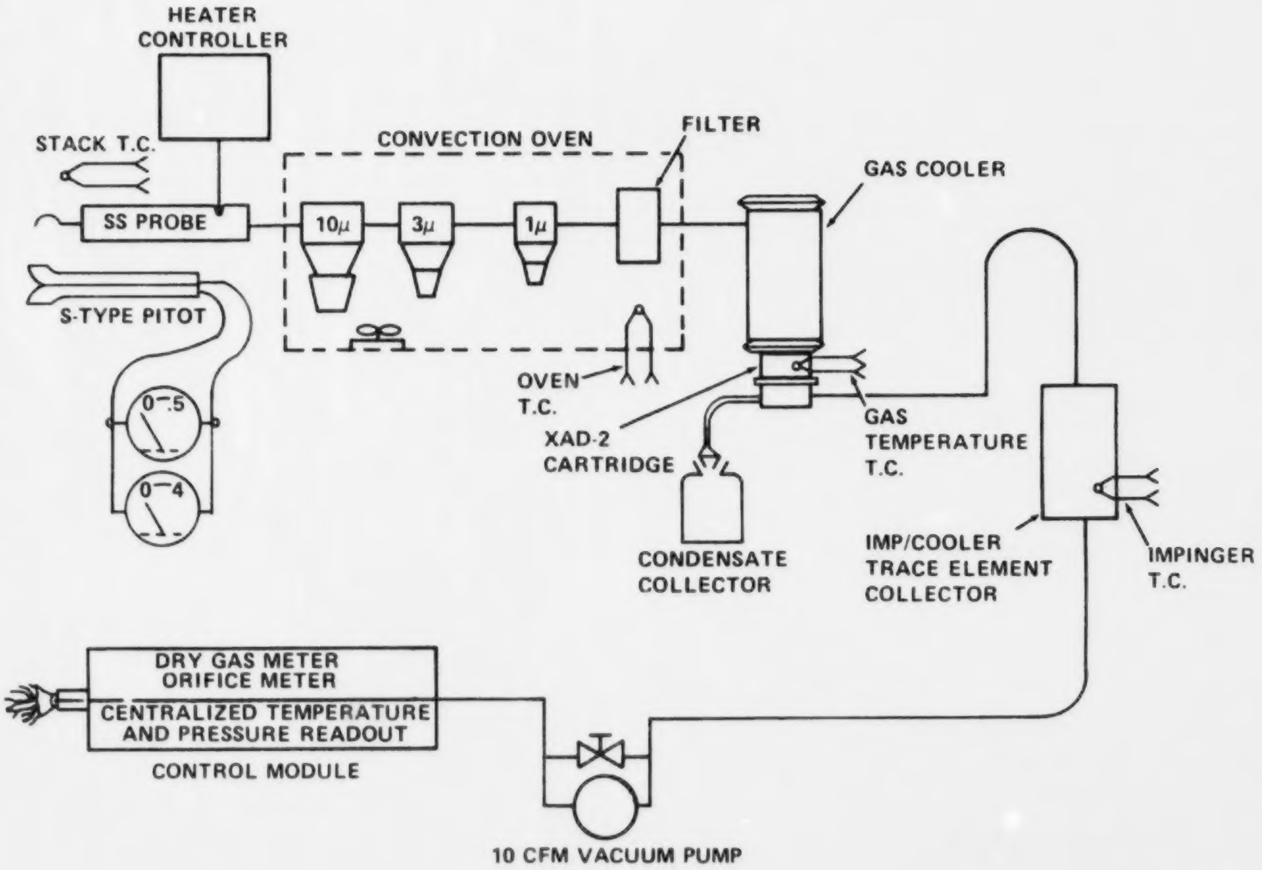
HEATER CONTROLLER
STACK T.C.
SS PROBE
S-TYPE PITOT
0–.5
0–4
CONVECTION OVEN
10μ
3μ
1μ
FILTER
OVEN T.C.
GAS COOLER
XAD-2 CARTRIDGE
GAS TEMPERATURE T.C.
CONDENSATE COLLECTOR
IMP/COOLER TRACE ELEMENT COLLECTOR
IMPINGER T.C.
DRY GAS METER
ORIFICE METER
CENTRALIZED TEMPERATURE AND PRESSURE READOUT
CONTROL MODULE
10 CFM VACUUM PUMP

Figure 7. Schematic of the Source Assessment Sampling System.

samples at suitable surface densities on the collection media, while still collecting a truly representative sample make the use of microscopy infrequent.

Details of particle size distributions from about 0.01 μm to about 0.5 μm (ultrafine particles) are desired or needed occasionally, but far less frequently than for the larger particles. Electron microscopy is sometimes used to provide information on the ultrafine particulate size distribution. Here again, difficulties in obtaining suitable representative, uncontaminated, unagglomerated samples make this an infrequently chosen method. The methods most frequently used for the determination of the concentrations and size distributions of ultrafine particles are diffusional and electrical mobility analyses.

Diffusional methods generally use condensation nuclei counters for measurement of particle concentrations and diffustion batteries for providing the necessary particle size discrimination. The condensation nuclei counter, illustrated in Figure 8, operates by causing a sample of the aerosol being measured to become supersaturated in the concentration of some condensible vapor--usually water or alcohol. The supersaturated vapor will condense on any particles present in the sample having diameters larger than some critical diameter which is determined by the particle solubility and the amount of supersaturation achieved. This critical diameter is typically about 0.002 μm. The condensation of the vapor results in the formation of a rather homogeneous, monodisperse fog containing one fog droplet for every particle in the sample which had a diameter larger than the critical nucleation diameter. Light scattering techniques are then used to determine the concentration of the fog droplets and hence the original concentration of the particles whose diameters were larger than the critical size. Size distributions are then determined by measuring the concentrations of a sample gas stream upstream and downstream of a series of tubes, narrow parallel rectangular channels, or screens, for which losses resulting from particle diffusion to the internal surfaces can be predicted as functions of particle size. Figure 9 illustrates a typical diffusion battery of the parallel rectangular channel type and penetration curves for a particular set of flow conditions. The condensation nuclei counters require samples which are essentially at ambient pressure and temperature and

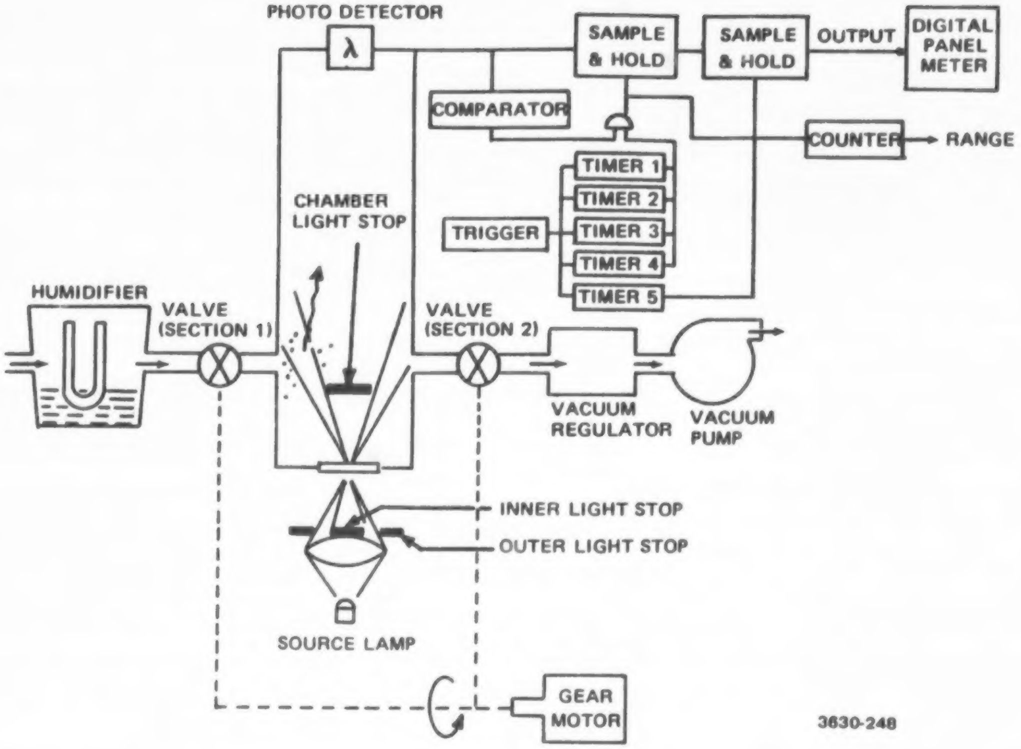
PHOTO DETECTOR
λ
SAMPLE & HOLD
SAMPLE & HOLD
OUTPUT
DIGITAL PANEL METER
COMPARATOR
COUNTER
RANGE
TIMER 1
TIMER 2
TIMER 3
TIMER 4
TIMER 5
TRIGGER
CHAMBER LIGHT STOP
HUMIDIFIER
VALVE (SECTION 1)
VALVE (SECTION 2)
VACUUM REGULATOR
VACUUM PUMP
INNER LIGHT STOP
OUTER LIGHT STOP
SOURCE LAMP
GEAR MOTOR
3630-248

Figure 8. Diagram of a condensation nuclei counter. After Haberl and Fusco.[5]

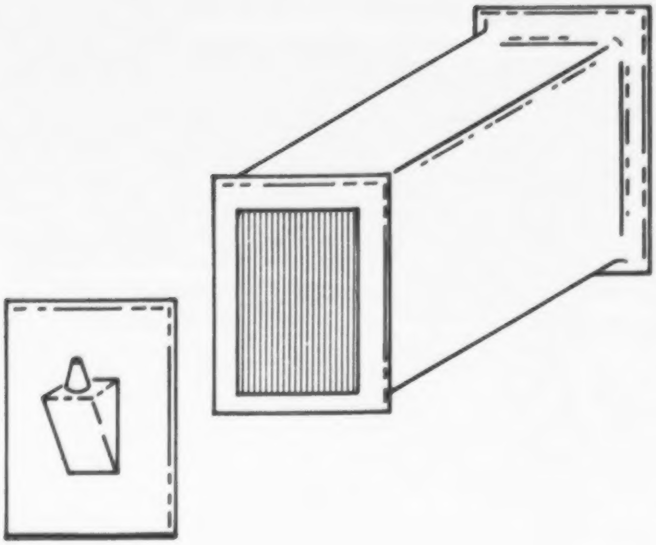

Figure 9a. Parallel plate diffusion battery.

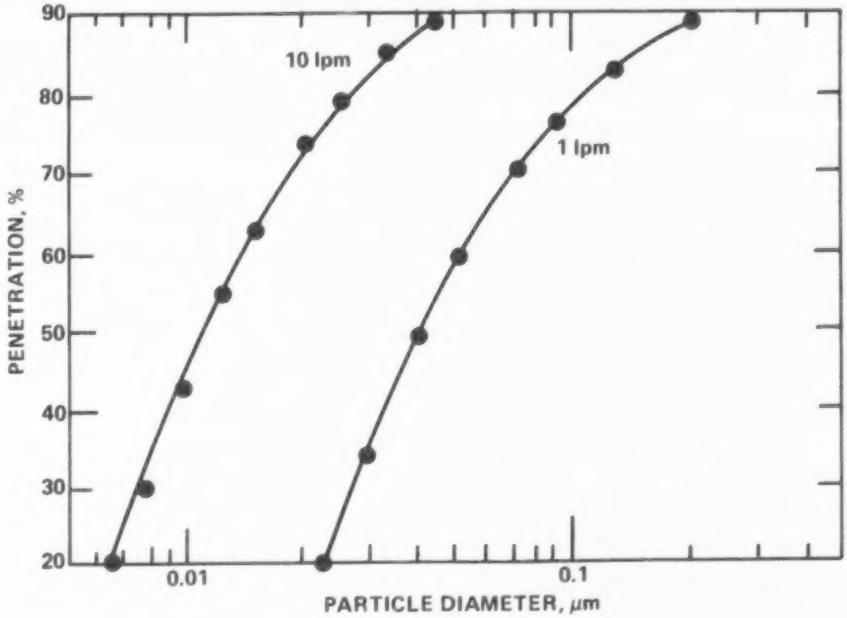

Figure 9b. Parallel plate diffusion battery penetration curves for monodisperse aerosols (12 channels, 0.1 x 10 x 48 cm).[4]

which have much lower particle concentrations than those typically found in industrial flue gases. Therefore extractive sampling is required followed by extensive dilution and sample conditioning to remove undesirable condensable vapors. A schematic diagram of a complete system used for such analyses by Southern Research Institute is shown in Figure 10. Dilutions from 10:1 to 4000:1 can be provided with the system. Diffusional analyses typically provide data over the size range from about 0.01 μm to 0.2 μm.

SAMPLING FUGITIVE EMISSIONS

SAMPLING STRATEGIES

Because they are not confined to a duct, or any particular area, fugitive emissions are more difficult to characterize than ducted emissions. The boundaries and velocity of the plume must be determined, and temporal variations and dilution must be taken into account. An important part of current research and development programs is the development of sampling strategies.

Measurements of fugitive aerosols may be made near the source, where essentially no dilution has occurred; in the air surrounding the source, where only limited dilution has occurred; or upwind and downwind of the source where dilution is essentially complete. Measurement methods used in each application are called quasi-stack, roof monitor, and upwind-downwind, respectively.

Figure 11 is a schematic showing the quasi-stack technique for sampling fugitive emissions. In this technique, the emissions are captured at their source in a temporary hood, and transmitted by means of an exhaust blower, through a duct where conventional, in situ sampling methods are used to measure the particulate concentration and the velocity of the gas. The emission rate of the pollutants can be calculated from these data.

The quasi-stack method is the most accurate technique for measuring fugitive emissions. Almost all of the emissions are captured with little dilution. Unfortunately, it may be difficult or impossible to apply in

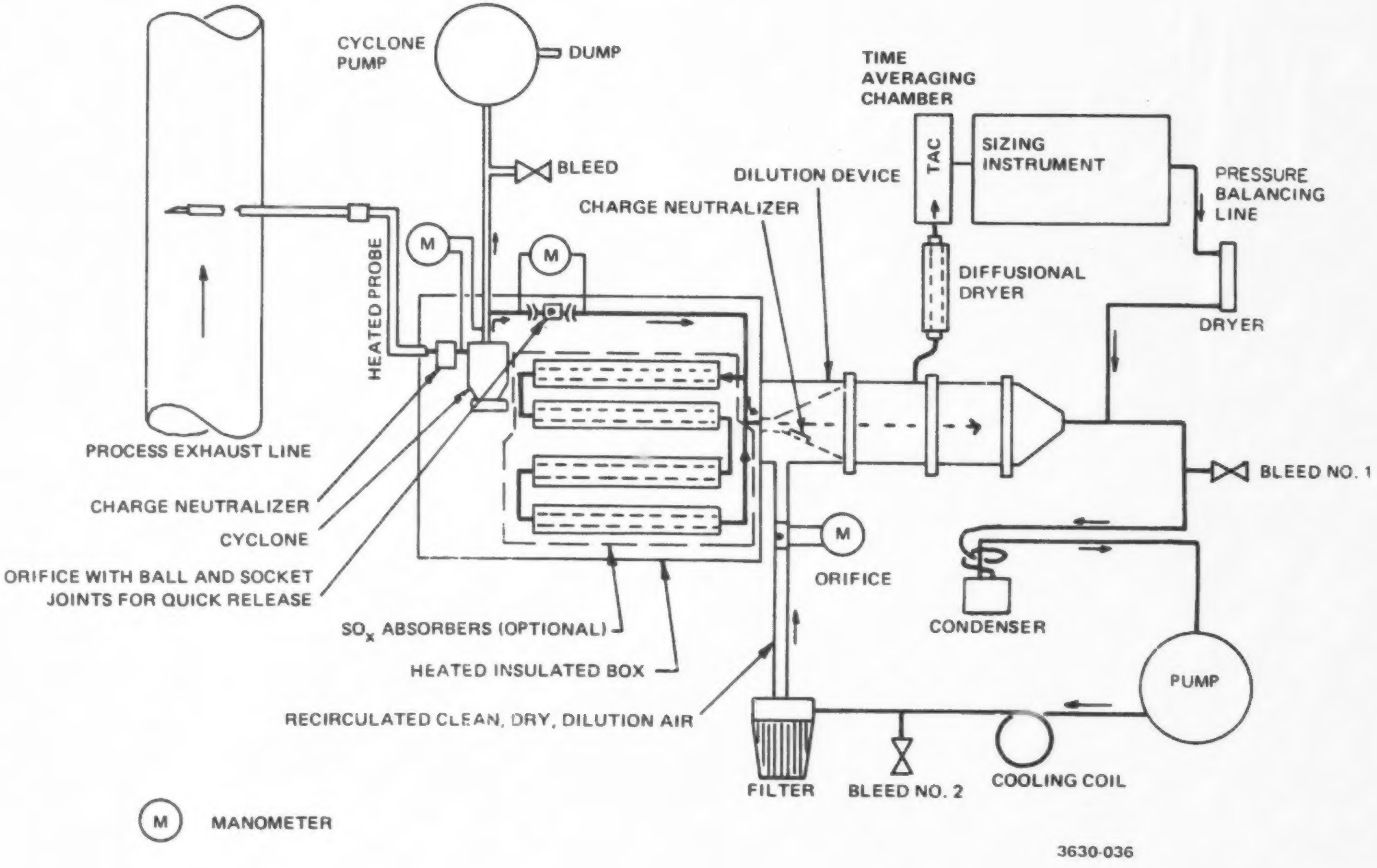
CYCLONE PUMP
DUMP
BLEED
TIME AVERAGING CHAMBER
TAC
SIZING INSTRUMENT
PRESSURE BALANCING LINE
DRYER
DILUTION DEVICE
CHARGE NEUTRALIZER
DIFFUSIONAL DRYER
HEATED PROBE
M
PROCESS EXHAUST LINE
BLEED NO. 1
CHARGE NEUTRALIZER
CYCLONE
ORIFICE WITH BALL AND SOCKET JOINTS FOR QUICK RELEASE
ORIFICE
SO$_x$ ABSORBERS (OPTIONAL)
CONDENSER
HEATED INSULATED BOX
PUMP
RECIRCULATED CLEAN, DRY, DILUTION AIR
FILTER
BLEED NO. 2
COOLING COIL
MANOMETER
3630-036

Figure 10. Sample Extraction-Dilution System (SEDS).[4]

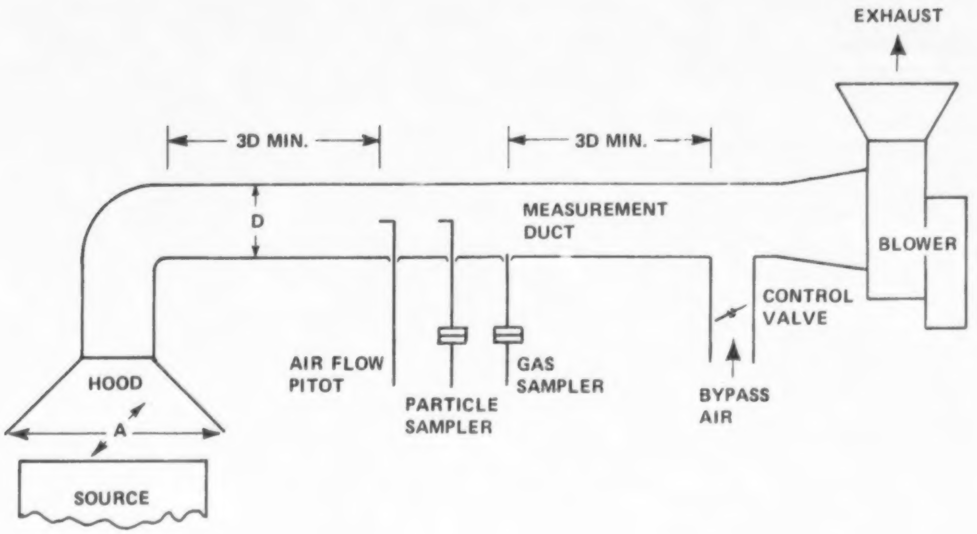
EXHAUST
3D MIN.
3D MIN.
D
MEASUREMENT DUCT
BLOWER
CONTROL VALVE
AIR FLOW PITOT
PARTICLE SAMPLER
GAS SAMPLER
BYPASS AIR
HOOD
A
SOURCE

Figure 11. Schematic of a quasi-stack sampling arrangement.

cases where the emissions from a source cannot be isolated, where the physical arrangement will not permit its installation, where the character of the emissions may be changed, or where the process operation might be interrupted.

Figure 12 illustrates the roof monitor method for sampling fugitive emissions. This method is applicable to methods or processes within buildings that have a small number of openings to the atmosphere. The structure of such a building serves as a large hood, confining the emissions to a limited volume of air (and hence dilution) before transmitting them through the openings to the outside.

As in the quasi-stack method, the particulate concentration and gas velocity are measured and used to calculate the emission rate. In the roof monitor method, the emission rate represents the combined strength of all the sources within the building.

The roof monitor method is less accurate than the quasi-stack method because of the higher dilution ratio and multiplicity of sources and exhaust openings. On the other hand, it can be applied to almost any process that operates indoors without interrupting the normal plant operations.

Although it is the least accurate of the three sampling techniques, the upwind-downwind method can be applied to any source of fugitive emissions. The particulate emission rate from a source is determined by taking the difference between particulate concentrations measured in the atmosphere by a network of samplers located upwind and downwind from a source. The samplers are normally arranged in a network near the ground, but in some applications have been attached to masts to form a two-dimensional, vertical array on the downwind side of the source. The data are used as input into dispersion models to estimate the strength of the source.

SAMPLING INSTRUMENTS

In using the quasi-stack technique to monitor fugitive emissions, the concentration of particles is generally high enough to allow the use of

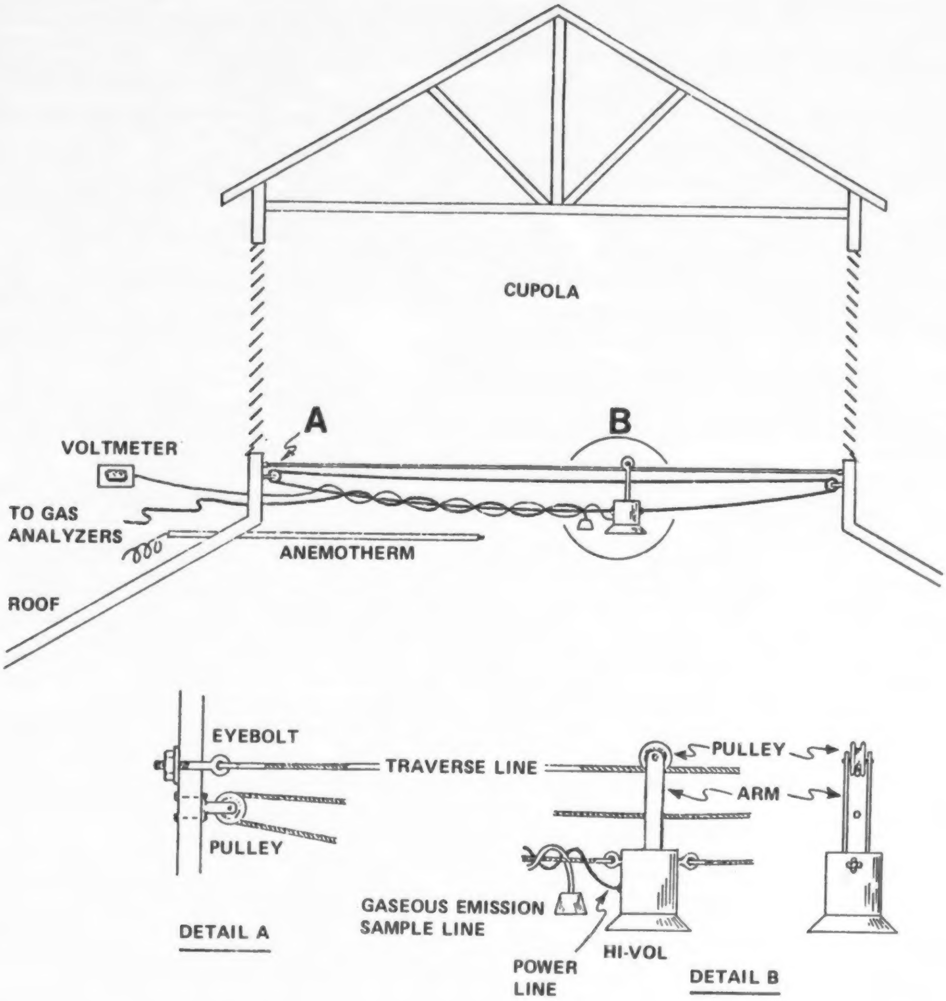
CUPOLA
A
B
VOLTMETER
TO GAS ANALYZERS
ANEMOTHERM
ROOF
EYEBOLT
TRAVERSE LINE
PULLEY
PULLEY
ARM
GASEOUS EMISSION SAMPLE LINE
POWER LINE
HI-VOL
DETAIL A
DETAIL B

Figure 12. Schematic of a roof monitor traversing sampler arrangement.

stack sampling instruments as described above. However, for roof monitor sampling and upwind-downwind sampling, the aerosol is diluted and it is desirable to use high volume samplers.

Figure 13 illustrates the high volume filter sampler that is used extensively in the USA to measure particulate concentrations. The sampler is enclosed in an aluminum enclosure to prevent rain and large particles from falling onto the filter. A blower is used to draw a gas volume of approximately 1130 ℓpm through a glass fiber filter (20.3 x 25.4 cm).

If a measure of the particle-size distribution is desired, cascade impactors are available that fit directly over the Hi-Vol filter, using the same blower and flow control system, to yield the additional data. Three models of cascade impactors for use with the Hi-Vol are illustrated in Figure 14.

A number of multiple jet impactors that operate at flowrates on the order of 30 ℓpm are also available for fugitive and ambient sampling.

Figure 15 is a schematic illustrating the operating principle of the dichotomous sampler, or virtual impactor, that has recently been developed for sampling fugitive and ambient aerosols. This instrument samples at a flowrate of 50 ℓpm. The separation of particles having aerodynamic diameters of 2.5 μm and larger from smaller particles is done by impingement into a dead air space, or virtual surface. In order to optimize the performance of the instrument, it has been found desirable to have a small flow from the stagnant volume. The main advantage of the dichotomous sampler is that it can be used to collect large samples without overloading.

A Fugitive Air Sampling Train (FAST) has been designed to utilize commercially available equipment to obtain a 500 milligram sample of particulate matter and a 15 milligram sample of organic vapors in an 8-hour sampling period at locations where the pollutant concentration levels are about 200 micrograms per cubic meter. The prototype unit has been constructed to contain the sampling devices in a single unit, as shown in Figure 16, about 2 x 1 x 1 meters in

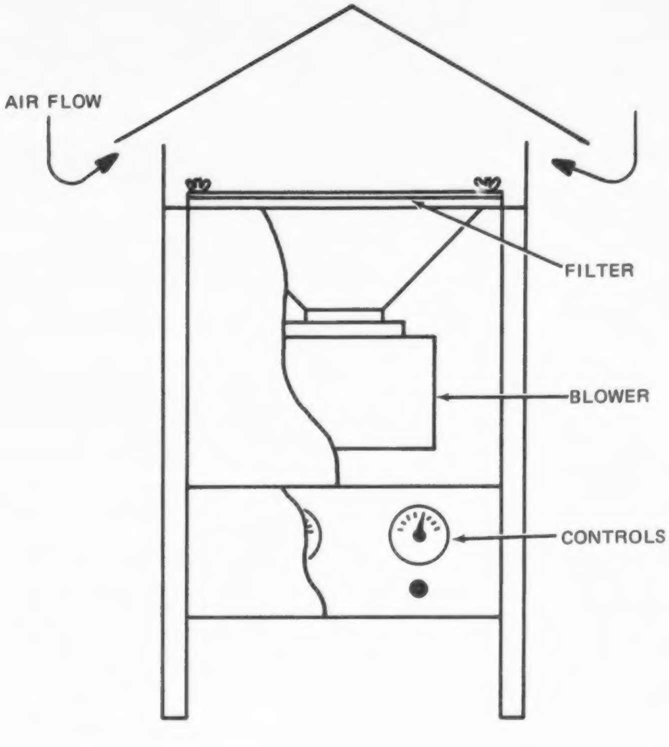
AIR FLOW
FILTER
BLOWER
CONTROLS

Figure 13. The standard high volume particle sampler.

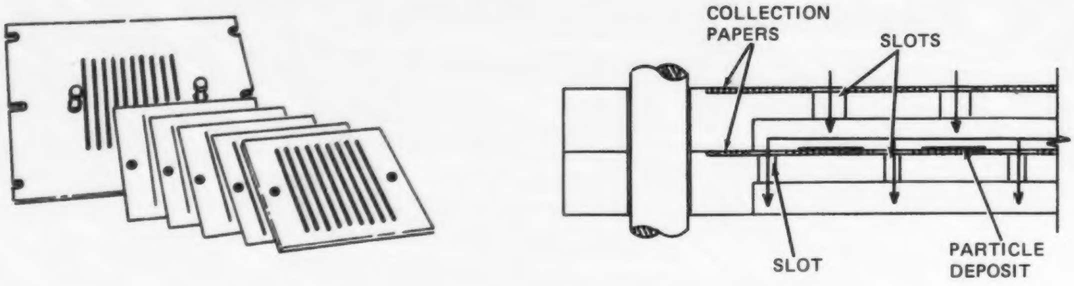
COLLECTION PAPERS
SLOTS
SLOT
PARTICLE DEPOSIT

Figure 14a. The Sierra Instruments Hi-Volume cascade impactor.

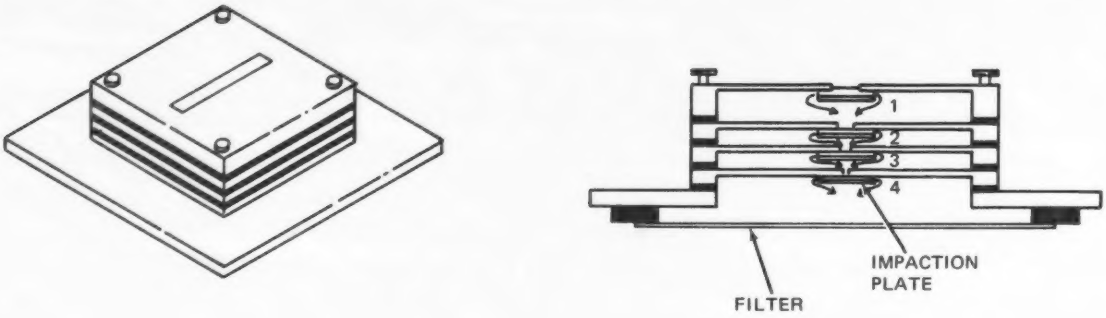
1
2
3
4
IMPACTION PLATE
FILTER

Figure 14b. The BGI Hi-Volume cascade impactor.

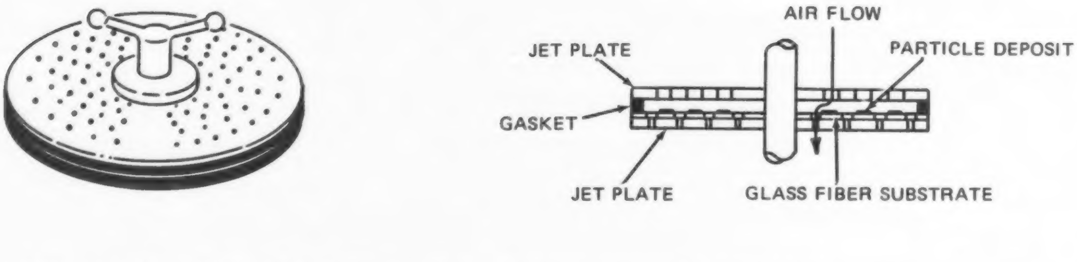
AIR FLOW
JET PLATE
PARTICLE DEPOSIT
GASKET
JET PLATE
GLASS FIBER SUBSTRATE

Figure 14c. The Andersen 2000 Hi-Volume cascade impactor.

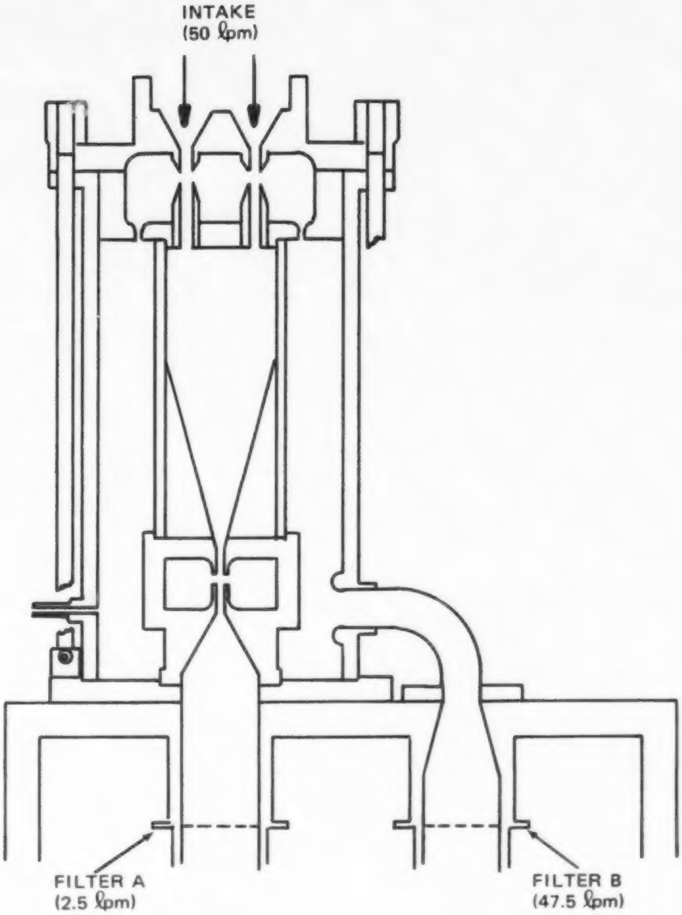
INTAKE
(50 ℓpm)
FILTER A
(2.5 ℓpm)
FILTER B
(47.5 ℓpm)

Figure 15. A schematic of the dichotomous sampler.

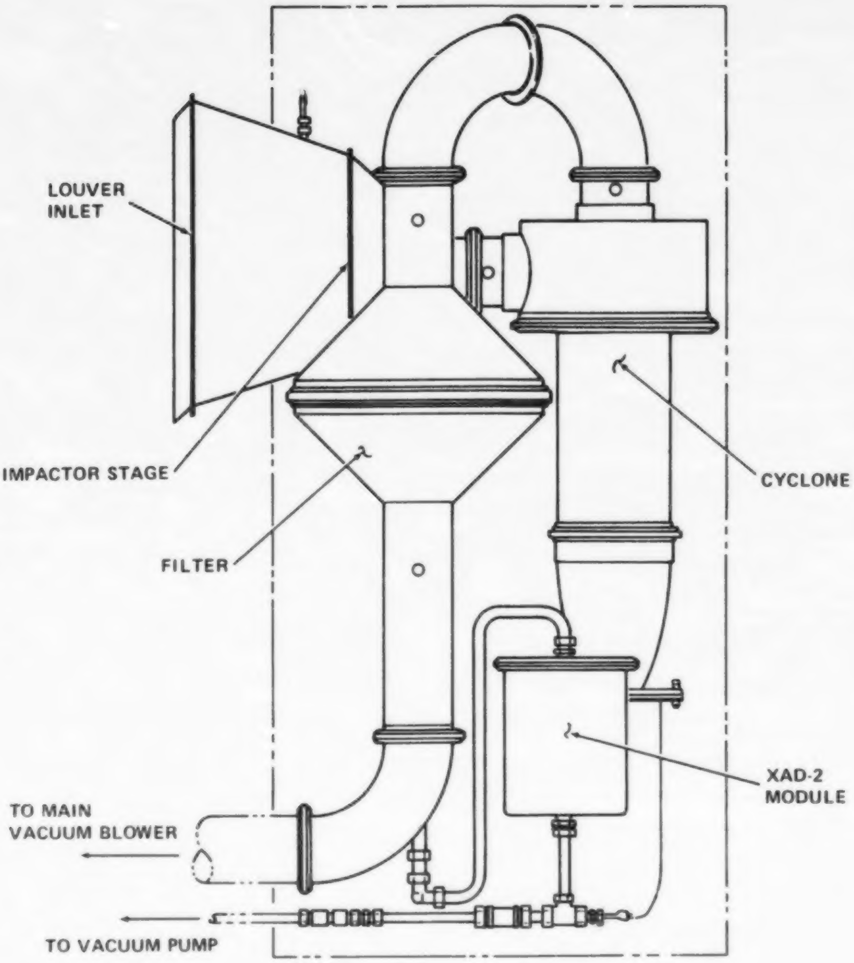
LOUVER INLET
IMPACTOR STAGE
FILTER
CYCLONE
XAD-2 MODULE
TO MAIN VACUUM BLOWER
TO VACUUM PUMP

Figure 16. Fugitive air sampling train assembly.

size. This sampling unit contains a single stage cascade impactor to collect about 90% of all particles larger than 15 μm, a cyclone separator to collect about 50% of the remaining particles larger than 3 μm, and a glass fiber filter to collect more than 99% of the particles still entrained in the sampling stream. The particulate sampling stream flowrate of about 300 m^3/hr is provided by a separately packaged Roots-type vacuum blower. A side stream of about 8 m^3/hr is taken from the main stream below the filter by a separately mounted vacuum pump and drawn through a canister of XAD-2 adsorbent resin to extract organic vapors. The component arrangement is shown schematically in Figure 17.

SAMPLING AMBIENT EMISSIONS

Sampling ambient aerosols is done with the same type of instruments as those used in sampling dilute fugitive emissions. A large network of Hi-Vol samplers is used to continuously monitor the total suspended particulate (TSP) burden in the USA.

Cascade impactors, dichotomous samplers, and the FAST, are all used as part of research studies or efforts to characterize urban aerosols in more detail.

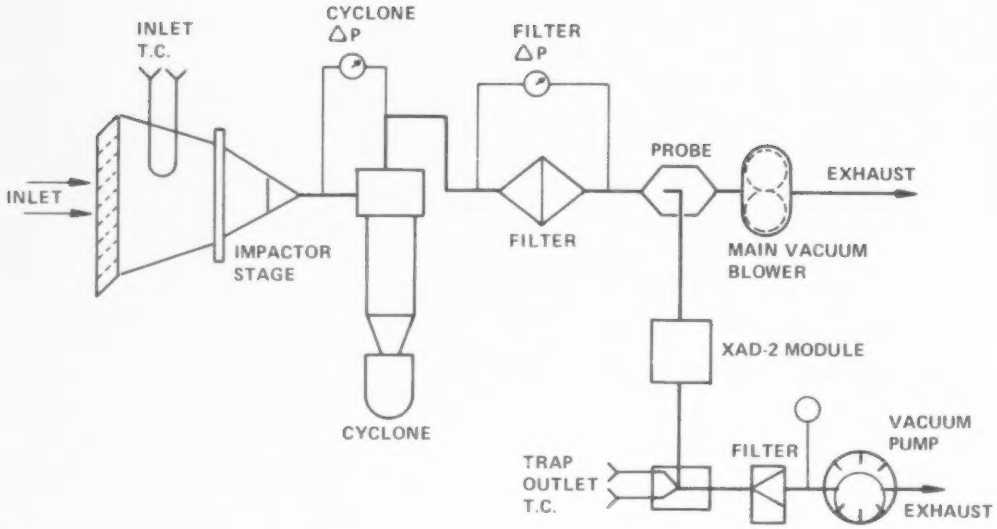
INLET
T.C.
CYCLONE
ΔP
FILTER
ΔP
PROBE
EXHAUST
INLET
IMPACTOR
STAGE
FILTER
MAIN VACUUM
BLOWER
XAD-2 MODULE
CYCLONE
VACUUM
PUMP
TRAP
OUTLET
T.C.
FILTER
EXHAUST

Figure 17. Fugitive air sampling train components.

REFERENCES

1. American Society for Testing and Materials
Standard Method for Sampling Stacks for Particulate Matter. Designation D2928-71, Annual Book of ASTM Standards, 1977.

2. Federal Register.
Standards of Performance for New Stationary Sources: Revision to Reference Methods 1-8. 42(160): 41753-51789, 1977.

3. Smith, W. B., and R. R. Wilson, Jr.
Development and Laboratory Evaluation of a Five-Stage Cyclone System.
Southern Research Institute, EPA, Research Triangle Park, NC. 66 pp, 1978.
EPA-600/7-78-008

4. Smith, W. B., K. M. Cushing, and J. D. McCain
Procedures Manual for Electrostatic Precipitator Evaluation.
Southern Research Institute, EPA, Research Triangle Park, NC. 430 pp, 1977.
EAP-600/7-77-059

5. Haberl, J. B., and S. J. Fusco
Condensation Nuclei Counters: Theory and Principles of Operation.
General Electric Technical Information Series, No. 70 POD 12, 1970.

6. Smith, W. B., P. R. Cavanaugh, and R. R. Wilson.
Technical Manual. A Survey of Equipment and Methods for Particulate Sampling in Industrial Process Streams.
Southern Research Institute, EPA, Research Triangle Park, N.C. 281 pp, 1978.
EPA-600/7-78-043

7. Helming, E. M., Compiler
Symposium on Fugitive Emissions Measurement and Control.
TRC, EPA, Research Triangle Park, NC., 1976.
EPA-600/2-76-246

D.L. Zelikson, N.G. Bulgakova

PRESENT-DAY TENDENCIES IN AEROSOL DISPERSION ANALYSIS

Improving methods for protecting the atmosphere from industrial emissions is based on the reliability of results from aero-mechanical and physio-chemical measurement. Measurement is strictly the basis of practically all aspects of environmental protection since it allows quantitative evaluation of efficiency of protection and of end results - the attainment of sanitary norms. The leading role of measurement in supplying technical process with the means of gas-cleaning may be realized only means of advanced development of concrete types of measuring techniques and of its basis, metrology.

Raising the question of lead development in measurement technology should above all accentuate research in an equipment oriented direction, deciding types of measurement directly necessary for reliable evaluation of gas-cleaning efficiency. Dispersion analysis and a survey of possible means of its development is the purpose of this report. An outline of literature (1-4) of various schemes of classifying methods for measuring aerosol particle diameter attests to the lack of a single common opinion on questions of selecting classifying features. Sufficiently arbitrary features are usually used applicable to this narrow problem. Disregarding attempts to set up a substantial classification model because of its complexity and the fact that it falls outside the limits of the given topic it is necessary as a consequence to select one basic type of dispersion analysis - dynamic dispersion analysis. Classification of measurement methods with regard to "dynamic features" is not found in the literature. At the same time, dynamic measurement type comprises a wide area of aerosol dispersion analyses to which in part relate more known methods of inertial precipitation and sedimentation.

Dynamic dipsersion analysis uses a fundamental property of particles - the presence of mass and inertia - and is realized by utilizing the effect of various forces on the suspended particle. Under the influence of these forces, particles acquire a given motion, therefore the problem of dynamic analysis is reduced to correct measurement of this motion's parameters.

From a metrological point of view, dynamic analysis is close to absolute measurements more preferable in result reliability when the magnitude of the measured value is found in agreement with the estimation of the given value's conception.

From determination of dynamic analysis follow basic classification features:

- the nature of the acting forces;
- types of particle motion;
- methods of measuring parameters of motion.

An enlarged classification is introduced in the table. Detailed classification is connected with clarification of concrete methods of force interaction with the particles and with each measurement method.

The classification provides five types of motion:

- equilibrial, when the particle is found at rest or is moving evenly and in a straight line;
- curvilineal, if when under the influence of applied forces the particle trajectory deviates in relation to its inertia;
- rotary motion has significance for non-spherical particles, mainly for those of elongated form and, obviously, it is almost the sole form of motion allowing evaluation of the particle's form;
- oscillatory, i.e. back-and-forth motion, whose amplitude and frequency dtermines the particle mass;
- impulse motion which has been practically unused until now and has a conditional character.

Active forces may be divided by their nature into aerodynamic, acoustic, electromagnetic, and distinct from the others, optical.

In the field of aerodynamic forces, the particle participates in any of the listed types of motion. In sedimentation methods, counterbalancing gravitational and centrifugal forces, other than aerodynamic, act upon the particle, which causes equilibrial motion. Aerosol stream flow against a barrier such as walls in cyclone analysors and impactors or against a counter flow of pure gas in so-called virtual impactors (5) is charaterized by the particle's curvilinear trajectory.

Aerosol gradient flow in a boundary layer or with stream vortex limits particle revolution. The submersed supersonic stream has periodic structure and and the stream velocity flow axis periodically changes from sonic to higher. The spatial modulation of

DYNAMIC DISPERSION ANALYSIS OF AEROSOLS

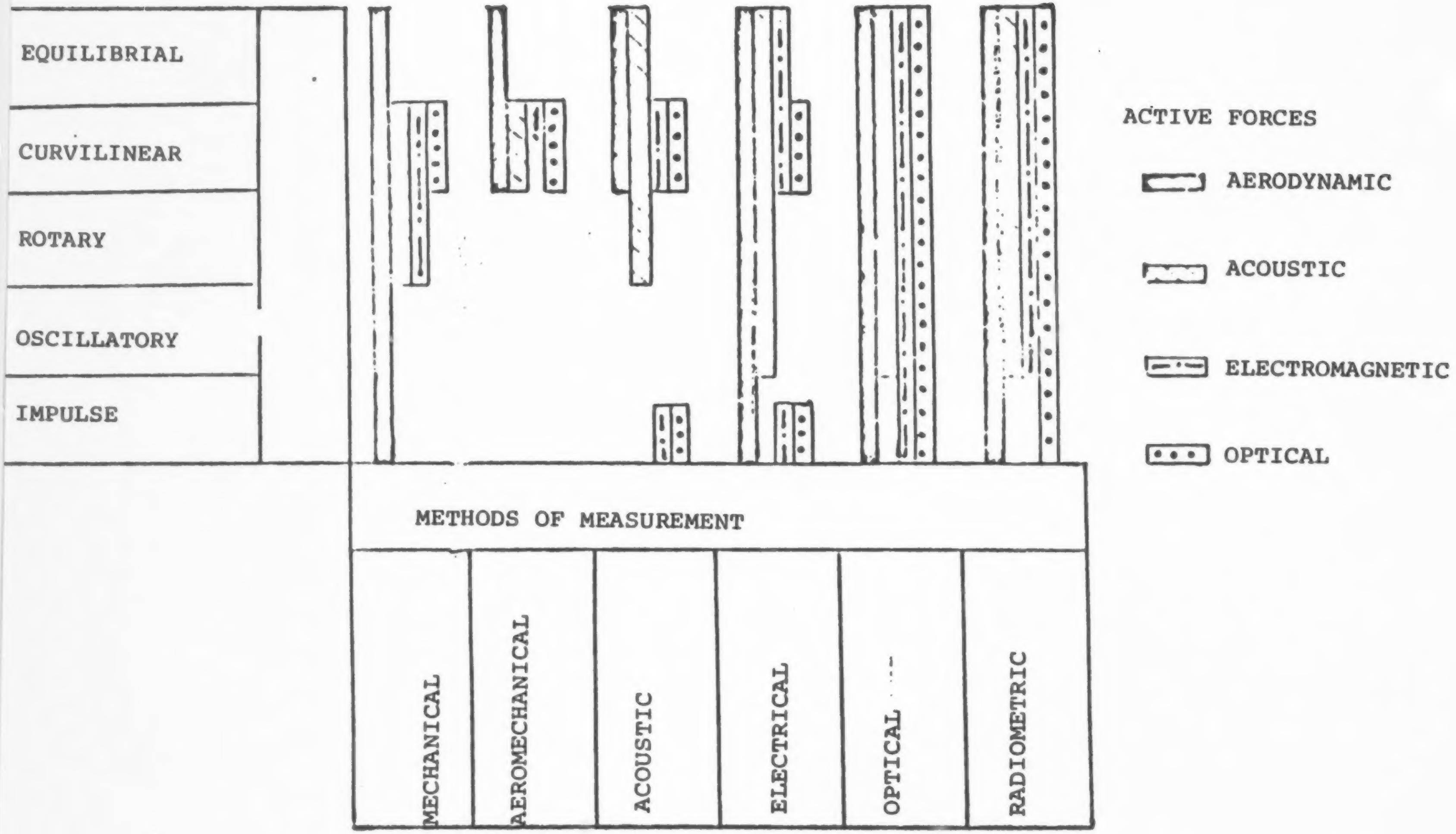

velocity results in particle separation(6). The shock wave transmits impulse motion to the particles.

In the acoustic standing wave, the particles, moving in loop motion, form an equilibrial spatial lattice(7), whose period of origin is a function of dispersion composition. Acoustically linear effects, accompanied by directed flows, perpendicular to the aerosol stream, may be used for fractional precipitation of particles moving curvilinearly. The travelling sonic wave draws particles into oscillation and revolution. The latter motion occurs due to the presence of velocity gradients in the wave (7). Sonic radio pulse or video pulse has an effect on the particle that is analogous to a shock wave.

Electrical, magnetic and optical forces influence the particle identically in equilibrial or curvilinear motion. In the first case, these forces counterbalance gravitational and/or aerodynamic forces, and in the second, the appearance of phoresis is used, acting perpendicularly to the aerosol stream(8). Revolution of elongated particles may be carried out by electro- or photophoresis. The specific action of the electromagnetic field appears in mass-spectometry. Mass-spectral analyzers used for high-dispersion charged aerosols separate particles according to curvilinear trajectories (9). The rotary electromagnetic field of the multi-phase flow holds wide possibilities for particle rotation (10). Spherical particle oscillation in the plane condensor's variable field is used for the most exact diameter measurements. Electrical discharge is the source of impulse movement.

In the standing optical wave are oscillating subatomic charged particles, the ions that form the spatial lattice analogous to the acoustic lattice. Irradiation of particles by a high-intensity laser source resulting in a piercing of the dispersion medium aids particle visualization (11) and may be conditionally related to impulse types, accompanied by transfer to the second aggregate state.

Methods of measuring movement parameters are based on partial usage of active field energies or on registration of the results of their influence.

Mechanical measurement methods reduce to determination of mass of the particles settled from the aerosol, the rate of their settling or revolution, the path travelled by the particles or the time taken to cover a given distance, and the amplitude of oscillations etc. in various combinations of types of motions and active forces given above. Aerodynamical measurement methods preclude those using aerosol flow parameter registration as a function of dispersion phase concentration. This hydraulic pressure variation of filters and other hydraulic systems, in particularly, in conjunction with changes in the viscosity of the dual-phase turbulent flow. Acoustic measurement methods include recording absorption or dispersion doses, which includes energy diffracted by particles of the sonic field. Measurement of the Doppler effect of frequency in relation to particle speed is possible, as well as recording sound pressure during particle impact.

Electrical discharge, transfered by particles directly to the collector electrode or induced, is measured in the electrical methods. For measurement of mass of settling, tuning fork or piezoresonance weights have been developed in which oscillation frequency of the resonance contour is set in relation to the amount of settling. The piezoelectrical effect is used also in pressure converters re= cording impulses during single particle impacts against the sensory element surface (12). Measurement of electrical beam absorption in the aerosol flow, magnetic and dielectric permeability dielectrical loss coeeficient, etc. is possible. Optical measurement methods present the widest possibilities. Equipment based upon these methods are universal, frequently automated, probeless means of measurement introducing the least interference in the measurement process and having maximum accuracy and sensitivity. Cinematographic, photographic and visual recording of movement parameters or fixation of particle position is related to these methods. Light absorption, scattering and difraction, polarization charactersistic variations, emission frequency Doppler effect and charactersitic illumination of exploding particles are used in this equipment.

Radiometric methods rival optical measurement. These methods include absorption, scattering and difraction of emissions, inherent emission of radioactive aerosols, and Doppler signal modulation down to the use of the Messbauer effect in special cases.

The considered methods of measurement are used for recording all types of particle movement in different combinations of active forces in wide ranges of fractional concentrations and dimensions particles of various forms. In aerosol measurement technology and industrial gas cleaning, particle size in the range of 5-6 orders of magnitude from 1 nanometer at concentrations also in the range of 5-6 orders of magnitude from 1 microgram/m^3 are of interest, and in experimental studies from one particle in the measured volume. The maximally attained accuracy of particle measurement on the order of 1 micron comprises 10^{-5} (13). Dynamic analysis methods of aerosol dispersed composition altogether meet the above demands and provide to a considerable degree the possibility for automating analysis in various conditions of use.

Two ways of of developing aerosol measurement techniques are possible. The first calls for creating universal means of measurement favorable for use in any, even extreme, conditions. According to the second, units that have been developed are specialized according to their branch of industry or according to gas-cleaning or dust removal systems. Universal equipment is more expensive, complex in its design and maintenance, requires more qualified operating personel during installation at experimental sites, but then is automated in a large degree and therefore simple in operation under conditions of sufficient reliability. Specialized equipment is distinguished by the simplicity of its design and mounting but practically excludes the possibility of changing the study site. Apparently, the technology of measurement in the area of dispersion analysis should be developed with determined relationship of these types of equipment with regard to the necessity of establishing calibration means to ensure accuracy.

BIBLIOGRAPHY

1.Klimenko, A.P. Methods and Equipment for Measuring Dust Concentration, Moscow, "Khimiia", 1978.

2. Methods, Equipment, and Systems for Monitoring the Industrial Environment : Interinstitutional Collection, Leningrad, LETI, 1976.

3. Larchenko, V.I., Filippov, V.P., Kulenev, Y.P., Modern Methods for Controling Aerosol Concentration : Survey Information TS-4 "Analytic Equipment and Equipment for Scientific Investigation", Moscow, TsNIITEI equipment construction, 1977.

4. Soprunyuk, P.M., Pau, A.A., Semen, N.P., New Dust Monitoring Equipment : Survey Information TS-4 "Analytic Equipment and Equipment for Scientific Investigation", Moscow, TsNIITEI equipment construction, 1977.

5. A Method for Measuring Particle Diameter, Japanese patent 113DO (G01N 15/02) No.52-22560, 1977.

6. Alkhimov, A.P., Papyrin, A.N., Predein, A.L., Soloukhin, R.I., Experimental Study of the Speed Lag Effect of Fine Particles in a Supersonic Gas Flow, PMFT Journal, 1977, No.4.

7. Mednikov, E.P., Acoustical Coagulation in Aerosol Settling, Moscow, USSR Academy of Sciences, 1963.

8. Kutukov,V.B., Ostrovskii, Y.K., Yalamov, Y.I., A Method for Separating Aerosol Particles from Gas Flow, USSR Author's Certificate, Patent no.558200, G01N 21/22, 1977.

9. Susoev, A.A., Chupakhin, M.S., Introduction to Mass-Spectometry, Moscow, Atomizdat, 1977.

10. Tolstoi, N.A., Spartakov, A.A., Trusov, A.A., Electrooptical Properties of Lyophobic Colloids, "Colloid Journal", 1966, 28, No.5, p. 735.

11. Zakharchenko, S.V., Kolomiets, S.M., Skripkin, A.M., Breakdown of Dispersion Medium By Laser Emission,"PMFT Journal", 1977, 3, No. 24, p.1339-1343.

12. Kozelkina, E.V., Kozelkin, V.V., Otroshko, N.G., Methods of Determining Solid Particle Concentration in Gas Suspension Flows, "Factory Laboratory", 1971, No.3, 307-308.

13. Ashkin, A., Recent Experiments with Optical Levitation, "Optical Communications", 1976, 18, No.1, 190-191.

INSTRUMENTS FOR AUTOMATICALLY MONITORING PARTICLE-SIZE DISTRIBUTIONS

W. M. Farthing
W.B. Smith

Southern Research Institute
2000 Ninth Avenue South
Birmingham, Alabama 35205

W. B. Kuykendal
Industrial Environmental Research Laboratory
Environmental Protection Agency
Research Triangle Park, N.C. 27711

(This document has been reviewed and approved for publication by the U.S. EPA.)

INSTRUMENTS FOR AUTOMATICALLY MONITORING PARTICLE-SIZE DISTRIBUTIONS

INTRODUCTION

Although the majority of size distribution measurements are still made using manual techniques, there is a clear need for automatic systems with real-time data output. Examples of such applications are: monitoring processes with periodic particle generation, process control, and optimizing control device performance.

The ideal measurement method is one which yields particle-size data conveniently, without perturbing the sample. Also, it is usually desirable to measure the diameter of the particles in terms of their aerodynamic behavior so that an estimate can be made of potential health effects. Some hybrid systems have been developed wherein the particles are size-segregated by impaction, with optical, piezoelectric, and β-particle monitor sensors after each stage; but, the greatest emphasis is now on the development of optical systems. The optical systems appear to offer greater convenience, speed, and reliability, but the accuracy will ultimately depend upon some knowledge of the optical properties of the aerosol being measured, and solving the problem of relating optical measurements to aerodynamic behavior.

In studies of process streams, the particle concentration, size range, and composition may present experimental difficulties, as well as the corrosiveness and temperature of the gas.

This paper includes descriptions of particle measuring systems now in regular use in the U.S.A., and some prototype systems that have been recently developed for in situ applications.

SYSTEMS NOW IN REGULAR USE[1]

CASCADE IMPACTORS WITH PIEZOELECTRIC CRYSTAL SENSORS

Piezoelectricity is a property of certain crystals, such as quartz, which involves the production of an electrical charge on certain faces of the crystal when the crystal becomes mechanically stressed. The converse process also occurs; that is, a piezoelectric crystal becomes mechanically stressed where an electrical charge is placed on certain faces. This two-way capability is responsible for the ability of a piezoelectric crystal to cause an oscillating electric circuit to oscillate at the natural vibrational frequency of the crystal. When foreign material, such as aerosol particles, adheres to the surface of a vibrating piezoelectric crystal, the natural frequency of vibration of the crystal decreases. The magnitude of the frequency change is directly proportional to the mass of the added material.

Carpenter and Brenchly and Chuan have developed and tested multiple-stage cascade impactors with piezoelectric crystals on each stage to monitor the rate and amount of mass collected. Chuan's impactor is now sold commercially by Berkeley Controls, Inc. (2700 Du Pont Drive, Irvine, CA 92714). Chuan's impactor has ten stages, with the cut points reported to be from 0.05 to about 25 μm. Because of the extreme sensitivity of the instrument (and upper limit on mass accumulation), it is more suitable for ambient than stack work, where sample extraction and dilution would be required. The impactor must be disassembled, and each crystal cleaned before the limits of the linear range are reached. In a typical urban atmosphere, this limit is reached in about two hours. When interfaced with a programmable calculator, the system will print out the measured size distribution at chosen time intervals. The piezoelectric impactor is shown in Figure 1.

ELECTRICAL MOBILITY ANALYZER

Figure 2 illustrates the relationship between the diameter and electrical mobility of small aerosol particles. If particles larger than those of minimum mobility are removed from the sample, the remaining particles exhibit a monotonically

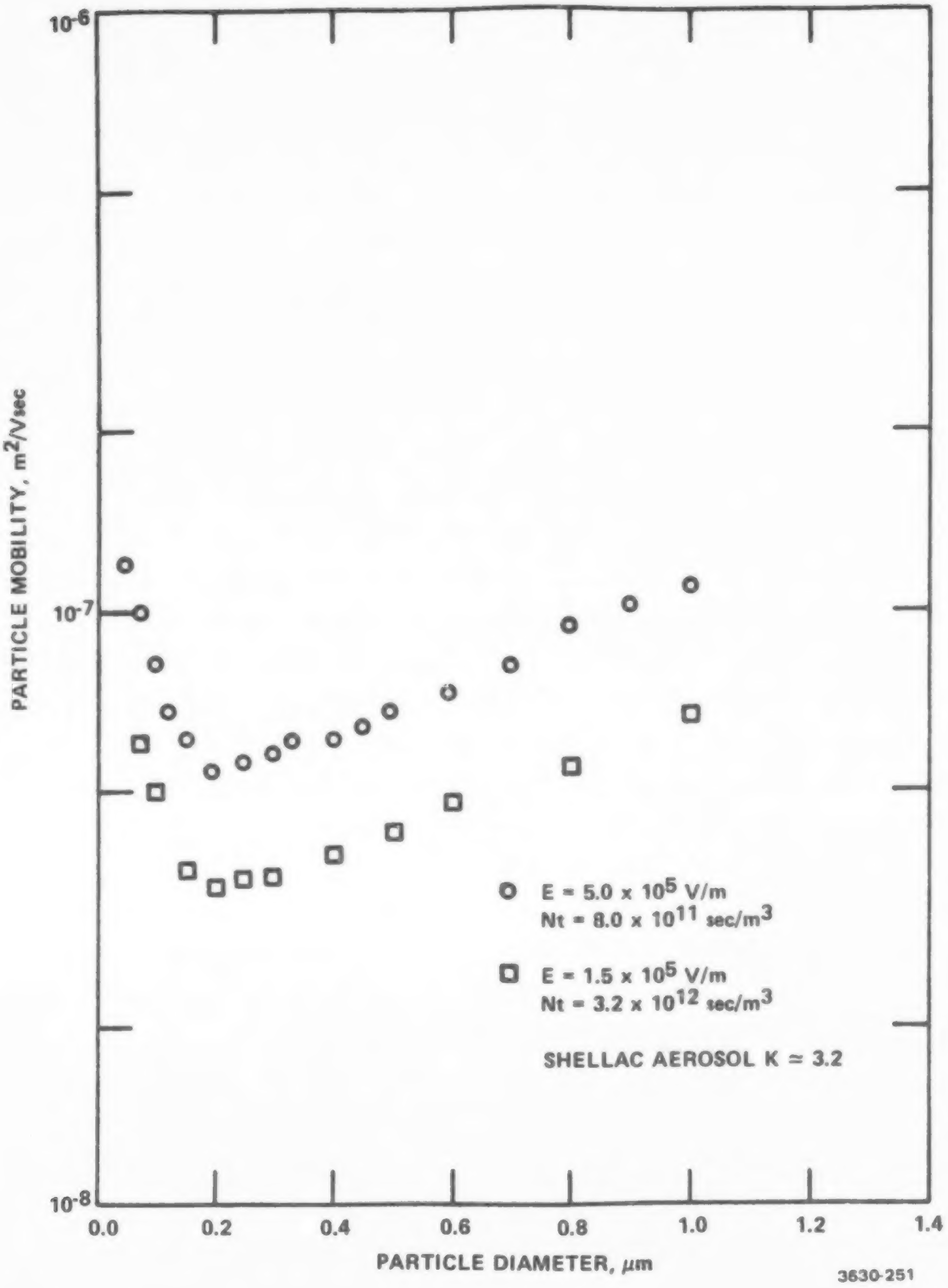

Figure 2. Particle mobility as a function of diameter for shellac aerosol particles charged in a positive ion field. K is the dielectric constant of the aerosol particles.

decreasing mobility with increasing diameter. Several aerosol spectrometers, or mobility analyzers, have been demonstrated that employ the diameter-mobility relationship to classify particles according to their size, and Figure 3 illustrates the principle on which these devices operate. Particles are charged under conditions of homogeneous electric field and ion concentration, and then passed into the spectrometer. Clean air flows down the length of the device and a transverse electric field is applied. From a knowledge of the system geometry and operating conditions, the mobility is derived for any position of deposition on the grounded electrode. The particle diameter is then readily calculated from a knowledge of the electric charge and mobility.

Difficulties with mobility analyzers are associated primarily with charging the particles to a known value with a minimum of loss by precipitation and obtaining accurate analyses of the quantity of particles in each size range. The latter may be done gravimetrically, optically, or electrically.

The concept described above has been used by Whitby, Liu, et al, at the University of Minnesota, to develop a series of models of the Electrical Aerosol Analyzer(EAA). A commercial version of the University of Minnesota devices is now marketed by Thermosystems, Inc., as the Model 3030 (Figure 4). The EAA is designed to measure the size distribution of particles in the range from 0.0032 to 1.0 μm diameter. The concentration range for best operation is 1 to 1000 $\mu g/m^3$, and thus dilution is required for most industrial gas aerosols.

The EAA is operated in the following manner. As a vacuum pump draws the aerosol through the analyzer (see Figure 4), a corona generated at a high voltage wire within the charging section gives the sample a positive electrical charge. The charged aerosol flows from the charger to the analyzer section as an annular cylinder of aerosol surrounding a cone of clean air. A metal rod, to which a variable, negative voltage can be applied, passes axially through the center of the analyzer tube. Particles smaller than a certain size (with highest electrical mobility) are drawn to the collecting rod when the voltage corresponding to that size is on the rod. Larger particles pass through the analyzer tube and are collected by a filter. The electrical charges on these particles drain off through an electrometer, giving a measure of current.

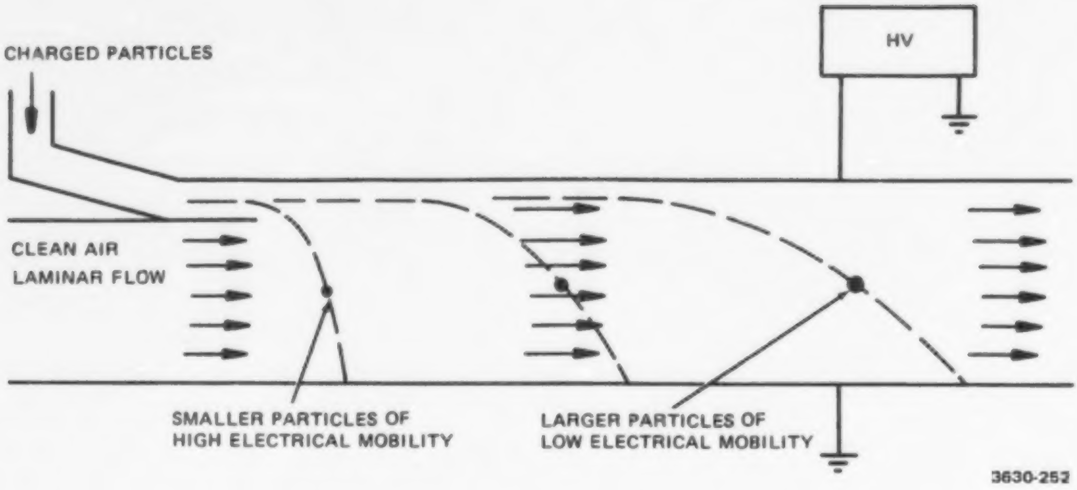
CHARGED PARTICLES
HV
CLEAN AIR
LAMINAR FLOW
SMALLER PARTICLES OF
HIGH ELECTRICAL MOBILITY
LARGER PARTICLES OF
LOW ELECTRICAL MOBILITY
3630-252

Figure 3. The electric mobility principle.

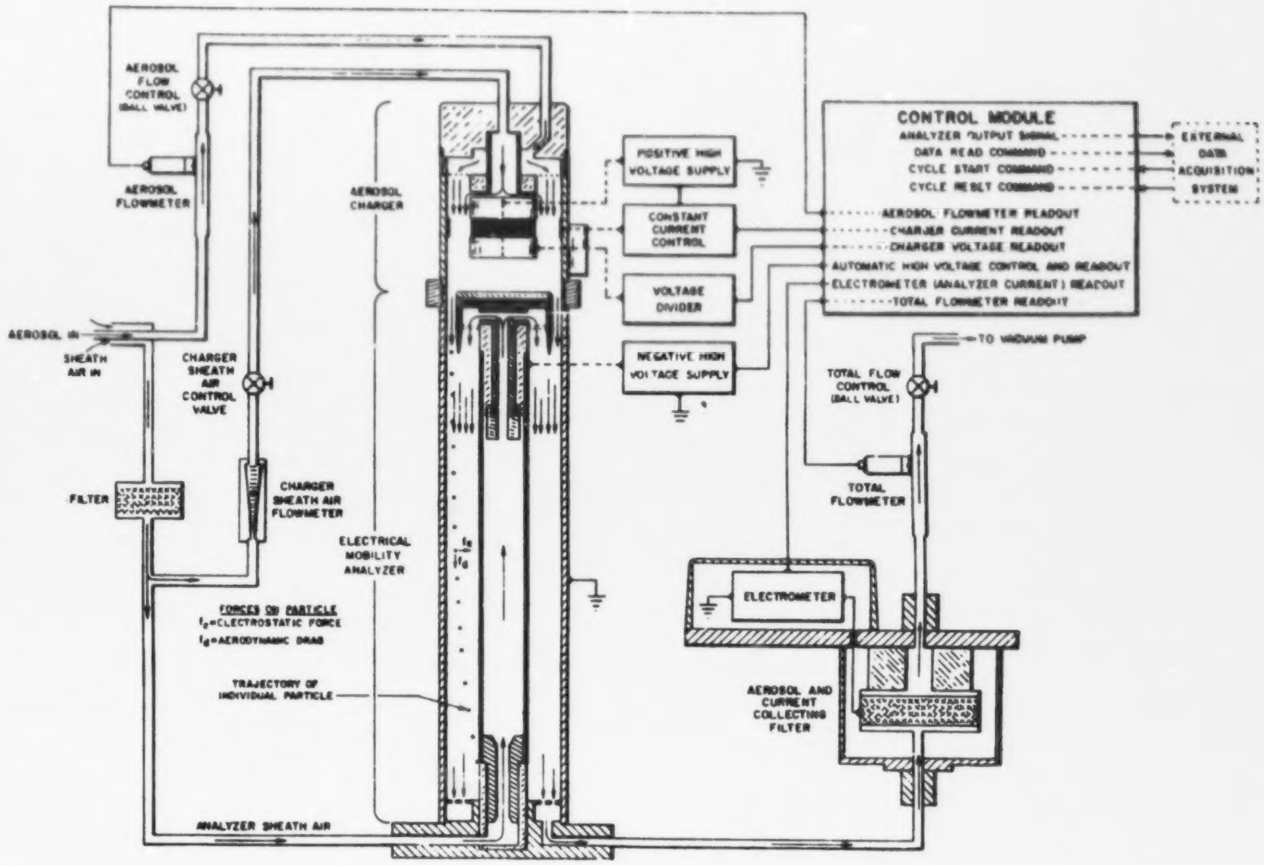
AEROSOL FLOW CONTROL (BALL VALVE)
AEROSOL FLOWMETER
AEROSOL IN
SHEATH AIR IN
CHARGER SHEATH AIR CONTROL VALVE
FILTER
CHARGER SHEATH AIR FLOWMETER
AEROSOL CHARGER
ELECTRICAL MOBILITY ANALYZER
FORCES ON PARTICLE
f_e=ELECTROSTATIC FORCE
f_d=AERODYNAMIC DRAG
TRAJECTORY OF INDIVIDUAL PARTICLE
ANALYZER SHEATH AIR
POSITIVE HIGH VOLTAGE SUPPLY
CONSTANT CURRENT CONTROL
VOLTAGE DIVIDER
NEGATIVE HIGH VOLTAGE SUPPLY
CONTROL MODULE
ANALYZER OUTPUT SIGNAL
DATA READ COMMAND
CYCLE START COMMAND
CYCLE RESET COMMAND
AEROSOL FLOWMETER READOUT
CHARGER CURRENT READOUT
CHARGER VOLTAGE READOUT
AUTOMATIC HIGH VOLTAGE CONTROL AND READOUT
ELECTROMETER (ANALYZER CURRENT) READOUT
TOTAL FLOWMETER READOUT
EXTERNAL DATA ACQUISITION SYSTEM
TO VACUUM PUMP
TOTAL FLOW CONTROL (BALL VALVE)
TOTAL FLOWMETER
ELECTROMETER
AEROSOL AND CURRENT COLLECTING FILTER

Figure 4. Flow schematic and electronic block diagram of the Electrical Aerosol Analyzer.

A step increase in rod voltage will cause particles of a larger size to be collected by the rod with a resulting decrease in electrometer current. This decrease in current is related to the additional number of particles being collected. A total of eleven voltage steps divide the 0.0032 to 1.0 micron size range of the instrument into ten equal logarithmic size intervals. Different size intervals can be programmed by means of an optional plug-in memory card.

The electrical aerosol analyzer can be operated either automatically or manually. In the automatic mode, the analyzer steps through the entire size range. For size and concentration monitoring over an extended period of time, the analyzer may be intermittently triggered by an external timer. The standard readout consists of a digital display within the control circuit module, although a chart recorder output is available. It is almost always advantageous to use a strip chart recorder to record the data. This allows the operator to identify a stable reading that may be superimposed on source variations and also gives a permanent record of the raw data. The EAA requires only two minutes to perform a complete size distribution analysis, which generally makes it advantageous to use, especially on stable sources.

OPTICAL PARTICLE COUNTERS

Figure 5 is a schematic diagram illustrating the principle of operation for optical particle counters. A dilute aerosol stream intersects the focus of a light beam to form an optical "view volume." The photodetector is located so that no light reaches its sensitive cathode except that scattered by particles in the view volume. Thus, each particle that scatters light with enough intensity will generate a current pulse at the photodetector, and the amplitude of the pulse can be related to the particle diameter. Optical particle counters yield real-time information on particle size and concentration.

In an optical particle counter, the intensity of the scattered light and the amplitude of the resulting current pulse depend on the viewing angle, particle refractive index, particle shape, and particle diameter. Different viewing angles and optical geometries are chosen to optimize some aspect of the

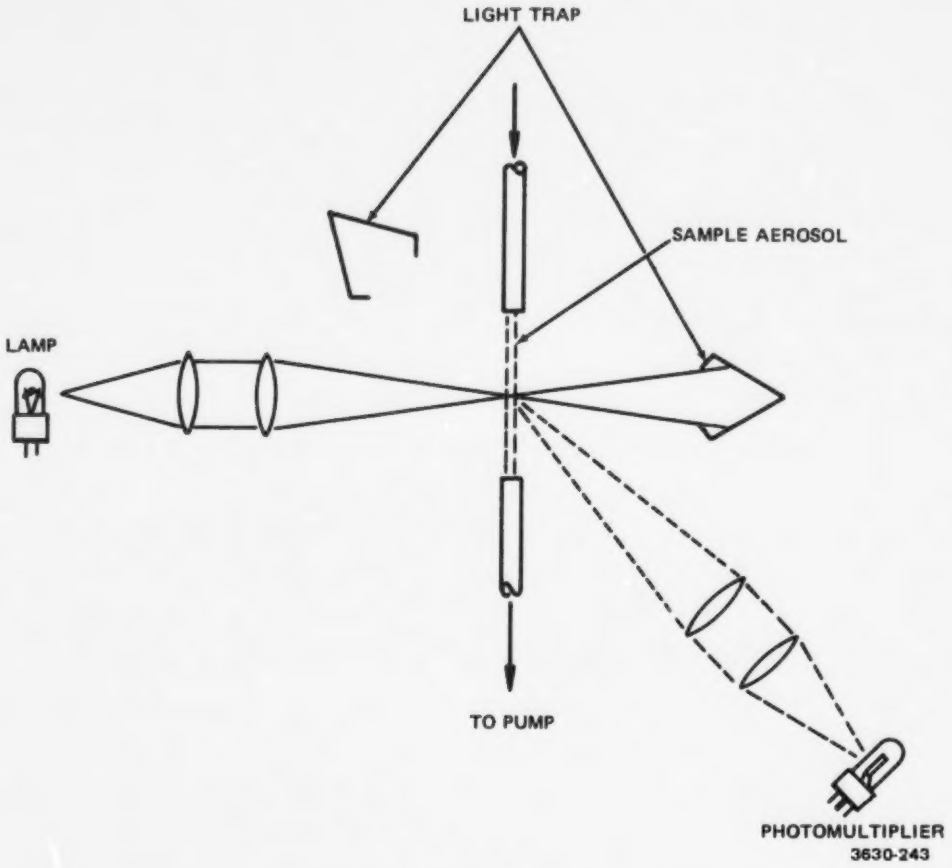
LIGHT TRAP
SAMPLE AEROSOL
LAMP
TO PUMP
PHOTOMULTIPLIER
3630-243

Figure 5. Schematic of an optical single particle counter.

counter performance. For example, the use of near forward scattering will minimize the dependence of the response on the particle refractive index, but with a severe loss of resolution near 1 μm diameter. The use of right angle scattering smooths out the response curve, but the intensity is more dependent on the particle refractive index.

Figure 6 illustrates some of the optical configurations that are found in commercial particle counters. The pertinent geometric and operating constants of the counters are summarized in Table 1.

The commercial optical counters that are available now were designed for laboratory work and have concentration limits of a few hundred particles per cubic centimeter. The lower size limit is nominally about 0.3 μm diameter. For use in studies of industrial aerosols, dilution of the sample is required and the useful upper limit in particle size has been limited by losses in the dilution system to about 2.0 μm diameter. In addition, the particle diameter that is measured is not aerodynamic, and some assumptions must be made in order to compare optical with aerodynamic data. However, it is possible to "calibrate" an optical counter, on a particulate source, to yield aerodynamic data. This is done by using special calibration impactors, or settling chambers.

DIFFUSION BATTERIES WITH CONDENSATION NUCLEI COUNTERS

Diffusion batteries with condensation nuclei counters have been standard equipment for measuring the size distribution of submicrometer particles for many years. Data acquisition with these systems, however, has been tedious and time consuming. Recently, Knutson and Sinclair developed and demonstrated an automatic diffusional sizing system.[2] Figure 7 shows their system. The aerosol is drawn through a 60ℓ tank to damp short-term fluctuations and into the miniature, screen-type diffusion battery. A motor driven valve having 15 ports is used to switch from port to port on the diffusion battery and to sample filtered air. The aerosol concentration at the inlet and outlet of the diffusion battery is measured using a continuous-flow condensation nuclei counter which has alcohol as a working fluid. The data are recorded on punched tape for later analysis by computer. Knutson and Sinclair's system has been

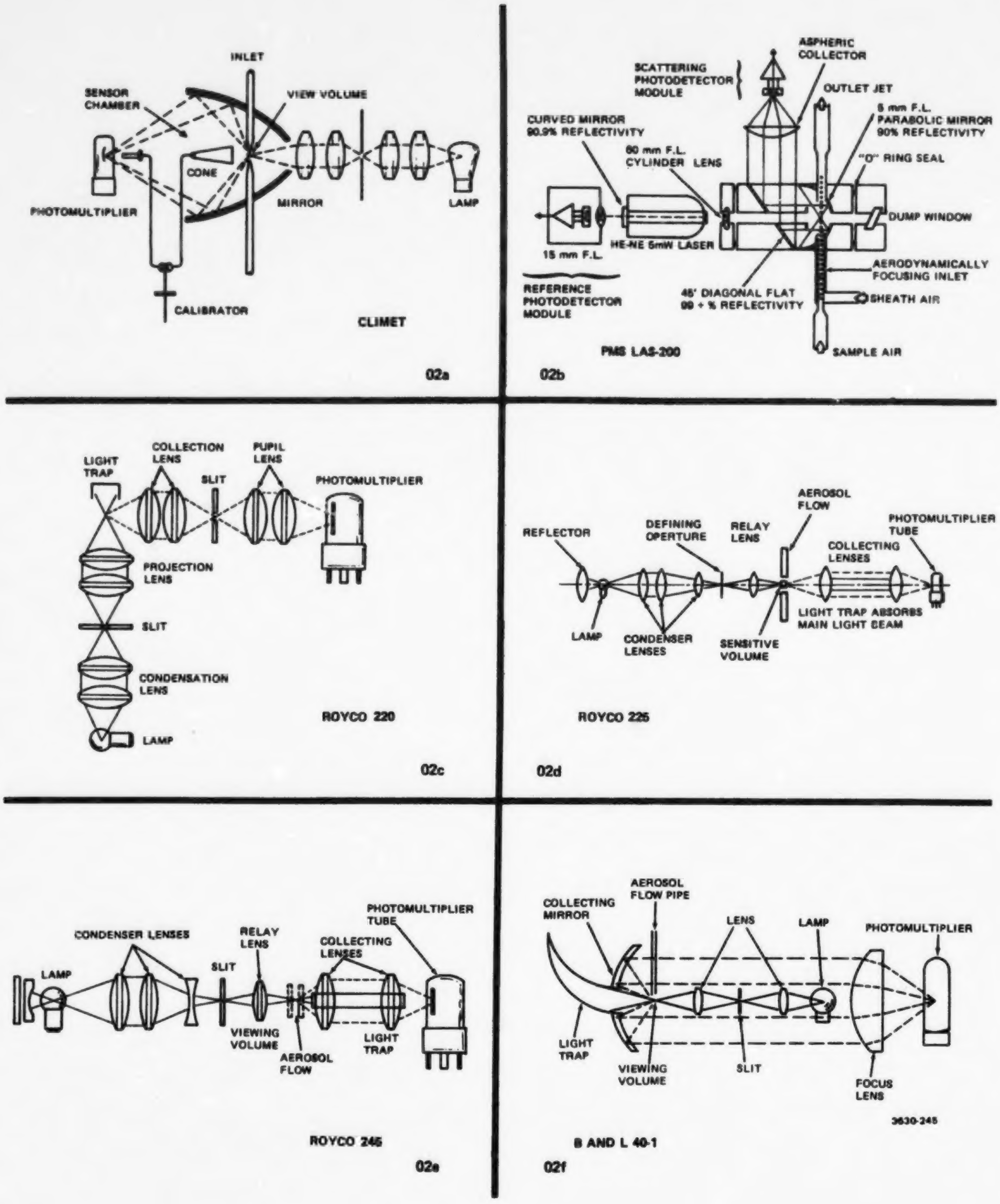
INLET
SENSOR CHAMBER
VIEW VOLUME
CONE
PHOTOMULTIPLIER
MIRROR
LAMP
CALIBRATOR
CLIMET
02a
ASPHERIC COLLECTOR
SCATTERING PHOTODETECTOR MODULE
OUTLET JET
CURVED MIRROR 90.9% REFLECTIVITY
8 mm F.L. PARABOLIC MIRROR 90% REFLECTIVITY
60 mm F.L. CYLINDER LENS
"O" RING SEAL
DUMP WINDOW
HE-NE 5mW LASER
15 mm F.L.
AERODYNAMICALLY FOCUSING INLET
REFERENCE PHOTODETECTOR MODULE
45° DIAGONAL FLAT 99 + % REFLECTIVITY
SHEATH AIR
PMS LAS-200
SAMPLE AIR
02b
LIGHT TRAP
COLLECTION LENS
SLIT
PUPIL LENS
PHOTOMULTIPLIER
PROJECTION LENS
SLIT
CONDENSATION LENS
LAMP
ROYCO 220
02c
AEROSOL FLOW
REFLECTOR
DEFINING OPERTURE
RELAY LENS
PHOTOMULTIPLIER TUBE
COLLECTING LENSES
LIGHT TRAP ABSORBS MAIN LIGHT BEAM
LAMP
CONDENSER LENSES
SENSITIVE VOLUME
ROYCO 225
02d
PHOTOMULTIPLIER TUBE
CONDENSER LENSES
RELAY LENS
COLLECTING LENSES
LAMP
SLIT
VIEWING VOLUME
AEROSOL FLOW
LIGHT TRAP
ROYCO 245
02e
AEROSOL FLOW PIPE
COLLECTING MIRROR
LENS
LAMP
PHOTOMULTIPLIER
LIGHT TRAP
VIEWING VOLUME
SLIT
FOCUS LENS
3630-245
B AND L 40-1
02f

Figure 6. Optical configurations for six commercial particle counters.

TABLE 1.
CHARACTERISTICS OF COMMERCIAL, OPTICAL, PARTICLE COUNTERS

	Illuminating Cone Half Angle, γ	Light Trap Half Angle, α	Collecting Aperture Half Angle, β	Inclination Between Illuminating And Collecting Cone Axis, ψ	Viewing Volume	Sampling Rate
Bausch & Lomb Model 40-1 820 Linden Avel Rochester, NY 14625	13°	33°	53°	0°	0.5 mm^3	170 cm^3/min
Climet Models 201, 208 Climet Inst. Co. 1620 W. Colton Ave. Redlands, CA 92373	15	35	90	0	0.5	7,080
Climet Model 150	12	18	28	0	0.4	472
Royco Model 218 Royco Inst. 41 Jefferson Dr. Menlo Park, CA 94025	5	11	30	0	0.25	283
Royco Model 220	24	-	24	90	2.63	2,830
Royco Model 245	5	16	25	0	4.0	28,300
Royco Model 225	5	7	25	0	2.0	283 or 2,830
Tech Ecology Model 200 Tech Ecology, Inc. 645 N. Mary Ave. Sunnyvalle, CA 94086	5	8	20	0	0.46	283
Tech Ecology Model 208	5	10	20	0	2.5	2,830
Particle Measurement Systems *Model LAS-200 Particle Measuring Systems 1855 S. 57th Ct. Boulder, CO 80301	0.5	35	120	0	0.003	120 or 1,200

*632.8 mm laser illum., all others are white light.

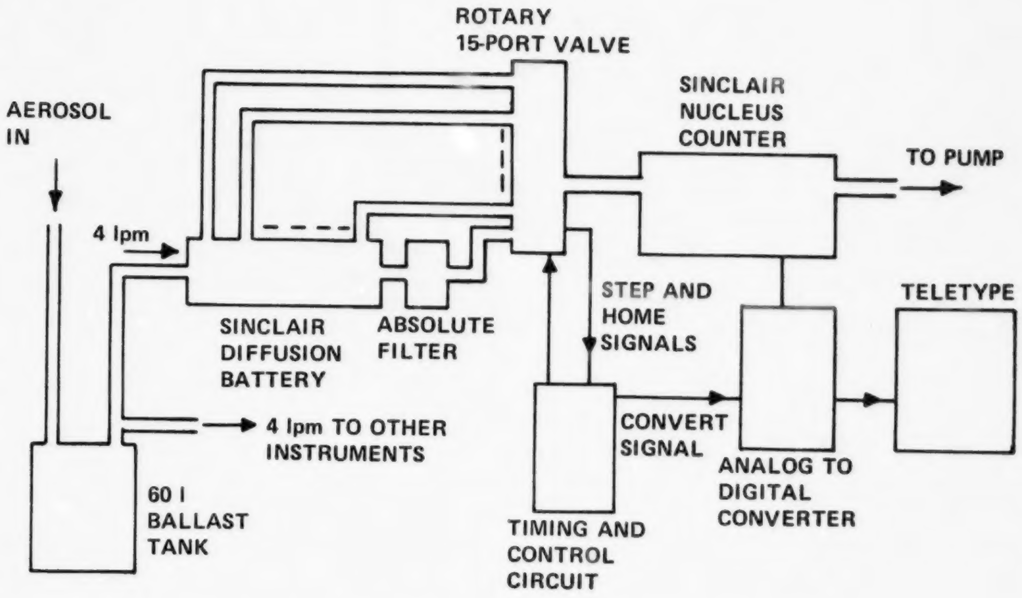
ROTARY
15-PORT VALVE
AEROSOL
IN
SINCLAIR
NUCLEUS
COUNTER
TO PUMP
4 lpm
STEP AND
HOME
SIGNALS
TELETYPE
SINCLAIR
DIFFUSION
BATTERY
ABSOLUTE
FILTER
4 lpm TO OTHER
INSTRUMENTS
CONVERT
SIGNAL
60 l
BALLAST
TANK
ANALOG TO
DIGITAL
CONVERTER
TIMING AND
CONTROL
CIRCUIT

Figure 7. Block Diagram of aerosol measurement system.

used to obtain over 1000 size spectra of urban aerosols. The diffusion battery and rotary switch are now sold commercially by Thermo-Systems, Inc., St. Paul, Minnesota.

SAMPLE EXTRACTION-DILUTION SYSTEMS FOR PROCESS STREAMS

The majority of instruments and systems for measuring particle-size distributions are designed to measure aerosols at conditions near ambient air with respect to temperature, gas composition, and pressure. Furthermore, the instruments are limited to aerosol concentrations much lower than those typically found in process streams. Therefore, some means of extracting samples, conditioning them, and diluting them, is required for measurements in process streams.

Figure 8 shows one sample extraction-dilution system (SEDS) that has been used by Ensor to measure aerosol properties in process streams.[4] It uses an in-stack impactor to remove particles larger than about 2.7 μm and a diffusional dryer for removing moisture, before the sample enters the dilution system. Dilution is done by a three-stage process employing venturi flow meters to measure the sample flowrate and orifice meters to measure the flowrate of the dilution air. Flow control is accomplished by manipulating the dilution air control valves. The dilution can be adjusted from a factor of 20:1 to 1000:1. Particle sizing can be done using the electrical aerosol analyzer or diffusional systems.

Figure 9 is a block diagram of the sample extraction-dilution system developed by Southern Research Institute.[3] The sample is removed from the flue by means of a heated probe which is connected to an oven by means of a heated, flexible hose. In the oven the sample gas flows through a cyclone, an orifice for metering sample flow, and an optional SO_x absorber assembly. Charge neutralization is done in the cone of the diluter by two 500 μc polonium-210 strips mounted as shown.

The sample gas enters the dilution chamber at the apex of a perforated cone into which clean, dry air is pumped through the perforations, creating a highly turbulent mixing zone. At a downstream point after adequate mixing

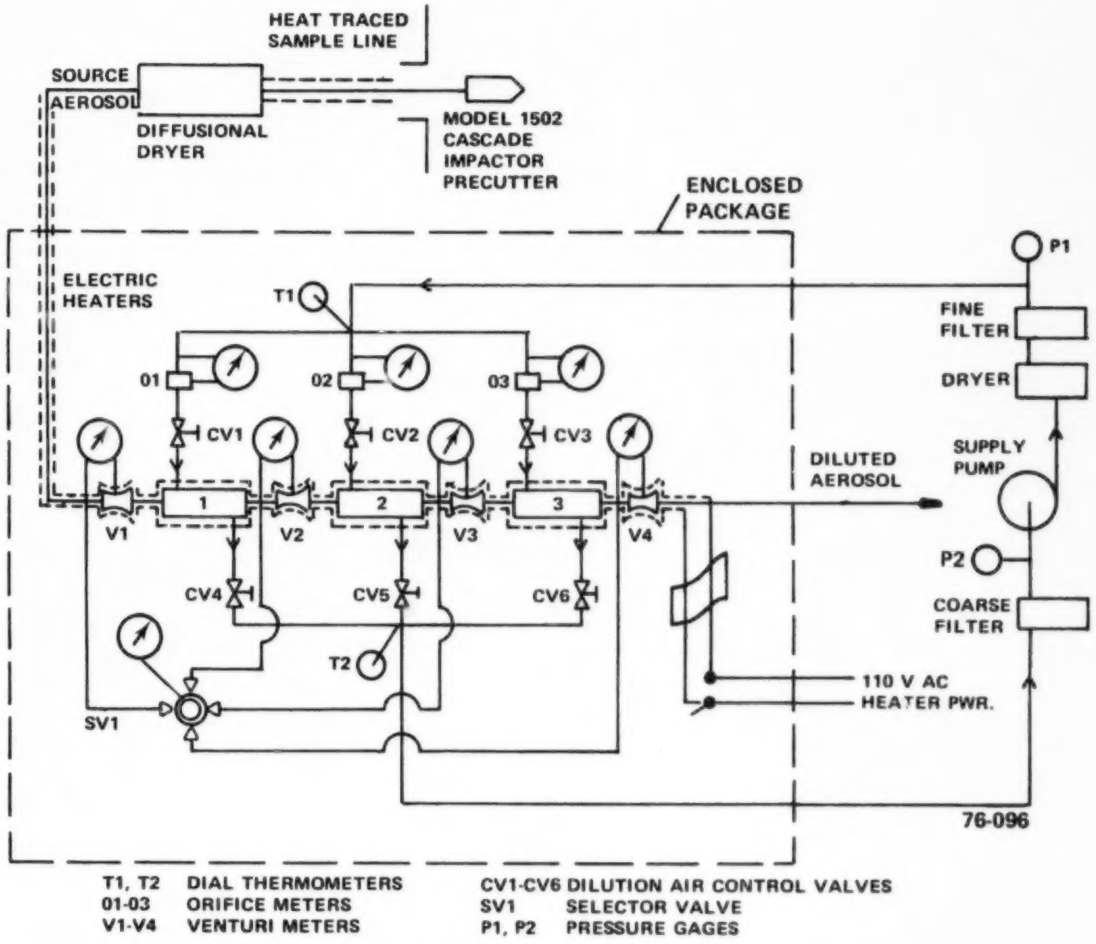
HEAT TRACED SAMPLE LINE
SOURCE AEROSOL
DIFFUSIONAL DRYER
MODEL 1502 CASCADE IMPACTOR PRECUTTER
ENCLOSED PACKAGE
ELECTRIC HEATERS
T1
01
02
03
CV1
CV2
CV3
1
2
3
V1
V2
V3
V4
CV4
CV5
CV6
T2
SV1
DILUTED AEROSOL
P1
FINE FILTER
DRYER
SUPPLY PUMP
P2
COARSE FILTER
110 V AC
HEATER PWR.
76-096
T1, T2 DIAL THERMOMETERS
01-03 ORIFICE METERS
V1-V4 VENTURI METERS
CV1-CV6 DILUTION AIR CONTROL VALVES
SV1 SELECTOR VALVE
P1, P2 PRESSURE GAGES

Figure 8. Meterology Research, Inc. - SEDS.[4]

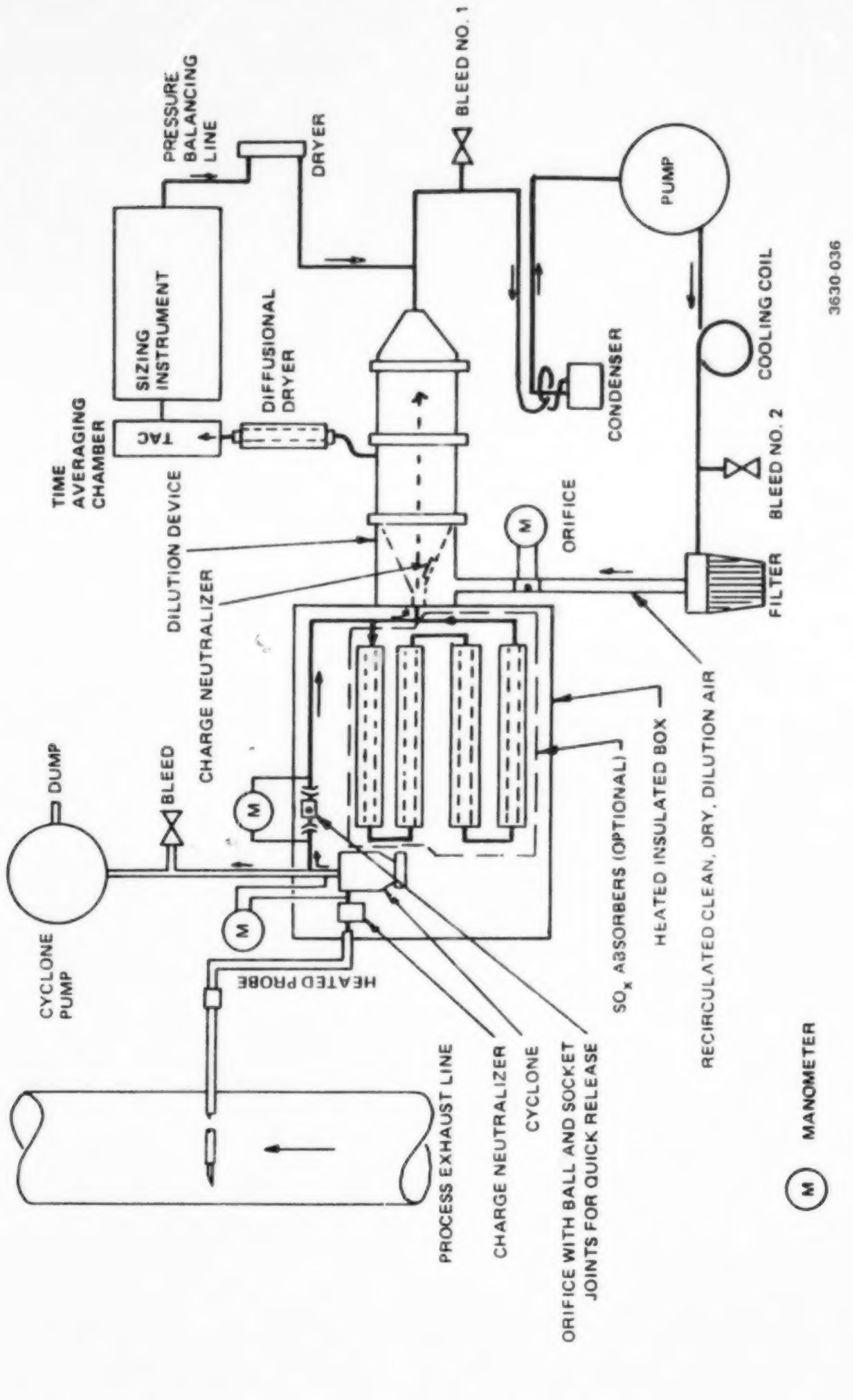
PROCESS EXHAUST LINE
CHARGE NEUTRALIZER
CYCLONE
ORIFICE WITH BALL AND SOCKET JOINTS FOR QUICK RELEASE
HEATED PROBE
CYCLONE PUMP
DUMP
BLEED
M
M
CHARGE NEUTRALIZER
DILUTION DEVICE
TIME AVERAGING CHAMBER
TAC
SIZING INSTRUMENT
DIFFUSIONAL DRYER
PRESSURE BALANCING LINE
DRYER
BLEED NO. 1
PUMP
CONDENSER
COOLING COIL
BLEED NO. 2
M
ORIFICE
FILTER
SO$_x$ ABSORBERS (OPTIONAL)
HEATED INSULATED BOX
RECIRCULATED CLEAN, DRY, DILUTION AIR
M MANOMETER
3630-036

Figure 9. Southern Research Institute SEDS.

has occurred, the dilution sample is extracted and conveyed to the sizing instrument. The diluted sample passes through a diffusional dryer where any remaining moisture is removed. The major drying action is accomplished by using dilution air which has been passed through an ice bath condenser. The sample then passes through an optional time averaging chamber and into the sizing instrument. The instrument exhaust lines are returned to the diluter to maintain a minimal pressure change across the instruments. Further drying of this recycled air is accomplished by passing this instrument exhaust gas through an absorption dryer.

Changing the sample air flow and the dilution air flow causes changes in the dilution ratio. Sample air and dilution air flowrates are controlled by two bleed valves on the dilution air pump, one upstream of the pump (#1) and one downstream (#2). Manipulation of these valves changes the internal pressure of the diluter which, in turn, sets the sampling rate. As the pressure in the diluter is reduced, the sample flowrate is increased.

In practice, the operation of these valves changes the dilution air flow only slightly (approximately ±10%) for a many-fold change in sample flow, or backflush condition, to the maximum flow value attainable with any particular sample metering orifice.

Particle sizing is done using optical particle counters, the electrical aerosol analyzer, and diffusional systems.

NEW SYSTEMS FOR AUTOMATIC PARTICLE SIZING

A variety of new systems has been developed for particle sizing work, some for in situ applications to process streams. Most of the systems employ light scattering from particles as their basic analytic principle. In this section some of the new instruments are described. None of the units described here are in widespread commercial use, and their performance may not have been fully evaluated.

INTENSITY RATIO AT TWO ANGLES

Hodkinson[5] was the first to point out that the ratio of the light intensity scattered by particles into two small angles is relatively insensitive to the particles' index of refraction.

Shofner et al,[6] Gravatt[7] and Chan[8] have developed prototype systems for particle sizing which are based on the intensity ratio concept of Hodkinson. Figure 10 is a schematic of Shofner's system which is called the "PILLS-IV". The intensities of the scattered light puses at the angles θ_1 and θ_2 are normalized to the reference pulse at $\theta = 0$ for synchronization and to account for fluctuations in intensity of the laser source. The optics and sensors are kept clean and cool by the use of a purge air system.

The laser used in this system is a semiconductor junction diode ($\lambda = 0.9\ \mu m$). The useful size range for particle sizing is from 0.2 to 3.0 µm although the ratio analysis is abandoned at radii less than 0.7 µm and the magnitude of scattered intensity is employed. Shofner states that the view volume of his system is approximately $2 \times 10^{-7}\ cm^3$. The upper concentration limit for single particle counters is determined by the requirement that the probability of more than one particle appearing in the view volume of a given time be much less than unity. For Shofner's system this would set the concentration limit at approximately 10^6 particles/cm^3, a value much higher than for conventional single particle counters.

Kuykendal[9] and Farthing[10] have done tests to evaluate the performance of the PILLS IV and compared its response to other instruments. The results of these tests indicate that further refinement will be required to achieve an acceptable level of accuracy.

OPEN CAVITY LASER

An optical particle sizing device developed by R. G. Knollenberg[11, 12] for atmospheric application might be applicable to industrial emission measurements. The device is, in some respects, similar to conventional near forward scattering optical single particle counters except that the sensing zone is

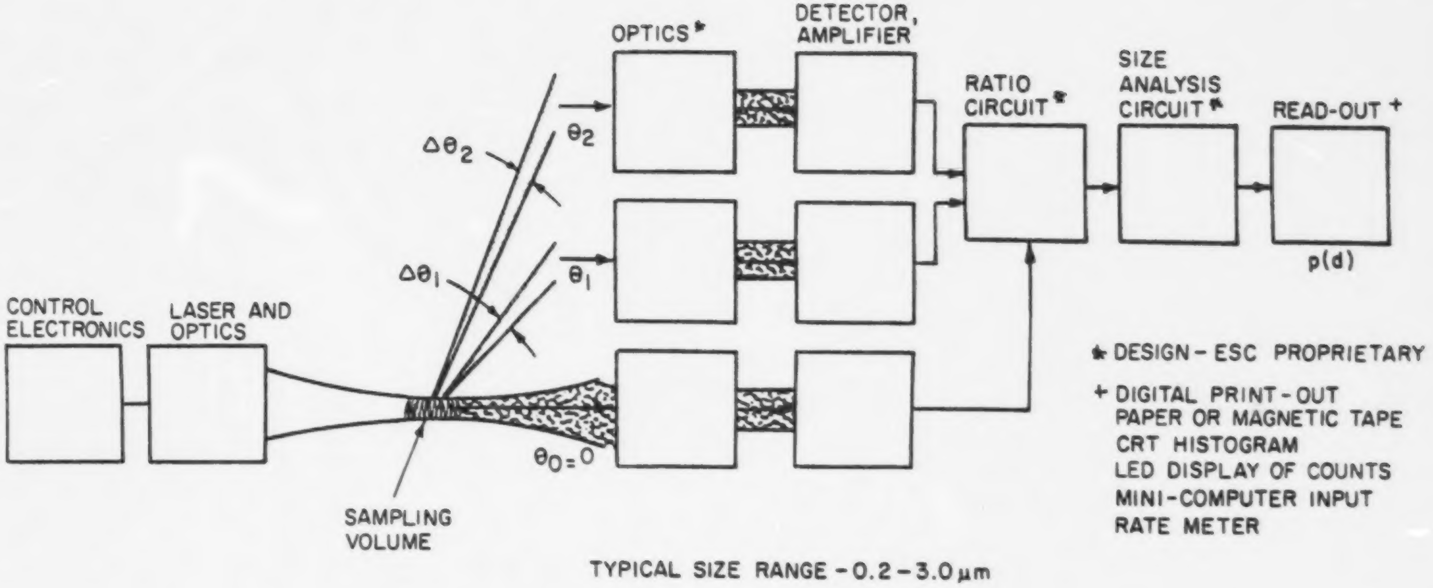
OPTICS *
DETECTOR, AMPLIFIER
RATIO CIRCUIT *
SIZE ANALYSIS CIRCUIT *
READ-OUT +
$\Delta\theta_2$
θ_2
$\Delta\theta_1$
θ_1
p(d)
CONTROL ELECTRONICS
LASER AND OPTICS
$\theta_0 = 0$
SAMPLING VOLUME
* DESIGN - ESC PROPRIETARY
+ DIGITAL PRINT-OUT
PAPER OR MAGNETIC TAPE
CRT HISTOGRAM
LED DISPLAY OF COUNTS
MINI-COMPUTER INPUT
RATE METER
TYPICAL SIZE RANGE - 0.2 - 3.0 μm

Figure 10. The PILLS IV optical Particle counter. After Shofner.[6]

contained within an open cavity laser as illustrated in Figure 11. This configuration results in very high illumination levels, permitting the detection of particles smaller than those sized by most light-scattering instruments and has been used in vacuum applications for sizing particles in the range from 0.1 to 30 μm.

An interesting characteristic of laser cavity scattering is the fact that the particle or particles in the beam effects the power incident upon it. This is due to the detuning effect of the laser because of the particles' presence, which is a function of the particle size. However, the scattering is normalized with the reference detector signal which is proportional to the actual intensity incident upon a particle. As with other particle counters which determine from the magnitude of scattered power, the inferred particle size from a measurement depends upon the refractive index.

The open cavity laser spectrometer is available commercially from Particle Measurement Systems, Boulder, Colorado.

SCATTERING AT FORWARD ANGLES FROM A COLLECTION OF PARTICLES

If a sufficient number of moments of the size distribution can be obtained, measurements of optical parameters of a collection of particles are, of course, more desirable than sequential single particle analysis. The latter is usually more restricted by concentration and particle size limits and more complicated mechanically.

Wertheimer and Wilcock[13] developed an approximate technique based upon diffraction theory to determine the second, third, and fourth moments of the size distribution. The technique utilizes three masks of different shapes to spatially filter the detected signal. The optical system is shown in Figure 12 and the three masks in Figure 13. With the a^2 mask the detected signal from a single particle is proportional to the second power of the particle radius. Similarly with the $a^3(a^4)$ mask the detected signal is proportional to the thrid (fourth) power of $\underline{a}$. For many such particles in the field of view of the detector then the three detected signals are proportional

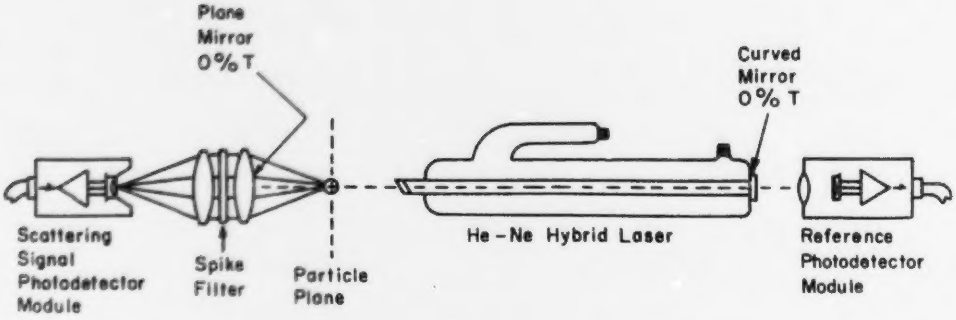
Plane
Mirror
0% T
Curved
Mirror
0% T
Scattering
Signal
Photodetector
Module
Spike
Filter
Particle
Plane
He - Ne Hybrid Laser
Reference
Photodetector
Module

Note: Mirrors are reversed for large particle size ranges.

Figure 11. Schematic of open cavity laser active scattering particle counter. After Knollenberg.[11]

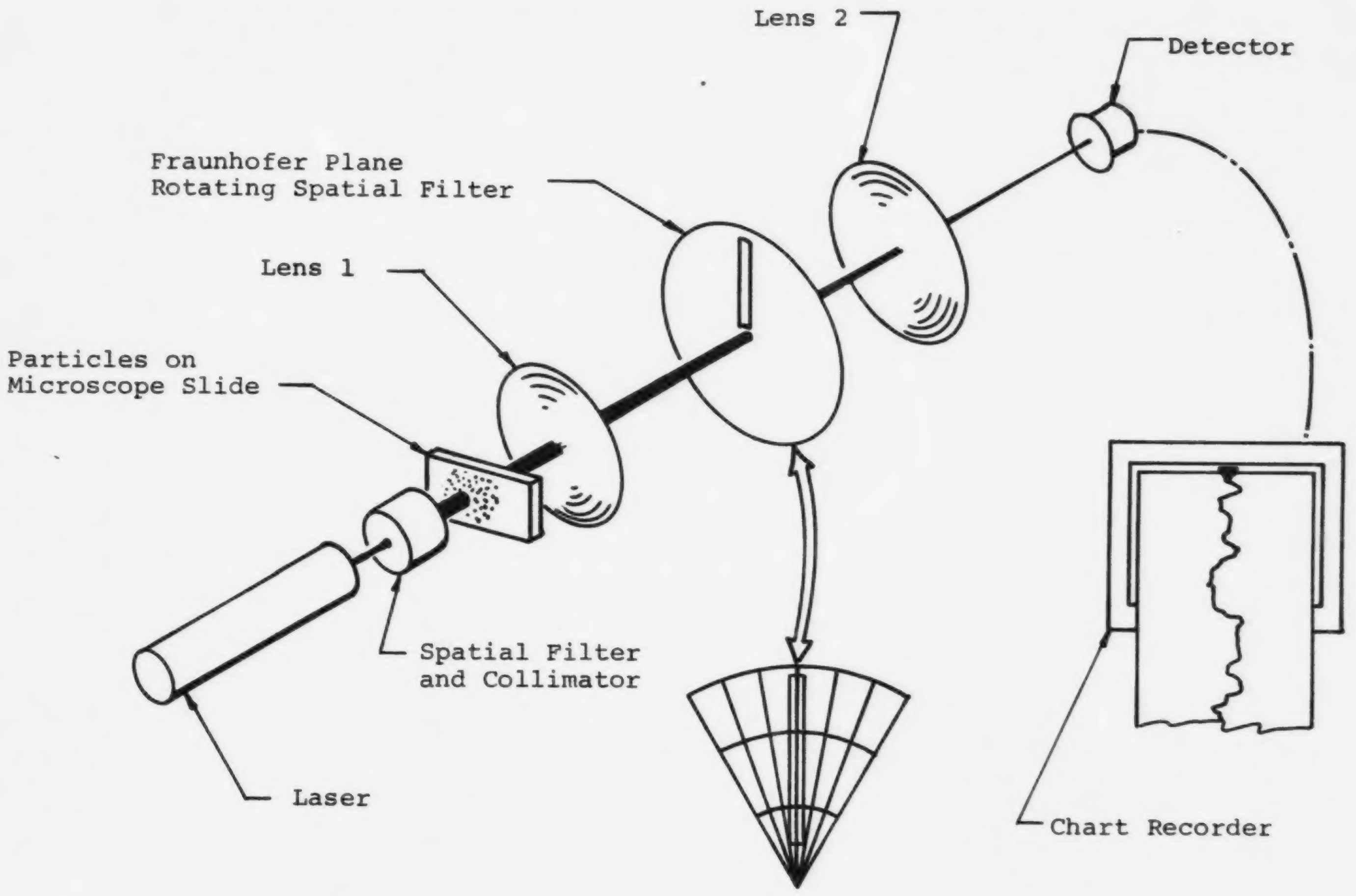
Lens 2
Detector
Fraunhofer Plane
Rotating Spatial Filter
Lens 1
Particles on
Microscope Slide
Spatial Filter
and Collimator
Laser
Chart Recorder

Figure 12. Optical system used to verify the response of the Fraunhofer plate filter. (After Wertheimer and Wilcock.[13])

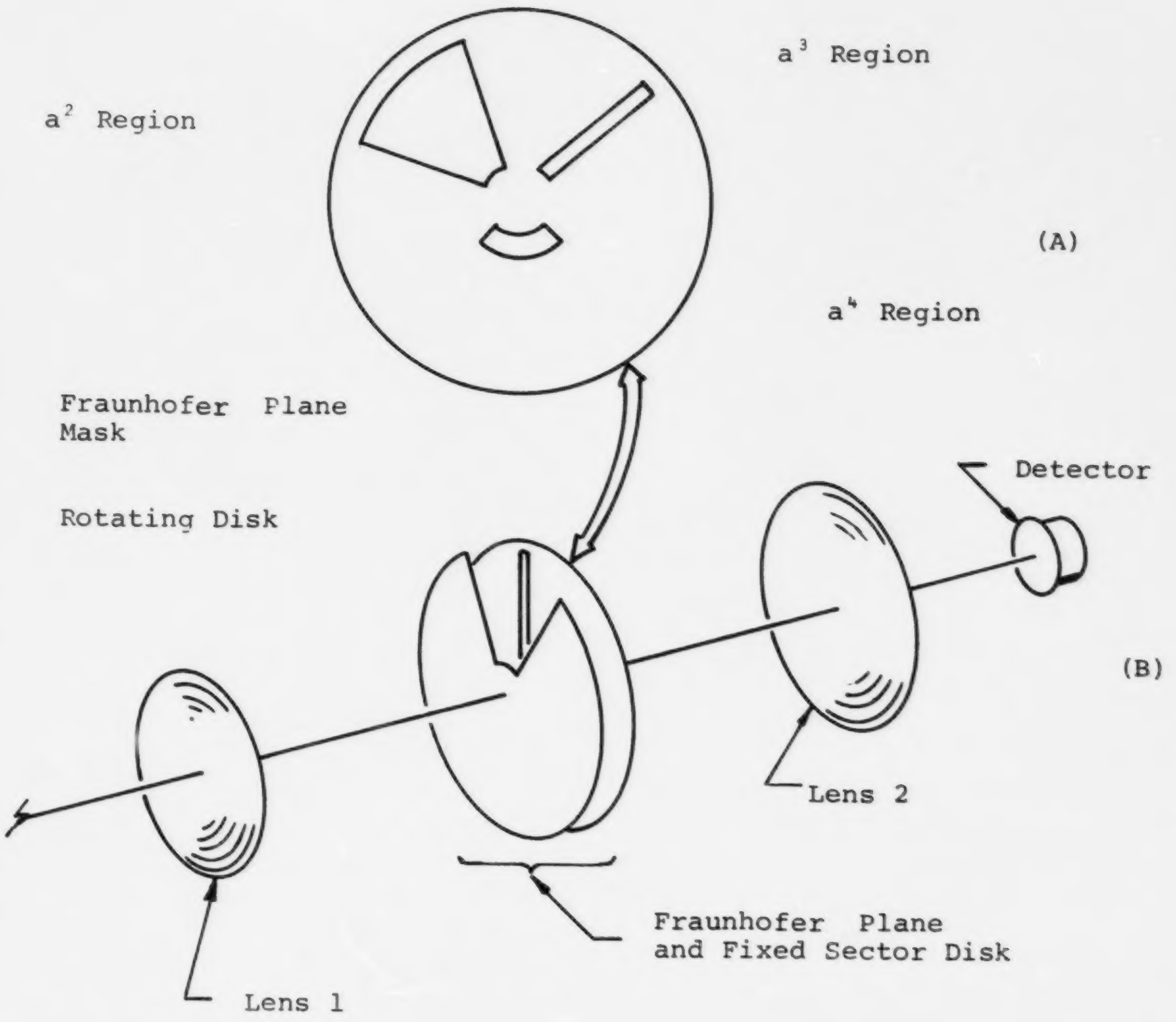
a^2 Region
a^3 Region
(A)
a^4 Region
Fraunhofer Plane Mask
Rotating Disk
Detector
(B)
Lens 2
Fraunhofer Plane and Fixed Sector Disk
Lens 1

Figure 13. (A) Schematic diagram of Fraunhofer plane mask with three response regions. (B) Instrument configuration for the three region mask. (After Wertheimer and Wilcock.[13])

to the second, third, and fourth moments of the distribution. These signals give the volume mean radius, the area mean radius, and the standard deviation of the area distribution.

The authors of this technique demonstrated its usefulness using particles from 4 to 83 μm in diameter. Since then the method has been incorporated into a commercial sizing system still being evaluated. From consideration of the principle upon which this method is based, it is sensitive to refractive index to the same degree as forward-scatter particle counters.

Figure 14 illustrates an optical particle counter that has been designed by R. Knollenberg for real-time, in situ particle sizing in process streams.[2] The instrument covers a particle size range of 0.3 to 10 μm with 60 channels of resolution. The counter uses small angle light scattering, and the uncertainty in sizing spherical particles is due to variations in the detected particle's index of refraction. Sizing errors of ±20% are possible, with ±10% expected to be more common. The concentration range for accurate measurements limited by coincidence counting is 5×10^4 particles/cm^3. The main effect of higher concentrations is said to be a decrease in the effective sizing range. An optical velocimeter is also included in the design. The prototype design allows temperatures up to 250°C and gas velocities to 30m/sec. The results of an initial in situ test at a coal-fired power plant were reasonable. The opacity calculated from the measured particle-size distribution was about 15%, while the measured opacity was 17%. The calculated mass loading was 0.01 to 0.02 g/m^3 with a volume median diameter of 1.3 μm.

Wertheimer et al[13] are developing another portable light scattering instrument for in situ particle sizing. This device measures the flux scattered from an ensemble of particles at three small angles relative to the forward direction, 4°, 8°, and 11°, and between 80°-100°. Each measurement is performed at two wavelengths, 0.45 and 0.9 μm, and the large angle scattering is measured at two orthogonal polarizations. The instrument relates the small angle signals dominated by Fraunhofer diffraction to the volume of particles in three size ranges, centered at 1.0, 3.5, and 7.0 μm. For the lower end of the size distribution, the differences in the two 90° signals, at two orthogonal polarizations, obtained with the 0.9 and 0.45 μm wavelengths

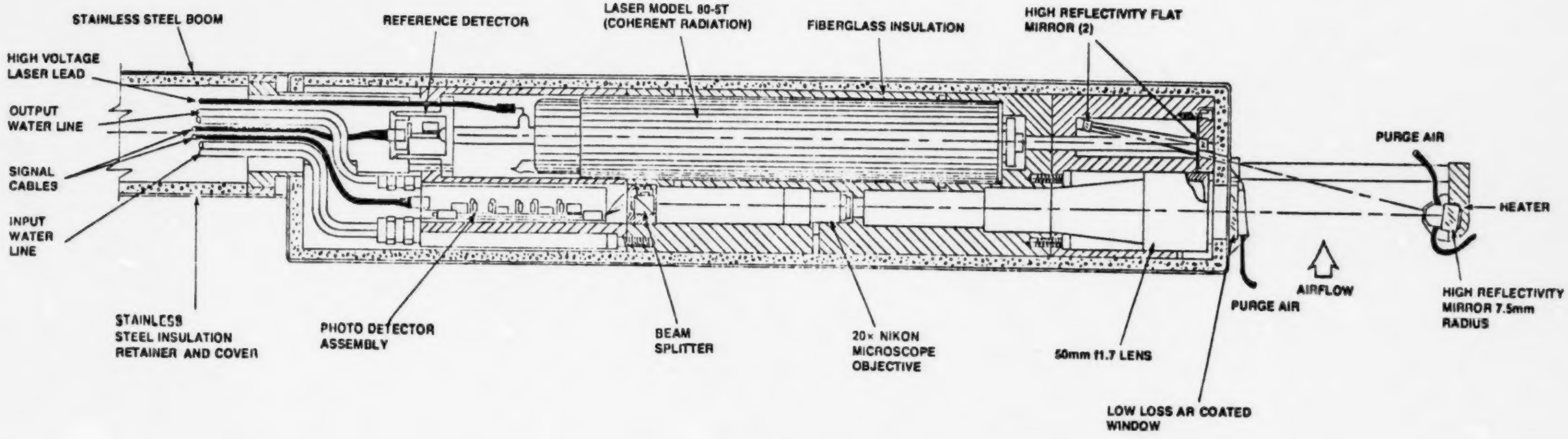
STAINLESS STEEL BOOM
REFERENCE DETECTOR
LASER MODEL 80-5T (COHERENT RADIATION)
FIBERGLASS INSULATION
HIGH REFLECTIVITY FLAT MIRROR (2)
HIGH VOLTAGE LASER LEAD
OUTPUT WATER LINE
SIGNAL CABLES
INPUT WATER LINE
PURGE AIR
HEATER
AIRFLOW
PURGE AIR
HIGH REFLECTIVITY MIRROR 7.5mm RADIUS
STAINLESS STEEL INSULATION RETAINER AND COVER
PHOTO DETECTOR ASSEMBLY
BEAM SPLITTER
20× NIKON MICROSCOPE OBJECTIVE
50mm f1.7 LENS
LOW LOSS AR COATED WINDOW

Figure 14. Sketch of the Knollenberg, in situ particle counter.

is related to the volume of particles in a size range centered about 0.4 μm and 0.2 μm, respectively. The size range, mass loading, and temperature ranges are 0.1 to 10 μm, 4 to 400 ppb by volume, and 0° to 260°C.

These principles have been incorporated into a prototype, portable stack monitor. The probe is 1.5 meter long and 9 cm in diameter, optical signals are carried through fiber optics cables contained in the probe. An arc source and silica photodetectors are outside the stack at the end of the probe, while a digital microprocessor is used to analyze the data. The microprocessor, air purge system, lamp power supply, and printer are housed separately from the probe.

Theoretical and experimental programs are continuing to investigate various approaches to using light scattering as an analytical tool for particle-size analysis. As progress is made it is anticipated that the data can be acquired and reduced more conveniently, quickly, and accurately.

REFERENCES

1. Smith, W. B., P. R. Cavanaugh, and R. R. Wilson
Technical Manual: A Survey of Equipment and Methods for Particulate Sampling in Industrial Process Streams.
Southern Research Institute, EPA, Research Triangle Park, NC, 1978. 281 pp.
EPA-600/7-78-043

2. Smith, W. B., Editor
Proceedings: Advances in Particle Sampling and Measurement.
Southern Research Institute, held in Asheville, NC, 1978. 1979, 389 pp.
EPA-600/7-79-065

3. Ragland, J. R., J. D. McCain, and W. B. Smith
Design, Construct, and Test a Field Usable, Prototype System for Sizing Particles Smaller than 0.5 Micrometers Diameter.
Southern Research Institute, EPA, Research Triangle Park, NC, 1978. 320 pp.

4. Ensor, D. S., R. G. Hooper, and R. W. Scheck
Determination of the Fractional Efficiency, Opacity Characteristics Engineering and Economic Aspects of a Fabric Filter Operating on a Utility Boiler.
EPRI-FP-297, Electric Power Research Institute, Palo Alto, Calif., 1976. 220 pp.

5. Hodkinson, J. R.
The Optical Measurement of Aerosols.
Aero. Sci., pp. 287-357, 1966.

6. Shofner, F. M., G. Kreikebaum, H. W. Schmitt, and B. E. Barnhart
In Situ, Continuous Measurement of Particle Size Distribution and Mass Concentration using Electro-Optical Instrumentation.
Presented at the 5th Annual Industrial Air Pollution Control Conference, Knoxville, TN, April, 1975.

7. Gravatt, C. C.
Real Time Measurement of the Size Distribution of Particulate Matter by a Light Scattering Method
J. of APCA 23(12): 1035-1038, 1973

8. Chan, P. W.
Optical Measurements of Smoke Particle Size Generated by Electric Arcs.
Colo. State University, EPA, Washington, D.C., 1974, 49 pp.
EPA-650/2-74-034

9. Kuykendal, W. B., and C. H. Gooding
New Techniques for Particle Size Measurements.
Presented at the Workshop on Sampling, Analysis, and Monitoring of Stack Emissions, Oct. 2-3, 1975, Dallas Texas. pp. 183-208.

10. Farthing, W. E., and W. B. Smith
Evaluation of the PILLS IV.
Southern Research Institute, EPA, Research Triangle Park, NC., 1978.
51 pp.
EPA-600/7-78-130

11. Knollenberg, R. G.
Active Scattering Aerosol Spectrometry.
Proceedings of Seminar on Aerosol Measurement, National Bureau of Standards, Washington, D.C., 1974.

12. Particle Measuring Systems, Inc.
Classical Scattering Aerosol Spectrometer Probe Model CSASP-100., Boulder, Colo., 1976. 2 pp.

13. Wertheimer, A. L., and W. L. Wilcock
Light Scattering Measurements of Particle Distributions.
Appl. Optics 15(6): 1616-1620, 1976.

A.I. Manyurov, N.G. Bulgakova, E.I. Akopov

METHODS AND DEVICES FOR MEASURING INDUSTRIAL GASES' DEW POINT

Measuring the dew point of industrial gases has great significance both in industrial processes as well as in gas cleaning. For example, operative monitoring of the dew point is necessary in the coal industry for retrieval of rare elements from coal during its burning in systems equipped with filter bags made from "nitron" fabric. The work of these systems is impossible without dew point monitoring due to the high sensitivity of the fabric to concentrating sulfuric acid. Continuous monitoring of the dew point is also necessary in coal-enriching plants for efficient control of corrosion in the elements of the gas-cleaning equipment.

In many branches of the industry, drying proceeds according to the temperature of the waste gases. Continuous monitoring of the dew point allows control of the drying process with regard to the degree of the stack gases' moisture content, which, apparently, is significantly more accurate than controlling the exhaust gases by temperature.

It has been established that corrosion most markedly appears when the surface temperature is close to the exhaust gases' dew point temperature for gases containing SO_3.

Implemetation of dew point operative monitoring permits the introduction of efficient corrosion control means such as, for example, slightly raising exhaust gas temperature, burning fuel with a low excess air ratio and introduction of an admixtures for neutralizing SO_3.

Chemical methods for determining the SO_3 concentration are complicated and cumbersome, and are therefore unusable for operational monitoring, whereas the method of evaluating SO_3 content in stack gas according to dew point temperature, which is highly sensitive even to insignificant changes of SO_3 concentration, is very simple and quick-responding.

Dew point temperature measurement consists of simultaneously measuring two values, one of which allows fixing the moment when condensation begins, and the other determnies the temperature of the condensation surface at the moment of its moistening.

Measurement of the condensation surface's temperature may be done by the usual monitoring and measuring devices working as a unit with a thermocouple, thermosensitive resistor, and thermistor, depending upon the range of dew point measurements and the unit's accuracy and speed requirements.

According to the principle of fixation of the moment of dew precipitaion on condensation surface, the "'direct' method of dew point measurement" and correspondingly, the hygrometer's "dew point" it is possible to make classifications in the following manner (1):

1. Optical, where occurence of the condensate film is judged according to variations of the optical properties of a polished condensational surface at the moment that dew precipitates on it (2,3);

2. Electrical, where changes in the electrical properties of a section of the condensational surface, for example, conductivity, capacitance, dielectric permeability, serve as the basis for this method.

3. Electrochemical, based on the occurence of galvanic

electromotive force during condensation of electrolyte vapor in the inter-electrode space, which is at that time the condensational surface;

4. Thermal, using temperature difference between the cooler and condensational surface, occuring at the moment of condensation;

5. Hygroscopic, based on physical regularities of absorption and release of water by a salt-saturated aqueous solution.

6. Radioactive, based on differences in the dispersion characteristic of particles in the presence or absence of condensate.

Analysis of possibilities and expediency for using the methods of measurement named above for purposes of continuous automatic monitoring of gas dew point temperature shows that use of the optical method is essentially limited because of the gas dust content.

The thermal and hygroscopic methods cannot be adapted for monitoring hot gases with complicated variable chemical composition.

The electrical (conductometric) method, using changes of ohmic resistance between two electrodes, received at the condensation surface, had the most widespread distribution.

The basis of this method gave rise to several domestic designs of equipment.

Research has shown that the electrical method principally allows measurement of dew point of hot, multi-component, gas mixtures, however it is not useful for work in a dusty environment (dust shorts out its contacts).

The most expedient means for measuring the dew point of hot dusty gases is the electrochemical method of fixing the moment of condensation. However, at the present time, series-produced equipment is not available.

Dew point hygrometers are also classified according to their method of cooling the condensing element.

Presently, the following methods of cooling have gained use:

1. Thermoelectric, based on the Peltier effect;
2. Gas expansion, for example, of CO_2, freon, etc;
3. Liquid nitrogen, propane or other coolants, for example, solid CO_2;
4. Cooling by use of the vortex effect of power energy separation. The complexity of accurately feeding the cooling agent lowers the operational characteristics and practically excludes the possibility of fully automating cooling by various cooling agents.

Gas expansion methodology is also sufficiently complicated, since it demands cumbersome equipment for increasing pressure on the expanded gas.

It is more reasonable to use the vortex effect of compressed gas power separation for cooling. A self-evacuating tube with slit-type over-speed diffusor, providing, by comparison with vortex tubes of different design, deep refrigeration is often used. This allows measurement of the dew point within a +20- -60°C range with a ±2°C error.

Using thermoelectrical units based on the Peltier effect is, from the point of view of automation, the most convenient method for cooling limited volumes. Multistage thermopiles produce significant (up to 50-70°C) temperature drops (fig.1.). This method of refrigerating condensing elements is the most widely used one in the USSR (3,6).

Indirect methods are used for determining dew points, when the dew point is determined by calculation on the basis of the moisture and pressure of the studied gas (4,5).

Recently, infrared methods for determining dew point have become widely used, due to their increased sensitivity and quick response.

An automatic infrared hygrometer, the IFO-459, is produced in the USSR (7). This is a dual-frequency absorption modulation (25 hertz) unit with compensation in the optical canal. It works within a wave length range of 1.4-2.1 μ using interference light filters. A lead-sulfur sensory element is used as a photodetector. This unit is used in various branches of industry during dew point determination, in determining moisture content in gases and in preparing industrial air for drying. The unit's high sensitivity and quick response in all ranges of water steam concentration are its advantages.

Dew point characteristics for hygrometers used in the USSR are represented in table 1.

For increasing hygrometer accuracy and operational stability, the differential and compensational methods are often used. This is done, for example, when two photodetectors, reacting correspondingly to the light stream reflected from and scattered by the condensation surface, are used, which provides automatic error compensation against contamination of the condensing element surface.

Under temperatures lower than -30°C, exact determination of phase condition of the condensate , which is often not considered and therefore introduces additional errors in determining dew point, is especially important (8). It is necessary under these temperatures to consider the different values of water vapor pressure over water and over ice (fig. 2). This feature of water steam determines to a great extent the metrological characteristics of dew point hygrometers in the negative temperature range in as much as, for example, temperature difference reaches 5°C at a saturation temperature level on the order of -60°C. Ice formation always passes through a liquid phase formation stage As an example, we can cite the photoelectri system for stabilizing the thickness of the condensate. Thanks to this system, it is possible to obtain a diagramic record (fig. 3) of the mirror temperature, in determining the phase diagram of the condensate and formation of the solid phase in the negative temperature dew point range for slow changing moisture content of the gas under analysis (the sloping nature of the curve). The points (1) correspond to dew point temperature at the moment of condensate precipitation in the liquid phase, and points (2) correspond to the frost point settled temperature at water vapor saturation over a constant ice layer. Any states between these two points are characterized by by the presence of the condensate's mixed phase. The absence of temperature difference between the points 1 and 2 (i.e. the absence of a a "peak" in the diagrammatic record) indicates the existence on the mirror of a condensate liquid phase on the surface during the entire period of observation, which occurs at temperatures above -30°C.

Difficulties in determining dew point at temperatures higher than 100°C are commonly known (1). In this temperature range absorption-type automatic hygrometers without sampling using semi-conductor-emittors can be widely applied. The latter are characterized by low cost, reliability, compactness, working convenience, possibility for modulating emission by feed current, large dynamnic range for re-tuning out-put capacity, long period of service (10^4 hrs.), small size of emitting area (less than $1mm^2$), feasibility of coverage with the aid of selection of composition of semi-conductive material of wide spectral range (0.56-20 microns), relatively large out-put capacity (1.0milliwatts-10 watts) (9). It is also necessary to consider the appearance of new types of semi-conductor lasers working at room temperature. Multi-wave matrices of semi-conductor emitters that may significantly simplify hygrometer design, especially for dual-frequency hygrometers, find a special place in use. Their high response ($\sim$10 newton seconds) allows operation in impulse conditions or with use of high frequency narrow-band modulation (30megahertz), which may significantly increase the signal-noise ratio.

The absorptional optical method for determining dew point without sampling may be accomplished in the unit whose lay-out is shown in fig.4.

In this instrument the amount of water vapor in the gases is determined by comparison with a standard amount in the calibrating cell. Also measuring pressure in the gas conduit by conversion exactly determines its dew-point. The optics are protected from pollution by traditional means used for optical dust measurement.

It is necessary to note the common features of optical absorptional hygrometers without sampling: quick response, due to using quick-response optic-electronic elements; high measurement exactness from the system's lack of sampling.

Water vapor molecule concentration value, measured by the optical absorption method is described by the following expression:

$$N_{\text{прк}} = \frac{\Delta J}{J_0 \sigma L}, \quad \text{см}^{-3}$$

where: $N_{\pi\rho\kappa}$ - maximally registerable water vapor (gas) concentration.
L - length of optical absorption path.
J_0 - initial intensity of the emission source
ΔJ - change of emission intensity due to absorption
σ - absorption cross-section.

To serve as an example, the sensitivity of this method may be introduced, relative to water vapor under normal atmospheric conditions using an emittor in a spectral range near to 1.34 microns, where intensity of the water vapor lines of absorption is comparatively small $\left(S \sim 10^{-4}\,\text{см}^{-2}\,\text{атм}^{-1}\right)$ and the optical path length is ~10m. In this case, sensitivity is taken as $N_{\text{прк}}/N \sim 6 \cdot 10^{-4}$ where N is the overall molecule concentration in the atmosphere. It is sufffficient to say, that $N_{\text{пдк}}/N \sim 10^{-4}$ where $N_{\text{пдк}}$ is maximum permissible concentration of water vapor molecules in air. If stronger absorption bands are used (for example 2.94 microns, 2.74 microns, 2.66 microns), sensitivity grows by 10^3-10^8 times (10).

Use of semi-conductive emittors in optical hygrometers based on measurement of reflected light also allows simplification of their design, lowering the size and increasing measurement accuracy thanks to a narrower spectral band of emission.

In determining the dew point of other components of process gases, especially elemental gases, the semi-conductor emittors shown above may also find wide usage. Due to the high coefficient of light ~~absorption by elemental~~ substances (sulfur, sodium, mercury, etc.), absorption methods using semi-conductor emittors will possess increased sensitivity (9,10).

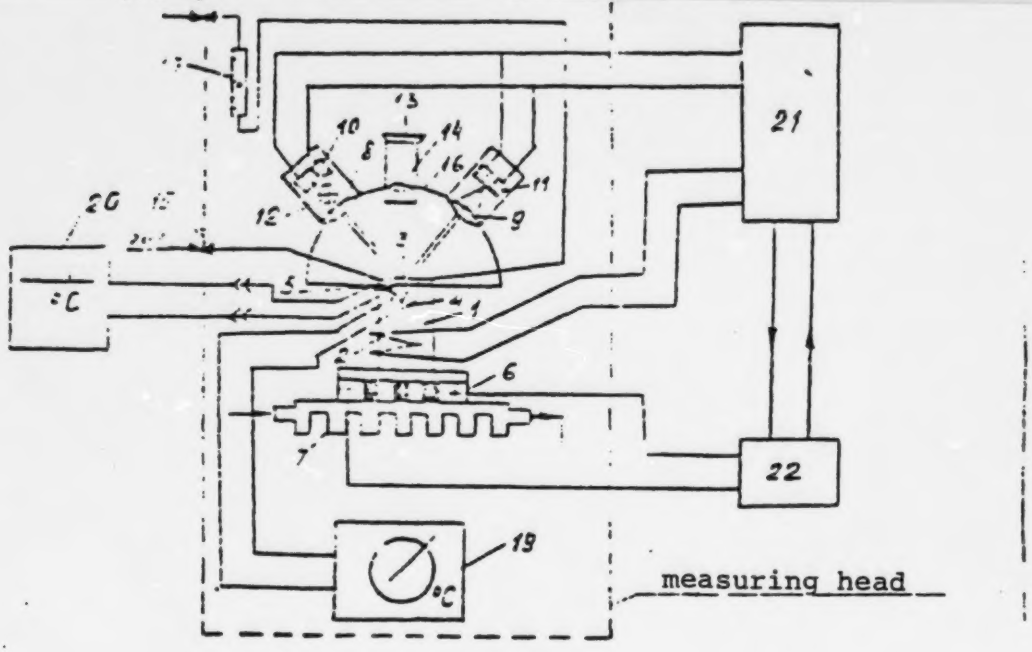
13
10
14
8
16
11
12
9
20
15
3
5
4
1
2
6
7
°C
21
22
19
°C
measuring head

Fig: 1

Dew-point hygrometer with thermoelectric cooling.
1. Copper rod. 2. nichrome spiral. 3. metal mirror. 4. resistance thermometer. 5. thermocouple. 6. thermopile. 7. radiator. 8,9. lenses. 10,11.photoresistors. 12. light source. 13. eyepiece. 14. magnifier. 15,18. rectifiers. 16. chamber. 17. rotameter. 19. microampermeter. 20. dew point register. 21. control elements. 22. thermopile supply unit.

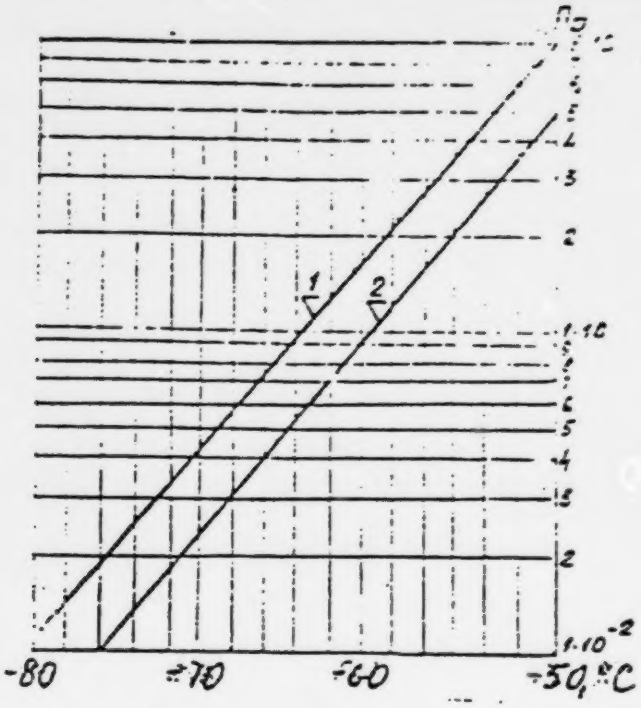

Fig.2. Dependence of water vapor pressure on temperature.

1. over water
2. over ice

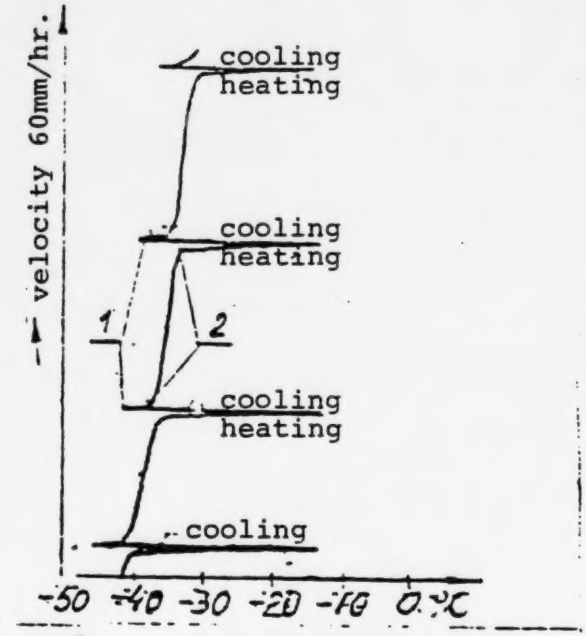

Fig.3. Diagrammatic record of mirror temperature.

1. Corrsponds to dew point temperature at the moment of condensate release in the fluid phase.

2. Corresponds to sustained frost point temperature during water vapor saturation under a constant ice layer.

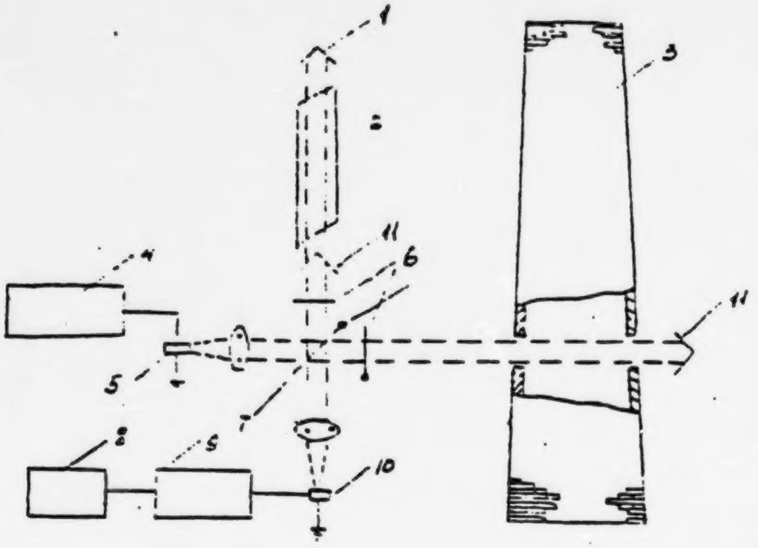

Fig. 4. Unit diagram - dew point hygrometer without sampling.

1,11. reflectors.
2. calibrating tray.
3. gas duct.
4. pumping generator.
5. semi-conductor emittor.
6. modulator.
7. beam splitter.
8. recorder.
9. amplifying unit.
10. photoreceptor.

BASIC DEW POINT MEASUREMENT TYPES

Unit type	measurement system	cooling type	of dew point measurement, °C	measurement error, °C	parameters of the studied gas			duration of measurement, mi
				0C	pressure in bars	temperature °C	flow rate kg/s	
VG-1	double beam	gas expansion (vortex tube)	- 60 ÷ + 20	± 2	0,5 - 6	± 50	$0,06 \cdot 10^{-3}$	
M-116	single beam	semi-conduct thermoelement	- 40 ÷ + 40	± 0,4		- 30 ÷ + 40		
APC-201	psychrometric	water cooling	+ 40,2 ÷ + 77	± I		40 - I50	air 3 m^3/hr steam 2 m^2/hr	
APV-201	psychrometric	water cooling	I0 - I00 % humidity	3%		30 - I00		
AGE-210	conductometric	semi-conduct thermoelement	- 20 ÷ + I50	± 0,5			I - 2 l/min	2
CA-1	single beam	semi-conductive thermoelement	- 20 ÷ + 20	± I	I00		I - 3 l/min	3 - 5
IFO-459	absorptional dual-frequency		optical density 0,002 0,05 0,2	10% 4% 3%				continuous

Reproduced from best available copy.

BIBLIOGRAPHY

1. Berliner, M.A., Moisture Measurement, Moscow, Energiia, 1973.

2. Merkulov, A.P., Kolyshev, N.D., Netsetaev, V.A., Karshin, A.I., "Basic Results of the Development and Testing of Dew Point Hygrometers with Vortex Cooling", in "Equipment and Means of Automation", 1974, no.10, p.21.

3. Dew Point Hygrometer M-116. Prospectus of the Achievements of the Soviet Economy.

4. Automatic Psychrometric APG-203 Hygrometer. Information leaflet no. 215-76, Interdisciplinary information, TsNIITEI Institute of Instrument Building, 1976.

5. APV-201-type Psychrometric Automatic Moisture Gage, Prospectus of the Achievements of the Soviet Economy, TsNIITEI Institute of Instrument Building, 1977.

6. Karpov, A.K. et al., "The Automatic Dew Point Hygrometer GA-1", in the collection "Industrial and Plant Processing of Natural Gas", Moscow, 1976, p.63-72.

7. Togulev, V.P., Ustimov, IU.N., Gross, L.G., Petrov, IU.A., "Automatic Infrared Hygrometer", "OMP", 1977, no.3, p.25.

8. Petukhov, V.P., "Determination of the Condensate's Phase State in Automatic "Dew Point" Hygrometers", "Measurement Technique", 1977, no.1, p.72.

9. Maniurov, A.I., "Perspectives on the Use of Semi-Conductor Emitting Diodes Made From Solid Solutions for the Quantitative Evaluation of Harmful Contaminants", in the interinstitutional collection "Ecology and Work Safety in Radioelectronics", Moscow, 1977.

10. Zuev, V.E., Propagation of Visible and Infrared Waves in the Atmosphere, Moscow, "Sov. Radio", 1970.

DESIGN OF AN IMPROVED IMPACTOR

W.B. Smith
K.M. Cushing

Southern Research Institute
2000 Ninth Avenue South
Birmingham, Alabama 35205

D.B. Harris
Industrial Environmental Research Laboratory
Environmental Protection Agency
Research Triangle Park, N.C. 27711

(This document has been reviewed and approved for publication by the U.S. EPA.)

DESIGN OF AN IMPROVED IMPACTOR

Over the past ten years cascade impactors have become commonly used measurement devices for the determination of particulate size distributions of industrial effluents. Data obtained with impactors are used to characterize particulate emissions from sources, to determine the performance of particulate control devices, and in the selection and design of control devices for specific sources.

Figures 1 and 2 show schematic diagrams of five commercial cascade impactors which are commonly used in stack sampling.[1,2,3,4,5,6,7] Particle separation by size interval takes place within these impactors by passing the sample gas stream sequentially through a series of dry impingement type inertial classifiers. The classifiers operate by impingement of the aerosol stream in an air jet against a plate, causing the air in each jet to sharply change direction and flow around the plate. (See Figure 3) Because of inertia, some particles cannot follow the flow streamlines and are deposited on the collection plate. Each cascaded impingement stage in the series operates at a higher impingement velocity (or as a higher energy separator) than the previous stage. Thus finer and finer particles are removed by the various stages as the sample gas stream proceeds through the impactor. An absolute filter is usually positioned after the final impaction stage to collect all remaining particulate.

Recently many researchers have undertaken investigations to better characterize cascade impaction operation. Both the development of better theories of operation[8,9,10,11] and the explicit calibration of existing commercial and prototype devices[12,13,14] has led to a better understanding of the interpretation and accuracy of cascade impactor data. The basic

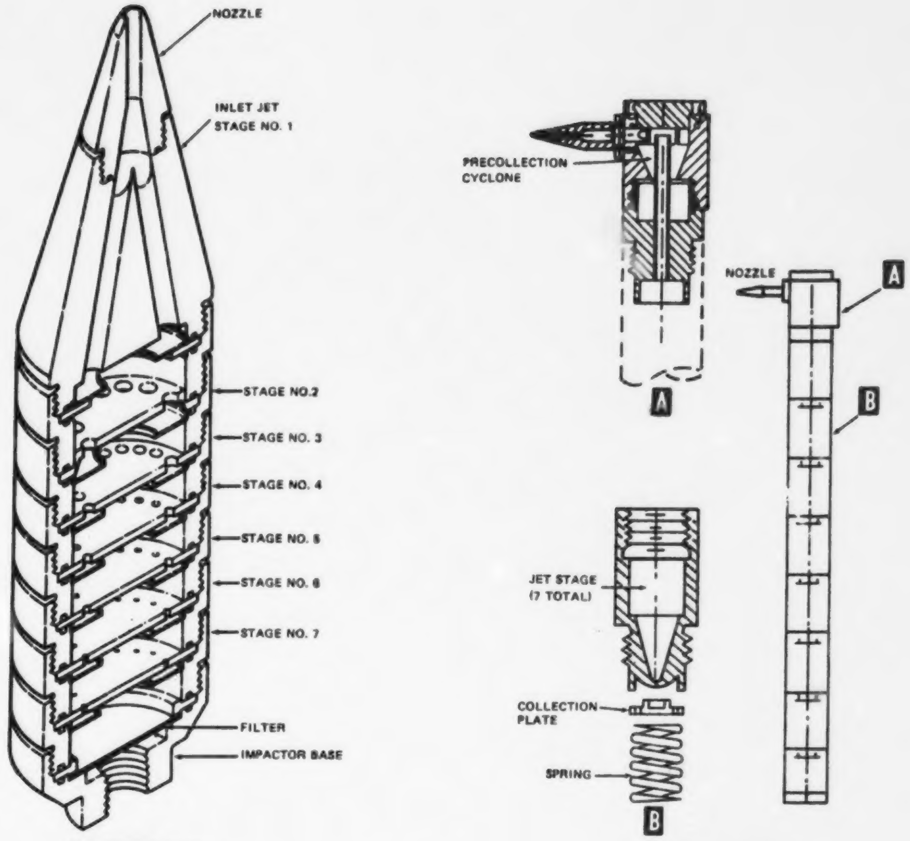
NOZZLE
INLET JET
STAGE NO. 1
STAGE NO.2
STAGE NO. 3
STAGE NO. 4
STAGE NO. 5
STAGE NO. 6
STAGE NO. 7
FILTER
IMPACTOR BASE
PRECOLLECTION
CYCLONE
A
NOZZLE
A
B
JET STAGE
(7 TOTAL)
COLLECTION
PLATE
SPRING
B
B

MRI MODEL 1502

MODIFIED BRINK

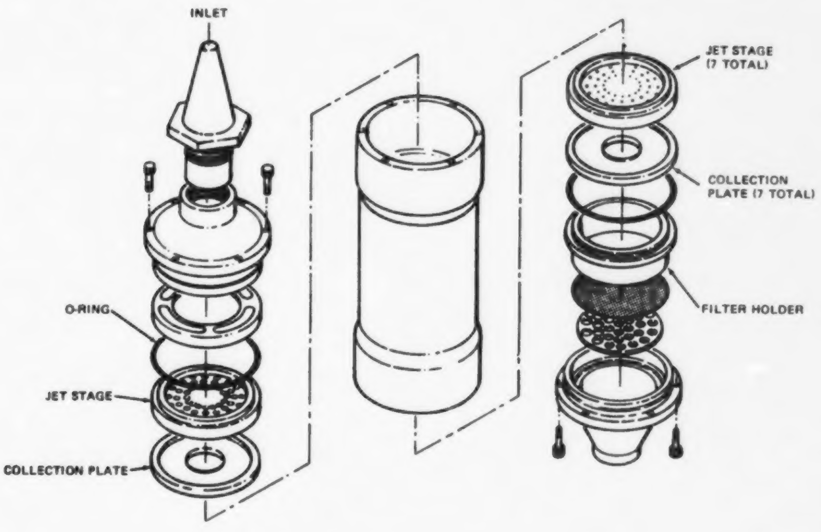
INLET
JET STAGE
(7 TOTAL)
COLLECTION
PLATE (7 TOTAL)
FILTER HOLDER
O-RING
JET STAGE
COLLECTION PLATE
3630-269

UNIVERSITY OF WASHINGTON MARK III

Figure 1. Schematics of three commercial cascade impactors.

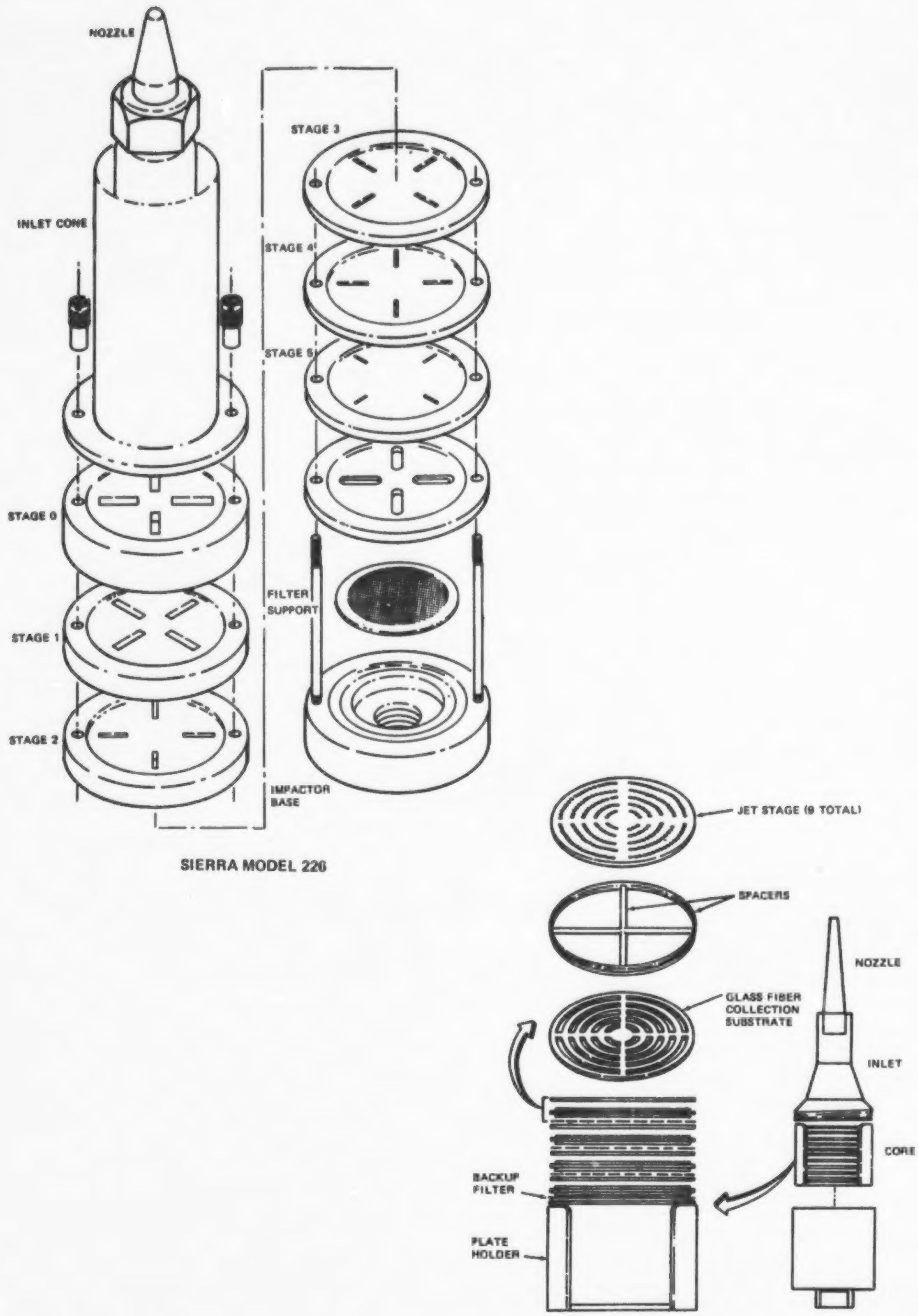
NOZZLE
STAGE 3
INLET CONE
STAGE 4
STAGE 5
STAGE 0
FILTER SUPPORT
STAGE 1
STAGE 2
IMPACTOR BASE
SIERRA MODEL 226
JET STAGE (9 TOTAL)
SPACERS
NOZZLE
GLASS FIBER COLLECTION SUBSTRATE
INLET
CORE
BACKUP FILTER
PLATE HOLDER
ANDERSON MARK III
3630-233

Figure 2. Schematics of two commercial cascade impactors.

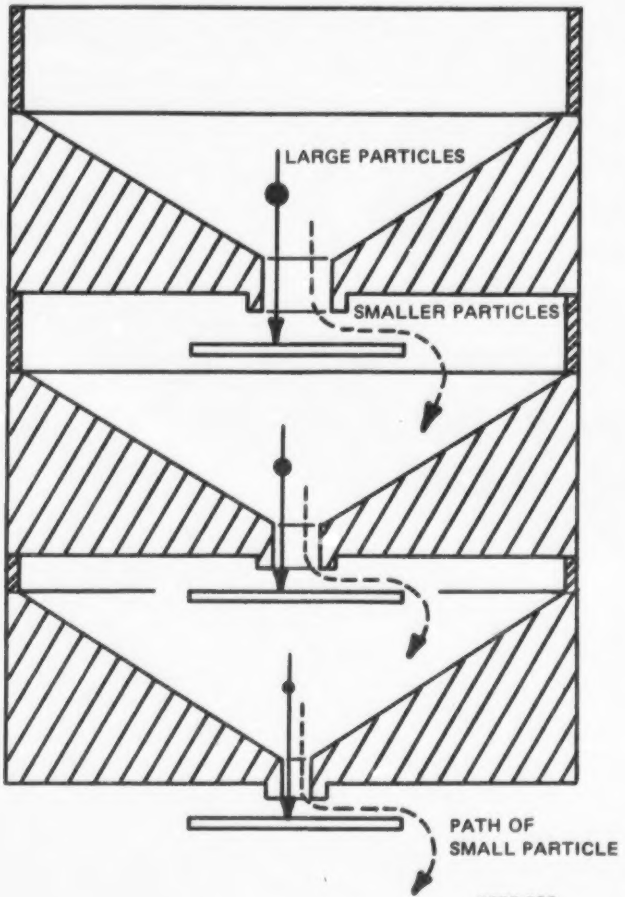
LARGE PARTICLES
SMALLER PARTICLES
PATH OF
SMALL PARTICLE
3630-230

Figure 3. Schematic diagram, operation of cascade impactor.

limitation of cascade impactors is that they provide data with only relatively low resolution and do not permit the exact reconstruction of the aerosol being sampled, even over the limited range of sizes normally covered by most impactors (approximately 0.5 to 10.0 microns). Improved methods of data reduction may reduce the reconstruction error.

The theory of the impaction process has been developed by several researchers to a state where the efficiency, E, of impaction can be estimated as a function of the particle size (D_p), Reynolds Number (Re), the jet diameter or width (D_j,W), the jet to plate distance (S), and the jet throat length (T). (Marple[9] specifically uses the dimensionless reduced quantities (S/D_j,S/W) and (T/D_j,T/W) when considering the jet to plate distance and the jet throat length, respectively.)

$$E = E\ (D_p,\ Re,\ S/D_j,\ T/D_j)$$

It is common practice to relate the particle diameter, D_p, to the square root of the inertial impaction parameter ($\sqrt{\psi}$), which is the ratio of the particle stopping distance (ℓ) to the jet diameter or width (D_j or W). Thus,

$$\psi = \ell/D_j$$

or

$$\psi = D_p{}^2\ \frac{C\rho_p V_o}{18\ \mu\ D_j}$$

where C = Slip Correction Factor,

V_o = Jet Velocity (cm/sec),

μ = Gas Viscosity (poise),

ρ_p = Particle Density (gm/cm), and

D_j = Jet Diameter (cm).

The square root of the inertial impaction parameter, $\sqrt{\psi}$, is used in impaction theories as a dimensionless quantity proportional to particle diameter,

$$\sqrt{\psi} = D_p \left[\frac{C\rho_p V_o}{18\ \mu\ D_j}\right]^{\frac{1}{2}} .$$

The inertial impaction parameter is useful in graphing impactor calibration data because information from all stages of an impactor can be placed on a single graph, and under many circumstances would, in theory, lie along a common curve. The value of $\sqrt{\psi}$ at 50% collection efficiency, $\sqrt{\psi_{50}}$, defines the impaction stage D_{50}, which is the particle diameter for which half of the particles are collected and half are passed to the next stage. For data reduction purposes the D_{50} is used as the effective stage cut diameter.

Recently Marple[9] has been able to calculate theoretical impaction efficiency curves for several values of the jet to plate distance, jet Reynolds Number, and jet throat length. Figure 4 shows the results of these calculations for both round and rectangular jet impactors. Using the data from Figure 4, a design chart for round jet cascade impactor can be formulated as shown in Figure 5.

Several basic problems have become areas of concern for researchers developing new cascade impactors, as well as users of current commercial devices. Several of these problems are discussed below:

1. Non Ideal Size Discrimination - Ideally each stage of a cascade impactor would remove all particles larger than a critical size and pass to the next stage everything smaller than that size. In reality the fractional efficiency curve for stage collection is a smoothly varying function which passes through the 50% efficiency point at a particle size designated as the stage cut point or D_{50}. Log normal approximations to stage efficiency curves generally have standard deviations on the order of 1.3. The overlapping stage efficiency curves result in particles of one particular size being collected on several impaction stages. This drastically complicates the data analysis procedure and the recovery of a reliable particle size distribution.

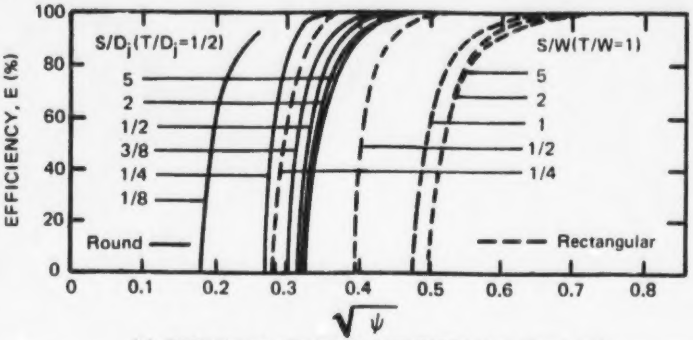

(a) EFFECT OF JET TO PLATE DISTANCE (Re=3,000)

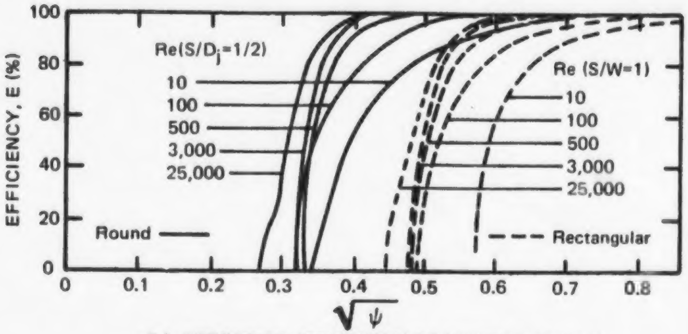

(b) EFFECT OF JET REYNOLDS NUMBER (T/W=1)

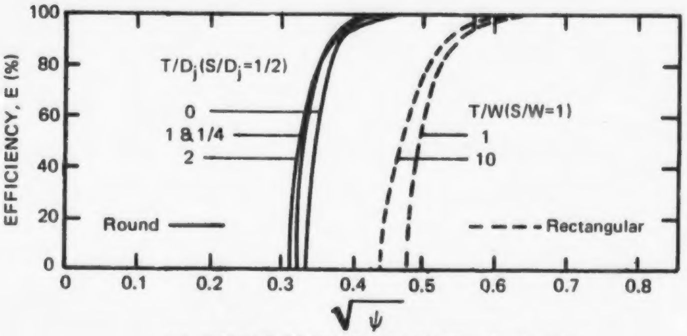

(c) EFFECT OF THROAT LENGTH (Re=3,000)

Figure 4. Theoretical stage collection efficiency versus $\sqrt{\psi}$ for round and rectangular jet cascade impactors. (After Marple.[9])

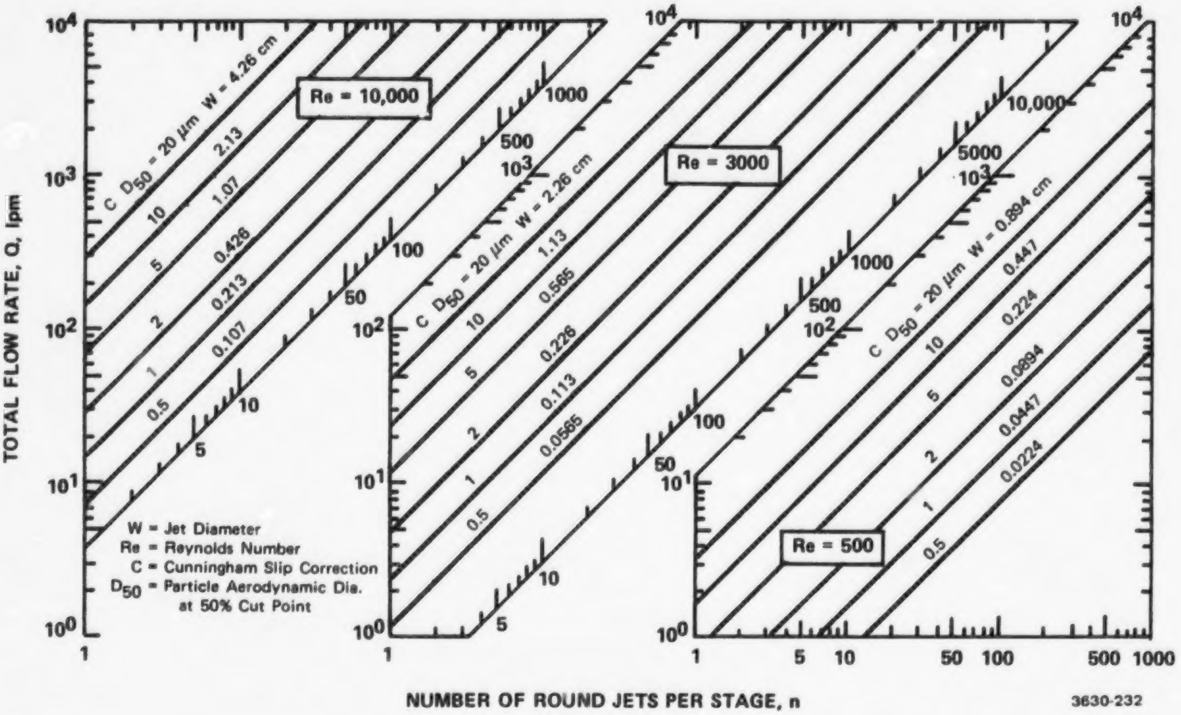

Figure 5. Design chart for round impactors (D_{50} = aerodynamic diameter at 50% cut point.) After Marple.[15]

2. Particle Bounce and Reentrainment - In an ideal impactor removal at each stage would become 100% at a certain size and remain constant for all larger particles. However, recent data[12,14] has shown most stage collection curves approach but never reach 100%, and roll over after a certain size and become less efficient for larger sizes. The fact that the particles do bounce and become reentrained can be attributed to several reasons including the type of collection surface, the nature of the particle, the jet velocity, and jet air flow interference on the collection surface. Each of these mechanisms contribute to particles not being captured initially and to subsequent particle reentrainment. This is evident in the calibration data shown in Figure 6 for an Andersen Mark III Cascade Impactor. Research has shown that these problems can be minimized by the use of collection substrates[16] (glass fiber mats or thin grease layers), the lowering of stage jet velocities, and the careful arrangement of multiple jets to reduce interference effects which cause blow off of the captured particles and their subsequent reentrainment. Because the collection of fine particles requires high jet velocities, lowering of jet velocities to improve capture efficiency reduces the size resolution of the device. Usually an attempt is made to reduce the jet velocities on the upper stages where particle bounce and reentrainment is more severe and causes a greater deformation of the recovered size distribution. The improvement of operation resulting from more jets and/or smaller jets is also bounded by the physical limits of placing many jets on a small jet plate and the ensuing increase in machining and tooling costs.

3. Wall Loss - Particle loss to the internal walls of impactors is an unavoidable situation which can be minimized by reducing surface area. Maintenance of proper flow streamlines and avoiding abrupt bends in the particle paths are also necessary. Particle wall loss is also attributable to settling and

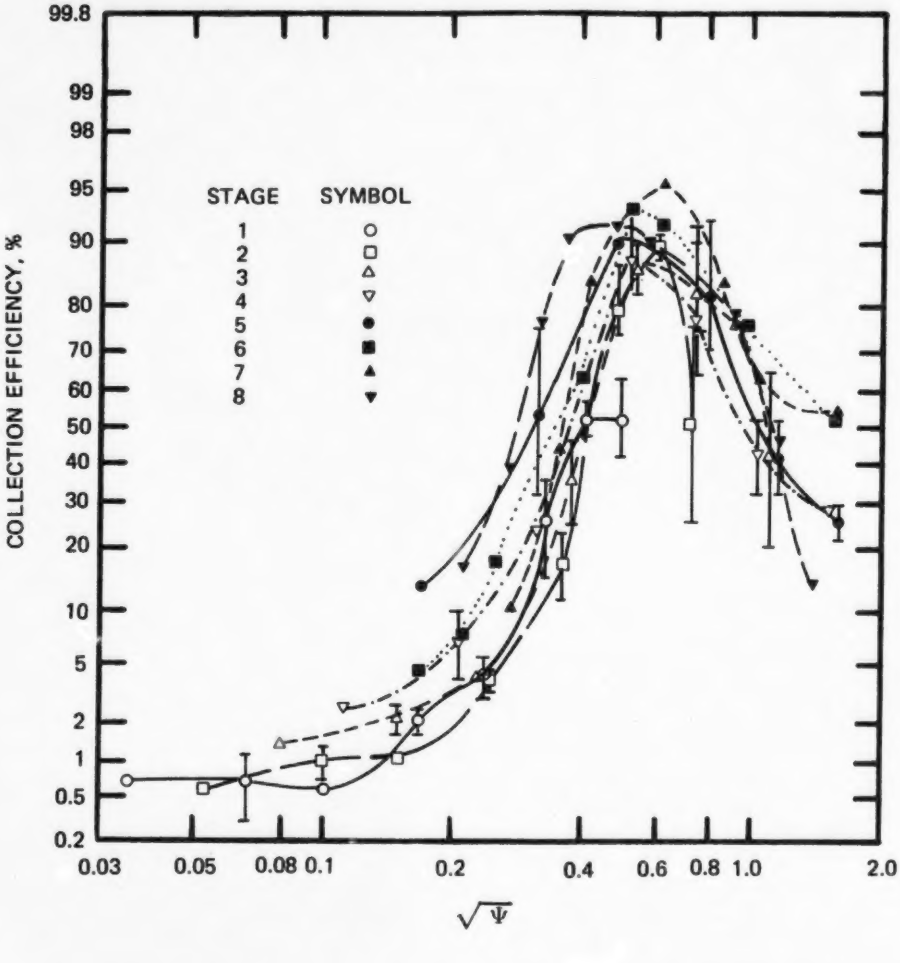

Figure 6. Stage collection efficiency versus $\sqrt{\psi}$ for Andersen Mark III Stack Sampler. (Flow rate = 14.2 lpm, particle density = 1.00 gm/cm^3, temperature = 20°C)

particle bounce, Van der Waal's forces, and, to a smaller degree, diffusion. Frequently particle bounce results in a dust pattern forming on the underside of the jet plates. This type of wall loss is an indication of poor impactor design, stage overloading, or high jet velocities. Recent wall loss data[12] for commercial cascade impactors is shown in Figure 7.

Based on the current knowledge of impactor theory and the result of field and laboratory testing of currently available commercial and prototype cascade impactors, high and low flow rate impactors are being designed and fabricated that attempt to conform to our criteria for optimized cascade impactors listed in Table 1. An optimized cascade impactor can be defined as one which is designed to operate both in a laboratory or field environment in such a way that the effects of particle bounce, particle reentrainment, wall loss, overlapping stage collection efficiency curves, etc. are minimized. Mechanical reliability and case of operation are also considered in this design program.

Design parameters for 0.1, 0.5, and 2.0 ACFM, optimized, cascade impactors have been generated by a special computer program written at Southern Research Institute. Six impaction stages with cut points of 9.6, 4.8, 2.4, 1.2, 0.6, and 0.3 micrometers aerodynamic diameter were chosen as a design goal for these cascade impactors. The actual theoretical stage D_{50}'s as calculated by the computer program were very close to the desired stage cut points, but varied slightly to limit the number of holes per stage and to allow the use of standard drill sizes. The final design parameters are presented in Tables 2, 3, and 4. An assembly drawing of the 0.5 ACFM impactor is shown in Figure 8.

A prototype of the 0.5 ACFM optimized cascade impactor is currently being fabricated by Southern Research Institute for calibration and testing purposes.

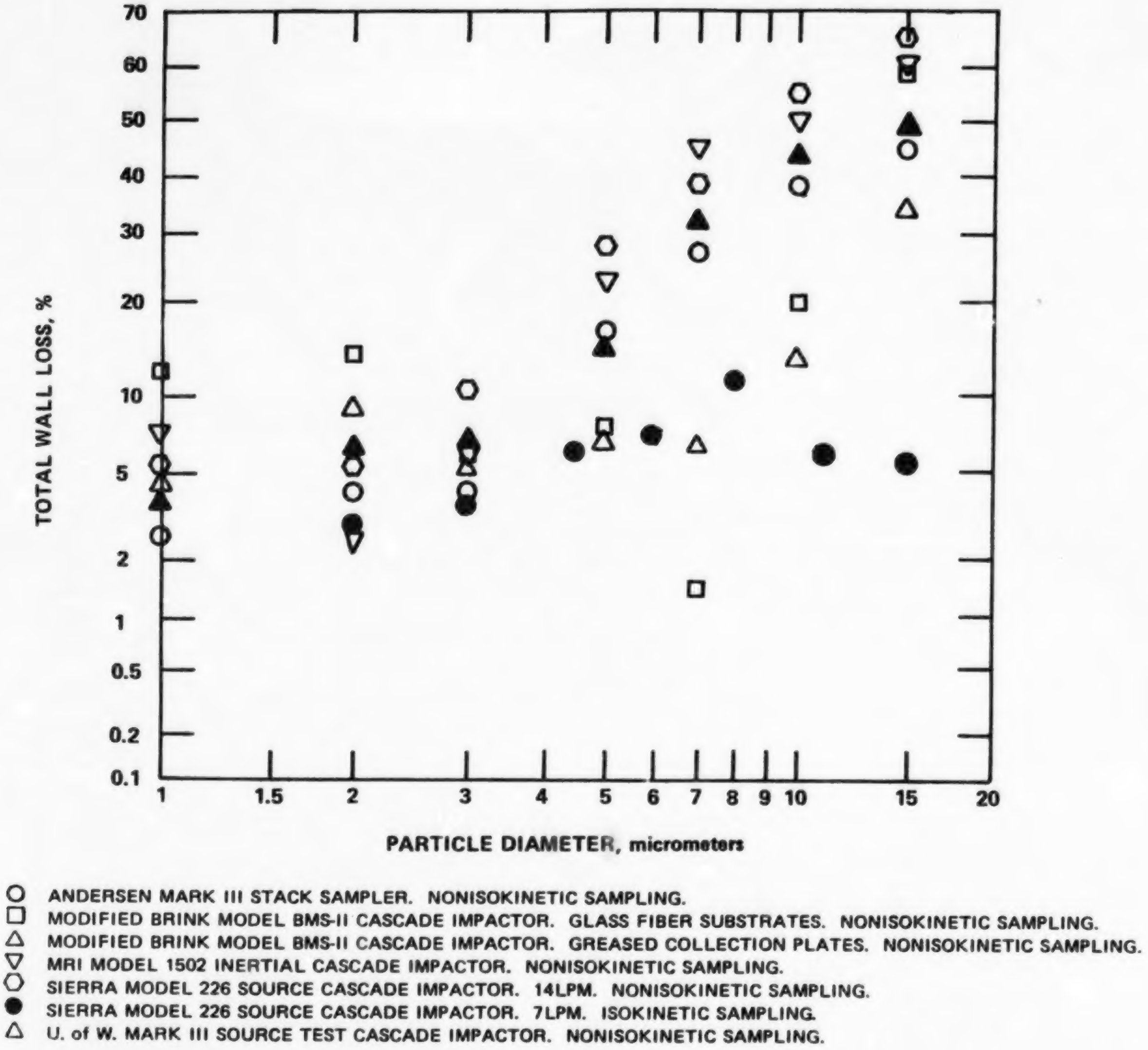

Figure 7. Recent cascade impactor particle wall loss data. After Cushing, et al.[12]

TABLE 1. CRITERIA FOR IMPACTOR DESIGN

1. The jet Reynolds number should be between 100 and 3000.
2. The jet velocity should be 10 times greater than the settling velocity of particles having the stage D_{50}.
3. The jet velocity should be less than 110 m/sec.
4. The jet diameter should not be smaller than can be attained by conventional machining technology.
5. The ratio of the jet-plate spacing and the jet diameter or width (S/W) should lie between 1 and 3.
6. The ratio of the jet throat length to the jet diameter (T/W) should be approximately equal to unity.
7. The jet entires should be streamlined or countersunk.

TABLE 2

0.1 ACFM OPTIMIZED CASCADE IMPACTOR DESIGN SPECIFICATIONS

Impactor Sampling Rate = 0.1 ACFM   Gas Temperature = 204.0°C   Particle Density = 1.0 gm/cc

Stage D_{50} - Design Goal (μm)	9.6	4.8	2.4	1.2	0.6	0.3
Jet Inlet Pressure (atm) (Ambient=0.987 atm)	0.987	0.986	0.985	0.975	0.953	0.921
Best Jet Drill Diameter (cm)	0.47	0.30	0.19	0.098	0.0254	0.0254
Number of Jets on this Stage	1	1	1	2	31	19
Actual Jet Reynolds Number	362.6	568.0	895.3	859.2	209.0	396.9
Jet Velocity (m/sec)	2.72	6.68	16.65	31.29	30.05	71.05
Actual Square Root of Stokes #	0.478	0.476	0.475	0.475	0.480	0.477
Cunningham Correction Factor	1.017	1.034	1.070	1.145	1.297	1.777
Computed Stage D_{50} (μm)	9.474	4.776	2.359	1.195	0.589	0.297

TABLE 3

0.5 ACFM OPTIMIZED CASCADE IMPACTOR DESIGN SPECIFICATIONS

Impactor Sampling Rate = 0.5 ACFM Gas Temperature = 204.0°C Particle Density = 1.0 gm/cc

Stage D_{50} - Design Goal (μm)	9.6	4.8	2.4	1.2	0.6	0.3
Jet Inlet Pressure (atm) (Ambient=0.987 atm)	0.987	0.986	0.981	0.970	0.931	0.901
Best Jet Drill Diameter (cm)	0.794	0.518	0.206	0.107	0.025	0.016
Number of Jets on this Stage	1	1	4	8	155	235
Actual Jet Reynolds Number	1073.6	1643.4	1030.1	981.5	204.4	206.9
Jet Velocity (m/sec)	4.77	11.19	17.75	32.99	30.05	49.95
Actual Square Root of Stokes #	0.474	0.471	0.474	0.474	0.480	0.480
Cunningham Correction Factor	1.017	1.035	1.070	1.146	1.304	1.707
Computed Stage D_{50} (μm)	9.221	4.797	2.372	1.212	0.588	0.316

TABLE 4

2.0 ACFM OPTIMIZED CASCADE IMPACTOR DESIGN SPECIFICATIONS

Impactor Sampling Rate = 2.0 ACFM Gas Temperature = 204.0°C Particle Density = 1.0 gm/cc

Stage D_{50} - Design Goal (μm)	9.6	4.8	2.4	1.2	0.6	0.3
Jet Inlet Pressure (atm) (Ambient=0.987 atm)	0.987	0.986	0.983	0.973	0.934	0.849
Best Jet Drill Diameter (cm)	0.794	0.404	0.206	0.107	0.045	0.022
Number of Jets on this Stage	4	8	17	32	119	355
Actual Jet Reynolds Number	1073.6	1054.1	971.0	984.3	602.5	375.6
Jet Velocity (m/sec)	4.77	9.21	16.71	32.99	49.88	69.95
Actual Square Root of Stokes #	0.474	0.474	0.474	0.474	0.476	0.478
Cunningham Correction Factor	1.017	1.035	1.070	1.145	1.324	1.844
Computed Stage D_{50} (μm)	9.221	4.694	2.448	1.212	0.598	0.300

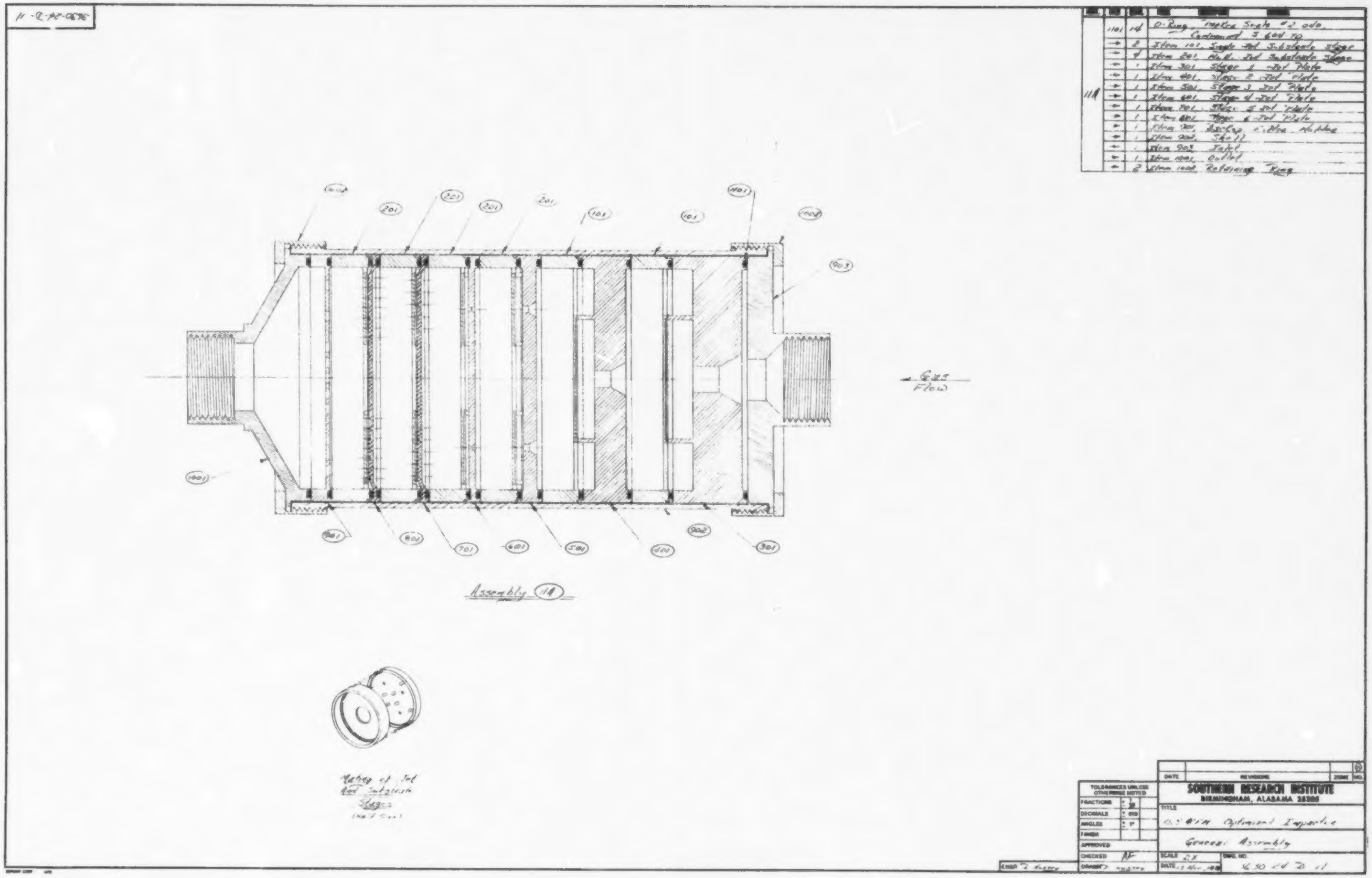
11-C-82-0676
O-Ring, Parker Single #2 odo, Continued 5-604-70
Item 101, Single Jet Substrate Stage
Item 201, Multi-Jet Substrate Stage
Item 301, Stage 1 Jet Plate
Item 401, Stage 2 Jet Plate
Item 501, Stage 3 Jet Plate
Item 601, Stage 4 Jet Plate
Item 701, Stage 5 Jet Plate
Item 801, Stage 6 Jet Plate
Item 901, Backup Filter Holder
Item 902, Shell
Item 903, Inlet
Item 1001, Outlet
Item 1002, Retaining Ring
11A
1101
1002
201
221
101
401
1001
903
802
701
601
501
902
301
Gas Flow
Assembly 11A
SOUTHERN RESEARCH INSTITUTE
BIRMINGHAM, ALABAMA 35205
TOLERANCES UNLESS OTHERWISE NOTED
FRACTIONS
DECIMALS
ANGLES
FINISH
APPROVED
CHECKED
DRAWN
DATE
REVISIONS
ZONE
NO.
TITLE
0.5 ACFM Optimized Impactor
General Assembly
SCALE 2X
DWG. NO.

Figure 8. Assembly drawing of the 0.5 ACFM, six-stage, optimized cascade impactor.

REFERENCES

1. Andersen A. A.
A Sampler For Respiratory Health Hazard Assessment.
Amer. Ind. Hyg. Assoc. J., pp. 160-165, 1966.

2. Brink, J. A., Jr.
Cascade Impactor For Adiabatic Measurements.
Ind. And Eng. Chem., 50(4), pp. 645-648, 1958.

3. Jackson, B., and D. Ensor
Preliminary Calibration Of The M.R.I. Inertial Impactor
Meteorology Research, Inc., M.R.I. Research & Development, 10 pp., 1974.

4. Lundgren, D. A.
An Aerosol Sampler For Determination Of Particle Concentration As A Function Of Size And Time.
J. of APCA, 17(4), pp. 225-259, 1967.

5. May, K. R.
A Cascade Impactor With Moving Slides.
A.M.A. Archives Of Ind. Health, 1956, Vol. 13, pp. 481-188.

6. Pilat, M. J., D. S. Ensor, and J. C. Bosch
Cascade Impactor For Sizing Particulates In Emission Sources.
Amer. Ind. Hyg. Assoc. J., 32(8), pp. 508-511, 1971.

7. Willeke, K.
Performance Of The Slotted Impactor.
Amer. Ind. Hyg. Assoc. J., 36(9), 683-391, 1975.

8. Cohen, J. J., and D. N. Montan
Theoretical Considerations, Design, And Evaluation Of A Cascade Impactor.
Amer. Ind. Hyg. Assoc. J., pp. 95-104, 1976.

9. Marple, V. A.
A Fundamental Study Of Inertial Impactors.
Dissertation, Univ. of Minn., University Microfilms, High Wycomb, England, 1970, 243 pp.

10. Mercer, T. T., and R. G. Stafford
Impaction From Round Jets.
Ann. Occup. Hyg., 12, pp. 41-48, 1969.

11. Ranz, W. E., and J. B. Wong
Impaction Of Dust And Smoke Particles On Surface And Body Collectors.
Ind. And Eng. Chem., 44(6), pp. 1371-1381, 1952.

12. Cushing, K. M., G. E. Lacey, J. D. McCain, and W. B. Smith
Particulate Sizing Techniques For Control Device Evaluation: Cascade Impactor Calibrations.
Southern Research Institute, EPA, Research Triangle Park, NC, 1976, 94 pp.
EPA-600/2-76-280

13. Dzubay, T. G., L. E. Hines, and R. K. Stevens
Particle Bounce Errors In Cascade Impactors.
Atmos. Environ. 10, pp. 229-234, 1974.

14. Rao, A. K.
An Experimental Study Of Inertial Impactors.
Dissertation, Univ. of Minnesota, 1975, 194 pp.

15. Marple, V. A., and K. Willeke
Impactor Design.
Atmos. Environ., 10, pp. 891-896, 1976.

16. Felix, L. G., G. I. Clinard, G. E. Lacey, and J. D. McCain
Inertial Cascade Impactor Substrate Media For Flue Gas Sampling.
Southern Research Institute, EPA, Research Triangle Park, NC, 1977, 89 pp.
EPA-600/7-77-060